SOLAR PHOTOCATALYTIC DECOMPOSITION OF PENTACHLOROPHENOL DISSOLVED IN WATER

Sixto Malato Rodríguez

Plataforma Solar de Almería

Centro de Investigaciones Energéticas, Medioambientales y Tecnológicas

Crta. Senés km 4 - 04200 Tabernas, Spain

January 1999

English version of Doctoral Thesis of Sixto Malato Rodriguez defended on the 19th of February 1997 in Chemical Engineering Department of Universidad de Almeria.

ACKNOWLEDMENTS

I wish to thank Dr. Manuel Romero Alvarez, who has directed and supervised with interest the development of this research.

Special thanks are due to Mr. Julián Blanco for his collaboration, which has been essential to the achievement of this research.

My gratitude to Mrs. Deborah Fuldauer and Mrs. Carmen Montesinos, without whose assistance the correct composition of this work would have been impossible.

To all PSA's staff for their great willingness and high skill, making possible the design and construction of the pilot plant as well as the performance of the tests, which are the bases of this doctoral thesis. I would also like to express special recognition to Jaime Aranda, Juan Antonio Camacho, Ginés García, Jose Manuel Molina and Angel Soler, together with the Operation and Maintenance team of the PSA.

To Dr. Christoph Richter (DLR-PSA), Dr. Jaime Giménez and Dr. David Curcó (Univ. Barcelona), Dr. Jean-Marie Herrmann (CNRS-Lyon), Dr. Claudio Minero and Dr. Ezzio Pelizzetti (Univ. Torino), as well as my colleagues in the Instituto de Energías Renovables Mr. Alfonso Vidal and Dr. Marcelino Sánchez for their help with their advise and comments, Mrs. Lucía Marroquín, for her valuable collaboration to obtain the bibliography used in this work.

To the direction of the Plataforma Solar de Almería and Centro de Investigaciones Energéticas, Medioambientales y Tecnológicas (CIEMAT) for the support given to carry out this doctoral thesis.

To the Departamento de Ingeniería Química de la Universidad de Almeria.

To my family, for their patience and moral support.

SOLAR PHOTOCATALYTIC DECOMPOSITION OF PENTACHLOROPHENOL DISSOLVED IN WATER

Table of Contents

1. INTRODUCTION

1.1 Photocatalysis

Recent decades have witnessed increased contamination of the Earth's drinking water reserves. To solve this problem, apart from reducing emissions, two main water treatment strategies are being followed: (i) chemical treatment of drinking water, contaminated surface and groundwater and (ii) chemical treatment of waste waters containing biocides or non-biodegradable compounds.

The decontamination of drinking water is done mainly by procedures that combine flocculation, filtration, sterilization and conservation, to which a limited number of chemicals are added. Normal human sewage water can be efficiently treated in conventional biological processing plants. The chemical treatment of polluted surface and groundwater or wastewater, is part of a long-term strategy to improve the quality of water by eliminating toxic compounds of human origin before returning the water to its natural cycles. This type of treatment is suitable when a biological processing plant cannot be adapted to certain types of pollutants that did not exist when it was designed.

The latest advances in water purification have been in the oxidation of very persistent organic compounds dissolved in water. The methods based on catalysis and photochemistry have been denominated Advanced Oxidation Processes. Among them, those which produce hydroxyl radicals ($^{\bullet}OH$) have had growing success *[Haag et al., 1992; Rupert et al., 1993a, 1994*]. Due to the strong oxidative nature of this compound (E°=2.8 V), much greater than other oxidants (ozone 2.07 V, peroxide 1.78 V, chloride dioxide 1.57, chlorine 1.36 V, etc.), is able to completely transform organic carbon to CO_2 [*Serpone et al., 1994a*]. Methods based on H_2O_2/UV, O_3/UV and H_2O_2/O_3/UV combinations utilize photolysis of H_2O_2 and ozone to produce the hydroxyl radicals. But these radicals can also be generated with a semiconductor (photocatalysis) which absorbs UV radiation when this is in contact with the water. The latter process is of special interest [*Kamat et al., 1990*], since it can use natural (solar) UV, if the semiconductor used has an appropriate separation between its valence and conduction bands which can be surpassed by the energy content of a solar photon ($\lambda \geq 300$ nm).

1.1.1 Definition

Photocatalysis may be defined as the "acceleration of a photoreaction by the presence of a catalyst". The catalyst activated by the absorption of light accelerates the process by interacting through a state of excitation (C*) or by the appearance of electron/ hole (e^- and h^+)

pairs if the catalyst is a semiconductor [*Pelizzetti, 1986a*]. In this case, the excited electrons are transferred to the reducible specimen, at the same time that the catalyst accepts electrons from the oxidizable specimen, which occupies the holes. In this way the net flow of electrons is null and the catalyst remains unaltered [*Fox, 1983*]. The work described here is based on this second process.

$$C \xrightarrow{h\nu} C^*$$
$$C^* + R \longrightarrow R^* + C^*$$
$$R^* \longrightarrow P$$

$$C \xrightarrow{h\nu} C(e^- + h^+)$$
$$h^+ + Red_2 \longrightarrow Ox_2$$
$$e^- + Ox_1 \longrightarrow Red_1$$

1.1.2. Heterogeneous Photocatalysis

It is not easy to define the ideal photocatalytic process, even for the most experienced researchers in the field [*Serpone et al, Chap. 1, 1989*]. In this sense, *Bahnemann et al.* [*1991b*] have proposed, not without strong reason, that a semiconductor particle is an ideal photocatalyst for a specific reaction if: (a) the products formed are highly specific, (b) if the catalyst remains unaltered during the process, (c) if the formation of electron/ hole pairs is required (generated by the absorption of photons with energy greater than that necessary to move an electron from the valence band to the conduction band) and (d) if photon energy is not stored in the final products, being an exothermic reaction and only kinetically retarded. These four characteristics are accepted as the optimum for a photocatalytic process to be ideal [*Pelizzetti et al., 1993c; Serpone et al. 1993a*] and are shown in the diagram in Figure 1.1.

Photocatalysis with irradiated semiconductors provides a method which permits effective oxidation and reduction of organic and inorganic compounds. Titanium dioxide particles (TiO_2) have been demonstrated to be an excellent catalyst for photo-oxidation of a multitude of organic substances such as: phenol [*Al-Ekabi et al., 1988; Augliaro et al., 1988, 1990; Okamoto et al., 1985a, 1985b; Sclafani et al., 1991*], chlorophenols [*Al-Ekabi et al., 1989; Barbeni et al., 1984, 1985; Minero et al., 1993*], dioxines [*Barbeni et al., 1986, Pelizzetti et al., 1988], DDT [Borello et al., 1989*], Lindane [*Vidal et al., 1994; Guillard et al., 1996*] and up to a total of some 600 others [*Blake, 1994, 1995*]. Its application is even being attempted as a bactericide [*Chang et al., 1994*].In this work TiO_2 suspensions were used as a reaction medium, (energy bandgap, E_G = 3.2 eV) in water and solar radiation as the source of photons.

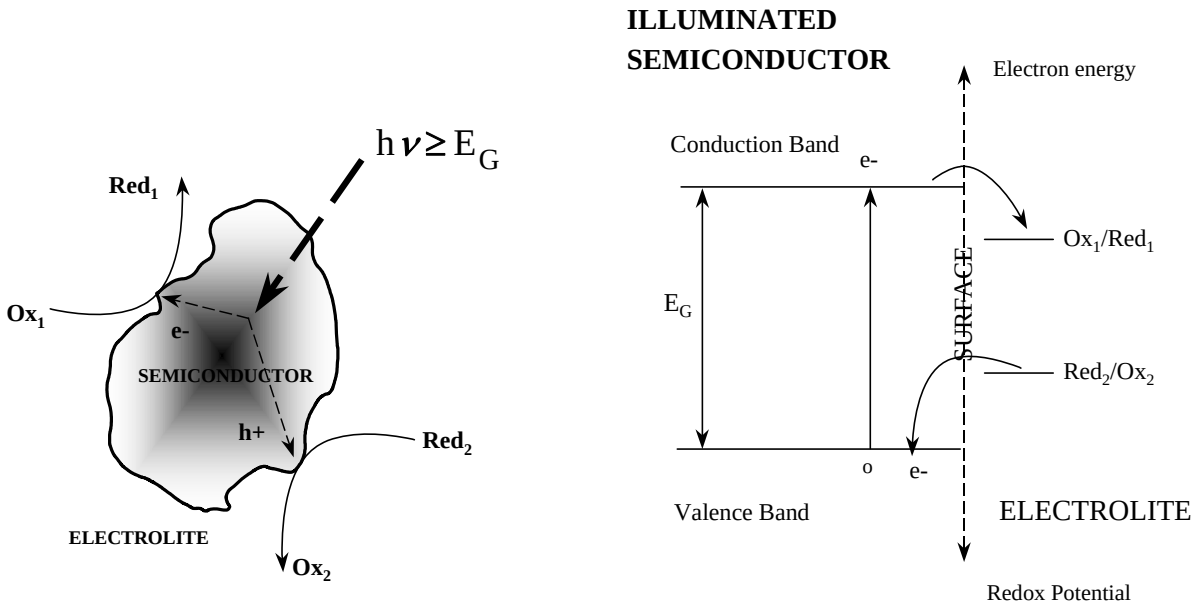

Figure 1.1 *Effect of the radiation on a semiconductor material*

1.1.3. Brief description of the mechanism

To date, evidence supports the idea that the hydroxyl radical ($^{\bullet}OH$) is the main oxidizing specimen responsible for photooxidation of the majority of the organic compounds studied, although the controversy on the importance of the role played in the process by the holes produced in the valence band remains open [*Pelizzetti, 1995a; Serpone, 1994a, 1995a; Spacek et al., 1995; Terzian et al, 1991*].

Serpone et al. [*1993a*] have compiled what has been proposed up to now on the formation of these radicals, as well as other reactions that may take place during the TiO_2 photocatalytic process. The first effect, after absorption of the radiation (near ultraviolet, $\lambda < 387$ nm), is the generation of electron/ hole pairs which are separated between the conduction and valence bands (Eq. 1.1). Both migrate quickly toward the surface [*Bahnemann et al., 1993a*] where h^+ is trapped by surface energy traps (Ti^{IV}-O^{2-}-Ti^{IV}) and e^- by surface traps (-Ti^{IV}-, Eqs. 1.3 and 1.4) [*Howe et al., 1987*], or by external traps through electron donors ($Red_{2,ads}$) and electron acceptors ($Ox_{1,ads}$) respectively (Eqs. 1.5 and 1.6).

In order to avoid recombination of the pairs generated (Eq. 1.2), Red_2 and Ox_1 have to have been previously adsorbed on the surface, before the catalyst excited by the light. If the dissolvent is oxidoreductively active (water) it also acts as a donor and acceptor of electrons. Thus, for a hydrated and hydroxylated TiO_2 surface, the holes trapped $^{\bullet}OH^-$ radicals linked to the surface (Eqs. 1.7 and 1.8). In any case, it should be emphasized that even trapped electrons and holes can rapidly recombine on the surface of a particle (Eq. 1.2). This can be

partially avoided through the capture of the electron by preadsorbed molecular oxygen, forming a superoxide radical (Eq. 1.9).

$$TiO_2 \xrightarrow{h\nu} e^- + h^+ + TiO_2 \quad (1.1)$$

$$e^- + h^+ + TiO_2 \longrightarrow TiO_2 + calor\ y/o\ h\nu' \quad (1.2)$$

$$(TiO^{IV}\text{–}O^{2-}\text{–}Ti^{IV})_{subsuperficie} + h^+_{BV} \longrightarrow (TiO^{IV}\text{–}O^{\bullet -}\text{–}Ti^{IV})_{subsuperficie} \quad (1.3)$$

$$(-Ti^{IV}-)_{superficie} + e^-_{BC} \longrightarrow (-Ti^{III}-)_{superficie} \quad (1.4)$$

$$h^+_{BV} + Red_{2,ads} \longrightarrow Ox_{2,ads} \quad (1.5)$$

$$e^-_{BC} + Ox_{1,ads} \longrightarrow Red_{1,ads} \quad (1.6)$$

$$(TiO^{IV}\text{–}O^{2-}\text{–}Ti^{IV})\text{–}OH^- + h^+_{BV} \longleftrightarrow (TiO^{IV}\text{–}O^{2-}\text{–}Ti^{IV})\text{–}OH^{\bullet} \quad (1,7)$$

$$(TiO^{IV}\text{–}O^{2-}\text{–}Ti^{IV})\text{–}OH_2 + h^+_{BV} \longleftrightarrow (TiO^{IV}\text{–}O^{2-}\text{–}Ti^{IV})\text{–}OH^{\bullet} + \quad (1.8)$$

$$O_{2(ads)} + e^-_{BC} \longrightarrow O^{-\bullet}_{2(ads)} \quad (1.9)$$

Whatever the formation pathway, it is well known that O_2 and water are essential for photooxidation with TiO_2. There is no degradation in the absence of either. Furthermore, the oxidative species formed (in particular the hydroxyl radicals) react with the majority of organic substances. The e^-/h^+ pairs are also able to cause reductive processes (e.g. $Cr^{6+} \rightarrow Cr^{3+}$), although the mechanisms would be different [*Curcó, 1994; Giménez et al., 1992a, 1994*].

In aromatic compounds, the aromatic part is hydroxylated (Fig. 1.2) and successive steps in oxidation/addition lead to ring opening. The resulting aldehydes and carboxylic acids are decarboxylated and finally produce CO_2. *Serpone et al.* [1*993a*] explain, with a drawing similar to the one shown in Figure 1.2, the main steps of this process using phenol as an example. Two different places can be identified on the surface of illuminated TiO_2 particles, reticular Ti^{III} and surface Ti^{IV}-OH^-. The compounds are adsorbed in surface hydroxyls, but the oxygen makes it in Ti^{III} forming $O_2^{\bullet -}$. The $^{\bullet}OH$ radicals are formed in surface Ti^{IV}-OH^- and can be spread in solution for reaction with the substrate, although this last affirmation originates controversies in the scientific community. *Pelizzetti and Minero* [*1993d, 1994a*] have concluded that the oxidative species generated do not migrate far from the catalyst surface and that the process of degradation must occur on the surface, or a few atoms away from it. In any case, the photodecomposition of phenol and many other organic substances takes place between the two specimens ($^{\bullet}OH$ and substrate) and begins with the displacement of a group of surface OH^- by a phenol molecule. In continuation the photogenerated e^- and h^+ are trapped in the surface entity Ti^{III} (e^-_{at}) and the subsurface Ti^{IV}-O-Ti^{IV} (h^+_{at}), process which competes with e^-/h^+ recombination. The molecular oxygen adsorbed captures the electrons yielding $O_2^{-\bullet}$, avoiding this recombination and generating in acid medium $HO_2^{\bullet}$. The h^+_{at} can

directly oxidize adsorbed phenoxide yielding phenoxyl radicals (pathway a) or oxidize the surface Ti-OH$^-$ groups giving rise to an $^{\bullet}$OH radical (pathway b) that can produce the phenoxy, dihydroxycyclohexadienyl or semiquinone radicals.

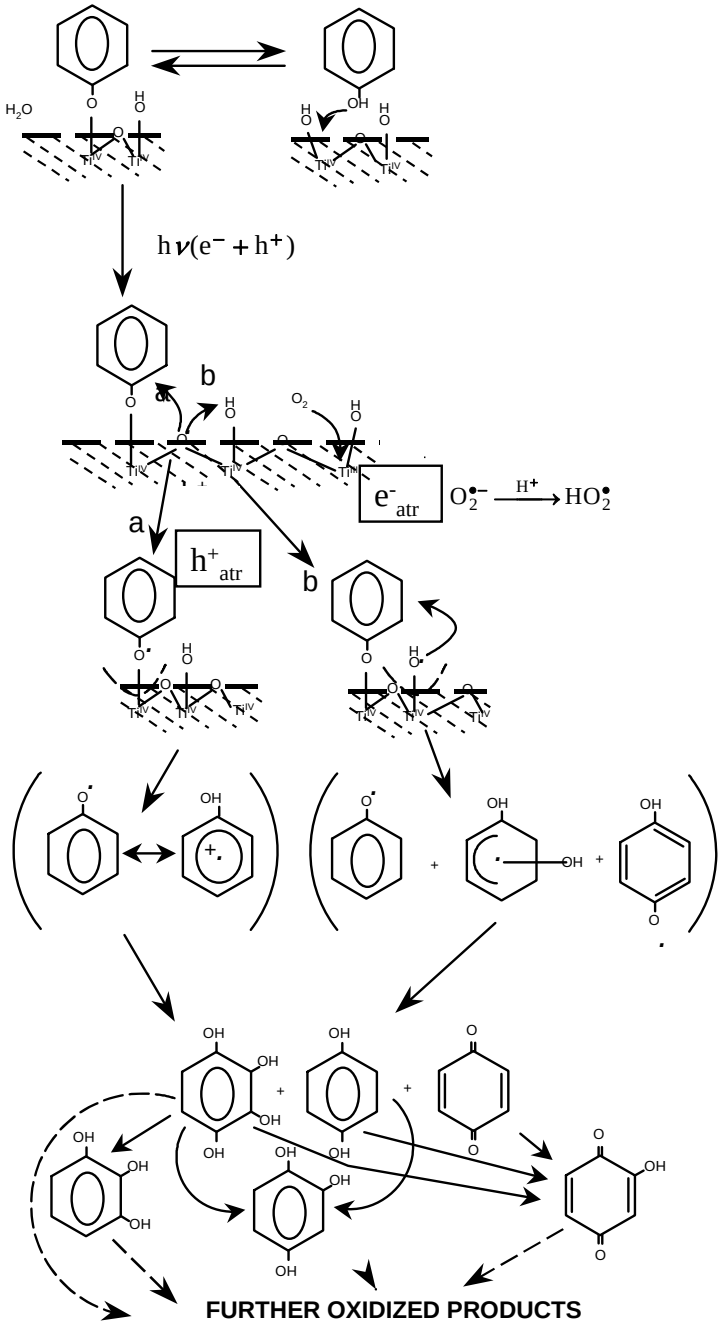

Figure 1.2 *Most important photocatalytic degradation steps of phenol.*

The data available to date [*Pelizzetti 1993c, 1995a; Serpone et al., 1993a*] suggest that all this occurs on the surface, but nothing is known about the point where the subsequent reactions

take place. The continuous oxidation of these intermediates terminates with complete mineralization, producing CO_2.

1.2 Application of the process to the decontamination of water

It should be noted that the microbial purification of water polluted by organic micropollutants at low concentrations (mg/L) is of extreme difficulty, as biodegradation, which is a major mechanism in wastewater treatment, is quite inefficient at low levels of substrate [*Muszkat et al., 1995*]. Something similar occurs when these compounds are very toxic, and the microorganisms need an extended period of adaptation, when they are not completely inviable. In recent years, research in new non-biological methods of water purification has led to processes that actually destroy the pollutant instead of simply changing its phase (adsorption by active carbon, air-striping, etc.). Therefore, the degradation of organic pollutants present in waste water using irradiated TiO_2 suspensions is a very promising process and R&D in this field has grown very quickly during the last years. Since *Carey et al.* [*1976*] published their results, about TiO_2-photocatalytic destruction of PCBs, many applications using the TiO_2/UV process, have been investigated. A recent study by *Blake* [*1994, 1995*] compiled up to 1200 references on the photocatalytic destruction of compounds in water and air, in which are included 117 products considered highly toxic. The most important features of this process making it applicable to the treatment of contaminated aqueous effluents are:

- The process takes place at ambient temperature
- The oxidation of the substances into CO_2 is complete
- The oxygen necessary for the reaction is obtained from the atmosphere.
- The catalyst is cheap, innocuous and can be reused.
- The catalyst can be attached to different types of inert matrices.
- The source of energy for the process is inexpensive and renewable, the Sun.

1.2.1. Development and state of the art

Since 1976 research on the subject has gradually increased, and is now in a period of total expansion, as shown in Figure 1.3, with new research groups in the field constantly appearing. The publications referred to in the following graphs (Figures 1.3, 1.4 and 1.5) were collected by *Blake* [*1994, 1995*] and there are probably more. In any case, the importance that photocatalysis has acquired for water purification is clear. In annual compilations, although articles on gas phase photocatalysis are also included, there is much less research being done on it, however it has acquired greater importance in recent years.

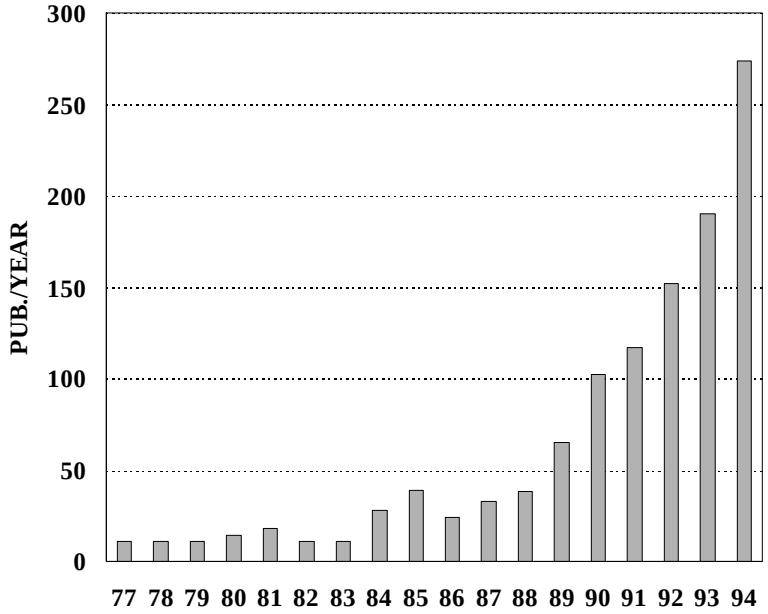

Figure 1.3 *Yearly distribution of the references reviewed by Blake [1994, 1995].*

In Figure 1.4, these publications, including no articles on experiments with different compounds in aqueous suspensions of TiO_2 but only those on advances that might improve process efficiency and recent bibliographic reviews, are distributed by subject matter. The most published aspects are:

(I) Modification of the catalyst (TiO_2) by doping or metallization, the use of dye sensitizers or treatment of the catalyst itself with processes that modify its properties.
(II) Immobilization of the catalyst on a support, avoiding the need to separate it from treated water after use.
(III) Use of other oxidants, besides O_2, which improve process rate.
(IV) Design of industrial reactors and systems that use this technology, as well as economic comparisons with other alternative processes.
(V) Alternative catalysts to TiO_2.

As seen in Figure 1.4, attempts to optimize the process have been mostly in the catalyst where surface characteristics as well semiconductor activity have been improved, making it sensitive to longer wavelengths and allowing lower-cost radiation to be used (e.g., sunlight) for its activation. On the other hand, it seems that there has not been much success in the search for alternative catalysts, either because they are not as active or because of their high cost. Research on catalyst immobilization on an inert support has received special attention in recent years (over 75% of the references after 1990). This has also been felt, as commented later, in international congresses on the subject.

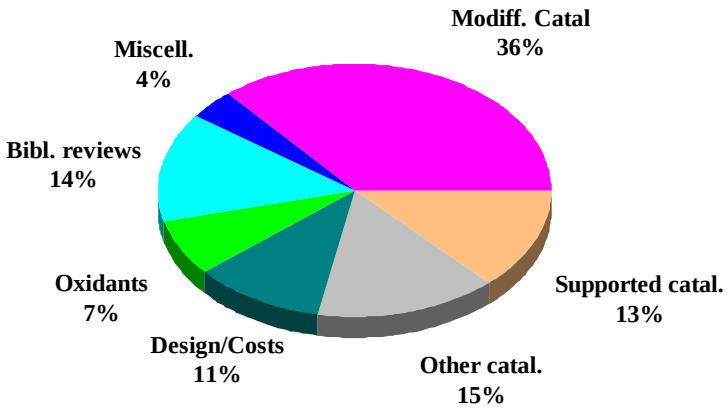

Figure 1.4 *Distribution by matters of all the references included in Figure 1.3.*

A search for substances that aid in oxidation and thereby improve process performance has also been pursued by many research teams, but it seems that no versatile product useful for all applications has yet been found. The incidence of industrial facility design studies and their cost would imply that this is an attractive process and its application to real problems is not very far in the future.

Hundreds of compounds have been the subject of degradation experiments with this technique. Water is the medium preferred, since organic and inorganic pollutants in ground water, rivers, lakes and even, at already detectable levels, in the sea, are a severe problem. Photocatalysis with TiO_2 has been demonstrated in over 30% of the compounds considered priority pollutants. A dearth of useful information has been generated, not only on the processes themselves, but on the environmental behavior of the pollutant. In addition, other compounds not considered dangerous at this time, but which may become so in the future have also been investigated. The technique has also been used in the treatment of toxic inorganic compounds (heavy metals, cyanide….) and even in the recovery of noble metals. Figure 1.5 summarizes these applications, as well as their relative importance.

Photocatalysis as a method of decontamination has acquired such relevancy that there have been several congresses on the subject [*Ollis, 1993; Al-Ekabi, 1994; Vogelpohl, 1996*]. Those aspects that have not yet been solved, those which have been and those which do not merit the attention given them in the beginning could also be identified.

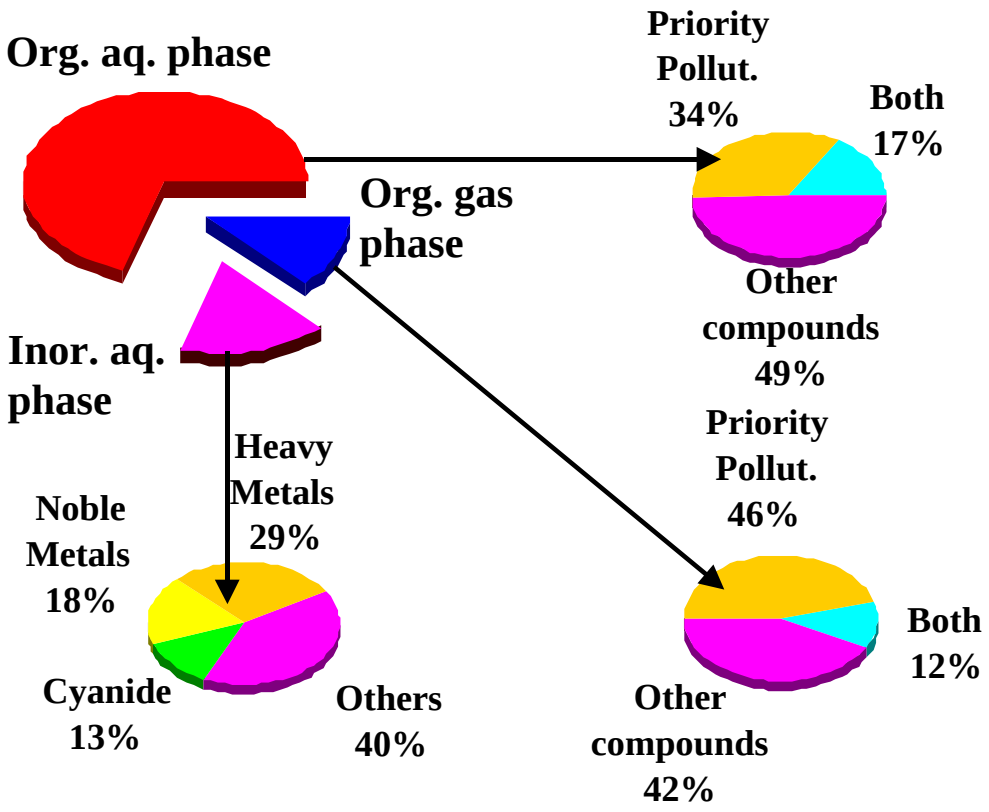

Figure 1.5 *Distribution by substances of the references included in Figure 1.3. Priority pollutants are the compounds included in the EPA lists [1988].*

1.2.2. Applications with artificial light. Photoreactors

The treatment of contaminated water necessarily includes the design of an efficient photoreactor. Basic laboratory research on the process has mostly been performed with experimental devices in which efficiency was not as important as obtaining appropriate conditions that would permit reproducibility of the results and exhaustive knowledge of the effects of all the important parameters. This is correct when the goal is a fundamental knowledge of the process, but not always sufficient to attempt a change of scale. Therefore, more work on several different aspects, such as the design of photoreactors for heterogeneous photocatalysis is still required.

The main factors to be optimized in these reactors are the energetic utilization of the radiation and the availability of the catalyst. As far as the energetic performance is concerned, the designs that place the source of energy (usually a UV lamp) in the center of an annular reactor have had the best results, and in fact commercial prototypes such as that patented by Nulite [*Al-Ekabi et al., 1991*], are based on this principle. The availability of the catalyst within the reactor, as well as the type of inert support used, if not in suspension, is still under

development, and no decision has yet been made as to which of the many proposals is the best [*Gao et al., 1992*].

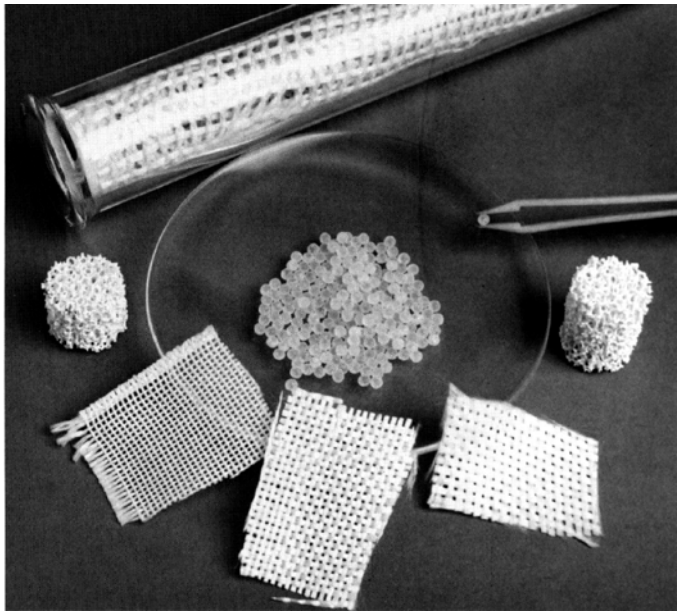

Figure 1.6 *Different possibilities for fixing the TiO_2 on inert materials.*

In Figure 1.6 [*SERI, 1991*], different types of catalyst fixation on porous and inert supports are shown. Glass (either on balls or by direct catalyst deposit on the surface of the tube through which the water circulates), as well as several ceramics, polymers and even some metals have been used for this. Supports may be nets, reticular, etc. The clear advantages of working with a fixed catalyst instead of a suspension are: it does not need to be separated from the water after treatment, to be recovered under optimum conditions that enable its reuse and to be resuspended as a prior step in the process. The different types of catalyst support inside the reactor are shown in Figure 1.7. The disadvantages of using such supports are:

- Decrease in activated TiO_2 surface in a specific reactor volume compared to the catalyst in suspension in the same volume [*Fox et al., 1994a*].
- Limitations in mass transfer at low flow rates [*Al-Ekabi et al., 1988, 1991; Barni et al., 1995a; Bellobono et al., 1995; Matthews, 1987a, 1987c, 1992; Ollis et al., 1991a*]. This effect is more intense when illumination is increased, since a good part of it cannot be used. When this occurs, the reaction rate does not increase with increased photon flow.
- Difficulties in obtaining correct illumination when the source of photons is not inside the reactor. This is a especially a problem for solar radiation.
- Increase in reactor pressure drop [*Pacheco et al., 1990c*]. The consequence is an increase in the cost of energy and capital since more powerful pumping systems have to be installed.

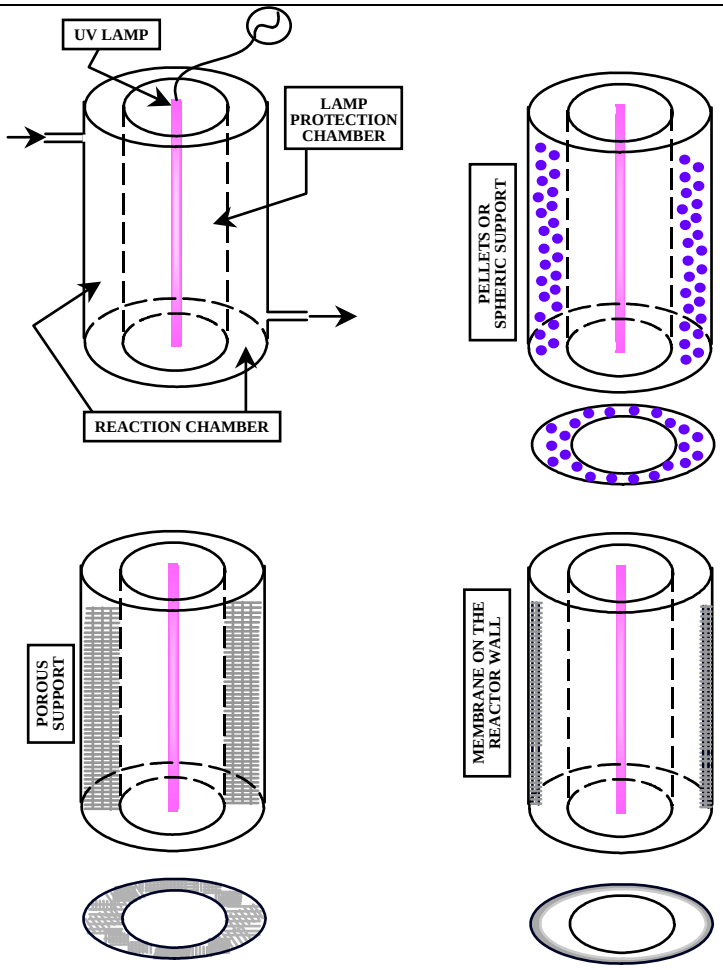

Figure 1.7 *Different types of catalyst support inside an annular photoreactor.*

1.3 Environmental problems caused by pentachlorophenol

Pentachlorophenol (PCP, CAS n° 87-86-5) was introduced in the thirties as a preservative of cut wood. It is also used in a great variety of industrial and agricultural applications (fungicide, bactericide, algaecide, herbicide, insecticide, etc.). Although its use has been diminishing progressively, production until up to a few years ago was in the tens of thousands of tons per year [*Kennes et al., 1991*]. It can presently be found on the market, under various trade names, among others: Penta®, Santophen®, PCP®, Penchlorol®, Dowicide 7®, Chlorphen® and Sontox®. It is useful because of its toxicity to harmful microorganisms, plants and invertebrates found on products that need to be preserved, but obviously, it is also harmful for man and the environment in general. It can be absorbed through the skin, it is corrosive, causes burns and blisters, and is very irritive in the respiratory tract (TLV 0.5 mg/m^3). In mammals a high level of exposure can cause fever, panting, hypertension, hyperglycemia and cardiovascular problems. It may be considered highly toxic (LD_{50} = 50

mg kg^{-1}). It is advisable to take extreme measures of precaution with this type of compound, since those over $LD_{50} \leq 50$ are considered especially harmful to the health [*ChemService, 1992*].

Residues of PCP are detected in man as much as in the environment that has been in contact with PCP. In spite of its low volatility, in exposed atmospheres (wood treatment plants) up to 2 $\mu g/m^3$ have been detected and in the air of industrial cities 6-7 ng/m^3 [*Crosby, 1981*]. In water it has reached very high levels (25-150 mg/L) in wood industry effluents and it is normally found in measurable amounts (0.1-0.7 μg/L) in human drinking water. It has also been confirmed that it joins trophic chains when any of their lower links are contaminated [*Kratz, 1989*]. In some studies [*Crosby, 1981*], it has been detected in 80% of human urine analysis samples. It is also known that PCP is toxic for many of the bacteria used in the biological waste water treatment [*Mäkinen et al., 1993; Manilal et al., 1992*] and therefore, may impede the correct functioning of these processes. Its degradation with certain types of bacteria has been demonstrated possible [*Froilán, 990; Jacobvsen et al., 1989; Kennes et al., 1994; Mäkinen et al., 1993; Suzuki et al., 1977; Valo et al., 1989*], but it always takes a relatively long time, hours or even days, to adapt the bacteria and, in any case, treatment capacity is low (0.7 mg $L^{-1}h^{-1}$ [*Froilán, 1990*]).

For all of these reasons, the production, transport and use of pentachlorophenol is subject to strict regulations *[Council Directive 91/173/CEC, DO n° L85, April 5, 1991, pg. 34*]. In Spain in particular, maximum dumping in waste waters must not be over 1 mg/l [*BOE, November 23, 1987, pg. 34793*]. The environmental danger of this compound is such that the CEE is considering its total prohibition *[Official Diary of the European Communities, November 12, 1994*].

2. SOLAR RADIATION

2.1 Introduction

The approach of solar radiation in general and its ultraviolet component in particular, is consider of interest being the existence of an ultraviolet radiation source the key of any heterogeneous photocatalytic process by means of TiO_2.

All the energy coming from that huge reactor the Sun, from which the earth receives $1.7x10^{14}$kW, means $1.5x10^{18}$ kWh per year, approximately 28000 times the consumption of all the world in that period. The radiation in the exterior of the atmosphere has a wavelength between 0.2μm and 50μm, which is reduced in an interval between 0.3 μm and 3 μm when reaching the surface, due to the absorption of part of it by different atmospheric components (ozone, oxygen, carbon dioxide, aerosols, steam, clouds). The solar radiation that reaches the ground level without being absorbed or scattered, is called direct radiation; the radiation which has been dispersed but reaches the ground level is called diffuse radiation and the addition of both is called global radiation. In general, the direct component of global radiation in cloudy days is minimum and the diffuse component is maximum, producing the opposite situation in clear days.

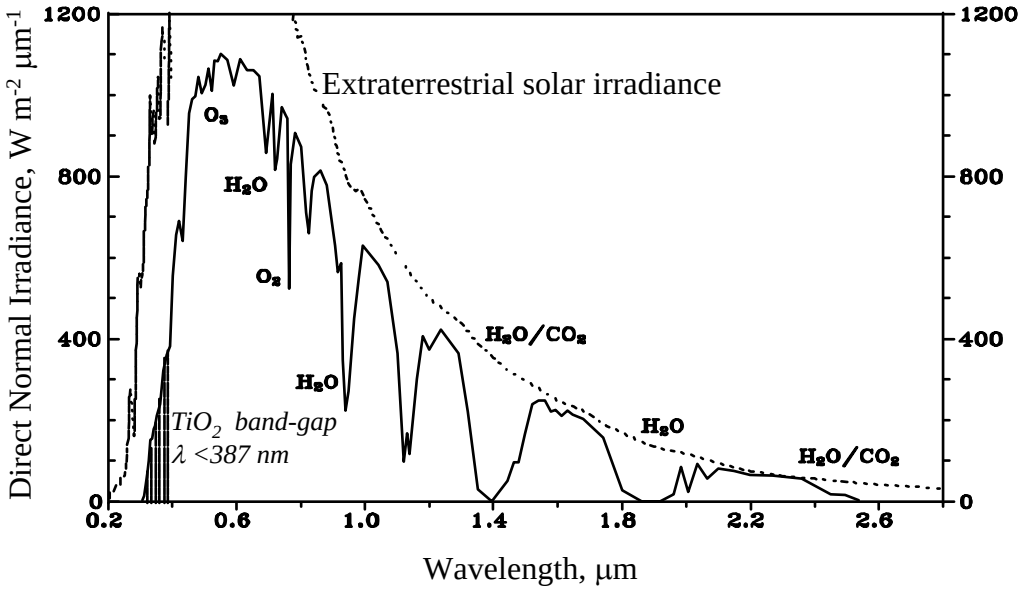

Figure 2.1. *Effect of atmospheric components on Solar spectrum*

Figure 2.1 shows the standard spectrum ASTM [*1987a*] of the direct solar radiation on the ground level on a clear day, reflecting the substances which absorb part of the radiation and

their absorption wavelength [*Iqbal, 1983*]. The dotted line corresponds to the extraterrestrial radiation in the same interval of wavelength. It is clearly seen the scarce part of the solar spectrum that can be used in the photocatalytic process with TiO_2 but, as the energy source is so cheap and abundant, even under these limitations it is interesting to use it [*Wilkins et al., 1994*].

2.2 Quantum Yield and UV Solar Radiation

Solar radiation is, as explained above, a very small part of the solar spectrum. The measurements carried out have demonstrated that the UV part of the solar spectrum represents between 3.5% and 8% of the total [*Riordan et al., 1990*], although this relation can change for a determined location between cloudy and clear days. The percentage of global UV radiation (direct + diffuse), with regard to total global, generally increases when the atmospheric transmisivity decreases, due mainly to clouds, but also to aerosols and dust [*Mehos et al., 1992a*]. In fact, the average percentage relation between UV and total radiation in cloudy days is up to two units (W m^{-2}) over the values in clear days. This means that the photocatalytic process has an acceptable efficiency even with clouds.

The efficiency of a chemical reaction is calculated from the relation between the products and the departing reactants. In photochemistry, it is very common to use the quantum yield concept, which is calculated knowing the photons absorbed in the reaction. Quantum yield (Φ) is defined as the relationship between, the number of reacting molecules (Δn) and the quantity of photons absorbed by the system (N_a):

$$\Phi = \frac{\Delta n}{N_a} \tag{2.1}$$

It can also be written in differential form:

$$\Phi = \frac{dn/dt}{P_a} \tag{2.2}$$

where dn/dt is the number of reacting molecules per unit of time and P_a is the number of absorbed photons during the same period. Experimentally, the quantum yield is expressed as the number of reactant moles in an interval of time t, divided into the number of moles of absorbed photons (Einstein) in the same period. The knowledge of the quantum yield is very important to understand the mechanism of the photochemical reactions. If every absorbed photon produces a molecular transformation, $\Phi = 1$. If it is smaller than 1, it means that there exist deactivation processes or other reactions competing with the studied one. If it is bigger than 1, indicates a sequence of reactions, which promoter has been excited by a photon. In the present case, photocatalysis by UV radiation, the number of photons that will reach the

reacting mixture and, so, will be susceptible to be absorbed, will be in relation with the UV solar spectrum (Fig. 2.2).

The two spectra shown in Fig. 2.2 correspond to the standard ASTM [*1987a*] for the UV range of the solar spectrum. The smaller of them refers to direct UV (radiation without scattering) and its value reaches 22 W m^{-2} between 300 and 400 nm, the bigger corresponds to the global UV (direct + diffuse) and its value is 46 W m^{-2}.

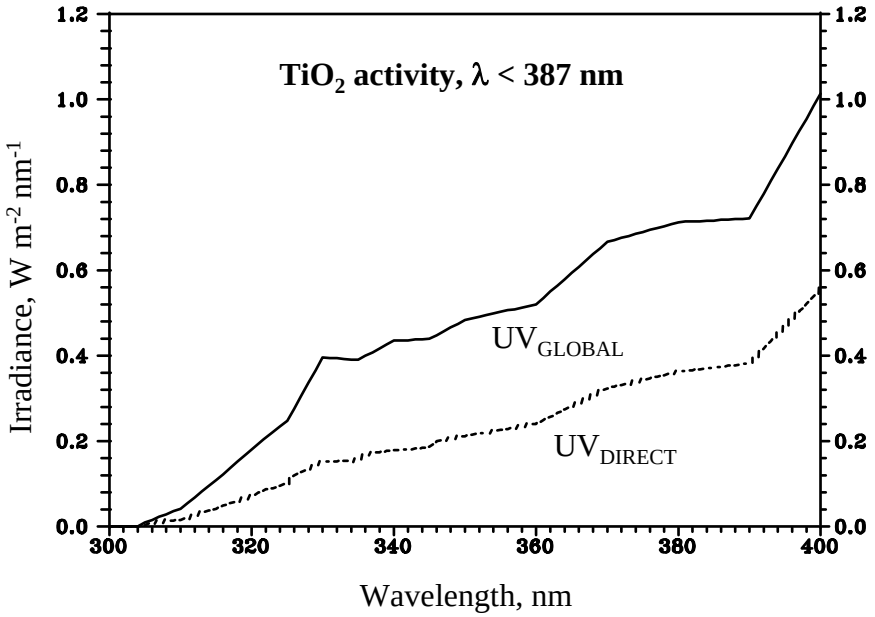

Figure 2.2. *Ultraviolet spectra on the earth surface (standard ASTM)*

The number of photons, N_λ, supplied by a monochromatic source of light of wavelength λ and energy Q_λ is related with the energy of one photon, W_λ, by Planck's equation:

$$W_\lambda = \frac{hc}{\lambda} \tag{2.3}$$

where h is Plank's constant and c the speed of the light, so:

$$N_\lambda = \frac{Q_\lambda}{W_\lambda} = Q_\lambda \frac{\lambda}{hc} \tag{2.4}$$

When the light source is polychromatic, as the solar radiation, the number of photons is given by an integral covering the whole range of wavelengths of that source:

$$N = \int_{\lambda_1}^{\lambda_2} N(\lambda) d\lambda = \frac{1}{hc} \int_{\lambda_1}^{\lambda_2} Q(\lambda) \lambda d\lambda \tag{2.5}$$

This expression gives the relation between photonic and radiometric quantities, defining from here the photon flux density I [Einstein s^{-1} m^{-2}], as the number of incident photons per unit of surface and time:

$$I = \frac{d^2 N}{N_0 \, dt \, dA} \tag{2.6}$$

where N_0 is Avogadro's number (6.023×10^{23}).

Using the spectrum data and the former equations in congruent units [S.I], it is possible to determine the photon flux density I ($I_{DIR} = 6 \times 10^{-5}$ Einstein m^{-2} s^{-1}, $I_{GL} = 14 \times 10^{-5}$ Einstein m^{-2} s^{-1}). These two values give an idea of the energy coming from the sun and available for photocatalytic reactions by TiO_2, which activity up to 387 nm only allows to use part of this UV spectrum, as it will be explained bellow. In any case, the described UV radiation values vary from one location to another, and obviously, during the day and between different seasons, for which it will be necessary to know these data in each location and in real time, although the first approach will be very useful in those cases where the latter is not possible. The corresponding spectra and radiometric measurements used in this report have been collected in the same location where the photocatalytic tests have been carried out, so the efficiency data are as real as they can be, as it will be seen further along.

2.3 Solar Collectors

Traditionally, the different solar collector systems have been classified depending on the concentration level attained with them (relation between the collecting surface and the surface where the final result is produced), which is directly related with the system working temperature. According to this criteria, there are three type of collectors:

I. No concentration or low temperature, up to 150º C
II. Medium concentration or medium temperature, from 150º C to 400º C
III. High concentration and high temperature, over 400º C.

This classification is done from a traditional point of view, considering only the thermal efficiency of the solar collectors. However, the important in photocatalysis is not only the amount of radiation collected, but its wavelength.

Non concentrating solar collectors (Fig. 2.3) are static, without any solar tracking device. They are usually a flat plate, in many cases aiming to the sun with a determined tilt, depending on the geographic situation. Their main advantage is the reduced cost and, for

many applications, the collected radiation is sufficient.

Medium concentration solar collectors concentrate the sunlight between 5 and 50 times. Parabolic Trough Collectors (PTC) and collectors with Fresnel lenses are within this group. The first ones have a parabolic reflecting surface (Fig. 2.4) which concentrates the radiation on a tubular receiver located in the focus of the parabola. They can be of one axis tracking, either azimuth (East-West movement around one axis North-South oriented) or elevation (North-South movement around one axis East-West oriented), or two tracking axis (azimuth + elevation). The Fresnel lenses collectors consist of refracting surfaces (similar to convex lenses) which deviate the radiation at the same time that they concentrate it into a focus.

High concentration collectors have a focal point instead of a linear one and are based on a paraboloid with solar tracking. Parabolic dishes and solar furnaces are among them.

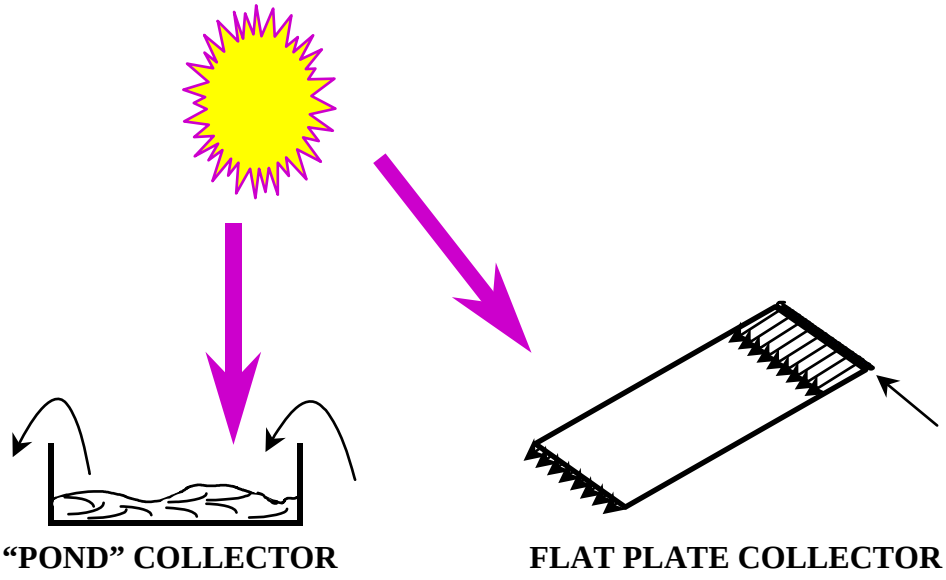

Figure 2.3. *Non-concentrating solar collectors.*

Up to now the solar collectors used for photocatalysis correspond to the two first categories. Within the non-concentrating ones must be mentioned:

a) Quartz tubes with TiO_2 suspension in the interior and exposed to the sun [*Ahmed et al., 1984*].
b) A flat glass plate, with a catalyst attached to the surface on which the liquid to be treated circulates [*Bahnemann et al., 1994a; Bockelmann et al., 1992, 1995*].
c) Another one very similar to the former, consisting in two plates between which water circulates using a separating walls. It is filled in with fibre with the catalyst attached.

[*Sullivan et al., 1994*].

d) Different types of small collectors [*Pacheco et al., 1993*] with many small tubes connected in parallel to make circulate the flow faster, but the functioning mode is basically like that in a flat plate.

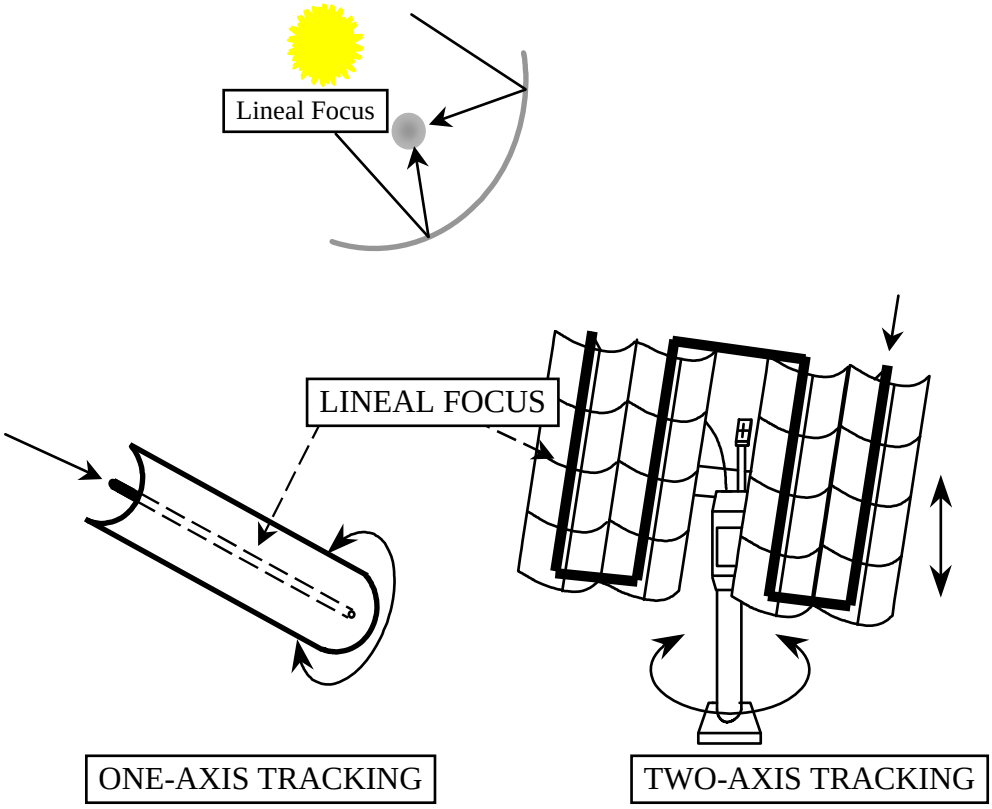

Figure 2.4. *Medium concentrating solar collectors. PTC type.*

Among the medium concentration collectors have been tested:

a) CPC collectors (compound parabolic collectors) with concentration ratio approximately 1[*Pacheco et al., 1993; Malato et al., 1996a, 1996b*]
b) One-axis parabolic trough [*Pacheco et al., 1990b, 1991; Anderson et al., 1991*].
c) Two-axis parabolic trough [*Minero et al., 1993, 1996a, 199b*].

From all of them, the two last ones correspond to pilot plants of considerable dimensions (hundreds of square meters of collecting surface) and have been the first step towards the industrialisation of the photocatalytic process. The rest are prototypes with different sizes but never more than a few square meters, with the problems to extrapolate the results that this implies. The present work has been carried out at pilot plant scale, with a photocatalytic reactor based on twelve two-axis PTCs (32 m^2 reflective surface per collector).

The utilisation of collectors of type I and II has been based on experiences at laboratory scale carried out by different researching groups [*Al-Sayyed et al., 1991; Blake et al., 1991; Egerton et al., 1979, Okamoto et al., 1985a; Ollis, 1991b; Trillas et al., 1994*]. During these experiences, they have detected that the ratio between the photocatalytic reaction rate and the intensity of radiation coming inside the reactor changes with the radiation power (see Figure 2.5). This modification does not seem to happen at a determined radiation intensity, as different researchers obtain different results. It is presumable that the experimental conditions affect significantly as it will be seen further along. However, in all the cases the graphics are very similar when representing the reaction rate as function of the amount of incident photons (Figure 2.5).

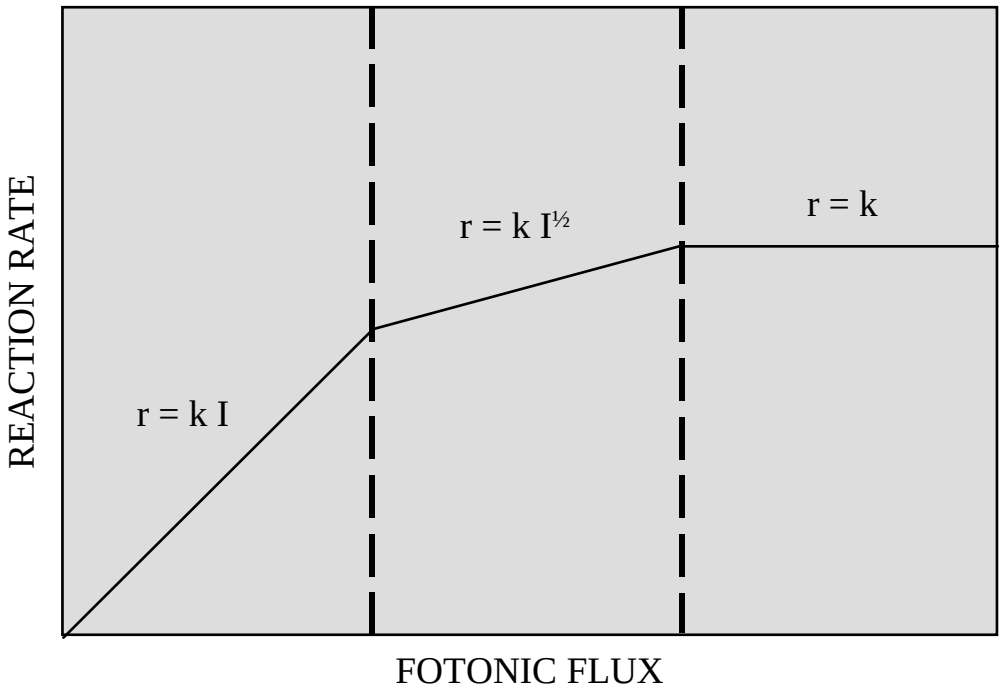

Figure 2.5. *Relation between the photocatalytic reaction rate and the intensity of the radiation received.*

Some authors [*Egerton et al., 1979; Kormann et al., 1991; Turchi et al., 1990a*] impute the transition of $r = f(I^{1.0})$ to $r = f(I^{0.5})$, to the excess of photogenerated species (e^-, h^+ and $^\bullet OH$). In chapter 6.5 of this report, devoted to the influence of radiation intensity over the reaction rate, all these will be treated in detail. At higher radiation intensities, another transition from $r = f(I^{0.5})$ to $r = f(I^0)$ is produced. At this moment, the photocatalytic reaction leaves its dependence on the received radiation, to depend only on the mass transfer within the reaction. So, the rate is constant although the radiation increases. This effect can own to different causes, as can be the lack of electrons scavengers (i.e. O_2), or organic molecules in the proximity of TiO_2 surface and/or excess of products occupying active centres of the catalyst,

etc. Really, this phenomena appears more frequently when working with supported catalyst, and/or at low agitation level. This implies low catalyst surface in contact with the liquid and smaller turbulence. This does not favour the contact of reactants with the catalyst and the diffusion of products, from the proximity of the catalyst to the liquid.

From all the above explained, the question is if to concentrate the radiation is really necessary for the photocatalysis technology and if a non-concentrating collector can be as efficient as a PTC. Initially it was thought that the last ones were the ideal alternative and in fact, the existing large pilot plants operate with them [*Pacheco et al., 1990b Alpert et al., 1991; Borthen et al., 1992; Minero et al., 1993;*]. However, their high cost and the fact that they can only operate with direct solar radiation (this implies their location in highly insolated areas) lead to consider the alternative of static non-concentrating collectors, which is currently under study.

Pacheco et al. [*1993*] have performed a comparative efficiency study, with seven different collectors, using photocatalytic trichloroethylene decomposition. All of them are of small dimensions (from 18 to 157 litres total capacity and from 0.4 m^2 to 53 m^2 reflecting surface) and some of them with the catalyst (TiO_2) fixed on to an inert matrix. Collectors with concentration ratio one (non-concentrating) gave better results, mainly when used with the catalyst in suspension. Therefore, the description given in the mentioned work, on the procedure followed to compare the results obtained with the different collectors, does not clarify if a very important consideration, the relation between reactors dead volume (without radiation) and useful volume of each photoreactor, has been taken into account. This relation depends on the way each one has been constructed (dimensions of the interconnection pipes between collectors, volume of the tanks employed for water recirculation, etc.) and can give rise to errors, with regard to the solar efficiency of the collector itself, if it is intended to give only an idea of the behaviour with regard to the radiation received. Also, the concentration ratio used in the parabolic trough collectors tested is rather high (about 20), which can be self-defeating if we consider the above mentioned, about the reaction rate (r) and the radiation intensity (I), according to Figure 2.5. The parabolic trough collectors employed in the cited work are “one-axis” type (Figure 2.4), which radiation efficiency is smaller than in the “two-axis” collectors used in this work.

Although for thermal applications of solar energy it has been demonstrated that the most (economically) suitable are those of one-axis tracking, this is not necessary for photocatalysis. In any case, the utilisation of PTCs with two-axis tracking has proven very efficient to know exactly the radiation that reaches the photoreactor at any time, as it will be explained below, also permitting to evaluate correctly all the other parameters related with the solar photocatalysis process. This accuracy has permitted to compare the experiences carried out in

this photoreactor with photoreactors at lab scale, where the calculation of incident radiation is a lot easier. It has also been possible to reduce the variables to tests, using the knowledge developed by other authors.

Figure 2.6 shows a comparative analysis of three types of collectors with regard to the incident direct radiation. It has been performed with the total radiation, because in the PSA there are a lot more of this data available than ultraviolet radiation data, assuming that the results are going to be identical. Data represented in Figure 2.6 [*Zarza, 1989*], correspond to the direct radiation in a typical sunny day (four years average) along the year. Direct radiation is the radiation that can be concentrated and consequently useful for parabolic-trough collectors. The total real value, in each case, will be reduced by the presence of clouds, but as the consequence would be the same for every one of them, this effect has been ignored. The curves in Figure 2.6 show the available energy (from the direct radiation) on the aperture plane of the three types of collectors (see Figures 2.3 and 2.4).

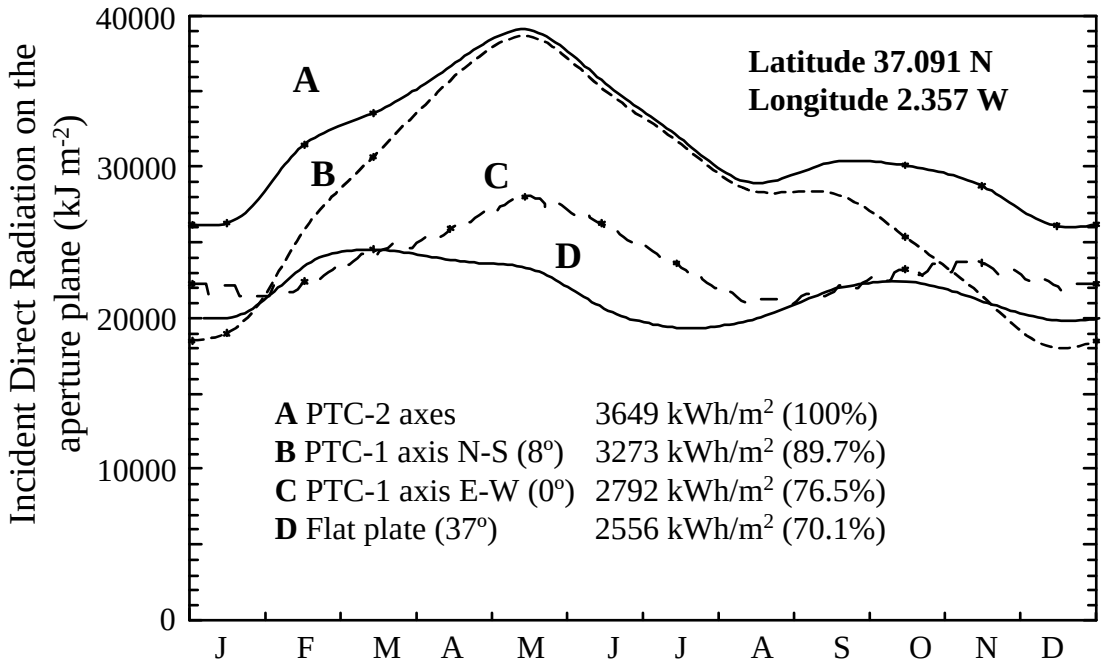

Figure 2.6. *Efficiency of solar collectors: PTC-one axis (two different dispositions), PTC-two axis and flat plate 37º tilted.*

The PTCs-one axis are in horizontal position (only elevation movement) and two different orientations: azimuth or 8 degrees elevation with regard to the horizontal. The calculations performed are only geometric and based in the incident angle, being this angle the one formed by the solar ray with the normal line to the aperture plane of the collector. These calculations

allow to know the amount of efficient direct radiation of each one available at any time, being the PTC-two axis the only one which can reach 100% efficiency [*Saltiel et al., 1992*]. In the PTC-one axis it is only possible to use a portion of the direct solar radiation. This introduces different efficiencies along the year with regard to PTC-two axis. Nevertheless, the consideration of other technical aspects can make that the most suitable collectors not always are the most efficient from the point of view of power collection. In fact, in the case of flat collectors, the diffuse radiation must be considered, which would be very important in cloudy conditions and could increased considerably the annual efficiency of this type of collectors.

2.4 Peculiarities of a solar collector to make use of UV radiation

This thesis is based on the utilisation of parabolic-through collectors for photocatalytic treatment of water contaminants, so this section will deal with them. Any way, the following is applicable to other type of collectors (including those that do not concentrate solar radiation), with certain peculiarities in every case. These peculiarities will depend on the type of reflecting surface to be used, or if this one is necessary or not (non concentrating collectors) and in the way the water circulates through them (tube, falling film or stirred vessel). The main characteristics which can make a non concentrating collector more efficient, with regard to PTC, is that also uses ultraviolet diffuse radiation. That is determinant in the case of cloudy days and increases considerably the yearly efficiency of an installation composed of this type of collectors.

The basic components of a parabolic-trough collector for photocatalytic applications are: the reflecting concentrator, the absorber tube (photoreactor), the tracking system and the overall structure. From them, the last two do not offer any particularity to photocatalysis, with regard to the applications they were originally designed for.

2.4.1. Reflecting surface

In this type of solar collector, this surface is parabolic (Figure 2.4) and must be made of a highly reflective material for ultraviolet radiation. The traditional mirrors silver coated have very low reflectivity (reflected radiation/incident radiation) between 300 and 400 nm, being the best option in this case the utilisation of aluminium coated mirrors (see Figure 2.7). On the other hand the glass, used as protective surface, is not satisfactory because it absorbs part of the UV radiation that reaches it. This effect is duplicated due to the light trajectory through the glass, to and from the metallic surface. Due to this, several solutions have been proposed [*Minero et al., 1993; Tyner, 1990*], but all of them lead to add to the old parabolic-mirrors (for thermal applications) a new flexible surface “sandwich” type. This is composed of three

parts: plastic-aluminium-plastic. This task has been carried out with a surface of this type, as explained below.

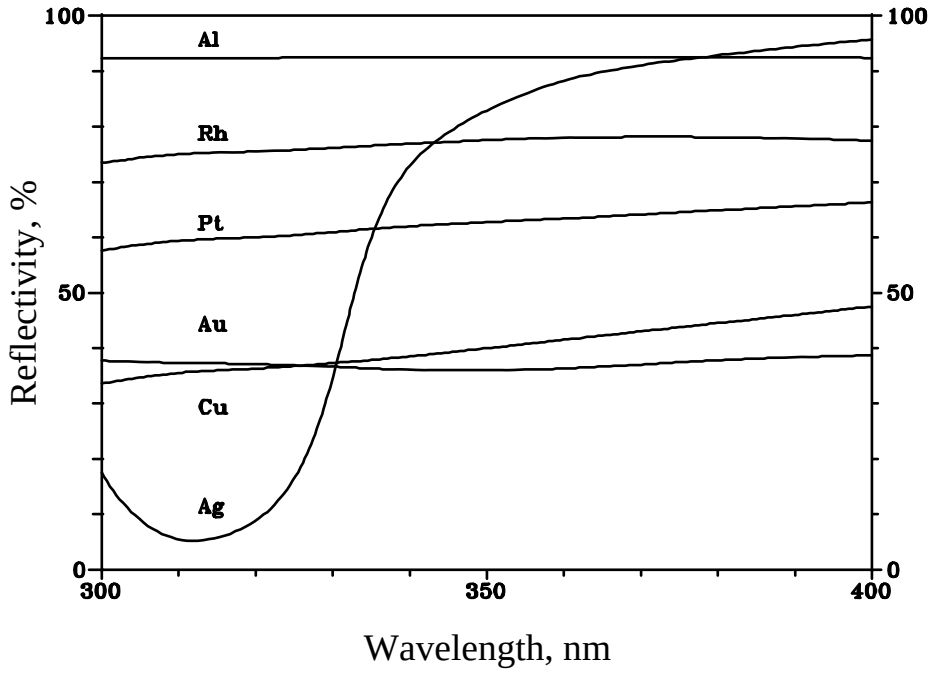

Figure 2.7. *Reflectivity of possible metallic coatings for mirrors* [*Hass, 1965*].

Nevertheless, it would be necessary to explain that the reflective surface question is not solved yet, as none of the surfaces used so far fulfils one of the main characteristics to make it optimum: a reasonable price combined with acceptable durability in outdoor conditions. *Jorgensen and Govindarajan* [*1991*] provide extended information on this matter and explain the state of the art in this field and the possible ways to follow to obtain the above mentioned objective.

2.4.2 Receiver tube

The receiver must be transparent to UV radiation and hard enough to work under high water pressure. The best solution would be quartz, but its high cost makes it completely unfeasible. The applying of a low-iron-content glass, such as borosilicated ones (see Figure 2.8) and similar, seams the most adequate.

Utilisation of plastic materials is also possible, if they fulfil the specifications of transmisivity, pressure and thermal resistance, as well as keeping its properties during outdoors operation. All this could be also applicable to any flat reactor, if it is covered to avoid direct contact with the atmosphere. To use an uncovered reactor is not recommended due to multiple factors: lose of volatile contaminants, dust and dirt inside the reaction mixture, difficulties to enrich the

water with oxygen, etc.

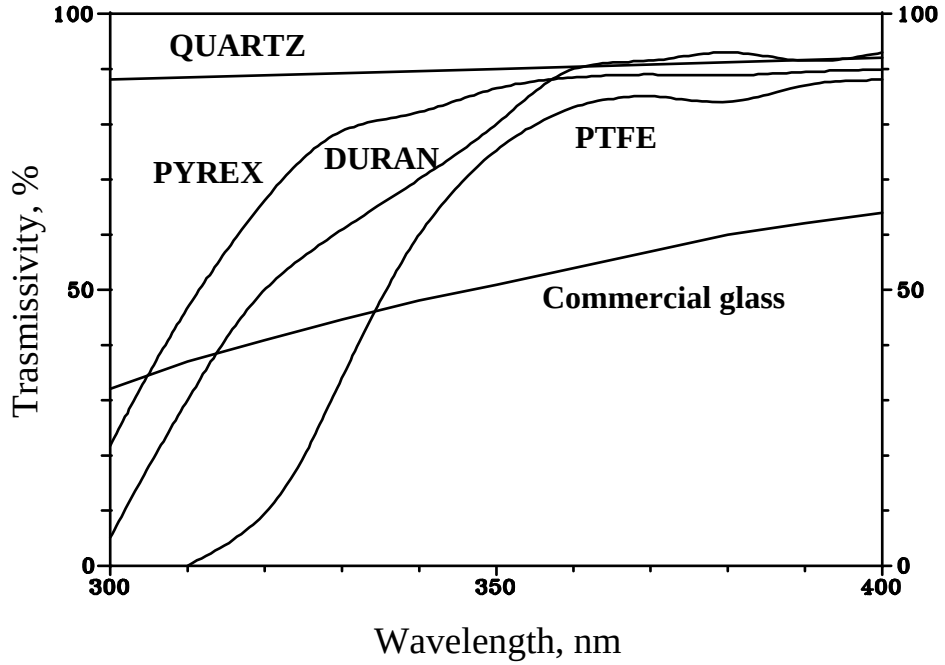

Figure 2.8. *Transmisivity of different materials suitable for to manufacture the photoreactor tubes.*

2.5. Comparison between PTCs and flat collectors

Parabolic-trough collectors make a more efficient use of the solar direct radiation and could allow the use, for other applications, of the thermal energy collected due to the concentration of the radiation. The size of the reactor is smaller, receiving more energy per unit of volume. So, the handling and control of the liquid to be treated is simpler and cheaper, also reducing the possibilities of leaks, which in many cases can be dangerous. If the utilisation of supported catalyst is considered, the required amount of catalyst can be considerably smaller.

Flat collectors (concentration ratio = 1), also use diffuse radiation. This is very important in locations where clouds are very frequent. They are, in principle, cheaper than PTCs as they do not have mobile elements or solar tracking devices. They do not concentrate radiation, so the efficiency is not reduced by factors associated to reflection, concentration and solar tracking. Maintenance costs are cheaper because their components are simpler than the PTC ones. The required surface for their installation are not as high, because being static they do not project any shadows on to the others.

2.6 Conclusions

(I) The effective Solar energy, for TiO_2 photocatalytic reactions, is a very small part (3.5%-8%) of the total.

(II) It is necessary to know the photonic flux density (I), corresponding to the incident radiation, to evaluate the efficiency of the photochemical reactions. This makes the measurement in real time of this parameter essential.

(III) From the different collectors available, those with low and medium concentration have characteristics applicable in photocatalysis with TiO_2.

(IV) Parabolic-trough collectors with two axis tracking system are the most efficient in direct solar radiation concentration. This does not mean that they are excellent for photocatalysis, but they are the best to know time the incident photonic flux in the reactor in real time.

3. DESCRIPTION OF THE EXPERIMENTAL SYSTEM

3.1 Introduction

The facility is part of the Spanish-German Plataforma Solar de Almería experimental centre, a dependency of the CIEMAT-DER (Centro de Investigaciones Energéticas Medioambientales y Tecnológicas - Department of Renewable Energies) located within the city limits of Tabernas (Almería). The Photocatalytic Detoxification Water Pilot Plant (see Figure 3.1) is in the area called the SSPS (Small Solar Power Systems) and was built with financing from the Commission of European Communities "Access to Large Scientific Installations" project. The solar collectors had already been used before for thermal applications. The parabolic troughs were used for the concentration of incident solar radiation on an absorber-black tube through which thermal oil circulated and was heated up to 290°C in order to produce water steam in a boiler and move a turbine connected to an alternator. Twelve of these collectors were selected from the "MAN I" field (see Figure 3.1) for modification for photochemical applications, keeping the original structure and solar tracking system intact.

3.2 Specifications of the solar modules

As mentioned above, a total of twelve modules have been modified for their use in photocatalytic applications. Each of these modules (Figure 3.2) consists of a turret on which a platform supporting four parabolic trough collectors with an absorber tube in the focus has been placed. The platform is moved by two motors which are controlled by a two-axis (azimuth and elevation) tracking system. The tracking system consists of a photoelectric cell which keeps the aperture plane perpendicular to the solar rays and these are reflected onto the focus (absorber), through which the water to be treated is circulated. The nominal aperture area is 32 m^2, although due to the separation between mirrors and the connections between the tubes, only 91% can be used. The solar tracking system has an error of less than 6' in azimuth and 3° in elevation. This means that the tracking cell corrects the collector position when it detects these differences between the real position and the correct position, so that the motors are not continually in movement. The modification of these collectors has affected the reflective surface, the absorber tubes and the connections between them and between the collectors. Modification of the connections was the easiest, since the old thermally insulated steel tubes (oil at up to 290°C had to flow through them without energy loss) were simply substituted with black HDPE (high density polyethylene) through which water was to circulate and thermal losses might even be desirable as they help keep the temperature down in a system made of plastic materials. Furthermore, if there are heat losses, less power is needed for the cooling system (see Figure 3.5). The reflective surface, on the other hand, was

transformed in such a way as to avoid loss of UV radiation produced by the reflection of conventional mirrors (made of silvered glass) and the original black absorber tubes had to be replaced by transparent tubes.

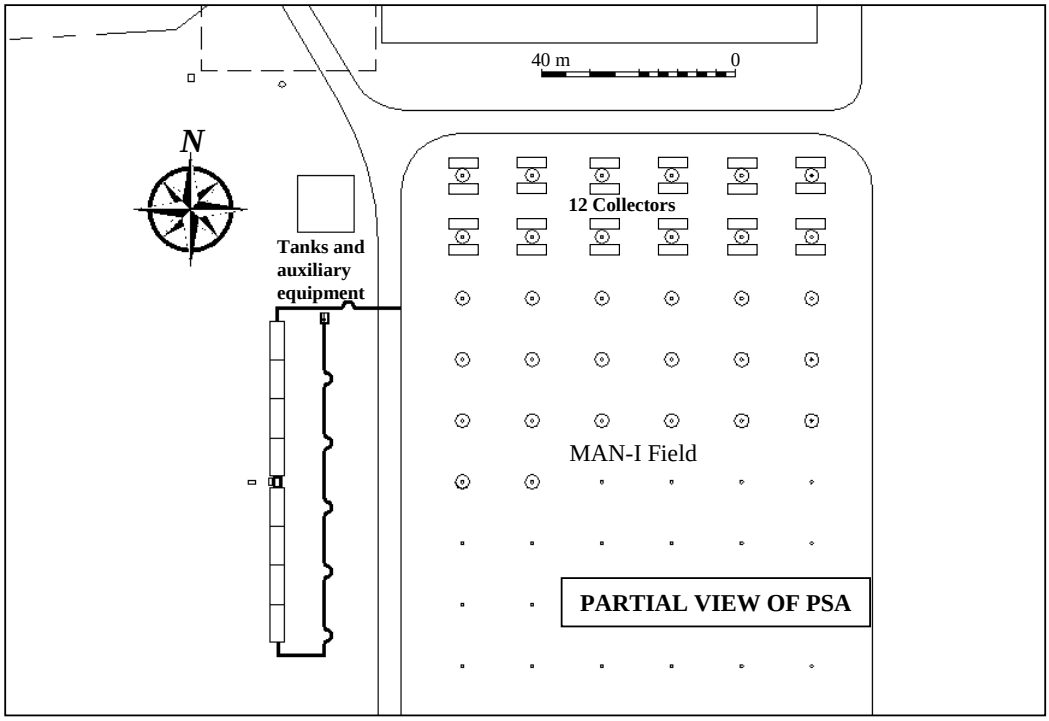

Figure 3.1. *Situation of the Pilot Plant inside the Plataforma Solar de Almería*

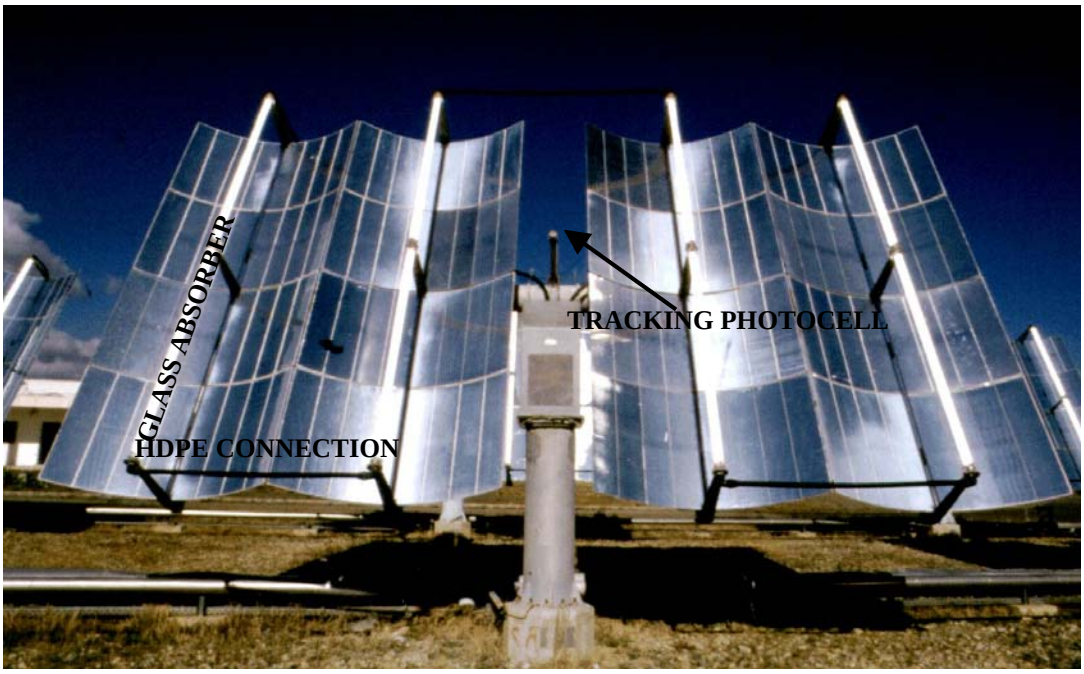

Figure 3.2 *One module of the Pilot Plant in tracking position.*

The complete PTC data are given in the following table:

COMPLETE MODULE		**COLLECTOR**	
Width	7.96 m	Shape	Parabolic trough
Height	5.27 m	Length	4.50 m
Nominal area	32 m^2	Width	1.81 m
Effective area	29 m^2	Focal length	0.64 m
Number of collectors	4	Aperture angle	70.5°
Maximum rotation	220°	Number of Elements	8
Maximum elevation	180°	Reflective Surface	Al-Polymer
Diameter of rotation	9.40 m	Concentration ratio	10.3
SOLAR TRACKING SYSTEM			
Two-axis cell, visual angle ≥ ± 60° on the two axes, response to insolation ≥ 300 W/m^2			
Axis of movement	Vertical	Axis of movement	Horizontal
Speed (°/min)	Fast 30-Slow 3	Speed (°/min)	6
Error	<6’	Error	< 3°
Security system: In case of problem (high water temperature, leaks, pump stopping) can be automatically defocused (4° to the East) so that the module is not damaged. Operation with wind under 50 km/h).			

Table 3.1

3.2.1. Reflective surface

The average reflectivity of the parabolic trough mirrors, initially mounted on the collectors, was approximately 50% between 300-400 nm (see Figure 2.7). For this reason, an aluminium-film was used because of its excellent UV characteristics (reflectivity >90% between 300 and 400 nm). Use of conventional glass (see Figure 2.8) as a support surface for the aluminium was discarded as a poor UV transmitter. The final characteristics of the surface had to be [*Jorgensen et al, 1991*]: (i) good reflectivity in the UV range, (ii) weather resistant and (iii) thick and flexible enough to permit good adherence to the old mirrors to make use of all the optical advantages of the original collectors (curvature, focal length, etc.). These three requirements are fulfilled by the three-layer film seen in Figure 3.3.

This type of film, developed and mounted [*Sánchez 1991, 1992*] for these collectors, has excellent weather resistance (accelerated ageing according to Standard ASTM G53-88). Its hemispheric reflectivity in the UV (300-400 nm) is also over 85%, according to measurements made with a PERKIN-ELMER spectrophotometer (model “Lambda-9”, with a 60 mm-integrating sphere, painted with barium sulphate, with a barium sulphate standard and a lead sulphate detector). Specular reflectivity was measured with a portable reflectometer (FH-PTL Wedel Reflectometer, λ measurement = 600 nm) immediately after gluing on the mirrors, and was found to be as high as 69.5% (average of measurements of 25% of the 384

mirrors modified, 32 per module × 12 modules). It should be noted that the value of 300 to 400 nm should not vary, since aluminium has a practically constant reflectivity over 300 nm (see Figure 2.7). In any case, reflectivity is determined periodically, in order to find out the situation on the reflective surface during the experiments.

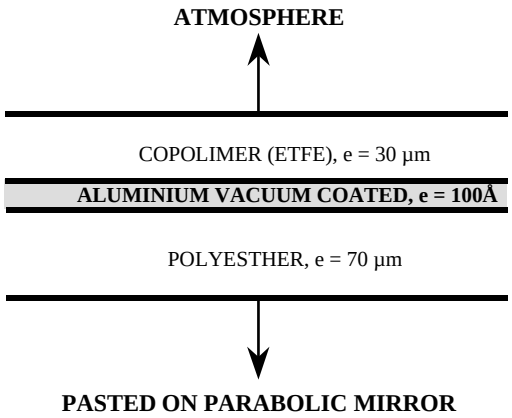

Figure 3.3. *Structure of the aluminised reflective surface glued onto the original parabolic trough surfaces.*

Reflectivity is very important in data handling, as seen later, since it determines the efficiency of the radiation collector surface which is outdoors and therefore gets dirty or can be damaged. Reflectivity measured in this way has to be corrected by a factor (f_{CR}, reflectivity measurement correction factor), in order to be used to calculate the photonic flux that enters the reactor. This factor is calculated based on reflectometer characteristics, the PTC collector characteristics and the aluminised surface reflectivity before gluing to the trough [*Blanco et al, 1991a; Lensch, 1983*]. As the tube on which the radiation is to be concentrated has an internal diameter of 56 mm (and is therefore not a point focus), a greater percentage of the radiation will reach the absorber than the measured by the reflectometer:

$$f_{CR} = \frac{\text{Effective reflectivity}}{\text{MeasuredReflectivity}}; \qquad f_{CR} = 1.22 \tag{3.1}$$

3.2.2. Absorber tube

The absorber tubes through which the water to be treated circulates are of borosilicate glass (Pyrex-type, Figure 2.8) and have an internal diameter of 56 mm, a 2-mm-thick wall and are 2.1 m long. Each module has eight absorbers located at the focus of the four troughs and connected two-by-two with stainless steel clamps. This makes a total of 16.8 m (illuminated volume of 41.4 L) of glass tube per collector. The connections between pairs is made by HDPE tube (I.D. 32 mm). They can withstand a pressure of 11 bar and its transmisivity in the

UV may be considered sufficient (see Table 3.2 and Figure 2.8), considering the savings in buying Pyrex instead of quartz.

λ, nm	% Tras.	λ, nm	% Tras.	λ, nm	% Tras.	λ, nm	% Tras.
300	21.71	318	62.94	336	81.74	360	88.44
302	26.75	320	66.19	338	83.66	365	88.93
304	31.62	322	69.66	340	82.13	370	87.82
306	36.92	324	71.37	342	84.76	375	88.03
308	42.01	326	74.36	344	85.88	380	88.77
310	46.67	328	76.82	346	85.72	385	88.90
312	50.39	330	78.70	348	86.20	390	89.39
314	55.14	332	78.98	350	86.44	395	89.80
316	58.69	334	80.44	355	87.76	400	89.80

Table 3.2

Figure 3.4a *View of the absorber with the illuminated catalyst inside*

3.3 Photocatalysis pilot plant

In Figure 3.5 a detailed drawing of the plant is given. A total of twelve modules (in two rows of six) constitutes the detoxification plant. All of them are connected in series, but with valves that permit to bypass any number of them. The separation among the modules is 12 m and

10.5 m between rows. This means that 433 meters of plastic tube are necessary to connect the whole system, broken down into: 157 m among the modules and 23 in each module to connect the four glass absorbers and reach the ground, where the main tube is located. All the tubes and valves are black HDPE, material chosen because it is strongly resistant to chemicals, weather-proof and opaque, in order to avoid any photochemical affect outside of the collectors.

Figure 3.4b *View of all the Pilot Plant in operation*

For the modules two nomenclatures were used “a (1,2)” and “b (1,2, …10)”. The first refers to those that must never come in contact with TiO_2, since it sticks to the glass and would not allow blank tests or tests with other catalysts to be carried out.

There are five storage-feeder tanks available, also made of HDPE and having different capacities: one 200 L (E), one 1200 L (D), and three 3000 L (A, B and C) where the test mixtures are prepared, the four larger tanks having electrically-powered stirrers. Four different operating modes are used: recirculation, once-through, partial recirculation, and system cleaning. Tank E was installed later, since A, B and C could not be used in recirculating experiments because too much dead volume would be involved. This originated an additional problem since large volumes of solution had to be prepared, sometimes with costly components, making operation much more expensive. For the same reason, a tube

allowing operation with just one module was installed as will be described later. Thus, the total volume (V_{TOT}) of the system in any given experiment is:

$$V_{TOT} = V_A + V_{HDPE} + n\ V_M \quad (3.2)$$

where V_A is the volume in the feed tank which can be varied as required, V_{HDPE} is the volume in the tube between the modules and the tank and V_M is the volume in each module, with n the number of modules in series.

Due to the concentration of the solar radiation on the absorber tubes, an important increase in temperature is produced in the water which flows through them. Obviously, that increase is that much greater the slower the flow rate used in the once-through experiments and the longer the recirculation experiments are. It is therefore necessary to use refrigeration in order to avoid vaporisation and damage to the plastic materials. In order to solve this problem, a closed-circuit cooling system was installed consisting of a small heat exchanger (28 tubes, 0.77 m^2 exchange surface, 4×10^5 kcal h^{-1}), where the process liquid is cooled in stainless steel tubes (AISI 316) by water, which, in turn, is cooled to ambient temperature by an air-cooler. This cooling water is recirculated through the heat exchanger/air-cooler using a tank and a centrifugal pump.

Another centrifugal pump (KSB, Ethacrom B 25-160) powered by a 3-kW electric motor (calculated to provide a maximum flow rate of 3800 L/h when the maximum length of the system was in use) was installed to move the treatment water through the reactor. A control loop, made up of a flow meter (FI, TECFLUID rotameter, model SC250), connected to a controller (FIC, FISCHER & PORTER, series MC5000, model 53MC5111), which in turns governs an automatic electric valve (FCV, SCHUBERT SALZER, model GS-8030), was designed to regulate the flow rate (see Figure 3.6). Different sensors and transmitters were installed throughout the system for pH(CRISON, model 261), temperature (INOR PT100, model RDT DIN 43760), pressure (ROSEMOUNT, model 1151GP) and dissolved oxygen (WTW, model 160-R). Two solar ultraviolet radiation sensors were also installed one for direct UV (INTERN. LIGHT, model SED 400) with a solar tracking unit (EPPLEY, model ST-1) and another global UV (EPPLEY, model TUVR) normal to the earth's surface.

A constant pure oxygen injection system consisting of a 50-litre bottle (200 bar) with a pressure regulator (from 1 to 10 bar) and an electro-valve, that allows the addition of oxygen to the reactor at intervals (opens and closes in a predefined cycle) or continuously, has been installed in the reactor inlet. To this circuit, a small (2-litre) tank has been added for the instantaneous gas-propelled injection of products into the reactor. This has been very useful for reactor flow characterisation tests with chemical tracers, described in greater detail in section 3.5.

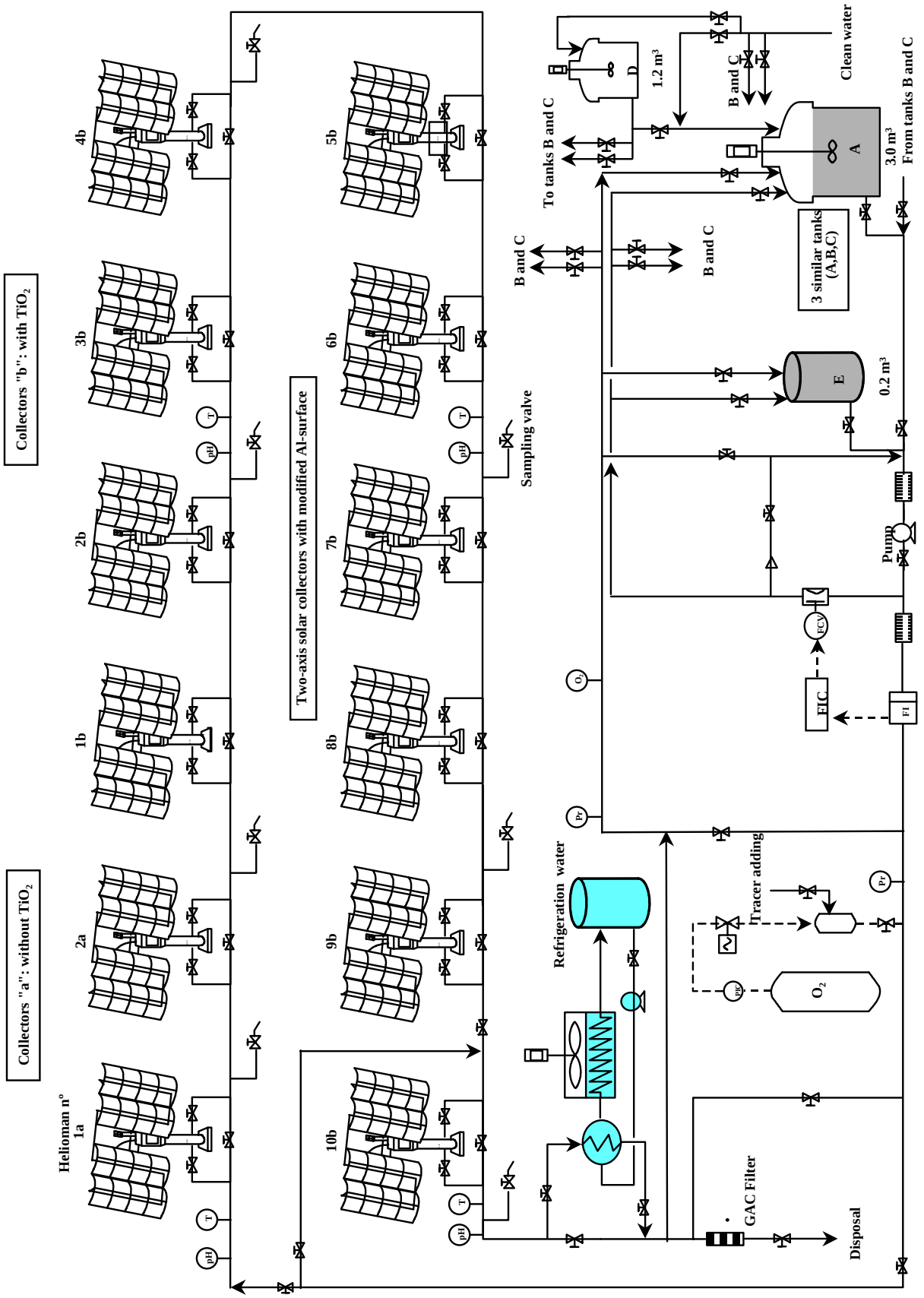

Figure 3.5a. *Photocatalytic Detoxification Pilot Plant*

Figure 3.5b. *Partial views of the pilot plant: tanks (above); instrumentation and main valves (below)*

All the data are sent to a computer which stores the results for later evaluation. This computer also controls all the solar modules through connection to the solar tracking system (see Table 3.1). For cleaning the system there is a tube connected to the PSA sewage system with an active carbon filter that retains any organic compound that could not be decomposed during the experiments. The water necessary for the tests and for cleaning is supplied by the PSA

desalination plant which produces demineralised water (conductivity of less than 10 μSiemens, organic carbon content < 0.5 mgr/L) by a multieffect evaporation system using solar energy. Periodically the aluminised mirrors are cleaned with this water by high pressure hosing. This is done when, due to its outdoor location, reflectivity is lowered by accumulated dirt on the surface.

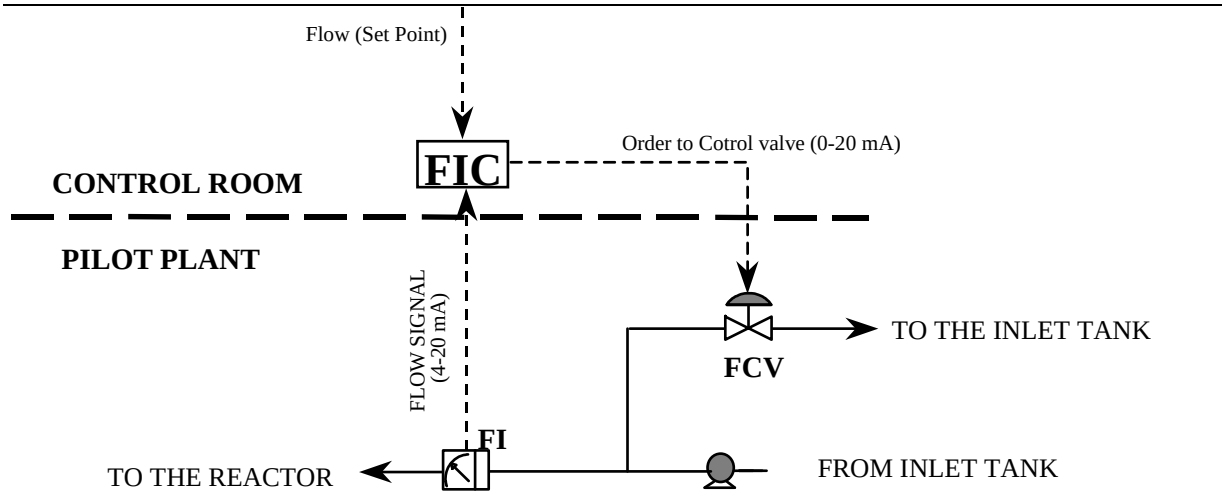

Figure 3.6. *Flow control loop installed in the Detoxification Plant*

3.4 Pilot Plant Operation

3.4.1. Once-through operation

When experiments are desired that circulate the reactant through the collectors only once, the procedure is the following:

1) The pump is connected and the entire system to be used is filled with clean water. The modules necessary are selected and the rest are bypassed by the valves next to each one. The electricity is also cut off for these so that they do not move. In continuation, the water is circulated through the circuit (Figure 3.7a), but returning it this time to feed tank (A).

2) The catalyst, the contaminant (PCP) and any other ingredient necessary for the experiment are added to the tank (A) in the amount required to obtain the initial concentrations of each as stipulated. Recirculation is continued until the mixture is homogeneous throughout the system. Obviously, the maximum flow the pump is capable of is used for this procedure. When the mixture is supposed to be complete, samples are taken, at the same time, at two different points of the reactor and they are analysed. A few minutes later two more samples are taken and if the four coincide, the concentration of the reactives may be considered the same throughout the reactor.

3) In continuation the modules that are going to be used are put into tracking position. Simultaneously, the FIC sets the flow (Q) to be kept constant during the experiment, oxygen injection is activated and the position of the valves is adjusted so that the fluid does not end up in Tank A and that it goes either to Tank B or C. This would be the beginning of the experiment and the liquid follows the path shown in Figure 3.7.a.

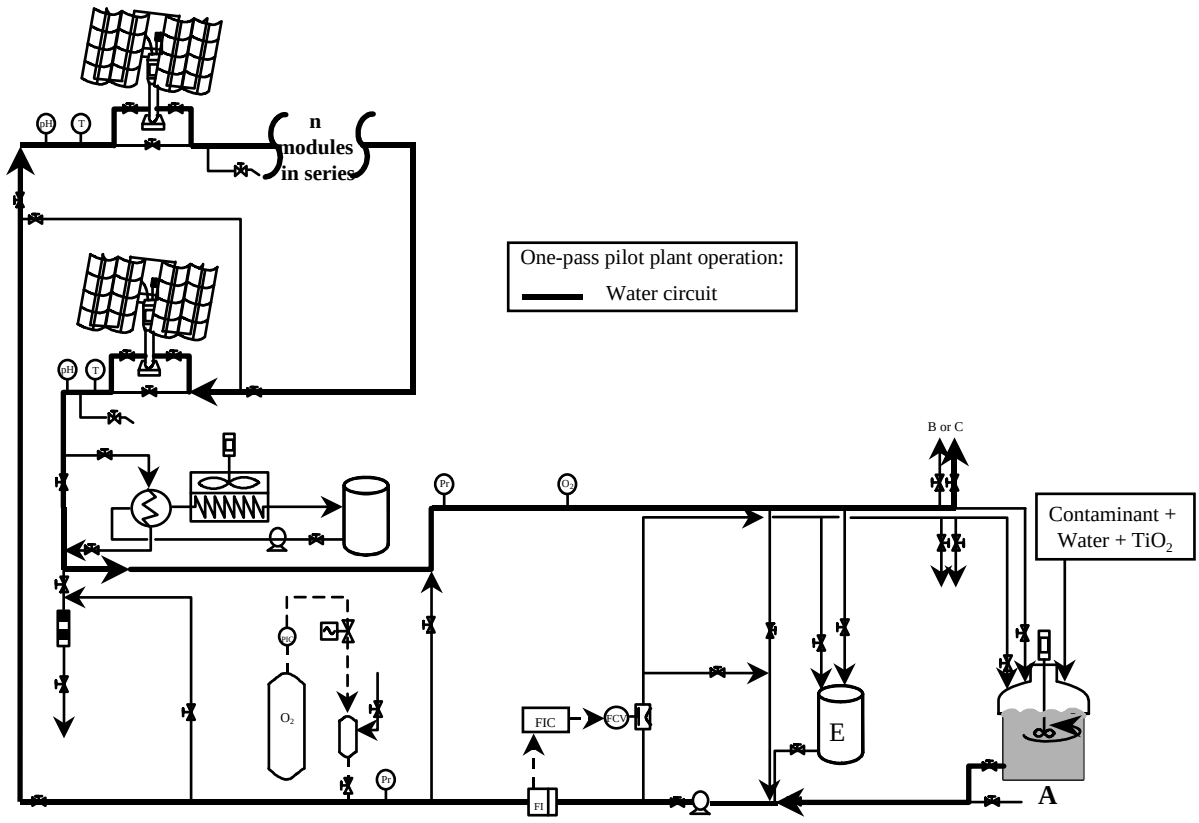

Figure 3.7.a *Simplified drawing of the working in once-through mode.*

4) The modules are kept in solar tracking, a little longer than necessary so that the water in Tank A has gone through the reactor and is approaching the outlet tank. This time (t_{exp}) is:

$$t_{exp} = (V_{HDPE} + n\ V_M)\ Q^{-1} \qquad (3.3)$$

5) At this time samples are taken at all the valves in the outlet of each of the modules used in the experiment. There will therefore be an "n" number of samples with different residence or illumination times ($t_{R,i}$) enable kinetics to be determined. Under these conditions the reactor behaves according to the ideal piston flow model as explained later. The residence

time corresponding to each sample collected at the end of the experiment is calculated with the following equation:

$$t_{R,i} = n_i \, V_R \, Q^{-1} \qquad (3.4)$$

where i (1, …12) is the number of modules through which the samples has passed before being collected and V_R is the volume in the (glass) absorber tube of each module (41.4 L).

Operating in this way it is not necessary to use the cooling system and therefore, the valves are in such a way that the liquid does not go through it. When the test is over, n samples have been obtained with a reactor residence time that is a function of the flow rate. Thus, if the procedure is repeated at a different flow rate, another group of samples with a different t_R will be obtained. Consequently, the number of points ($t_{R,I}$, Concentration) necessary to evaluate any experiment can be obtained.

3.4.2. Operation in recirculation mode

This type of operation differs little from the previous one. However, the modifications may be included in each one of the sections of the previous point, as described below:

1) The test tank used is E (except in some cases when A, B or C is used), since it is the smallest (200 L) and therefore, leaves very little dead volume. If only one module is to be used (10b, Figure 3.5) for the test, the valves are set to pass through the loop which has been especially set up to work under these conditions, avoiding water flow through many of the HDPE tubes. The flow rate is set (approx. 4000 L/h) high enough so that the flow attains a perfect mixture.

2) Same as above.

3) Recirculation is kept up and when the modules enter into tracking (beginning of test), the cooling system is activated (cooling pump + air-cooler). The rest is the same as the once-through experiments.

4-5) The test lasts the desired time (even several days) and samples may now be taken at any of the sampling ports since as the system is in recirculation mode, t_R is the same for samples taken at any point in the system. The pairs ($t_{R,i}$, Concentration) are thus obtained. The calculation of illumination time in this type of experiments is done in the following manner:

$$t_{R,i} = n \, V_R \, (V_{TOT})^{-1} \, t_{E,i} \qquad (3.5)$$

where n is the number of modules connected in series, V_R is the same as equation 3.4, V_{TOT} is calculated with equation 3.2 and $t_{E,i}$ is the time since the experiment began until collection of sample i.

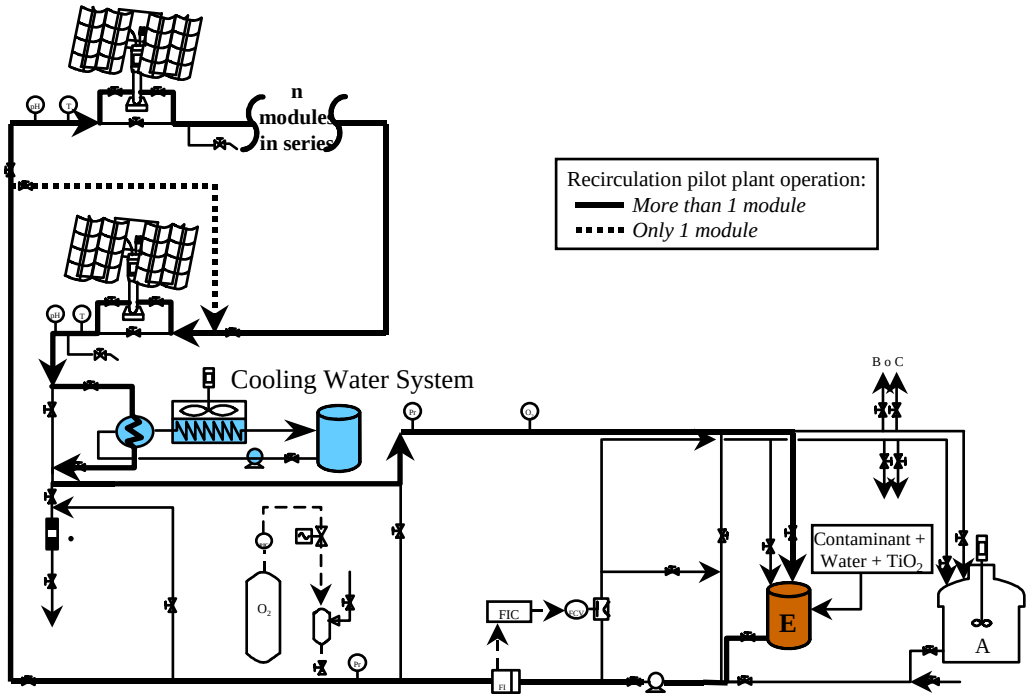

Figure 3.7b. *Simplified diagram of the plant working in recirculation mode.*

3.5 Type of flow in the reactor

For the experiments carried out in once-through mode, the flow characteristics inside the reactor have to be known, since while they are going on, samples are taken from several points in the reactor at the same time. Furthermore, in order to assure that equation 3.4 adjusts to reality, reactor behaviour has to follow a "piston flow" model. That is, flow is not channelled, there is no partial recirculation, stagnant zones, etc., that could invalidate the representativety of the samples taken.

The flow model was checked by a stimulation-response technique. A tracer, specifically 20.6 g of Cl^- (added in the form of $CaCl_2$) dissolved in 100 mL of deionized water, was injected under pressure of oxygen from a small vessel connected to the reactor inlet (see Figure 3.5), into the stream of water almost instantaneously (9.6 sec.). Before injection, the flow rate was set on the FIC. Shortly before it is time for this tracer-signal to get to the end of the reactor (t_{exp}, Eq.3.3), sampling is begun (at the sampling port in the last module) at fixed intervals for

several minutes, in order to find out when the entire injection has passed. In these samples, the concentration of chlorides is analysed as a parameter for use in later calculations.

Twelve tests were carried out (plus some preliminary tests to set the optimum test conditions) in four different situations (each type is repeated three times) with extreme text conditions (Q minimum-12 modules and Q maximum-6 modules) and two intermediate conditions. In each experiment 50 samples are collected at short time intervals (30"at 500 L/h, 15" at 1000 L/h and 10" at 2000 L/H), as shown in Table 3.3 for an example of one of the tests carried out with 500 L/h in 12 modules.

The various elements of fluid, when different paths are followed in the reactor, take different times to pass through it. The distribution of these times in the outlet stream is called the distribution of outlet age (E) and it is recommended to represent them in a standardised manner, so that the area under the curve is the unit.

$$\int_0^\infty E\, dt = 1 \qquad (3.6)$$

No. sample	Cl^- (mg/L)	No sample	Cl^- (mg/L)	No sample	Cl^- (mg/L)	No sample	Cl^- (mg/L)
1(1)	0.0	13	343.4	25	34.3	37	1.6
2	0.0	14	328.5	26	27.9	38	1.5
3	2.1	115	298.4	27	21.5	39	1.3
4	10.6	16	263.5	28	16.5	40	1.2
5	28.2	17	216.9	29	13.0	…	
6	61.2	18	185.3	30	9.6	47	0.0
7	102.5	19	155.7	31	7.2		
8	158.4	20	115.8	32	5.3		
9	221.7	21	95.8	33	3.7		
10	283.0	22	69.2	34	3.2		
11	309.3	23	49.2	35	2.6		
12	343.4	24	37.3	36	2.1		

(1) Sample 1 is taken 5700 seconds after tracer injection, after which the rest are taken at 30 second intervals. The last is collected after 7080 seconds.

Table 3.3

When the outlet signal does not contain a tracer and one is injected virtually instantaneously, the standardised tracer response in the outlet stream over time is called Curve **C** [*Levenspiel,*

1975]. In order to obtain this standardisation, the concentration (c) is divided by A_C, the area under the concentration-time curve:

$$\int_0^\infty \mathrm{C}\, dt = \int_0^\infty \frac{c}{A_C} dt = 1, \text{ being } A_c = \int_0^\infty c\, dt \tag{3.7}$$

When the distribution of residence times is to be characterised, it is important to know what the centre, called the average or centroid of distribution.

$$\bar{t} = \frac{\int_0^\infty t\, c\, dt}{\int_0^\infty c\, dt} \tag{3.8}$$

In continuation, $\bar{t}$ is compared with the expected residence time (V_{TOT}/Q). Since this is only known for a discrete number of values of time, t_i, then:

$$\bar{t} = \frac{\sum t_i c_i \Delta t_i}{\sum c_i \Delta t_i} \tag{3.9}$$

In Table 3.4 a summary of the results obtained in the twelve experiments is given. The flow rate (Q') value corresponds to the average of minute-by-minute data taken, from the time of injection to the last sample. The total volume considered (V_{TOT}) corresponds to the entire path of the fluid and is obtained with equation 3.2. Each experiment was repeated three times under identical conditions.

Exp. No.	**Q', L/h**	**N**	**t, sec**	**V_{TOT}/Q, sec**	**Δt*, sec**
1a	498	12	6249	6195	54
1b	499	12	6441	6183	258
1c	498	12	6130	6195	-65
2a	1987	6	887	900	-13
2b	1982	6	887	903	-16
2c	2000	6	887	895	-18
3a	997	6	1744	1800	-56
3b	96	6	1800	1796	4
3c	1000	6	1821	1789	32
4a	497	6	3760	3600	160
4b	528	6	3428	3388	40
4c	499	6	3464	3586	-122

*$\Delta t = t - (V_{TOT}/Q)$

Table 3.4

In Figure 3.8 the C curves for experiments 1 and 4 are given, in which greater differences are seen between the average times calculated by the injection of the tracer ($\bar{t}$) and those calculated using the system characteristics. In all cases, the differences existing between the mean times, calculated by the tracer experiment and those expected from the ratio of volume to flow rate may be due to three reasons: (i) error in flow measurement, (ii) error in available volume, (iii) the tracer is absorbed or retained by the system. Since the error is sometimes in

one direction and others in another, the first reason seemed the most logical (the other do not produce a random error). In order to find out the amplitude of the distribution, the variation σ^2 is calculated, which in the case of discrete values, takes the form of:

$$\sigma^2 \cong \frac{\sum \left(t_i - \bar{t}\right)^2 c_i \Delta t_i}{c_i \Delta t_i} \tag{3.10}$$

If the experiments are carried out in closed vessels (those which are in neither inlets nor outlets) and the tracer signal is injected instantaneously (injection time ≈ 0), curves C and E coincide and the expression of the variation is simpler.

$$\sigma^2 \cong \sum t_i^2 E_i \Delta t_i - \bar{t}^2 \tag{3.11}$$

Time should be measured as a function of the average residence time, giving an undimensional unit:

$$\theta \cong \frac{t}{\bar{t}} \text{ and } d\theta = \frac{dt}{\bar{t}}, \text{ therefore } E_\theta = \bar{t}E \text{ and } \bar{\theta}_E = 1 \tag{3.12}$$

The expression of variation is thus finally:

$$\sigma_\theta^2 \cong \sum \theta_i^2 E_{\theta,i} \Delta\theta_i - 1, \text{ being } \begin{cases} \sigma_\theta^2 = 1 \text{ Perfect Mixture Reactor} \\ \sigma_\theta^2 = 0 \text{ Plug Flow Reactor} \end{cases} \tag{3.13}$$

The results of this calculation for all the experiments carried out appear in Table 3.5.

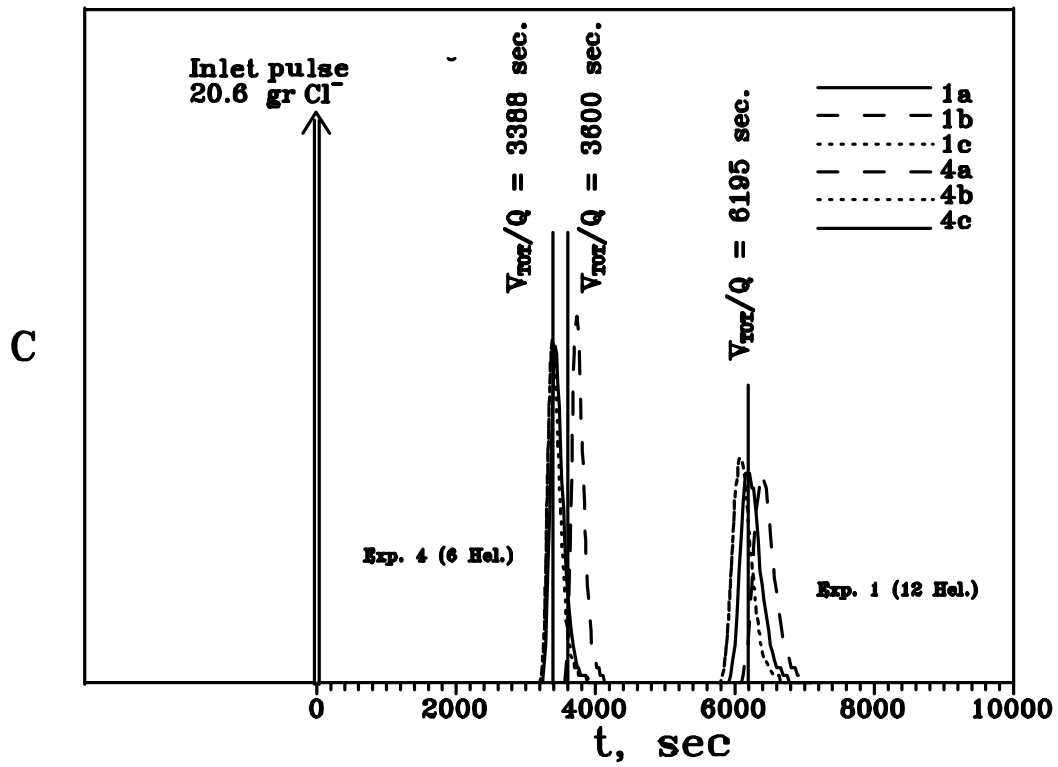

Figure 3.8. *Type of flow (representative curves), in the reactor, obtained with tracer experiments.*

The variation in concentration (dc) over time of residence or illumination ($t_{R,i}=n_i V_R Q^{-1}$) for once-through experiments and for first order reactions (typical in photocatalysis) would be:

$$r = -\frac{dc}{dt} = kc, \text{ which integrated is: } \ln\frac{c}{c_0} = -k\, t_{R,i} \qquad (3.14)$$

In experiments with recirculation using the small tank (Fig. 3.7b), type of behaviour similar to the perfect mixture may be achieved using a very high flow so that the residence time in the reactor is low enough (each time through) for the conversion to be considered negligible. Therefore, the concentration (c) at all points in the system is the same at any given moment.

No.	1a	1b	1c	2a	2b	2c	3a	3b	3c	4a	4b	4c
σ_θ^2	0.0002	0.0013	0.0000	0.0006	0.0002	0.0006	0.0013	0.0031	0.0005	0.0010	0.0004	0.0005

Table 3.5

3.6 Evaluation of ultraviolet radiation

The measurement of the solar ultraviolet radiation (UV) is an essential parameter for the correct evaluation of the data obtained during the photocatalytic experiments carried out in a solar water decontamination pilot plant. The following equipment was used for this:

(I) Sensor for global UV radiation measurement (Eppley, model TUVR) with a typical sensitivity of 150 µVolts W^{-1} m^2 and 2% accuracy. It is placed horizontally in a fixed position, sending its signal to the computer where data (UV_G) are stored.

(II) Sensor for direct UV radiation measurement (INTERNATIONAL LIGHT, model SED 400). The angle of vision has been adjusted to 5.7° with two collimating tubes. The complete unit is installed on a solar tracking system (EPPLEY, model ST-1). The data (UV_D) are treated in the same way as global UV.

These radiometers provide data in terms of incident W_{UV} m^{-2} on each of them, which gives an idea of the energy reaching any surface in the same position as they are with regard to the sun. Likewise, for some calculations, other weather data extracted from PSA weather station (certified by the Spanish National Institute of Meteorology, n° 321-0) have also been used (ambient temperature, total direct and global solar radiation, hours of sunlight, etc.).

Both UV instruments are sensitive, according to the manufacturer, to ultraviolet radiation. But in their technical description, the interval of wavelengths covered in their calibration is not reported. Therefore, there was no certification as to this data, so important in the calculation

of photonic flux (Eq. 2.3 and following) and thus, the determination of quantum performance (Φ) of the reactions that were taking place in the pilot plant. In order to solve this uncertainty, calibration was verified by comparing the data provided by these two instruments with those obtained by a spectroradiometer (LICOR-1800) placed in the same position as each of the radiometers. The spectroradiometer provides radiation data, $UV_{i,\lambda}$(W m^{-2} nm^{-1}), between 300 and 1100 nm in 2 nm intervals during a 26-second scan. This provides:

$$UV_{\Sigma,D} = \sum_{\lambda=300nm}^{\lambda=n} UV_{D,\lambda} \tag{3.15a}$$

$$UV_{\Sigma,G} = \sum_{\lambda=300nm}^{\lambda=n} UV_{G,\lambda} \tag{3.15b}$$

where $UV_{\Sigma,D}$, W m^{-2}, is the summation of the direct radiation measurements (above 300 nm up to n in 1 nm intervals) provided by the spectroradiometer and $UV_{\Sigma,G}$, W m^{-2}, is for the global radiation. In Table 3.6, the two ways of measuring UV_D at different times of day are compared considering n = 400 nm, which is the ultraviolet-visible threshold, after which the radiometers should not measure.

Local time	**UV_D** **W m^{-2}**	**$UV_{\Sigma,D}$** **W m^{-2}**	**UV_D-$UV_{\Sigma,D}$** **W m^{-2}**	**$100(UV_D-UV_{\Sigma,D})/UV_{\Sigma,D}$** **%**
10:31	13.69	11.68	2. 01	+17.2
10:48	16.57	15.29	1.28	+8.4
11:00	17.43	16.01	1.42	+8.9
12:41	25.97	24.49	1.48	+6.0
12:56	27.06	25.53	1.53	+6.0
12:59	26.96	25.42	1.54	+6.1
15:25	17.78	15.62	2.16	+13.8
15:34	17.68	16.00	1.68	+10.5

Table 3.6

In view of these results, the conclusion was that the UV_D radiometer measures beyond 400 nm. The facts that the difference between the measurements taken with the spectroradiometer and the radiometer are practically constant and therefore, the percentage of error, $100(UV_D-UV_{\Sigma,D})/UV_{\Sigma,D}$, varies depending on the value it is measuring and always in the same direction, suggested that the radiometer is active for wavelengths above 400 nm. In order to find this interval the same procedure was carried out for n values over 400 nm at 1 nm intervals. The results are given in Table 3.7, together with the % of error.

It seems that, taking as the upper limit a wavelength of 404 nm, the radiation measured by both instruments is in agreement. Therefore, this indicates that installed in the pilot plant. A similar procedure was followed for the UV_G and in this case the UV_G radiometer measures solar radiation up to a wavelength of 393 nm. The measurement interval is fundamental for the calculation of the photon flux which reaches the interior of the reactor. In each one of the experiments carried out, the measurement of UV_D and UV_G have been on-line while experiments have being performed.

UV_D W m^{-2}	$UV_{\Sigma,D}$; $100(UV_D-UV_{\Sigma,D})/UV_{\Sigma,D}$ [(1)] W m^{-2}; %				
	n=401	**n=402**	**n=403**	**n=404**	**n=405**
13.69	11.99; +14.2	12.33; +11.0	12.67; +8.1	13.03; +5.1	13.38; +2.3
16.57	15.69; +5.6	16.13; +2.7	16.57; 0.0	17.01; -2.6	17.46; -5.4
17.43	16.42; +6.2	16.87; +3.3	17.33; 0.0	17.79; -2.1	18.25; -4.7
25.97	25.06; +3.6	25.69; +1.1	26.34; -1.4	26.99; -3.9	27.64; -6.4
27.06	26.12; +3.6	26.77; +1.1	27.43; -1.4	28.11; -3.9	28.78; -6.4
26.96	26.01; +3.6	26.66; +1.1	27.32; -1.3	27.98; -3.8	28.65; 0.0
17.78	15.99; +11.2	16.40; +8.4	16.81; +5.8	17.24; +3.1	17.66; 0.0
17.68	16.39; +7.6	16.81; +5.2	17.24; +2.5	17.67; 0.0	18.11; -2.4

(1) Under each n in the table, the UV obtained with the data from the spectroradiometer when Eq. 3.15a is applied, is given. To the right of each value, the percentage of error between these measurements and the UV_D that appears in the column to the left is indicated.

Table 3.7

3.7 Materials and reactives

All the products were used directly, without any prior treatment or purification. The contaminant selected for this work was PCP (Pentachlorophenol, C_6Cl_5OH, CAS n° 87-86-5) because of its extensive use and highly contaminating nature [*Crosby, 1981; Jacobsen et al., 1989; Kratz et al., 1989; Kuelh et al., 1980; Weber et al., 1978*]. Initial PCP concentrations were between 6 and 200 mg L^{-1}. The aqueous solutions used were prepared from the pure compound (Aldrich, 99%). The natural pH usually obtained with the addition of PCP (pKa=4.7) to deionized water is 5 and under these conditions solubility is only 18 mg L^{-1} (20°C). However, at pH 10 increases to 20 g L^{-1}. In order to dilute large quantities (tens of grams) in a small volume of water (several hundreds of mL) in the laboratory and later add this mixture to the large tanks in the pilot plant, the pH of the solutions had to be elevated with sodium hydroxide. On adding these concentrated solutions of PCP to large volumes of water (hundreds of litres) the final pH was around neutral (6-8) and, therefore, was close enough to the conditions under which it is normally found in the environment: at pH 7.3 (very

common in fresh water [*Crosby, 1981*]) it is 99% ionised and at pH 8.1 (very common in sea water [*Crosby, 1981*]) it is 99.9% ionised.

The catalyst used was titanium dioxide (CAS 13463-67-7), TiO_2 Degussa P-25, since it is the most widely used in photocatalytic decontamination. It also produces the best results compared to other semiconductors [*Herrmann et al., 1983, 1990a; Minero et al., 1991b*]. Specifically, it has been demonstrated to be the most appropriate for PCP decomposition [*Barbeni et al., 1985*], other chlorophenols [*Pelizzetti et al., 1985*], highly toxic chlorinated compounds as PCBs and dioxines [*Pelizzetti et al, 1988*] and, in general, for the production of OH^- radicals [*Riegel et al., 1995*]. Another very important advantage which has been considered was its economical price compared with other semiconductors, since it has to be used in large quantities and the treatment proposed for the destruction of PCP should be economically viable. The mixtures of TiO_2 and water were prepared by adding the solid directly into the experimental tank, rapidly obtaining a homogeneous milky suspension. The main physical-chemical properties of the TiO_2 used (P-25) were [*Degussa Corp., 1986, 1988, 1990, 1991; Nargiello et al., 1993*]:

Surface area:	35-65 m^2/g
Average diameter of elemental particle	20 nm
pH at 4% aqueous suspension	3.0-4.0
Anatase-Rutile ratio	70:30 approx.
Apparent density:	100 g/L
Purity	>99.5%
Toxicity	Biologically inert.

The water used in the laboratory for the preparation of the concentrated PCP solutions was normal distilled. This provides a typical conductivity lower than 4 μSiemens cm^{-1} and TOC (total organic carbon) of less than 0.1 mg L^{-1}. The water used in the pilot plant experiments comes from the PSA Desalination Plant and has an equivalent laboratory quality (Type III-IV ASTM), with a TOC content of a little over (<0.5 mg L^{-1}) but that, in no case, causes distortion of results obtained.

The rest of the reactives used in the pilot plant for the experiments were: hydrogen peroxide (Probus, PRS), sodium persulphate (Merck or Riedel-de Häen, PA), sulphuric acid (≥96% Probus, PRS) and pure oxygen (SEO, industrial quality). The reactives necessary for the analytical methods used are listed in the following section in each case.

3.8 Methods of analysis

The analyses performed on the samples which were collected throughout the experiments, attempted to be as complete as possible. This makes it possible to adjust the mass balance for

the photocatalytic decomposition of PCP. At the same time, the analyses should be sufficiently simple to permit a large number of samples to be treated and, thereby, the greatest number possible of experiments to be performed. Since this was a pilot plant study, the formation of intermediate degradation compounds was not studied in depth. However, several PCP degradation intermediates were identified, confirming that the mechanism of the solar photocatalytic degradation of PCP does not differ substantially from that known up until now, in laboratory experiments using lamps. The PCP decomposition reaction to which all mass balances should be adjusted is the following:

$$C_6Cl_5OH + \frac{9}{2}O_2 + 2H_2O \xrightarrow[TiO_2]{h\upsilon} 6CO_2 + 5HCl \qquad (3.16)$$

Obviously, an energy contribution from the radiation (in this case, solar UV) is necessary to activate a semiconductor (TiO_2) to permit the complete oxidation of the PCP within a reasonable period of time.

Each of the samples taken from the pilot plant had a volume of approximately 250 mL. The sample flasks were not transparent in order to avoid any photochemical reactions after collection and were covered and identified. An attempt was made to analyse all the parameters immediately. If this is not possible, they were stored in a refrigerator at 4°C for the least amount of time possible. In any case, tests were made to determine its stability over time and no change was detected in any of the values analysed after one month of storage.

The total sample was divided into several parts, each one of which was analysed by a different technique, according to the following scheme:

$$\text{250 mL (pH determination in the flask)} \longrightarrow \begin{cases} \sim 15mL\ Filtration\ 0.45\mu m \rightarrow PCP\ Analysis \\ \sim 25mL\ TOC\ Analysis \\ \sim 50mL\ Cl^{-}\ analysis \\ Remaining\ volume \rightarrow Rest\ of\ parameters \end{cases}$$

3.8.1 PCP Analysis

This compound was determined by liquid chromatography with UV detection. The equipment used for it was an HPLC (Hewlett-Packard, series 1050) made up of the following components:

- High pressure pump for dosing of up to four different solvents by means of a proportional system valve (low pressure mixing).
- Variable wavelength detector (190nm-600 nm) with 10 mm pathlength cell
- Electronic integrator (HP 3396 series II)

- Degasification system using direct helium purge in the solvent bottles.
- Sample injection system made up of sample valve (Rheodyne model 7125) with 20 μl injection loop and thermostatic column container for temperatures above ambient.
- Reverse phase column C-18 (Merck, LiChroCART RP-18, 5μm , I.D. 4 mm and 125 mm length).

The optimum chromatographic conditions (a typical chromatogram is shown in Figure 3.9) for correct and rapid identification and quantification of PCP are:

- Methanol (Merck or Riedel-de Häen, HPLC gradient grade)/water (bidistilled) 80/20 at pH 3 (H_2SO_4), to keep PCP from dissociating and avoid peek tailing.
- Flow 1.5 mL min^{-1}.
- Detector wavelength 220 nm
- Column temperature 30°C
- Injection by complete filling of the injection 25 μL loop (using 100 μl sample syringes to assure total occupation of loop volume.)

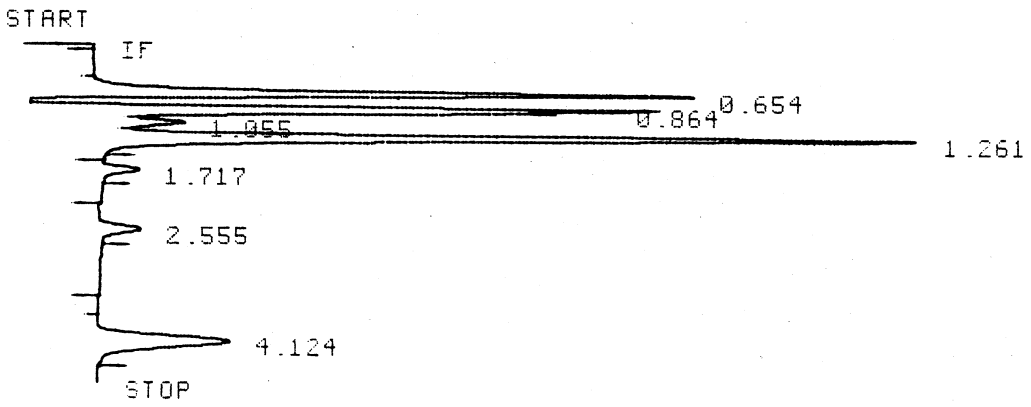

Figure 3.9 *PCP chromatographic analysis by HPLC (t=4.124 min), after several minutes of illumination. The rest of the peaks correspond to degradation intermediates.*

With this method the concentration of PCP may be quantified with total confidence until 1 mg L^{-1} (quantification limit, LOQ) and its presence may be detected in concentrations of over 0.04 mg L^{-1} (limit of detection, LOD). The only treatment that samples require before injection in the equipment is filtering (to get out TiO_2 and any other particles that could damage the chromatographic column). A device made up of a syringe (glass, 10 mL) and 0.45 μm membrane filters (Millipore, HVLP 13 and 25 mm) is used for this purpose. The calibration curves, which enable quantification, were made using diluted solutions prepared from concentrated solutions (~1000 mg L^{-1}) in methanol of a chromatographic highly pure

standard (Riedel-de Häen, PESTANAL®). These solutions are unaltered for at least a month, if kept refrigerated.

The intermediate products of the photocatalytic decomposition of PCP, from one of the degradation experiments, were analysed by the Dept. of Analytical Chemistry. of the University of Torino (Italy). They were identified by mass spectrometry of organic extracts obtained by a continuous extractor, where 45 mL samples were placed in contact with 30 mL of CH_2Cl_2 for 40 min. The organic phase was concentrated under vacuum and injected into a GC-MS (Varian 3000 GC-Finnigan MAT 95Q MS). A capillary column (SGE PB-5, 30m × 0.25 mm) was used and the separation method was programmed according to the following sequence: 35°C for 3 min, from 35ºC to 300°C at 10° min^{-1}, 300° for 10 min. The spectrum was recorded at 70 eV and was compared to the mass spectra of the pure compounds. The quantification of intermediates was done by HPLC-UV under the same conditions described above.

3.8.2 TOC analysis

The total organic carbon analyses of the samples generated during PCP degradation experiments were vital for the following reasons:

1. Determination of all the intermediates that might be generated during the photodecompositon of PCP is not possible and therefore, it is crucial the identification of the moment at which only CO_2 remains and water is considered completely decontaminated.
2. The determination of the CO_2 produced might be reasonable, since this must be stoichiometric with the organic carbon present at the beginning in the PCP molecule (6 atoms of C). However, since the reactor is enormously large and not airtight, the loss to atmosphere of the carbon dioxide produced prevents this. Besides, for the same reason, the samples might become contaminated by atmospheric CO_2 and falsify results.
3. Due to the great majority of the organic compounds produced from PCP, in the first stages of the photodegradation, they are in equimolar form (1 mol of PCP $\rightarrow$ 1 mol of intermediates, as seen later), the measurement of TOC is a reflection of the number of moles of product that still remain as organics. Therefore, it is possible to get an idea of the remaining quantity of intermediates: (moles of TOC/6) - (moles of PCP) = (moles of remaining intermediates).
4. It is a reliable, rapid and simple way to close the mass balance at any moment, since if only PCP and identifiable intermediates were determined, one could not be sure of having reduced the contaminating load of the water.

The instrument employed to determine TOC (Heraeus-Foss Electric, model LiquiTOC-2001) uses the wet chemical oxidation method with IR detection (EPA method 415.1). The operation of the analyser is automatic, all functions being computer-controlled. The operator only has to inject the sample and set the two basic parameters: type of analysis (TIC, TOC, TC) and range of analysis (from 0 to 1 mg L^{-1}, to 10 mg L^{-1}, …. 10000 mg L^{-1}). The procedure is the following:

1. Injection of the sample directly (without filtering out TIO_2) into the instrument, where orthophosphoric acid (10% v/v) is added automatically, which transforms all the inorganic carbon (TIC) into CO_2. The sample is then purged with O_2 (ultrapure, 99.999%) and the CO_2 is forced out of the sample toward the IR detector. The CO_2 produced in this way is originated from all the carbonates present in the water and its determination by IR is possible, by comparing with standard solutions treated in the same manner. As explained previously, this is not useful in this case. The usefulness of this step is in ridding the sample of any trace of inorganic carbon that might distort the measurement of TOC to be carried out in continuation.
2. The sample, free of TIC, is injected with sodium persulphate (1.5 M) and put into a reactor placed around a UV lamp ($\lambda \approx 250$ nm). In this way all the TOC present in the water is converted into CO_2, which is again purged with a stream of oxygen (which is also used as a source of oxygen for oxidation) and directed toward the IR detector. The device is calibrated with standards (free of CO2), prepared with KHP (potassium hydrogen phthalate, MERCK, 47% TOC) in bidistilled water. The results are obtained in mg of carbon per litre.
3. After the analysis is performed, waste is washed out of the system by clean water (bidistilled) and another sample is injected. The entire process lasts 10 minutes per sample.

One aspect of the TOC analysis detected during continued use of the instrument is worthy of comment. Since to inject the sample, it is not necessary to take out the TiO_2, this has an accelerating effect on the UV/persulphate oxidation reaction. It considerably prolongs the life of the lamp and improves quantification of the samples. In fact, there are already some TOC analysers on the market based on the use of TIO_2 [*Matthews, 1990; Millipore, 1995; SGE Scientific, 1993*].

3.8.3. Analysis of chloride and other parameters.

When PCP decomposes (Eq. 3.26), a stoichiometric increase in the concentration of chlorides is produced in the water treated (5 moles of Cl^- per mol of PCP) and, likewise, an increase in the concentration of hydrogen ions (decrease in pH). For this reason, the analysis of these two products of the reaction is of interest for the final mass balance. However, the decrease in pH

is not a very reliable parameter of this balance, save in some cases, because it is influenced by other processes which take place in the medium: the effect of the TiO_2 suspension , the formation of CO_2, the decomposition of $S_2O_8^{-2}$ and H_2O_2 when these are used as additional oxidants, the NaOH used to dissolve the PCP, etc. The methods used to determine the concentration of H^+ and Cl^- were:

- Measurement of pH with selective electrode (combined electrode, CRISON) calibrated with pH 4 and 7.02 buffers (MERCK).
- Measurement with Cl^- selective electrode with $AgCl/Ag_2S$ membrane (CRISON, measurement range 5×10^{-6} M to 1 M) with Ag/AgCl reference electrode (CRISON) filled with KNO_3 1M. The calibrating curve (mV/log[Cl^-]) was made, according to the requirements detailed in the electrode manual for measurement of low-chloride concentrations, with chloride standard solutions in bidistilled water. The concentrations of these standards were appropriate for the measurement range necessary at any given moment, depending on the initial PCP concentration in the experiments and therefore, the maximum molar concentration of chlorides expected in the samples ($5\times[PCP]_0$). In both cases the electrodes are connected to a pHmeter (CRISON, model micropH-2002).
- Besides the selective chloride electrode, in some cases, the Mohr method was used: titration with silver nitrate and potassium chromate indicator. This procedure was followed when there was no way to use an electrode (broken or other reasons) and the results were very confident.

During experiments carried out with the addition of oxidants that accelerate the photocatalytic reaction ($S_2O_8^{2-}$, H_2O_2, the effect of which on the reaction will be described later), it was necessary to analyse them. This is because these are compounds that are used up during the reaction and certain amounts have to be added in order to keep the concentration constant. The techniques used were:

- To find out the concentration of persulphate, sulphates were analysed, since during photocatalysis $S_2O_8^{2-}$ becomes $2SO_4^{2-}$. Therefore, when the initial amount of sulphate and the amount at any given moment are known, the amount of persulphate that has decomposed can also be known and thereby the amount that has to be added. The sulphates were measured by turbidimetry (400 nm) in a spectrophotometer (Spectronic 100) with $BaCl_2$, after filtering the samples to take out the TiO_2. The calibrating curves were made with standard solutions of sodium sulphate (MERCK, P.A.)
- The concentration of hydrogen peroxide was determined by titrating the samples taken from the pilot plant with potassium permanganate (0.1 N, MERCK standard solution) in acidic medium.

3.9 Conclusions

(I) The facility used for the photocatalysis experiments is based on solar collectors originally built for thermal applications. The collector surface has been modified (aluminised, fig. 3.3) and the absorber tube substituted by UV-transparent glass.

(II) The pilot plant is made up of twelve twin parabolic trough modules with 384 m^2 of radiation collector surface. They may be operated in once-through (piston flow behaviour), or recirculation mode (perfect mixture behaviour). The calculation of residence time in the reactor is different in each case and thereby, the conversion.

(III) The knowledge of the wavelength interval at which the two UV radiometers used are active is basic to data treatment. It is therefore necessary to calibrate them in situ by comparison with a spectroradiometer.

(IV) The adjustment of the mass balance of the PCP photodecomposition reaction assures that the analytical data are reliable and the organic compounds have not disappeared in some other way (evaporation, adsorption in the reactor, adsorption in the catalyst, etc.) besides photocatalysis.

4. CALCULATION OF THE PHOTON FLUX

4.1 Introduction

Referring to the explanation given in Chapter 2 (Eq. 2.1 and following) on the need to know the quantum yield (Φ) of any photochemical reaction and, thereby, the amount of photons that enter in the reaction while in process, for a large reactor using solar radiation, this is, if possible, even more important for the following reasons:

- The radiation (sunlight) that reaches the earth surface is not constant. This prevents a correct comparison between experiments carried out at different times of the day or seasons of the year or under different atmospheric conditions. There must be a real time radiation measurement and precise knowledge of the spectrum that reaches the earth's surface.

- The extensive bibliography of the photocatalytic decomposition of organic compounds, indicates that the majority of the experiments in which the photon flux in the experimental system is known are carried out in laboratory reactors illuminated by lamps. In order to compare these results with solar radiation or to use the information contained in those reports, it is necessary to know the flux inside the solar reactor. Therefore, it is necessary to find a relationship between the radiometer measurements and the photons that actually reach the reaction.

- The quantum yield of the reaction tested, under each of the experimental conditions used, gives information on the optimum conditions for the decomposition of the contaminant. Knowledge of the photon flux in this situation is fundamental for the determination of the efficiency of the components of the solar reactor (reflective surface, absorber tube, control system, concentration factor, etc.) and the possible modifications to be undertaken, in each case, to improve the conditions of photodegradation.

- Any economic comparison desired between solar radiation and electric lamps, as the UV photon source, requires a knowledge of the photon flux incident on the solar reactor.

The calculation of the photon flux within the PSA photochemical reactor has been undertaken following the flow diagram shown in Figure 4.1.

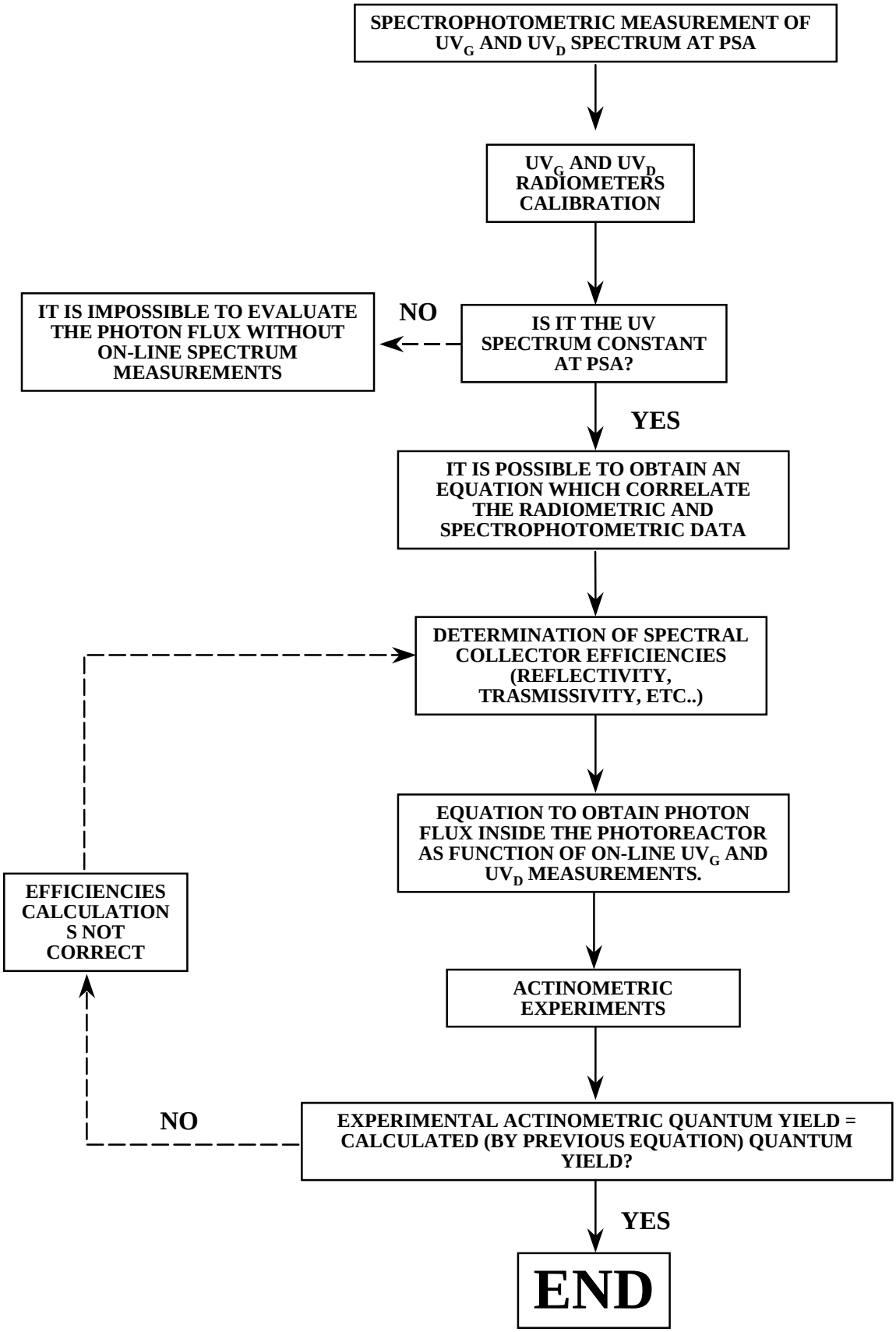

Figure 4.1 *Calculating procedure followed to find out the photon flux inside the reactor as a function of UV radiometer measurements.*

4.2 UV spectra at the PSA

4.2.1 Measurement of UV spectra

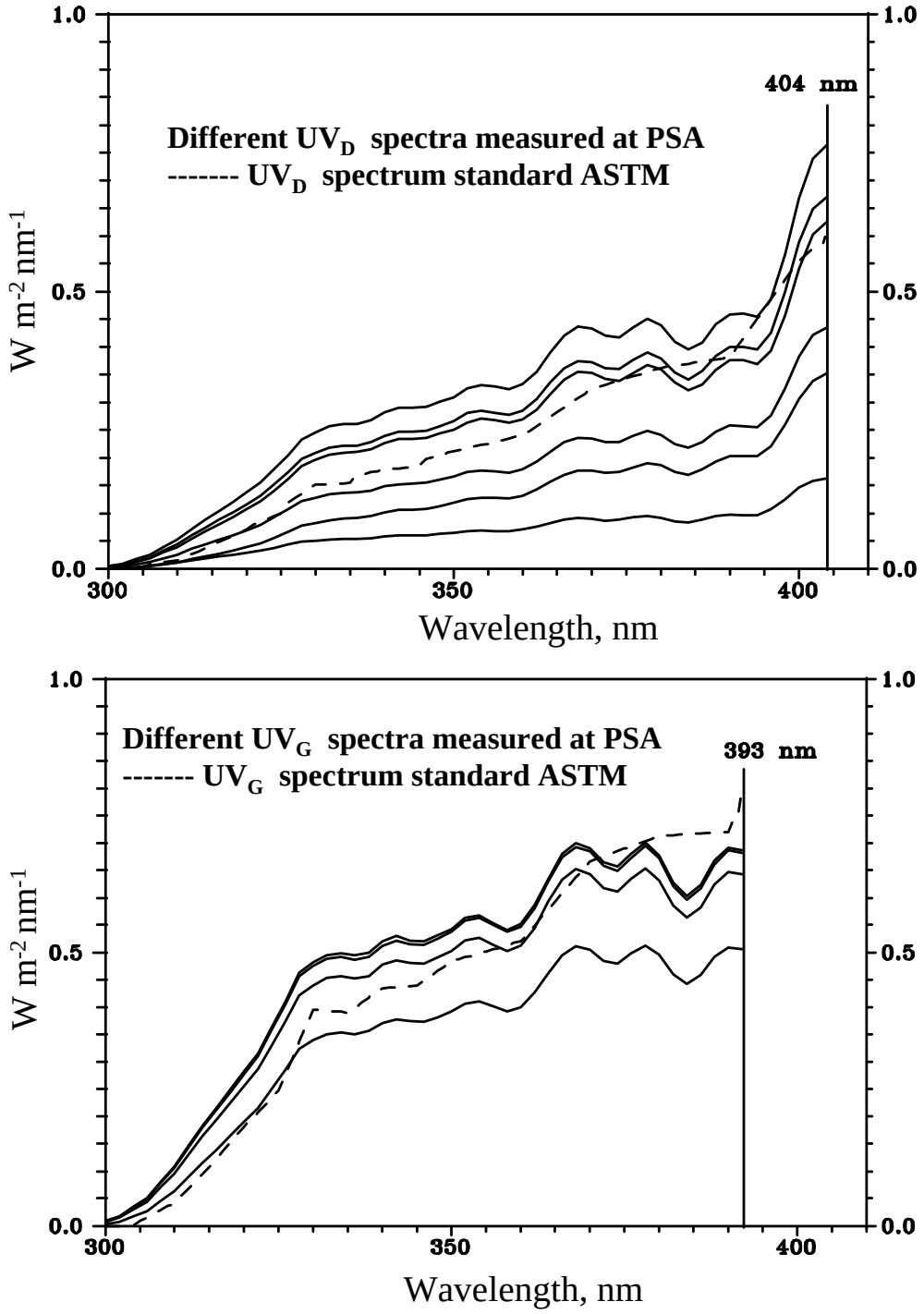

Figures 4.2 and 4.3 *Spectroradiometer measurements taken at the PSA*

The solar UV radiation spectra at the PSA were found with a spectroradiometer (LICOR-1800, see chapter 3) in the same position as each radiometer, so that results are comparable, in order to find a fixed relationship between the spectroradiometer and radiometer measurements. In Figures 4.2 and 4.3 direct and global radiation spectra are shown for different times of the day on different days. The fact that direct UV spectra are up to 404 nm and global up to 393 nm has to do with the calibrating intervals of the radiometers as explained in the previous chapter. The use of spectral data in this way is fundamental to the calculation of photon flux as will be seen later. It may be observed that the spectra measured do not differ substantially from the ASTM standard [*1987a, 1987b*]. However, this cannot be guaranteed if the data for all the spectra are not represented in a standardized manner as in Figures 4.4 and 4.5, when they can then be compared at different times of the day and different seasons of the year (with different radiation). This standardization can be done for any wavelength interval applying the following operations. Summations have been used to treat the discrete values nm to nm:

$$f_{D,\lambda} = \frac{UV_{D,\lambda}}{\sum_{\lambda=300nm}^{\lambda=404nm} UV_{D,\lambda}}, \text{ therefore } \sum_{\lambda=300nm}^{\lambda=404nm} f_{D,\lambda} = 1 \qquad (4.1)$$

and likewise for global UV:

$$f_{G,\lambda} = \frac{UV_{G,\lambda}}{\sum_{\lambda=300nm}^{\lambda=393nm} UV_{D,\lambda}}, \text{ therefore } \sum_{\lambda=300nm}^{\lambda=393nm} f_{G,\lambda} = 1 \qquad (4.2)$$

where $f_{i,\lambda}$, is the fraction of power associated with the wavelength λ and $UV_{i,\lambda}$ is the irradiance, W m^{-2}, corresponding to each wavelength and measured with the spectroradiometer. In Figures 4.4 and 4.5 the homogeneity of all the spectra recorded and their great similarity to the ASTM standards may be observed. In order to obtain a constant relationship between spectroradiometric data and the data recorded by the global and direct UV sensors, sufficient historical data must be available to assure that the direct and global UV spectra at the PSA is constant, that is, the fraction of irradiance corresponding to each wavelength is always the same.

As it was not possible to obtain historical data, to find out the solar UV radiation spectrum behavior and the measurements that have been made in other places, these were taken from literature. *Riordan et al.* [*1990*], compiled a large part of the existing information on UV measurements in the world and atmospheric conditions effects on it.

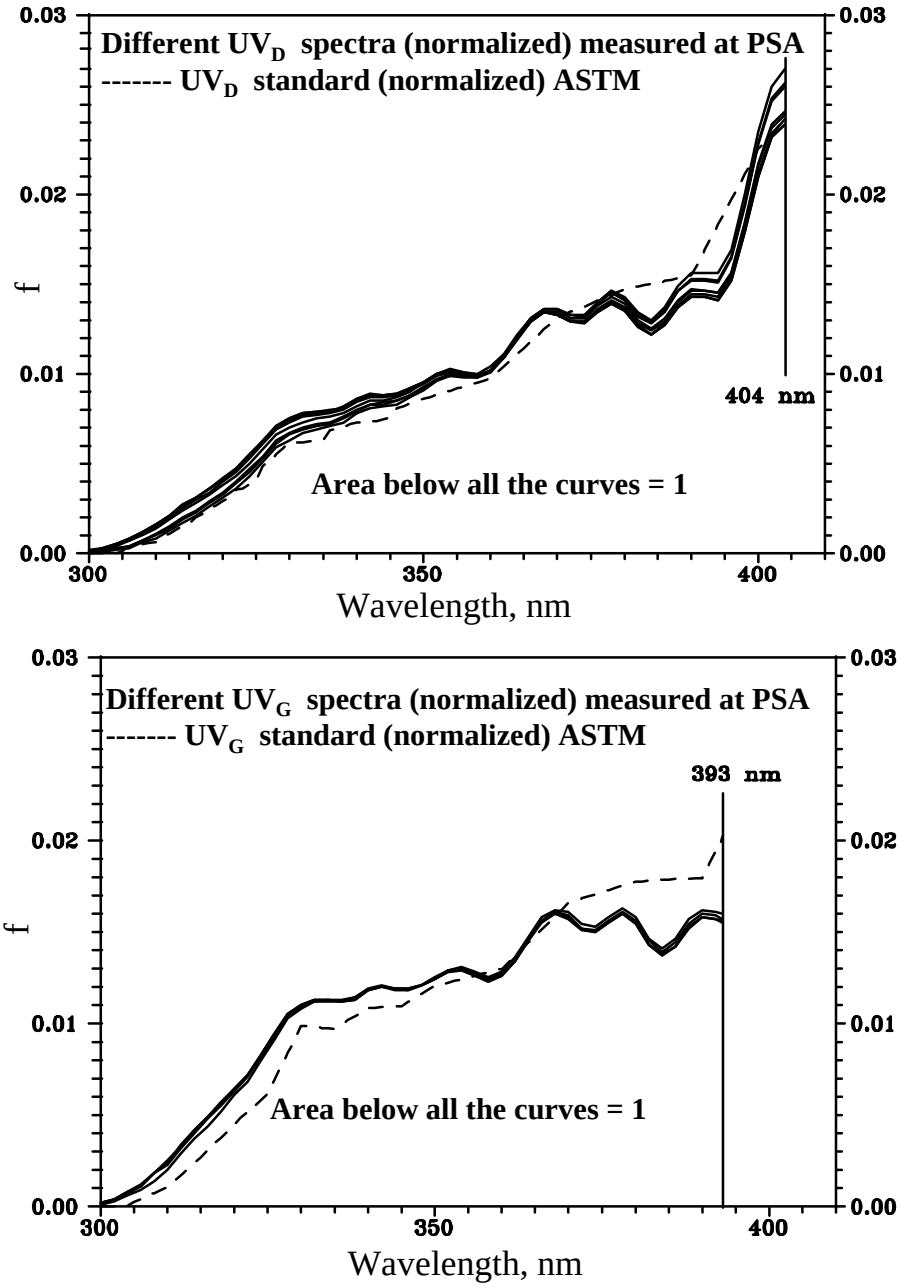

Figure 4.4 and 4.5 *Spectra from Figures 4.2 and 4.3 standardized to obtain the fraction of power ($f_{i,\lambda}$) associated with each wavelength.*

Transmittance (T_λ) of the atmosphere against a definite wavelength radiation is represented by the following expression [*Iqbal, 1983*]:

$$T_\lambda = T_{R,\lambda} T_{a,\lambda} T_{o,\lambda} T_{g,\lambda} T_{v,\lambda} \tag{4.3}$$

$T_{R,\lambda}$ is the spectral transmittance resulting from the dispersion produced by the molecules of air (many of which have dimensions ≈1Å, Raleigh dispersion). $T_{a,\lambda}$ is the spectral transmittance related to absorption and dispersion by aerosols (solid or liquid particles suspended in the air). $T_{o,\lambda}$ corresponds to the effect of the ozone layer. $T_{g,,\lambda}$ is the

transmittance resulting from absorption of atmospheric gases (such as carbon dioxide and oxygen). $T_{v,,\lambda}$ corresponds to the absorption by steam. The effect of each one of these parameters in the range in question (300 nm-404 nm) would be the following:

- $T_{R,\lambda}$ = exp (-0.008735 $\lambda^{-4.08}$ M'), where M' is the air mass corrected according to its density, which depends on the pressure and, therefore, the altitude. According to this, this factor would be practically constant for given site.
- $T_{a,\lambda}$ = exp ($-\lambda^{-\alpha}$ β M) where M is the mass of air, β is the coefficient of turbidity, which usually varies between 0 and 0.5, and is a reflection of the amount of aerosols in the air and α is an index of the size of those aerosols molecules. As the PSA site is practically in a desert (with few environmental variables) exempt of atmospheric contamination, making β low (<0.1) and varying only slightly, if the existing data for similar zones (Albuquerque, El Paso, Phoenix) in the United States [*Hulstrom et al., 1985*] are kept in mind. For the same reasons, α is practically constant.
- $T_{o,\lambda}$ is constant for a specific site since the ozone layer has a practically constant thickness.
- $T_{g,\lambda}$ only influences wavelengths over UV.
- $T_{v,\lambda}$ does not affect the UV spectrum either.

Keeping in mind then, the different transmittances, it may be assumed that the solar UV spectrum does not vary substantially within a specific site throughout the year, unless atmospheric conditions (except clouds) do so. In fact, in Madrid [*Fabero et al., 1992*] the UV spectrum has been demonstrated to stay the same in different seasons of the year, and therefore, at the PSA, where the conditions are much more stable due to its location, the UV spectral distribution (300nm-404nm) may be considered constant. If this consideration is erroneous, the results must show it since it is used as photon flux calculation basis.

4.2.2. Calculation of the UV spectrum based on radiometric data

If the spectrum of direct and global UV radiation is assumed to have fixed form, similar to that in Figures 4.4 and 4.5, then two average standardized spectra are available in all spectra (between the wavelengths measured by the radiometers) measured with the spectrophotometer and can be considered as standards for the PSA. These are given in Figure 4.6 and tabulated at 2 nm intervals in table 4.1. Therefore, using the average standardized spectrum and the irradiance data (W m^{-2}), measured by each radiometer, the spectral distribution can be calculated for all of these data:

$$\begin{aligned} UV^{*}_{D.\lambda} &= f_{D,\lambda} UV_D \\ UV^{*}_{G.\lambda} &= f_{G,\lambda} UV_G \end{aligned} \qquad (4.4)$$

where $UV^{*}_{D,\lambda}$ and $UV^{*}_{G,\lambda}$ are the spectra data calculated with $f_{i,\lambda}$ and the radiometer data

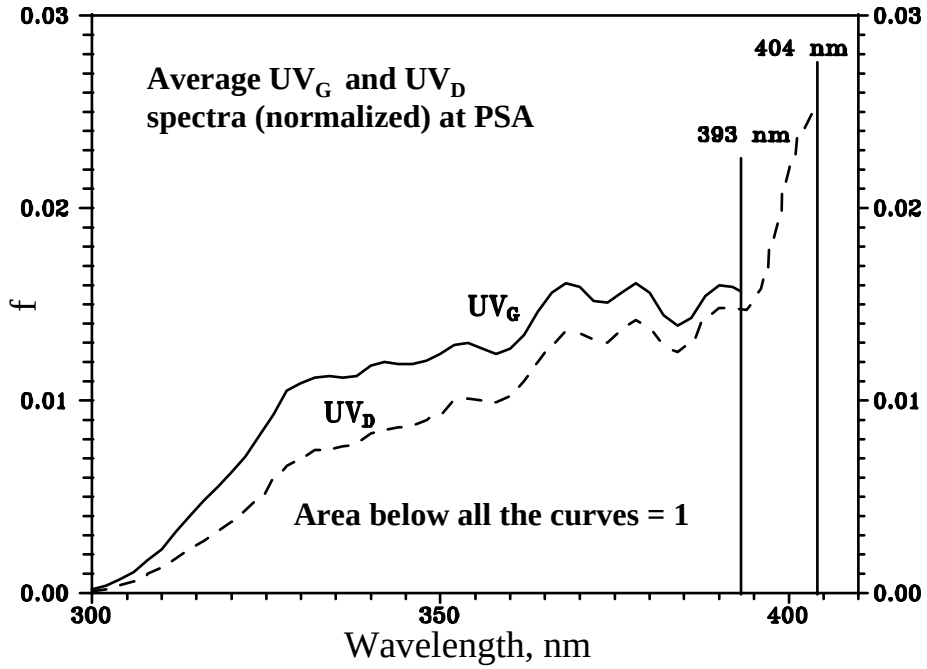

Figure 4.6 *Average spectra obtained from those given in Figures 4.4 and 4.5.*

λ, nm	$f_{G,\lambda}$	$f_{D,\lambda}$	λ, nm	$f_{G,\lambda}$	$f_{D,\lambda}$	λ, nm	$f_{G,\lambda}$	$f_{D,\lambda}$
300	0.0002	0.0001	336	0.0112	0.0076	372	0.0152	0.0131
302	0.0004	0.0002	338	0.0113	0.0078	374	0.0151	0.0130
304	0.0007	0.0004	340	0.0118	0.0083	376	0.0156	0.0137
306	0.0011	0.0006	342	0.0120	0.0085	378	0.0161	0.0142
308	0.0017	0.0010	344	0.0119	0.0086	380	0.0156	0.0138
310	0.0023	0.0013	346	0.0119	0.0087	382	0.0144	0.0129
312	0.0032	0.0018	348	0.0121	0.0090	384	0.0139	0.0125
314	0.0040	0.0023	350	0.0124	0.0094	386	0.0143	0.0131
316	0.0048	0.0037	352	0.0129	0.0099	388	0.0154	0.0142
318	0.0055	0.0032	354	0.0130	0.0101	390	0.0160	0.0148
320	0.0063	0.0037	356	0.0127	0.0100	392	0.0159	0.0148
322	0.0071	0.0043	358	0.0124	0.0099	393	0.0157	0.0147
324	0.0082	0.0050	360	0.0127	0.0102	394	0.0156*	0.0147
326	0.0093	0.0058	362	0.0134	0.0110	396	0.0167*	0.0158
328	0.0105	0.0088	364	0.0146	0.0120	398	0.0195*	0.0186
330	0.0109	0.0070	366	0.0156	0.0130	400	0.0227*	0.0220
332	0.0112	0.0074	368	0.0161	0.0135	402		0.0242
334	0.0113	0.0075	370	0.0159	0.0135	404		0.0250

*The values for $f_{G,\lambda}$ of 394 nm to 400 nm were also obtained with equation 4.2 with the spectrum data corresponding to those wavelengths. They are included to complete the table of values up to 400 nm, although they are not used in the calculations made in this work.

Table 4.1

4.2.3 UV Photon flux at the PSA

Once the spectral distribution of the radiometer measurements is known, the number of photons incident per unit of time and surface are (N) corresponding to those measurements can be found. Remembering Eq. 2.5, which relates the number of photons from a given polychromatic source of light to the energy corresponding to each wavelength, this can be transformed for this case into the following (using summations of discrete values):

$$N_D = \frac{1}{hc}\sum_{\lambda=300nm}^{\lambda=404nm} UV^*_{D,\lambda}\lambda \quad for\ direct\ UV$$
$$N_G = \frac{1}{hc}\sum_{\lambda=300nm}^{\lambda=393nm} UV^*_{G,\lambda}\lambda \quad for\ global\ UV \qquad (4.5)$$

where N is incident photons between 300 and 404 nm (N_D), or 300 and 393 nm (N_G), per m^2 and second, when UV is measured in W m^{-2} and λ in nm, with speed of light c = 2.998 × 10^{17} nm s^{-1} and the Planck's constant h = 6.626 × 10^{-34} J s. But, as the spectral distribution is assumed to be constant, equation 4.4 yields:

$$N_D = \frac{UV_D}{hc}\sum_{\lambda=300nm}^{\lambda=404nm} f_{D,\lambda}\lambda \quad for\ direct\ UV$$
$$N_G = \frac{UV_G}{hc}\sum_{\lambda=300nm}^{\lambda=393nm} f_{G,\lambda}\lambda \quad for\ global\ UV \qquad (4.6)$$

Therefore, the wavelength considered equivalent to each of the summations would be:

$\sum_{\lambda=300nm}^{\lambda=404nm} f_{D,\lambda}\lambda$ = 368.79 nm

$\sum_{\lambda=300nm}^{\lambda=393nm} f_{G,\lambda}\lambda$ = 357.53 nm

To calculate the values corresponding to other intervals, the same procedure is followed. The next values correspond to the other two intervals of interest to this work, 387 nm, which is the maximum wavelength of radiation that can produce an e^-/h^+ pair on the TiO_2 surface and 400 nm, which is the visible UV threshold.

$\sum_{\lambda=300nm}^{\lambda=387nm} f_{D,\lambda}\lambda$ = 248.57 nm $\sum_{\lambda=300nm}^{\lambda=400nm} f_{D,\lambda}\lambda$ = 330.41 nm

$\sum_{\lambda=300nm}^{\lambda=387nm} f_{G,\lambda}\lambda$ = 320.71 nm $\sum_{\lambda=300nm}^{\lambda=400nm} f_{G,\lambda}\lambda$ = 407.60 nm

Returning to equation 4.6, the number of photons corresponding to the average radiation at any given instant for each of the radiometers is:

$$N_{D,300-404nm} = 1.856 \times 10^{18} UV_D \quad ; \quad N_{G,300-393nm} = 1.798 \times 10^{18} UV_G \qquad (4.7)$$

where N is the incident photons between 300 and 404 nm (N_D), or 300 and 393 nm (N_G), per m^2 and second, when UV is measured in W m^{-2} and λ in nm, with speed of light c = 2.988 ×

10^{17} nm s^{-1} and the Planck's constant h = 6.626 × 10^{-34} J s. If Einsteins (moles of photons) are used as the unit, the result is:

$$I_{D,300-404nm} = \frac{N_{D,300-404nm}}{N_0} = 3.083 \times 10^{-6} UV_D$$
$$I_{G,300-393nm} = \frac{N_{G,300-393nm}}{N_0} = 2.985 \times 10^{-6} UV_G \quad (4.8)$$

where I is obtained as Einstein m^{-2} s^{-1}. The equations for the other intervals of interest are:

$$I_{D,300-387nm} = 2.087 \times 10^{-6} UV_D \qquad I_{D,300-400nm} = 2.762 \times 10^{-6} UV_D$$
$$I_{G,300-387nm} = 2.678 \times 10^{-6} UV_G \qquad I_{G,300-400nm} = 3.403 \times 10^{-6} UV_G \quad (4.9)$$

If compared with the data corresponding to the standard UV-ASTM spectrum, which appears in chapter 2.2:

UV_D = 22 W m^{-2} →I = 6 × 10^{-5} Einstein m^{-2} s^{-1}
UV_G = 46 W m^{-2} →I = 14 × 10^{-5} Einstein m^{-2} s^{-1}

4.3 Photon flux inside the reactor

4.3.1 Collector Efficiency

In Figure 4.7 all the factors related to collector efficiency are shown, the majority of which have already been described in detail in chapter 3, where the original characteristics of the collectors, given their initial thermal application and the modifications made for their use in photochemistry, were explained.

The definition of each of those factors and their values are:

- η_s originates from the error produced during solar tracking, attributable to the control system (photocell and azimuth+elevation motors) The value of this factor was determined experimentally and is 0.92 [*Blanco et al., 1991*].
- η_C, has to do with the construction of the module and is 0.91 (see section 3.2).
- $\eta_{R,\lambda}$ is the reflectivity (which is a function of the wavelength) of the aluminized surface of the parabolic mirrors. Since the hemispheric reflection spectrum does not vary over a wide range (between 85% and 89% of the incident radiation) and that variation is uniformly distributed over the whole interval of interest (300-404 nm) an average spectral distribution will be considered. This average was 87.2*% [Sánchez,1991, 1992*] with the material in its original film form. However it should be noted that after being glued to the collector surface, this is lowered to 69.5% (measured with a portable reflectometer at 660 nm),

percentage which must be corrected by a factor of 1.22 (see Section 3.2.1) and therefore $\eta_{R,0}$ = 0.85%. As the surface is outdoors and could get dirty or be damaged, this has to be measured periodically and in each case the value is $\eta_{R,i}$ = 1.22 R/100, where R is the portable reflectometer measurement (%).

- $\eta_{T,\lambda}$ is the spectral transmissivity of the absorber tube and its value appears in Table 3.2.

With the combination of these factors and equations 4.7 to 4.9, the photon flux for each case has been calculated as explained below.

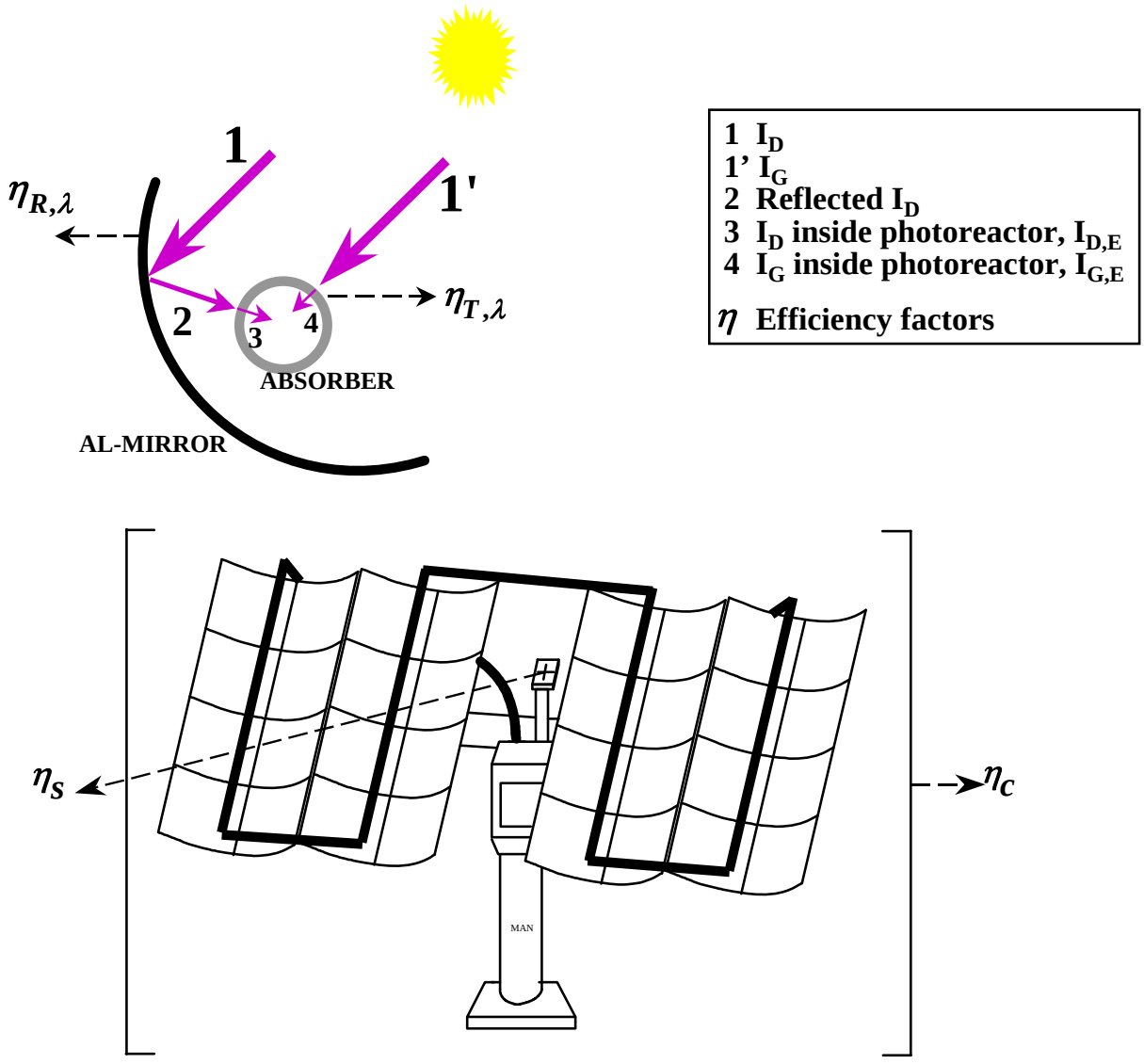

Figure 4.7. *Drawing of the various loss factors (η) affecting the photon flux (I) inside the photoreactor.*

4.3.2 Photon flux from direct UV radiation

In Figure 4.7 the path followed by I_D until it arrives inside the absorber tube is shown. It must arrive at the surface and be reflected (part is lost due to $\eta_{R,\lambda}$) in the right direction (here η_s affects) by the real mirror surface (η_C), before penetrating ($\eta_{T,\lambda}$) in the tube. Furthermore, the parabolic trough concentration factor must also be considered (ratio of surface area of the parabola capturing the radiation and surface area of the tube, S_p/S_T). Therefore, the effective photon flux corresponding to the direct UV inside the absorber ($I_{D,E}$) is:

$$I_{D,E} = f\left(I_D, \frac{S_P}{S_T}, \eta_C, R, \eta_{T,\lambda} \right) \tag{4.10}$$

Since $\eta_{T,\lambda}$ depends on the wavelength, in order to evaluate $I_{D,E}$ equation 4.6 must be recalculated as follows:

$$N_{D,E} = \left(0.92 \times \frac{S_P}{S_T} \times 0.91 \times 1.22 \frac{R}{100} \right) \frac{UV_D}{hc} \sum_{\lambda=300nm}^{\lambda=404nm} f_{D,\lambda} \frac{\eta_{T,\lambda}}{100} \lambda \tag{4.11}$$

Consequently, the weighted up wavelengths, corresponding as much to the interval of the Eq. 4.11 as to the other two of interest in this case, which result from the combination of tables 3.2 and 4.1 are:

$$\sum_{\lambda=300nm}^{\lambda=404nm} f_{D,\lambda} \frac{\eta_{T,\lambda}}{100} \lambda = 319 \text{ nm}$$

$$\sum_{\lambda=300nm}^{\lambda=400nm} f_{D,\lambda} \frac{\eta_{T,\lambda}}{100} \lambda = 284 \text{ nm}$$

$$\sum_{\lambda=300nm}^{\lambda=387nm} f_{D,\lambda} \frac{\eta_{T,\lambda}}{100} \lambda = 211 \text{ nm}$$

and equations 4.8 to 4.9 are now, for direct radiation:

$$I_{D,E(300-404)} = 2.724 \times 10^{-8} UV_D R \left(\frac{S_P}{S_T} \right) \tag{4.12a}$$

$$I_{D,E(300-400)} = 2.428 \times 10^{-8} UV_D R \left(\frac{S_P}{S_T} \right) \tag{4.12b}$$

$$I_{D,E(300-387)} = 1.803 \times 10^{-8} UV_D R \left(\frac{S_P}{S_T} \right) \tag{4.12c}$$

where, if UV_D is W m^{-2} and R is %, the units of $I_{D,E}$ are Einstein m^{-2} s^{-1} incident in the inside of the tube.

The knowledge, as precise as possible, of S_p/S_T is used to determine the values of $I_{D,E}$ in each case. For this it is necessary to make the corresponding trigonometric calculations based on

Figures 4.8 and 4.9. These figures are meant only as illustrations of the calculations carried out in order to understand them better and, therefore, they are not made to scale and the curve of the parabola does not coincide exactly with that of the parabolic troughs used.

The calculations for the modules with half the mirrors covered (Figure 4.9) corresponds to experiments performed under these conditions. Tests have also been carried out with modules without concentrating the radiation (in horizontal position and without solar tracking), but the calculation used in this case is very simple and does not need to be illustrated with schematic drawing, as will be seen later. These experiments were carried out to evaluate the relationship existing between the reaction rate and photon flux (see Figure 2.5), since under these conditions less radiation reaches the absorber tube. This permits to know the zone of that relationship where the reactor tested is at: $r = f(I)$, $r = f(I^{0.5})$ or $r = f(I^{0})$.

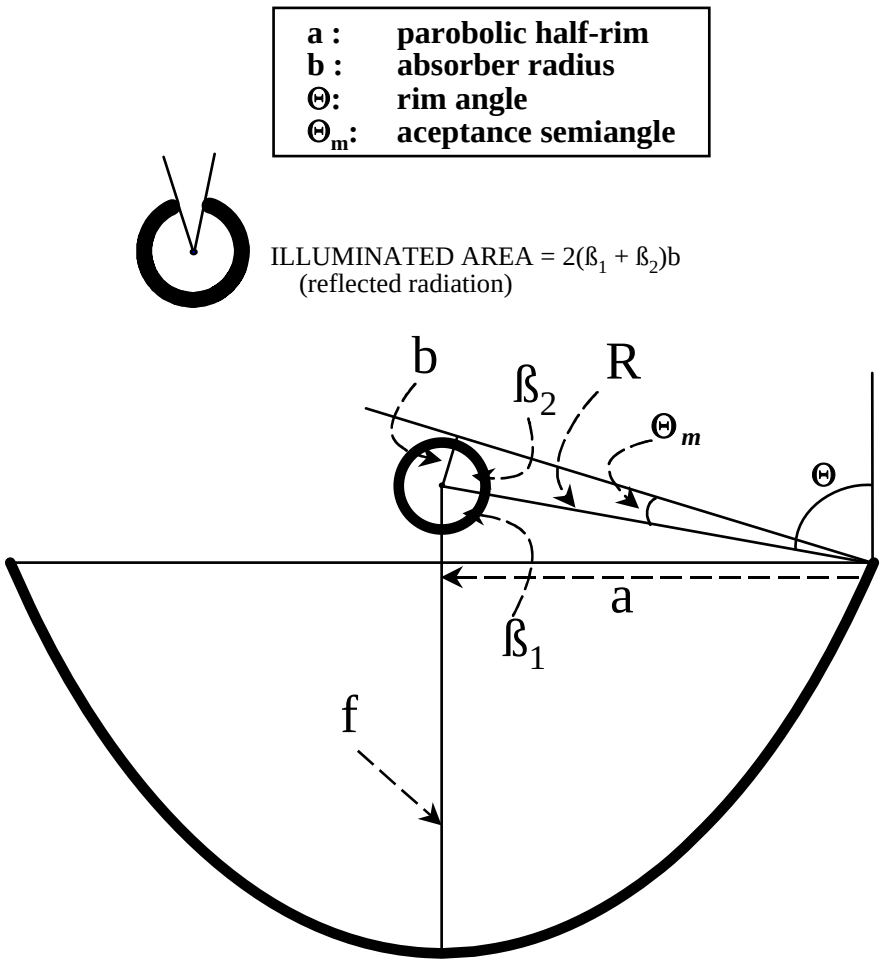

Figure 4.8. *"Trigonometric" drawing used for the calculation of the absorber surface illuminated by the radiation reflected on the parabolic surface.*

Some of the parameter values have already been described in detail (chapter 3): a = 905 mm, b (tube inner radius) = 28 mm, θ = 70.52° (0.392π radians), f = 640 mm. This known, R = a/senθ = 960 mm and therefore, the semiangle of acceptance is θ_m = arcsen (b/R) = 1.67° (0.00928π radians). In a parabolic concentrator, the value of S_p/S_T maybe defined from two different points of view: geometric concentration ratio ($R_{C,g}$) and the concentration ratio calculated from the collector optics ($R_{C,op}$). In both, the length of the parabola (4.5 m) and the absorber (2×2.1 m) is obviated, since this difference (0.93 = 4.2 m/4.5 m) has already been considered in η_C and it is incorrect to include it here.

$$R_{C,g} = \frac{surface\ area\ collecting\ the\ radiation}{absorber\ cylinder\ area} = \frac{2a}{2\pi\ b} \tag{4.13a}$$

$$R_{C,op} = \frac{unshaded\ area}{area\ where\ reflected\ radiation\ incides} = \frac{2(a-b)}{2b(\beta_1+\beta_2)} \tag{4.13b}$$

according to this $R_{C,g}$ = 10.3 and, if $\beta_1 = \theta$ = 0.392π rad and $\beta_2 = (\pi/2) - \theta_m$ = 0.491π rad, then $R_{C,op}$ = 11.3, valid only for the modules used in these experiments.

If half of each parabola is covered, the outline of work would be what is represented in Figure 4.4. In this case equations 4.13 would be different, since the collecting surface is half and the illuminated surface is different:

$$R_{C,g} = \frac{surface\ area\ collecting\ the\ radiation}{absorber\ cylinder\ area} = \frac{a}{2\pi\ b} \tag{4.14a}$$

$$R_{C,op} = \frac{unshaded\ area}{area\ where\ reflected\ radiation\ incides} = \frac{(a-b)}{b(\alpha_1+\alpha_2+\alpha_3)} \tag{4.14b}$$

therefore $R_{C,g}$ = 5.15 and $R_{C,op}$ = 7.37, angles α having been calculated in the following manner:

$$\alpha_1 + \frac{\pi}{2} + \theta'_m = \pi;\ \text{where,}\ \theta'_m = arcsen\frac{b}{R} = 2.51^\circ = 0.0139\pi\ rad$$

$$\underline{\alpha_1 = 87.5^\circ = 0.4861\pi\ rad}$$

$$\alpha_2 = \theta - \hat{f}R$$

$$where:\ \hat{f}R + \frac{\pi}{2} + \arccos\frac{b}{R'} = \pi; \qquad y = \frac{b^2}{4f}; \qquad (R')^2 = (f-y)^2 + b^2$$

$$\underline{\alpha_2 = 68.0^\circ = 0.378\pi\ rad}$$

$$\alpha_3 = \arccos\frac{b}{R}$$

$$\underline{\alpha_3 = 88.3^\circ = 0.491\pi\ rad}$$

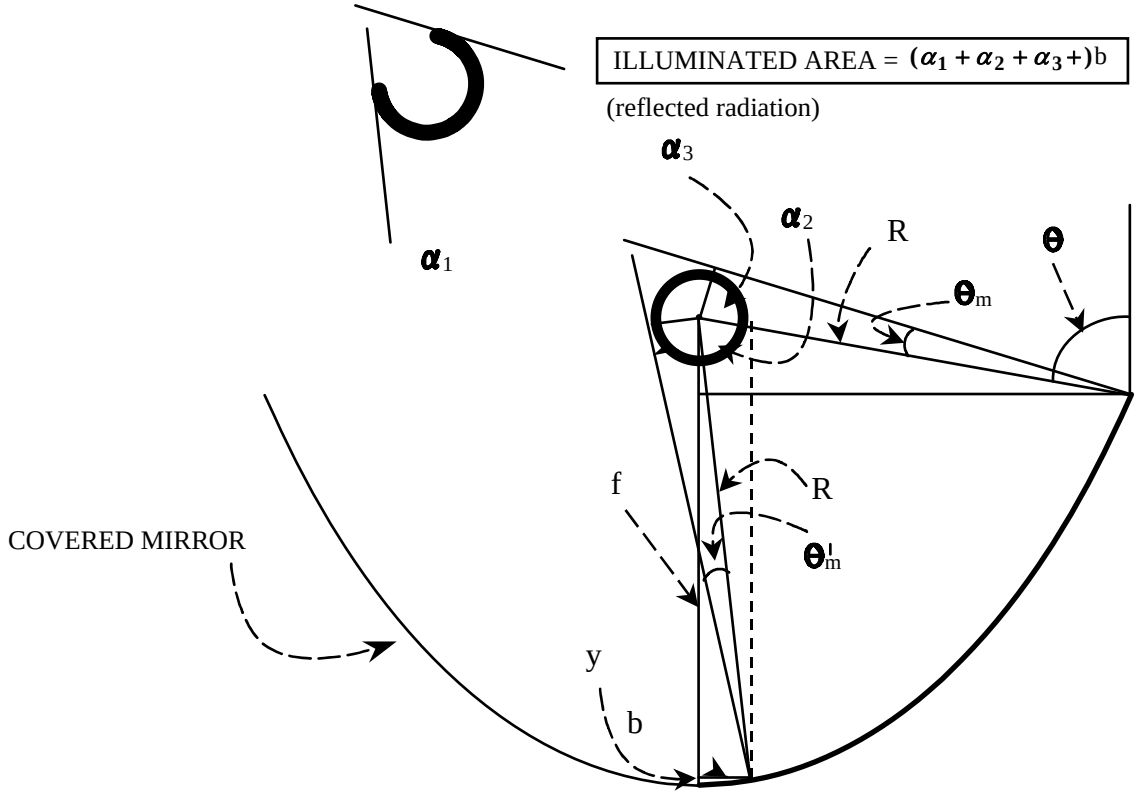

Figure 4.9. *Drawing of the calculation of the absorber surface illuminated by the radiation reflected on "half" of the parabolic mirrors.*

Thus, the simplest expression of equations 4.12, for the case of completely uncovered mirrors and using the "optic" concentration ratio is:

$$I_{D,E(300-404)} = 3.078 \times 10^{-7} UV_D R \quad (4.15a)$$

$$I_{D,E(300-400)} = 2.744 \times 10^{-7} UV_D R \quad (4.15b)$$

$$I_{D,E(300-387)} = 2.037 \times 10^{-7} UV_D R \quad (4.15c)$$

and for the half-covered case:

$$I_{D,E(300-404),1/2} = 2.008 \times 10^{-7} UV_D R \quad (4.15d)$$

$$I_{D,E(300-400),1/2} = 1.789 \times 10^{-7} UV_D R \quad (4.15e)$$

$$I_{D,E(300-387),1/2} = 1.329 \times 10^{-7} UV_D R \quad (4.15f)$$

where, if UV_D is W m^{-2} and R is %, the units of $I_{D,E}$ are Einstein m^{-2} s^{-1} incident inside the tube through the surface illuminated by direct irradiance.

Once this is known, the same ratio can be calculated (using equations 4.12) for the reactor volume (41.4 L/module). The unshaded area per module is: 2(a-b) × 4.5 m × 4 = 31.57

m^2/module. Consequently the ratio is 0.763 m^2/L. Therefore, S_p/S_T is substituted for this amount in equations 4.12. In this way, photon flux is obtained in units congruent with reaction rate (M s^{-1}) so that a estimate quantum yield for direct radiation can be obtained ($\Phi_{E,D}$) similar to that in equation 2.2, but using moles of incident photons instead of moles of photons absorbed by the catalyst.

$$I^*_{D,E(300-404)} = 2.078 \times 10^{-8} UV_D R \quad (4.16a)$$

$$I^*_{D,E(300-400)} = 1.852 \times 10^{-8} UV_D R \quad (4.16b)$$

$$I^*_{D,E(300-387)} = 1.376 \times 10^{-8} UV_D R \quad (4.16c)$$

$$\Phi_{E,D} = \frac{reaction\ rate}{I^*_{D,E}} \quad (4.17)$$

where $I^*_{D,E}$ are Einstein $L^{-1}s^{-1}$ incident inside the tube by direct irradiance and, for the partially covered mirrors, the value is exactly one half:

$$I^*_{D,E(300-404),1/2} = 1.039 \times 10^{-8} UV_D R \quad (4.16d)$$

$$I^*_{D,E(300-400),1/2} = 9.260 \times 10^{-9} UV_D R \quad (4.16e)$$

$$I^*_{D,E(300-387),1/2} = 6.88 \times 10^{-9} UV_D R \quad (4.16f)$$

4.3.3. Photon flux from global UV radiation

It is possible to define global radiation in the same way as Eq. 4.10, which depends on the path followed by direct radiation until it enters the tube, with the following considerations:

- Values directly obtained from the global radiation sensor (Eppley-TUVR), as well as those obtained with the spectrophotometer will be used.
- The range of measurement of this radiometer is up to 393 nm and therefore the power fraction data in table 4.1 corresponding to the global UV spectrum should be used, that is $f_{G,\Psi}$.
- Global radiation is collected directly by the transparent absorber tube without intervention of the collector characteristics. Only the transmissivity of the glass, $\eta_{T,\lambda}$, affects it.

$$I_{G,E} = f(I_G, \eta_{T,\lambda}) \quad (4.18)$$

where $I_{G,E}$ is the effective photon flux corresponding to global UV inside of the absorber and therefore, equation 4.6 would be as follows:

$$N_{G,E} = \frac{UV_G}{hc} \sum_{\lambda=300nm}^{\lambda=393nm} f_{G,\lambda} \frac{\eta_{T,\lambda}}{100} \lambda \quad (4.19)$$

The following calculation is similar to that with direct UV. The value of the summations for the three ranges of interest for global radiation are:

$$\sum_{\lambda=300nm}^{\lambda=400nm} f_{G,\lambda} \frac{\eta_{T,\lambda}}{100} \lambda = 347 \text{ nm}$$

$$\sum_{\lambda=300nm}^{\lambda=393nm} f_{G,\lambda} \frac{\eta_{T,\lambda}}{100} \lambda = 302 \text{ nm}$$

$$\sum_{\lambda=300nm}^{\lambda=387nm} f_{G,\lambda} \frac{\eta_{T,\lambda}}{100} \lambda = 270 \text{ nm}$$

and equations 4.8 and 4.9, in the case of global radiation in the absorber are:

$$I_{G,E(300-400)} = 2.905 \times 10^{-6} UV_G \quad (4.20a)$$

$$I_{G,E(300-393)} = 2.530 \times 10^{-6} UV_G \quad (4.20b)$$

$$I_{G,E(300-387)} = 2.254 \times 10^{-6} UV_G \quad (4.20c)$$

where if UV_G is expressed in W m^{-2}, the units of $I_{G,E}$ are Einstein m^{-2} s^{-1} inside the tube.

To calculate the relationship with reactor volume, the procedure is the same as for direct. The total absorber tube area of each module is considered the total surface of incident global radiation (2πbl x 4), since there is no shading, this is 2.96 m2, and the volume is 41.4 L. Therefore, the ratio is 0.071m^2/L, and the global UV equations equivalent to 4.16 are:

$$I^*_{G,E(300-400)} = 2.077 \times 10^{-7} UV_G \quad (4.21a)$$

$$I^*_{G,E(300-393)} = 1.796 \times 10^{-7} UV_G \quad (4.21b)$$

$$I^*_{G,E(300-387)} = 1.600 \times 10^{-7} UV_G \quad (4.21c)$$

where the units of $I^*_{G,E}$ are Einstein L^{-1} s^{-1} incident in the interior of the tube through the illuminated surface by global irradiance, when the units of UV_G are in W m^{-2}.

In this case, for experiments with half of the mirrors covered, the expressions are the same since this time there is no effect from the reflected radiation. In the experiments performed without using concentrated radiation, this is, with the modules completely horizontal and face up, the incident radiation is calculated only with these expressions.

4.4 Actinometric experiments

An actinometer is a chemical or physical system by which the number of photons incident on said actinometer may be determined. In a chemical actinometer, the photochemical conversion is directly related to the amount of photons absorbed. This method has been used since the 30's [*Leighton et al., 1930*], but due to recent progress in radiation sensors, semiconductor and electronic equipment development, physical measuring devices have

become more popular in the photochemical community [*Feister et al., 1992*]. In the case of reactors with simple geometries, they are preferable because they are very quick, simple and precise. Furthermore, they permit the radiation to be determined at the same time that the experiments are being performed. In the case in hand, the chemical actinometer was used as a method of validation (see outline of work in Figure 4.1) for all the calculations performed to obtain the equations detailed in section 4.3. Based on this, all the calculations of this thesis are carried out, for which a method of checking that all these equations are reasonably correct was necessary due to the multitude of parameters involved during their deduction (Eq. 4.10 and 4.18). A good chemical actinometer meets the following *specifications [Kuhn et al., 1989; Rabek, 1982*]:

- The photochemical system should be simple and the reaction should be reproducible, under well-defined and easily controlled conditions. The quantum yields should be well known for a wide range of wavelengths, if polychromatic wavelength radiation has to be measured.
- The quantum yield should be independent of the intensity of radiation, actinometer concentration and temperature (the pilot plant cannot be thermostatized.)
- The reagents and products should be reasonably stable, so errors do not arise between the time the sample is taken and the time it is analyzed.
- The analytic methods should be simple.
- The reagents should be easily synthesized and, even better, commercially available. This is, if possible, much more important in the case of pilot plants, because of the large volumes of actinometer that have to be prepared.
- The system should be sufficiently sensitive for low radiation intensities and the evaluation of photons absorbed should be simple.

In this case a common uranyl-oxalate system was used (Eq. 4.22) [*Cassano, 1968; Rabek, 1982; Curcó, 1994*]. It is characterized by: a) kinetics of zero order with regard to the concentration of oxalic acid (r_{OXALIC}=k I), b) the simplicity of the analysis to be performed (as explained below), c) having quantum yield independent of intensity of radiation (in the working range) and experimental temperature and, d) it does not react in the dark. In addition to this, the products used are all commercially available and quantum yield stays practically constant within a wide range of wavelengths, as can be seen in table 4.2. The reactions that take place, when the radiation is incident in the actinometric mixture, go through a state of excitation ($UO_2^{2+} \rightarrow UO_2^{2+}$*), and another of real oxidation:

$$\begin{aligned} UO_2^{2+} &\xrightarrow{h\nu} \left(UO_2^{2+}\right)^* \\ \left(UO_2^{2+}\right)^* + H_2C_2O_4 &\longrightarrow UO_2^{2+} + CO + CO_2 + H_2O \end{aligned} \tag{4.22}$$

Oxalic acid 0.05 M (prepared from $H_2C_2O_4$-$2H_2O$, Merck A.G.) and 0.01 M uranyl (prepared from $(NO_3)_2UO_2$-$6H_2O$, Probus, A.G.) were used. Absorptivity of this solution may be estimated from:

$$\frac{Absorbed\ Photons}{Incident\ Photons} = 1 - \exp\left(-\mu_\lambda 2b\right) \tag{4.23}$$

where b is the inside reactor radius (2.8 cm), 2b being the light pathlength and μ_λ [*Cassano, 1968*] is the coefficient of absorptivity, which appears in table 4.2. This coefficient was calculated for the experimental conditions described using $\mu_\lambda = \varepsilon_\lambda c$, where ε_λ is the coefficient of molar absorvance (also called the coefficient of extinction, M^{-1} cm^{-1}) and *c* is the solute concentration (M). μ_λ remains constant during the experiment, according to equation 4.22, since it depends only on the concentration of uranyl.

The quantum yield (Φ_λ) of this reaction may vary, if high oxalic conversion rates are attained or if the oxalic/uranyl ratio is not constant and, therefore, in all the actinometric experiments, the conversion was less than 20% [*Cassano, 1968*]. The experimental set-up for these measurements was the pilot plant, with the configuration shown in Figure 3.7b, with only one module and working in once-through mode (Eq. 3.3 and 3.4). The use of large tanks for this experiment was undesirable, since the minimum volume possible was to be used, due to the high price of uranyl. The total volume of water was 230 L and the amount of oxalic acid and uranyl was added proportionally to it. V_R is 41.4 L and Q is different in each experiment, so t_R is also.

λ, nm	μ_λ, cm^{-1}	Φ_λ, mol/Eins	λ, nm	μ_λ, cm^{-1}	Φ_λ, mol/Eins
295*	19.63	0.57	425	0.340	0.58
305	13.27	0.56	435	0.325	0.58
315	9.61	0.56	445	0.258	0.57
325	5.79	0.54	455	0.187	0.54
335	3.65	0.51	465	0.110	0.47
345	1.67	0.51	475	0.055	0.37
355	0.81	0.50	485	0.029	0.29
365	0.41	0.49	495	0.016	0.22
375	0.37	0.49	505	0.009	0.18
385	0.37	0.52	515	0.006	0.12
395	0.37	0.54	525	0.004	0.08
405	0.37	0.56	535	0.003	0.02
415	0.35	0.57			

*Obviously, the actinometer is active for lower wavelengths, but since only solar radiation on the earth's surface was considered, no values under 295 nm were taken into account.

Table 4.2

After adding the chemicals to tank E, the whole solution was recirculated through the reactor during enough time to obtain total homogeneity in the system. A sample was taken (t_R=0) to test whether the concentration was correct and the module was placed in tracking. After the time foreseen for the water to have gone once through the system (Eq. 3.3), another sample, having a residence time which can be calculated by Eq. 3.4, was taken at the reactor outlet and the same procedure was repeated for each of the tests carried out. The concentration of uranyl remains inalterable. The concentration of oxalic acid is determined with potassium permanganate 0.1 N in a acid medium (H_2SO_4 1:1). At the end of each experiment, the amount of oxalic acid necessary to reach the original level is added again, so that, another experiment can be started. At the same time that the actinometries are being performed, the corresponding solar spectra, in the desired range of wavelengths (λ<536 nm), are collected with the spectroradiometer described above. The results of these experiments appear in table 4.3:

Exp No.	Q, L/min	t_E, s	t_R, s	C_0, M	C_F, M	r, M/s	X, %
1	1018	780	137	0.0482	0.0403	$5.71\ 10^{-5}$	16.4
2	1308	600	103	0.0465	0.0370	$9.22\ 10^{-5}$	20.4
3	2155	360	66	0.0517	0.0460	$8.64\ 10^{-5}$	11.0
4	1400	540	106	0.0545	0.0500	$4.25\ 10^{-5}$	8.3

C_0 = Initial concentration of oxalic acid; C_F = Final concentration; $r = (C_0-C_F)/t_R$; X = Conversion

Table 4.3

Photon flux inside of the reactor during the actinometric experiments may be calculated from equations 4.11 and 4.19. However, in this case the range of wavelengths is widened to 536 nm and, instead of using $f_{D,\lambda}$ and $f_{G,\lambda}$ and the UV_D and UV_G measured by the radiometers as factors the solar spectra up to 536 nm measured during the actinometric tests are used. Therefore, the value of I_E (N_E/N_0, where N_0 is the Avogadro number) is in this case:

$$I_{E(300-536)} = I_{D,E(300-536)} + I_{G,E(300-536)} \tag{4.24}$$

when

$$I_{D,E(300-536)} = \left(0.92 \times \frac{S_P}{S_T} \times 0.91 \times 1.22 \frac{R}{100}\right) \frac{1}{hcN_0} \sum_{\lambda=300nm}^{\lambda=536nm} RAD_{D,\lambda} \frac{\eta_{T,\lambda}}{100} \lambda$$
$$I_{G,E(300-536)} = \frac{1}{hcN_0} \sum_{\lambda=300nm}^{\lambda=536nm} RAD_{G,\lambda} \frac{\eta_{T,\lambda}}{100} \tag{4.25}$$

where $RAD_{i,\lambda}$ are the data supplied by the spectroradiometer, in W m^{-2}, corresponidng to each wavelength.

If the photon flux inside the reactor and the characteristics of the actinometer are known, the oxalic acid degradation rate can be calculated from $I_{E(300,536)}$, μ_λ, Φ_λ and the area/volume ratios in each case (0.763 m^2/L for the direct and 0.071 m^2/L for global). The absorptivity coefficient as well as the quantum yield depend on wavelength, so these values must be introduced in the summation, in this case yielding an expression for the oxalic acid reaction rate as function of global and direct radiation:

$$r_{D,OXAL} = 7.36 \times 10^{-10} R \sum_{\lambda=300nm}^{\lambda=536nm} \left(\prod_{i,\lambda} RAD_{D,\lambda} \frac{\eta_{T,\lambda}}{100} \left[1 - \exp\left(-\mu_\lambda 2b\right)\right] \Phi_\lambda \right) \quad (4.26)$$

where:

$$7.36 \times 10^{-10} = 0.92 \times \frac{S_P}{S_T} \times 0.91 \times \frac{1.22}{100} \times \frac{0.763}{hcN_0}$$

and

$$r_{G,OXAL} = \frac{0.071}{hcN_0} \sum_{\lambda=300nm}^{\lambda=536nm} \left(\prod_{i,\lambda} RAD_{G,\lambda} \frac{\eta_{T,\lambda}}{100} \lambda \left[1 - \exp\left(-\mu_\lambda 2b\right)\right] \Phi_\lambda \right) \quad (4.27)$$

therefore

$$r_{CALC} = r_{D,OXAL} + r_{G,OXAL} \quad (4.28)$$

where r_{CALC} supplies the oxalic acid degradation rate (M s^{-1}), from the radiometric data and collector characteristics. The comparison between this calculated acid decomposition rate and the rate measured in the actinometric experiments (r, table 4.3) will give an idea of the validity of the equations developed in points 4.3.2 and 4.3.3. In the following table the results of this calculation and the differences found between the two procedures are reflected.

Exp n°	**R, M/s**	$\mathbf{r_{D,OXAL}}$	$\mathbf{r_{G,OXAL}}$	$\mathbf{r_{CALC}}$	**Δr%**
1	$5.71\ 10^{-5}$	$5.49\ 10^{-5}$	$1.23\ 10^{-5}$	$6.72\ 10^{-5}$	17.7
2	$922\ 10^{-5}$	$7.78\ 10^{-5}$	$1.55\ 10^{-5}$	$9.33\ 10^{-5}$	1.2
3	$8.64\ 10^{-5}$	$7.95\ 10^{-5}$	$1.56\ 10^{-5}$	$9.51\ 10^{-5}$	10.1
4	$4.25\ 10^{-5}$	$3.54\ 10^{-5}$	$1.10\ 10^{-5}$	$4.64\ 10^{-5}$	9.2

$\Delta r = 100(r_{CALC} - r)/r$

Table 4.4

The oxalic acid degradation rate calculated by the actinometric experiments (r) or by Eq. 4.28, are really very similar, keeping in mind the large number of parameters involved in this equation. Therefore, all the equations developed in sections 4.3.2 and 4.3.3 are assumed to be valid, among which Eq. 4.28 (combination of 4.26 and 4.27) is a version extended to 536 nm. It was only slightly modified to directly obtain the oxalic degradation rate (r_{CALC}), but with all

the collector parameters treated in the same way as in the equations that it attempts to validate.

4.5 Conclusions

Recalling the outline of work at the beginning of this chapter, it must be concluded that the loop has been closed. Equations that permit estimation of photon flux inside the reactor during photocatalytic experiments have been obtained. At the same time, a series of conclusions have been arrived at that permit the experimental set-up used to be much better known:

(I) The equipment used to measure the direct and global radiation are not sensitive with the 300 nm-400 nm range exactly, but within a range of 300 to 393 for global and 300 to 404 for direct. This is basic to the calculation of photon flux as a function of the data supplied by those devices.

(II) The spectral distribution of the UV radiation at the PSA is constant (and moreover very similar to the ASTM standard). Therefore, the number of photons corresponding to this range of wavelengths is only a function of the intensity (measurable in real time with the radiometers).

(III) The overall efficiency (ratio of incident radiation inside the tube and that available on the aperture plane of the parabola) of the collector is approximately 60%, as long as the reflective surface and the absorber tube are kept clean. For this reason, the concentration ratio (whether $R_{C,g}$ or $R_{C,op}$) is also 60% of the original.

(IV) The basic equations for the experiments carried out with TiO_2 are 4.16c and 4.21c, similar to those obtained by different authors for their experimental set-ups [*Bideau et al., 1980; D'Oliveira et al., 1990; Herrmann et al., 1980; Jenny et al., 1991; Pruden et al., 1983a*]. Therefore, in order to calculate the moles of photons incident at any given moment, an expression combining both of these has been used:

$$I^*_{E(300-387))} = I^*_{D,E(300-387)} + I^*_{G,E(300-387)} \tag{4.29}$$

The estimated quantum yield (Φ_E), for all the experiments performed with TiO_2 and considering the influence of the factors corresponding to each type of radiation, is:

$$\Phi_E = \frac{reaction\ rate}{I^*_{E(300\text{-}387)}} \tag{4.30}$$

where the rate is expressed in moles $L^{-1}\ s^{-1}$ and the radiation in Einstein $L^{-1}\ s^{-1}$.

(V) The actinometric experiments have been shown to be useful to contrast the validity of equation 4.29 and all those related to it in this chapter. However, this technique would not be useful for finding the photon flux, at any moment, inside any photoreactor illuminated by solar radiation. The variations in the solar intensity, due to changes in weather, and the impossibility of using an actinometer within the reactor, at the same time as the photocatalytic experiments are being performed, make it impossible. It would be ideal in this case to have the solar spectrum at all times. If only the UV range is being worked with (as in this case, where atmospheric variation does not appreciably affect this range of the solar spectrum), with the radiometric data and knowledge of the spectrum, from a measurement campaign, equations can be obtained that enable calculation of the number of photons inside the reactor with reasonable precision and in real time.

(VI) The estimate of quantum yield using equation 4.30 enables results obtained in the photoreactor used to be compared of the with others and thereby, make use of existing literature on the compounds that are going to be tested. This is very important when working with a large reactor, where any test means a considerable outlay of time and expense. So the more information available “a priori”, the fewer experiments are necessary and the faster useful conclusions may be arrived at. The equations obtained in this work have been used to foresee the behaviour of other substances tested in this reactor, that are not the subject of this thesis and in order to be able to reduce the number of experiments performed with them [*Curcó et al., 1994, 1996a, 1996b; Giménez et al., 1996a, 1996b, 1996c; Karpa, 1995; Malato et al., 1996a; Minero et al., 1996b*].

5. DATA TREATMENT

5.1 Introduction

The kinetic constants of photocatalytic processes can be obtained by varying the concentration with regard to three different variables: time, incident photon flux inside the reactor and photon flux absorbed by the catalyst. Depending on the adjustment chosen, it is more or less complicated to obtain the constants and the possibilities for their application are different.

Using Equations 3.4 and 3.5, the independent variable is $t_{R,i}$, which is the time the sample taken has been exposed to the radiation at any given moment. In this case, $t_{R,I}$ is always less than the time since the start of the experiment, as the reactor is composed of illuminated and non-illuminated areas (see section 3.4). This type of calculation is common for photochemical reactors [*Acher et al., 1990*; *Blake et al., 1991; Bockelmann et al., 1991; Goswani, 1995; Li et al., 1992; Magrini et al., 1990; Muradov, 1994; Oberg, 1994; Ollis, 1991b; Pacheco et al., 1990a; Tinuzzi et al., 1993; Turchi et al., 1989*]. The existence of illuminated and dark areas could give rise to misinterpretation of the results if the experimental time were used as the unit of calculation (t_{exp}, Eq. 3.3 o $t_{E,i}$, Eq. 3.5). Also, in a large pilot plant, quite a lot of instrumentation is necessary in order to make it as versatile as possible, which substantially increases the non-illuminated volume in the reactor. If t_{exp} or $t_{E,i}$ were used instead of $t_{R,i}$ to calculate the reaction rate, and installation efficiency were in turn calculated from this, the conclusions would be erroneous, because they would be much lower than for a commercial photoreactor designed to minimise dark areas.

If the incident photon flux inside the reactor is selected as the independent variable (chapter 4), calculated to correspond only to the useful photons for the reaction under study ($\lambda < 387$ nm), it is possible to obtain conclusions helpful for extrapolating results from one scale to another, as well as avoiding the problem that rises from working with a radiation source of variable intensity. Referring the kinetic constant to the radiation flux inside the reactor represents an important improvement with regard to the previous procedure.

On the other hand, if the photon flux absorbed by the catalyst is used as the independent variable, the possibility for extrapolating the results increases. However, a series of parameters (those photons that enter inside the reactor, but do not excite the catalyst; directions in which light, interacting several times with catalyst particles in the interior of the reaction, is scattered; size and distribution of the TiO_2 particles suspended in the liquid, etc.) must be known and this is not possible for the reactor used in these experiments. So to obtain

the quantum yield (Eq. 2.1) the calculations have been performed using the photon flux at the reactor inlet. The estimated quantum yield, obtained in this way, will be called Φ_E, as mentioned before.

5.2 Photon flux versus illumination time

The use of photon flux instead of residence time (in the illuminated part of the reactor) is justified by the graphic in Figure 5.1.

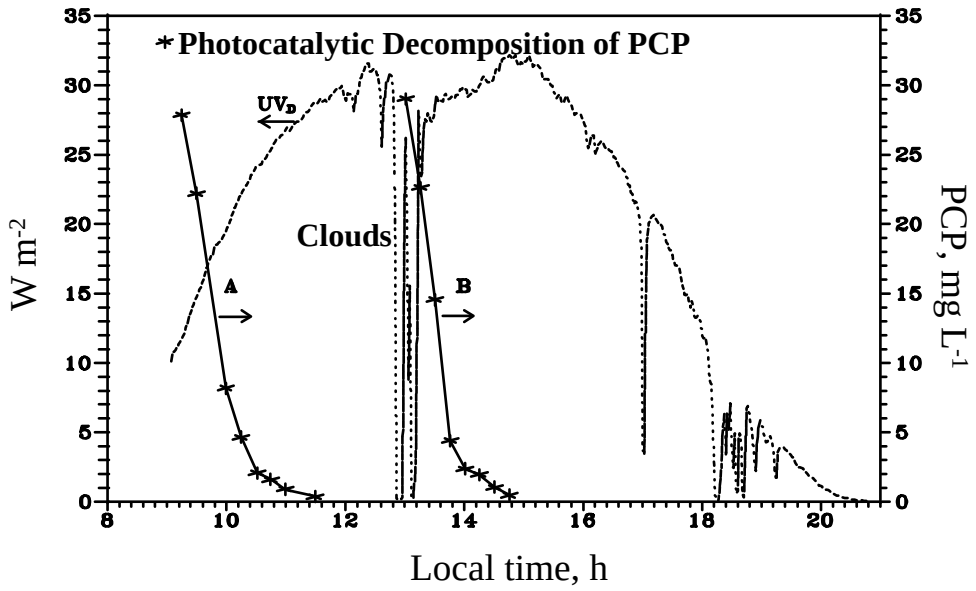

Figure 5.1. *Photocatalytic degradation of PCP in different periods in the same day.*

Figure 5.1 shows the results of two PCP decomposition experiments (catalyst TiO_2, 200 mg L^{-1}) performed in recirculation mode (See Figure 3.7.b). Obviously, UV power varies during the day and clouds during the tests also make this variation more noticeable. PCP concentration (*) decreases during both experiments. Experiment A started at 9:15 and B at 13:00. If the time of illumination (t_R) is calculated with Eq. 3.5 (n=1, V_R = 41.4 L, V_{TOT} = 260 L), a graphic is obtained by which, among other things, the initial decomposition rate may be found from the points of the beginning of the experiments.

Test conditions were the same for both experiments, however, their initial rates are considerably different. The slope of the lines in the insert are very similar. Although this may look incongruent, it is because in this last situation a larger number of experimental points are used, attenuating the effect of the variation in the intensity of the radiation. Since time is used as an independent variable, the differences in incident radiation inside the reactor during the

day are not taken into account. This is more serious when the environmental conditions during the experiments being compared are different (different days, different season of the year or atmospheric variations). The only solution for this problem is to use the equations developed in chapter 4.

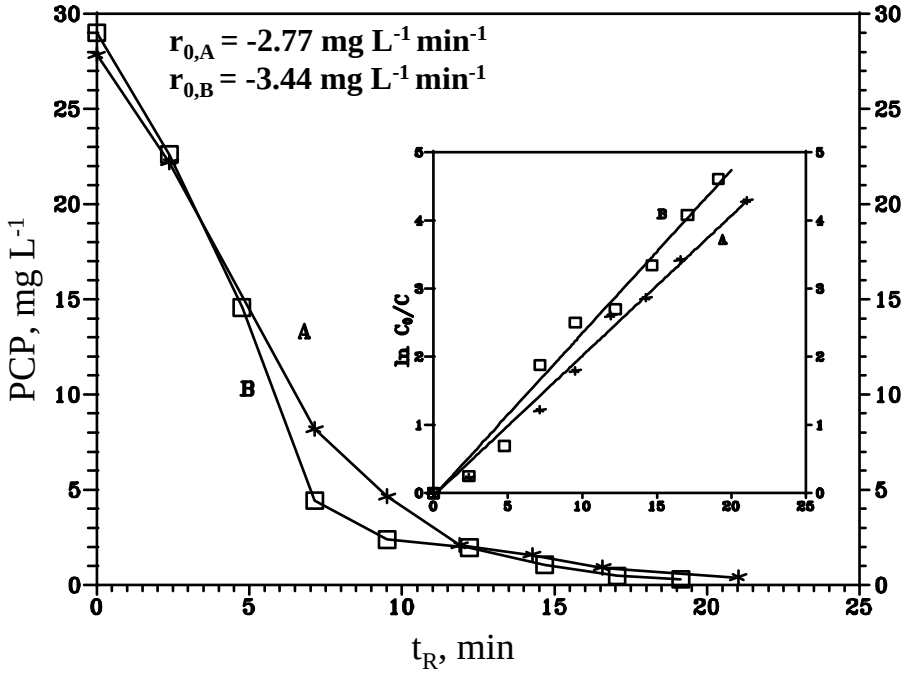

Figure 5.2. *PCP decomposition (experiments in Figure 5.1) as a function of illumination time (t_R). The insert shows data adjusted to Eq. 5.4.*

According to Equation 4.29, the value of $I^*_{E(300\text{-}387)}$ was given in Einstein L^{-1} s^{-1}, as calculated from the measurements of direct and global UV radiation. As radiation data is collected every minute (section 3.6), it is very easy to gather the average incident radiation in the reactor, in any time range, and use that average in Equation 4.29. It is possible to find the amount of photons collected in the reactor (per unit of volume) from the start up of the experiment until each sample is collected:

$$E_{E,n} = E_{E,n-1} + \Delta t_R \; I^*_{E(300\text{-}387),n} \qquad (5.1)$$

$$\Delta t_R = t_{R,i} - t_{R,i-1}$$

where $t_{R,i}$ is the time each sample has been illuminated, $E_{E,\,n}$ is the energy accumulated (per unit of volume, Einstein L^{-1}) inside the reactor for each sample taken during the experiment and $I^*_{E(300\text{-}387),\,n}$ are the moles of incident photons corresponding to the average UV radiation during the sampling period. Figure 5.3 shows the accumulated energy as the independent variable. The improvement in reproducibility of the results may be observed.

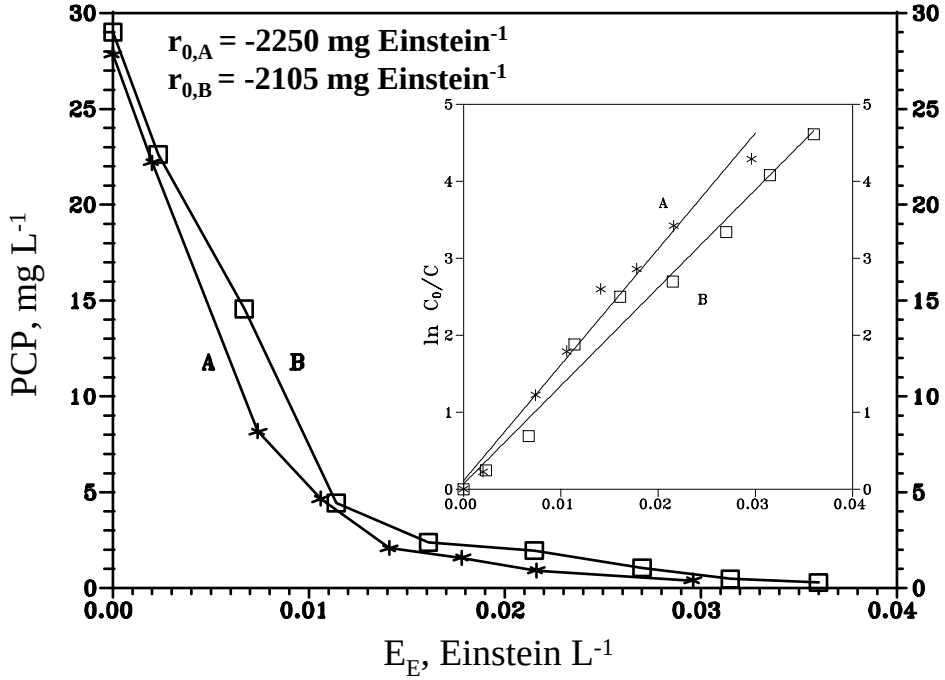

Figure 5.3. *Same data as in the previous graphic, but as a function of the incident photons inside the reactor, that is, accumulated energy (E_E).*

The inserted graphic is equivalent to that in Figure 5.2, but using E_E as the independent variable. Here no improvement is obtained and the slopes are only inverted, A being greater in this case than B in Figure 5.2. This is due, as already commented, to the attenuation of the effect of variation in incident radiation. The last samples of experiment A were exposed to similar photonic flux density as those in experiment B, as shown in Figure 5.1.

In this thesis, E_E has been used preferentially as the independent variable for kinetic calculations, substituting t_R, although in some specific cases the illumination time is used, or I_E and I^*_E, according to the needs of the calculations to be made.

5.3 Kinetics of the photocatalytic reactions in the heterogeneous phase

Photocatalysis (a heterogeneous catalytic process) demands that data treatment takes into account that the reaction takes place between a liquid (water and diluted PCP) and a solid phase (TiO_2 in suspension). It must therefore first be established whether the reaction initially takes place: on the catalyst surface through PCP adsorption, or in the liquid phase with the active specie ($^{\bullet}OH$) desorbed and reacting with the PCP. A Langmuir-Hinselwood kinetics (L-H) model is commonly used for quantitative descriptions of the gas-solid reactions between two adsorbed reactants that take place on the interface of the two systems. It has also been efficient as a standard quantitative description of liquid-solid reactions (l-s) [*Al-Ekabi et*

al., 1988, 1989]. Extrapolation of the L-H model for l-s reactions requires some modification for a TiO_2 solid surface in aqueous suspension, as it is known that it is covered by hydroxyl groups and molecular water (See Figure 1.2).

Rigorous treatment of kinetics by *Turchi and Ollis* [*1990a*], and mentioned by *Pelizzetti and Minero* [*1993d*], of the photocatalytic oxidation of organic compounds by irradiated semiconductors distinguishes four possible situations: (i) the reaction takes place between two adsorbed substances; (ii) the reaction occurs between a radical in the solution and the adsorbed substrate; (iii) the reaction takes place between the radical linked to the surface and the substrate in the solution; and (iv) the reaction occurs with both species in solution. In all cases, the expression of the equation rate is similar to the L-H model. By kinetic studies only, it is not possible to find out whether the process is on surface or in solution [*Serpone et al., 1993a; Terzian et al., 1990*].

Due to the earlier, for a L-H standard data treatment, it is assumed that the reaction occurs on the surface, which is also the assumption most widely accepted as possible. Under these conditions, two extreme situations [*Al-Ekabi et al., 1988*] are defined to illustrate the adsorption on the catalyst surface: (I) PCP and water compete for the active sites of the catalyst and (II) the reactant and the solvent are adsorbed on the surface without competing for the same active catalyst sites. According to the L-H model, the reaction rate (r) is proportional to the fraction of surface covered by PCP (θ_X). In each case the following expression can be obtained:

$$r = -\frac{dC}{dt} = k_r \theta_x = \frac{k_r K C}{1 + KC + K_S C_S} \tag{5.2a}$$

$$r = -\frac{dC}{dt} = k_r \theta_x = \frac{k_r K C}{1 + KC} \tag{5.2b}$$

where k_r is the reaction rate constant, K is the reactant (PCP) adsorption constant, C is the PCP concentration at any time, K_S is the solvent adsorption constant and C_S is its concentration (for water $C_S \approx 55.5$ M). As $C_S >> C$ and, C_S remains practically constant, the part of the catalyst covered by water is unalterable over the whole range of C and the previous equations can be integrated:

$$\ln\frac{C_0}{C} + \frac{K}{1 + K_S C_S}(C_0 - C) = \frac{k_r K}{1 + K_S C_S} t \tag{5.3a}$$

$$\ln\frac{C_0}{C} + K(C_0 - C) = k_r K t \tag{5.3b}$$

When C_0 is very small, both equations can be reduced to a order one reaction rate equation [*Amalric et al., 1995*]:

$$\ln \frac{C_0}{C} = k't \tag{5.4}$$

So, if ln (C_0/C) is represented versus t (in this case t_R or E_E), a line, the slope of which is the apparent reaction rate constant k', should be obtained. In the graphic inserts in Figures 5.2 and 5.3, the adjustment to this equation is correct and, therefore, the data may be treated with this simplification. At lower C_0 the adjustment improves considerably, as seen in the following chapters. Likewise, at higher concentrations both equations can be simplified by adjusting them to a zero order one, (C_0 - C) = k_rt [A*l-Ekabi et al., 1989*], as might be the case of the beginning of the experiment represented in Figures 5.2 and 5.3. Using L-H model, graphics similar to those depicted in Figure 5.4 may be obtained from the experimental data and from the linearization of the previous equations:

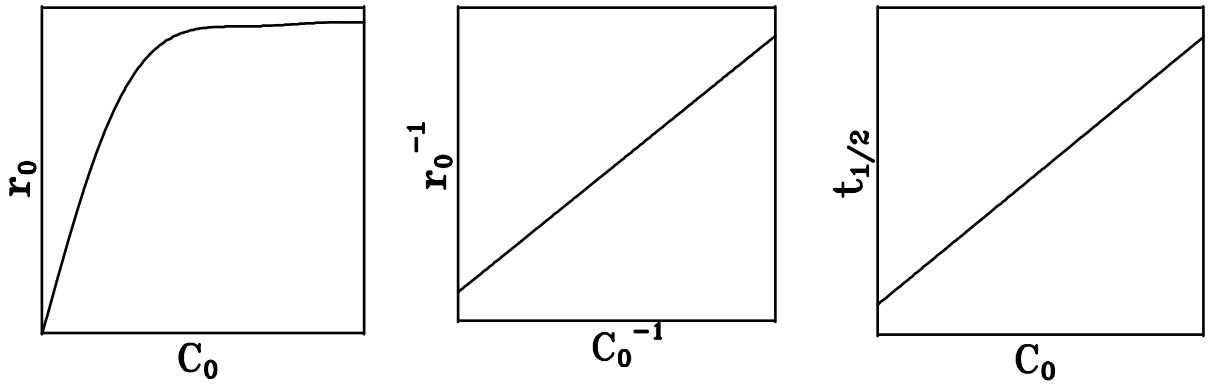

Figure 5.4. *Graphics related to the adjustment of data to a L-H type kinetic model.*

The effect of the initial PCP concentration in the degradation rate is shown in Figure 5.4a, where, due to the saturation produced on the semiconductor surface as the concentration of the reactant increases, it reaches a point at which the rate becomes steady. This agrees with what is proposed in this L-H-type model, where it is assumed that the reaction occurs on the surface. Figure 5.4b shows a linearisation of Eqs. 5.2, where the slope of that straight line is $(1+K_SC_S)/k_rK$, but could also be $1/k_rK$. Finally, Figure 5.4c is obtained from Eqs. 5.3 when the concentration is half of the initial (C/C_0 = 0.5):

$$t_{1/2} = \frac{0.693(1+K_SC_S)}{k_rK} + \frac{0.5C_0}{k_r} \tag{5.5a}$$

$$t_{1/2} = \frac{0.693}{k_rK} + \frac{0.5C_0}{k_r} \tag{5.5.b}$$

In both cases, it is not possible to discriminate between situations I and II commented at the beginning of this section.

It should be emphasised that PCP photodecomposes giving rise to intermediates, which could

also be adsorbed competitively on the surface of the catalyst. The concentration of these intermediates varies throughout the reaction up to their mineralization and thus, Eq. 5.2a may also take the following form [*Al-Ekabi et al., 1989*]:

$$r = \frac{k_r KC}{1 + KC + \sum_{i=1}^{n} K_i C_i \left(i = 1, n\right)} \tag{5.6}$$

where i is the number of intermediates formed during degradation (the solvent is also included in the summation).

During the eighties, this type of reasoning was followed to justify photocatalytic oxidation on the surface. Many authors [*Chen-Yung et al., 1983, Fernández et al., 1995; Hermann et al., 1983; Kawaguchi, 1994; Matthews, 1988; Nguyen et al., 1984; Ollis, 1984; Pruden et al, 1983a; Vidal, 1991a]* present their data in this way. They give to k_r and K values in an attempt to define the superficial reaction rate and the adsorption of the contaminant on TiO_2. But recently, further studies in the kinetics [*Davis et al., 1993; Minero, 1995; Serpone et al., 1993b]* make one wonder whether the values obtained by adjusting data by L-H really give an idea of the superficial adsorption and reaction rate, or whether they are only apparent constants.

Terzian et al.[*1991b*] propose a series of equations based on the results obtained from cresol photodegradation, a compound slightly adsorbed (5% in darkness) in TiO_2. They assume that a constant fraction of cresol is adsorbed on the surface of the catalyst and the reaction occurs there, although the adsorption does not have to coincide with that produced in darkness. They comment that if all the reactions that can be produced during the photocatalytic oxidation process are taken into account, that is, if a compound is considered to not directly mineralise, its decomposition goes through a series of intermediate steps leading to CO_2. In this way, a scheme similar to the one reflected in Eq. 5.7 would be obtained. In this reaction, cresol has been replaced by S and its intermediates by D in order to generalise.

$$(Active\ sites) + S \underset{k_d}{\overset{k_{ad}}{\leftrightarrow}} S_{ads} \xrightarrow{k_S} \left\{D_{ads} + D_{sol}\right\} \xrightarrow{k_I} \cdots \rightarrow \rightarrow \ CO_2 \tag{5.7}$$

where, k_{ad} and k_d are the adsorption and desorption constants of the compound to be degraded (S), k_s represents the sum of the constants of formation of the different intermediates in the first steps of the degradation and k_I represents the constant of decomposition of these intermediates. According to this reaction, Eq. 5.8 shows the intermediates formation rate (proposed by *Terzian et al.* [*1990, 1991b*], which has been commented on and accepted by *Minero et al* [*1991a*] and *Serpone et al* [*1993a, 1993b*], for different types of substrates).

$$r = \frac{k_s K_S N_C [S]}{1 + \alpha K_S [S]} \tag{5.8}$$

N_C is the number of active sites on the catalyst surface, $\alpha = (k_S + k_I)/k_I$ and $K_S = k_{ad}/(k_d + k_S)$. But $^{\bullet}OH$ radicals must also be taken into account in the general expression of the product formation rate. The concentration of these radicals (considering that the source is reaction 1.2, which can produce de radicals by 1.7 and 1.8 and also $k_R > k_{OH}$) at any given moment is:

$$\left[{}^{\bullet}OH\right] = \frac{\Phi_{OH}\, I\, k_{OH}\, \beta\, A_{TiO_2}\, \tau}{k_R} \tag{5.9}$$

where Φ_{OH} is the quantum yield of $^{\bullet}OH$ radical formation, I are the moles of incident photons, A_{TIO2} is the catalyst area, β gives an idea of the fraction of illuminated catalyst particles, k_{OH} is the sum of reaction 1.7 and 1.8 constants (responsible for $^{\bullet}OH$ radical formation), τ is the lifetime of these radicals and k_R is the e^-/h^+ recombination reaction rate constant (Eq. 1.2).

Equation 5.10 is obtained by combining 5.8 and 5.9. A term corresponding to the adsorption of other intermediates (D_n) which can compete for the same adsorption sites as the compound for degrading and therefore, avoid the formation of D, is also included in it.

$$r = \frac{[{}^{\bullet}OH]\, k_S\, K_S\, N_C [S]}{1 + \alpha K_S [S] + \sum K_n [D_n]} \tag{5.10}$$

Turchi et al. [*1991b*] indicate that this is one of the reasons for which, when using L-H, very good adjustments of the experimental results are often obtained. If the experimental device employed is the same in all the experiments and the catalyst concentration does not vary, the fraction of illuminated TiO_2 particles is constant. At the same time, if the radiation intensity is constant, so is the number of $^{\bullet}OH$ radicals. In this way, L-H-type representations can be obtained from Eq. 5.10. If the constants in Eq. 5.6 are compared with Eq. 5.10 under the same conditions, the result is that they may be equivalent:

$$k_r <=> \frac{\Phi_{OH}\, I\, k_{OH}\, \beta\, A_{TiO_2}\, \tau}{k_R}\ \frac{k_S\, N_C}{\alpha}$$

$$K <=> \alpha\, K_S \tag{5.11}$$

In the present case, this simplification may be correct. Using Eq. 5.1, the radiation may be considered constant. Also, in the experiment to find k_r and K, the concentration of TiO_2 used was constant (this is the optimal concentration for the pilot plant tested, as seen further below). In this way, constants useful for extrapolating results are obtained, but without the meaning that the L-H model attempts to give to these constants.

6 RESULTS

6.1 Overview of current research on PCP photodecomposition

6.1.1 PCP Photolysis

Pentachlorophenol water solutions absorb radiation in the solar spectrum range (λ_{max} 320 nm). *Wong and Crosby* [*1981*] comment that PCP photodecomposition has been referenced since the seventies and even several compounds that originate through PCP photolysis had been isolated and identified: tetrachlororesorcinol, chloroanilinic acid and chlorinated ethers. They present results about PCP photolysis under artificial (UV lamps) and solar radiation, obtaining the maximum decomposition rate at pH 7.3 (C_0=0.38 mM, $t_{1/2}$ = 48h, solar radiation). The degradation path includes many intermediates (See Figure 6.1). The authors comment that it was impossible to detect any organic compound after exposing a solution for 2-3 weeks to solar radiation. However, they do not provide a mass balance by CO_2 or HCl analysis, which would be the indicator of total mineralization. All this indicates that PCP residues can remain in a river or lake for a long time, because the incident solar radiation at a depth of a few centimetres is usually very low. In this same article, they refer to the detection of dioxines (highly toxic compounds) during photodegradation of PCP at high concentrations (C_0 = 3.8 mM).

In a later work [*1983*] *Mille and Crosby* evaluate PCP photodecomposition in sea water. There was no significant difference in the degradation path and only a decrease in the degradation rate was detected (in the order of three times less than the obtained in distilled water). This lag is due to the presence of large amount of chlorides (~20 g L^{-1}), which can produce nucleophilic interchanges with the PCP chlorides. In the same paper, this effect is determined by experiments in distilled water with different chloride concentrations. A logarithmic relationship is found: $r = r_0 - k \log [Cl^-]$, r_0 being the PCP decomposition rate in the presence of a few mg L^{-1} of chlorides and r the rate in the presence of a large amount. The effect produced by these anions when working in drinking water should be negligible, because the reaction rate decreases only 15% in the presence of a few hundred mg L^{-1}.

A similar effect occurs in an acid medium (pH<3) in the presence of TiO_2 (Degussa P-25, pH_{zpc} = 6.25), but this time due to Cl^- adsorption on the positively charged catalyst surface [*Kormann et al., 1991, Pelizzetti et al., 1993d; Terzian et al., 1991*], or, as proposed by *Abdullah et al*. [*1990*], by the antioxidant effect of the chloride anions: $Ox^{\bullet} + Cl^- \rightarrow Cl^{\bullet}$. In any case, to obtain a significant effect in the decomposition rate, the presence of chlorides in the

range of several grams per litre is necessary. All this will be explained in detail in the section devoted to the effect of pH on PCP photocatalytic decomposition.

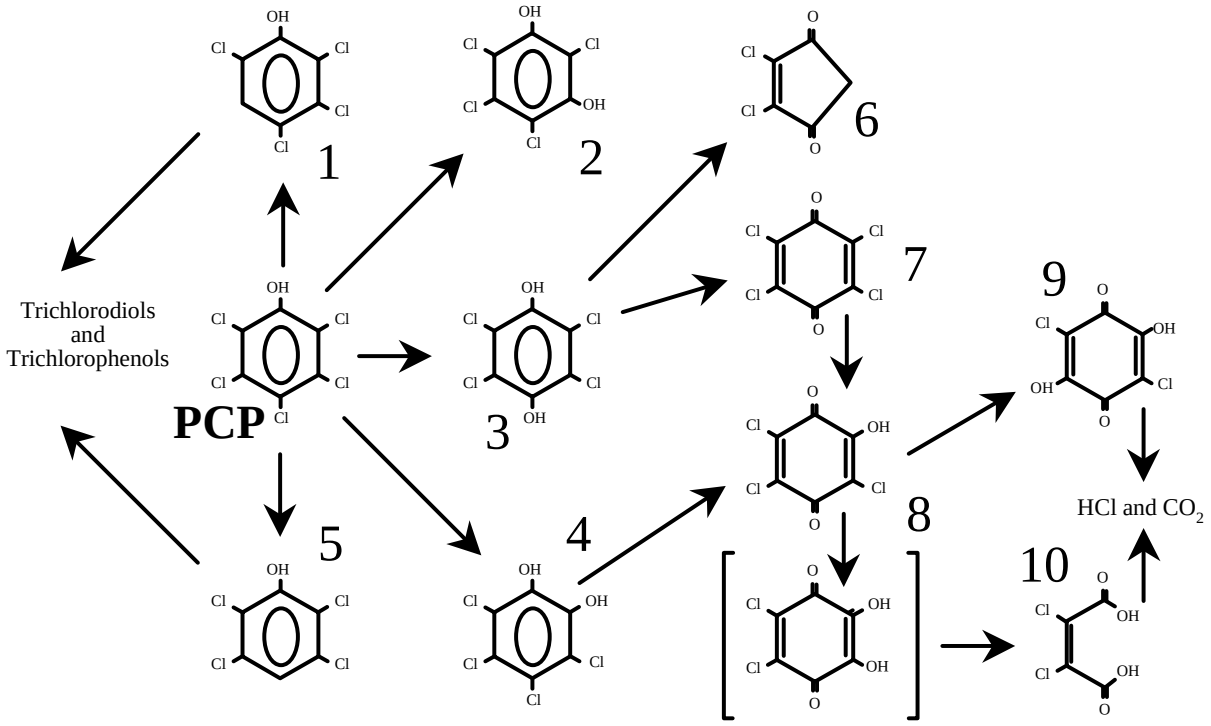

Figure 6.1. *PCP photolytic decomposition, proposed by Wong and Crosby [1981]*

Manilal et al. [*1992*] were able to reduce PCP toxicity in an aerobic cell culture by exposing it to direct solar radiation, as pre-treatment prior to cell inoculation. However, the toxicity was not completely eliminated and therefore, they tried photocatalytic treatment, as will be seen later. That same year a work by *Li et al.* [*1992*] was published in which they try to break down PCP using methylene blue as a light absorber. The dye, in an excited state, transfers part of its energy to other molecules present in the medium and the oxygen becomes single oxygen, which is much more reactive. Their reactor (similar to the basic one in Figure 1.8) was illuminated by lamps. These lamps generate radiation very similar to a sunny day. Under these conditions, the degradation rate was 1.15 mg L^{-1} min^{-1}, yielding all the chloride present in the molecule as Cl^- in solution, which does not completely ensure mineralization, as will be seen later.

6.1.2 Photocatalysis of PCP

The first work on heterogeneous photocatalytic decomposition of pentachlorophenol was published in 1985 [*Barbeni et al., 1985*], by two research groups from Torino University and Quebec University, headed by Professors E. Pelizzetti and N. Serpone, who have become two

of the most renown world experts in this subject. In this work, a "SOLARBOX", a device usually used in laboratory tests, was employed to simulate solar radiation. An incident radiation of 3.3 x 10^{-5} Einstein min^{-1} in 20 mL of catalyst suspension was estimated by chemical actinometric techniques. Nevertheless, the specific wavelength range was not given, mentioning only "near UV". Moreover, the actinometric method employed is also sensitive to photons outside the UV band, so this is not very clear. Taking the available value (3.3 x 10^{-5} Einstein min^{-1}), an incident radiation per unit of volume of 2.75 x 10^{-5} Einstein L^{-1} s^{-1} is obtained. This is very similar to the radiation inside the reactor used in this work (see Eq. 4.16 and 4.21), assuming similar $\Delta\lambda$.

As first step, they study several semiconductor suspensions (2 g L^{-1}, pH_0 = 3) and obtain PCP degradation (C_0 = 0.045 mM) with all of them, although with very different rates: TiO_2 > ZnO > CdS > WO_3 > SnO_2. The best results were obtained with titanium dioxide Degussa P-25, later used not only in the work described in this thesis, but also in most of the research done on this topic. The rest of the experiments performed with this catalyst are summarised in table 6.1.

pH_0	**r_0, mg L^{-1}**	**Comments**
3	<0.01	No TiO_2 + hν>310 nm
10.5	≈0.1	No TiO_2 + hν>310 nm
3	<0.01	No light + TiO_2
10.5	<0.01	No light + TiO_2
3	≈0.3	TiO_2+ hν(1)
10.5	≈0.4	TiO_2+ hν(1)
3	≈0.3	TiO_2+ hν(1) + ClNa 1mM
3	≈0.6	TiO_2+ Sunlight(2)

(1) SOLARBOX, λ > 310 nm

(2) July, k' = 0.069 min^{-1} (see Eq. 5.4)

Table 6.1

In view of the results shown in table 6.1, the necessity of combining both radiation and catalyst to produce a photocatalytic process is clear. Therefore, PCP decomposition is observed at similar rates in its protonated (pH = 3) as well as deprotonated form(pH = 10.5) and the presence of small amounts of chlorides is irrelevant. Total contaminant mineralization was also confirmed (see Eq. 3.16), although it took longer than indicated by r_0 in table 6.1, since the mass balance could be closed by the CO_2 and Cl^- produced.

Until 1991, no more work is published on pentachlorophenol, possibly due to the lethargy in the development of this technology till the beginning of the nineties, coinciding with the

epitome of the processes meant to solve environmental problems. In one of them, *Tseng and Huang* [*1991*] reported the photodecomposition of different chlorophenols by TiO_2 (suspensions 10 g L^{-1}, but with rutile-TiO_2 from Dupont) and radiation from UV lamps (mercury, medium pressure). Nothing is specified about the radiation incident in the solution. They obtained an initial PCP decomposition rate of ~0.02 mM min^{-1}. However, they did not achieve PCP mineralization (no CO_2 is produced). The reason for this effect is not explained, although it is assumed that the use of rutile has a lot to do with it.

That year, *Al-Ekabi et al*. [*1991*] also used PCP in their preliminary tests with a photoreactor (patented for commercial use) based on a design very similar to the one shown in Figure 1.8 (membrane in the outer wall), with a UV lamp in the 300-400 nm range. Obviously, because it is patented, no more details are available and the decomposition rate is not very useful: C_0 = 0.1 mg L^{-1}, r_0 = 0.03 mg L^{-1} min^{-1} and k'(Eq. 5.4) ≈ 0.44 min^{-1}. No comment is made on the mass balance (Eq. 3.16) and, as the only analytical method employed is gas chromatography, it is not clear whether the rate corresponds to PCP mineralization.

In 1992, work by *Sabin et al.* [*1992*] was published, where the photocatalytic destruction of 23 compounds is studied (among them PCP, C_0 = 1 mM) with 1 g L^{-1} of TiO_2 (Degussa P-25) and a Xenon lamp as the source of radiation. Under these conditions k'(Eq. 5.4) = 0.33 min^{-1}. In that same year, *Manilal et al.* [*1992*] published their results on the photocatalytic treatment of PCP to reduce its toxicity in microbiological cell cultures, however, with photolytic treatment alone the inhibition effect of this contaminant on cell growth did not disappear. They did determine that, after exposing a 0.6-L solution (75 mg/L PCP, 1 g/L P-25) to sunlight for 9 hours, it can be used without any inhibiting effect. The analytical method employed is a bit rough; they determined only the absorption spectrum of the PCP solution. After a 9-hour treatment, no absorption appears from 220 nm. It is therefore not possible to know the decomposition rate.

In 1993, *Puma et al*. [*1993*] tested PCP solutions (0.045 mM) with a reactor equipped with medium-pressure mercury lamps (emission at 254 and 366 nm). They obtained total mineralization after approximately 30 minutes, although the initial compound disappeared in 15 minutes, using 3 g L^{-1} of TiO_2 (P-25) in a reactor similar to the one shown in Figure 1.8. The use of such short wavelengths makes the comparison of this rate with those obtained in this thesis of little interest. In fact, they tested the photodecomposition with H_2O_2 without TiO_2 and completely mineralised the PCP. They assumed (although they do not enter into detail) that this is due to the generation of oxidant radicals by $H_2O_2 + h\nu \rightarrow 2\ OH^{\bullet}$. This reaction does not take place with solar radiation [*Pelizzetti et al. 1993d*].

The same year, the most complete work [*Mills and Hoffmann, 1993*] on the mechanism of PCP photocatalytic decomposition by simulated solar radiation (Xenon lamp with filter limiting the incident radiation to 330-370 nm) on a small scale (30 mL of water with 0.2 g L^{-1} of TiO_2 Degussa P-25) was published. Formic acid was proposed as the final product of the reaction:

$$C_6Cl_5OH + \frac{7}{2}O_2 \xrightarrow[TiO_2]{h\nu} 2HCOOH + 4CO_2 + 5HCl \qquad (6.1)$$

This does not agree with the results obtained by other authors (or in this thesis), who have observed total mineralization of PCP to CO_2. Before the appearance of this work, *Bideau et al*. [*1980*] had already published the first results on formic acid photodecomposition with TiO_2, which was confirmed by subsequent papers [*Bideau et al., 1987, 1990, 1991*] as well as by other authors, such as *Blake* [*1991*], *Matthews* [*1987b, 1988, 1990*] and *Sczechowski* [*1993*]. It does not seam logical that the acid would remain unalterable only when it is a product of PCP degradation. TOC, which could have avoided this error, was not determined. However, this does not discredit the rest of the very interesting questions dealt with in this article and detailed below.

During photocatalysis, only 3 (TCHQ), 4 (TCC) and 7 (p-TCBQ) are detected among those appearing in the photolytic decomposition mechanism (Figure 6.1) besides tetrachloro-1,2-benzoquinone (o-chloranil, o-TCBQ). Nevertheless, they did not detect tetra and trichlorophenols, which play an important role in photolysis (see Figure 6.1) and have only quantified compounds 3 and 7, because the instability of the rest in water made their determination impossible. To find the quantum yield, they followed the same procedure proposed in this thesis, that is, incident photonic flux is considered instead of the photonic flux absorbed by the catalyst (Eq. 4.30). Quantum yield was calculated for PCP decomposition, Cl^- produced and H^+ generated. For that, they chose the early periods, when the reaction is of a zero order, $C_0 \geq 0.023$ mM. They observed that the molar ratio of chloride produced/PCP decomposed increases ($1.8 \rightarrow 4$) as degradation progresses, until the final stoichiometric quantity is reached. The total amount of chlorides is obtained only after twice the illumination time necessary for complete disappearance of PCP. On the other hand, pH did not decrease as much as expected for the amount of H^+ generated in the process, which they believe to be caused by a buffer effect by PCP (pKa = 4.7), intermediates and the final products detected (acetate and formiate). The results are the following:

I (Einstein L^{-1} s^{-1})	**$\Phi_{E.PCP}$(%)**	**$\Phi_{E.Cl^-}$(%)**	**$\Phi_{E.H^+}$(%)**
3.2×10^{-6}	1.0	2.0	1.4

2.2×10^{-6}	1.3	2.7	1.6
1.1×10^{-7}	1.3	-	-

0.047 mM PCP, $pH_0 = 5$

Table 6.2

Regarding the mechanism proposed by the authors, it is accepted that $^{\bullet}OH$ radicals are responsible for oxidation (also confirmed by *Terzian et al* [*1990*]) and not the h^+ holes. Also, the hydroxylation is usually produced at the "ortho" and "para" positions, the first being quicker because a higher quantum yield has been determined for the production of o-chloranil and TCC. Figure 6.2 shows the pathway of p-hydroxylation.

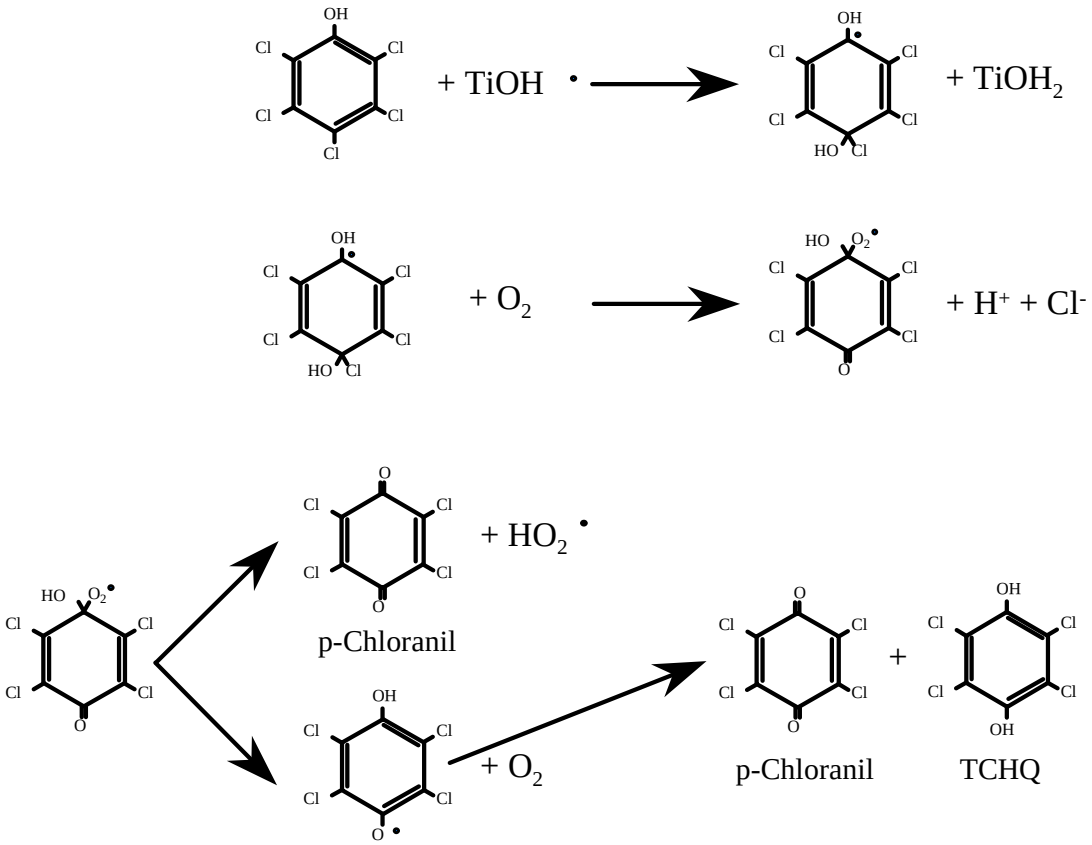

Figure 6.2. *Primary intermediates, proposed by Mills and Hoffmann [1993], of PCP photocatalytic decomposition*

In 1995, *Serpone et al*. [*1995b*] employed PCP (together with phenol and 2-chlorophenol) as a standard compound for demonstrating the possibility of improving the photocatalytic process. This combination of semiconductors ($CdS\text{-}TiO_2$) permits the transfer of e^- and h^+ between the two catalysts, so the total efficiency of the system can be increased. To achieve

this, they performed tests at pH 12, obtaining an increase in PCP decomposition rate from 0.96 mg L^{-1} to 1.30 mg L^{-1} in an experimental device similar to that used by Mills and Hoffmann ($\lambda \geq 320$ nm). However, they do not comment on disappearance of TOC or production of Cl^-, so, the improvement obtained in detoxification is questionable. Besides, the utilisation of Cd may be self-defeating due to its high toxicity.

Also that year, *Martin et al.* [*1995b*] treated PCP, with Degussa P-25 (1 g L^{-1}), obtaining $\Phi_{E.PCP} = 0.4\%$ with a radiation source between 310 and 330 nm. Nothing else is specified in this article about the experimental device utilised.

In conclusion, these studies could be summarised in the following:

(i) By solar radiation alone, it is impossible to mineralise PCP.
(ii) The photocatalytic process, by means of TiO_2/solar radiation, is able to mineralise PCP completely.
(iii) The reaction takes place within a very wide range of pH and passes through many intermediates, ending with CO_2 and HCl.
(iv) The estimated quantum yield (Φ_E) is approximately 1%.
(v) To date, the experimental devices used have been: small laboratory reactors illuminated by lamps or small transparent flasks, exposed directly to the sunlight.
(vi) Current solar technology, based on large-area collectors, has never been used to mineralise PCP.

6.2 PCP Photolysis in the PSA pilot plant

The preliminary tests with PCP in the pilot plant described in chapter 3 were performed in order to find out its decomposition rate without the semiconductor. As TiO_2 readily sticks to glass, it was decided to carry out these tests at the beginning, before the photoreactors came into contact with the catalyst. Removal of the thin coating of catalyst on the tubes after TiO_2 suspensions have circulated through them, is a very hard, complex and expensive task due to the dimensions of the tubes and the plant itself. This was known beforehand, as the glass equipment used in the laboratory tests became stained after containing TiO_2 suspensions and could only be removed with an ultrasonic cleaner or by abrasion.

Recirculation tests were carried out (see Figure 3.7.b and Eq. 3.5) with the largest number of modules possible in order to obtain significant degradation in a short time. Figure 6.3 shows the results obtained in one of these tests.

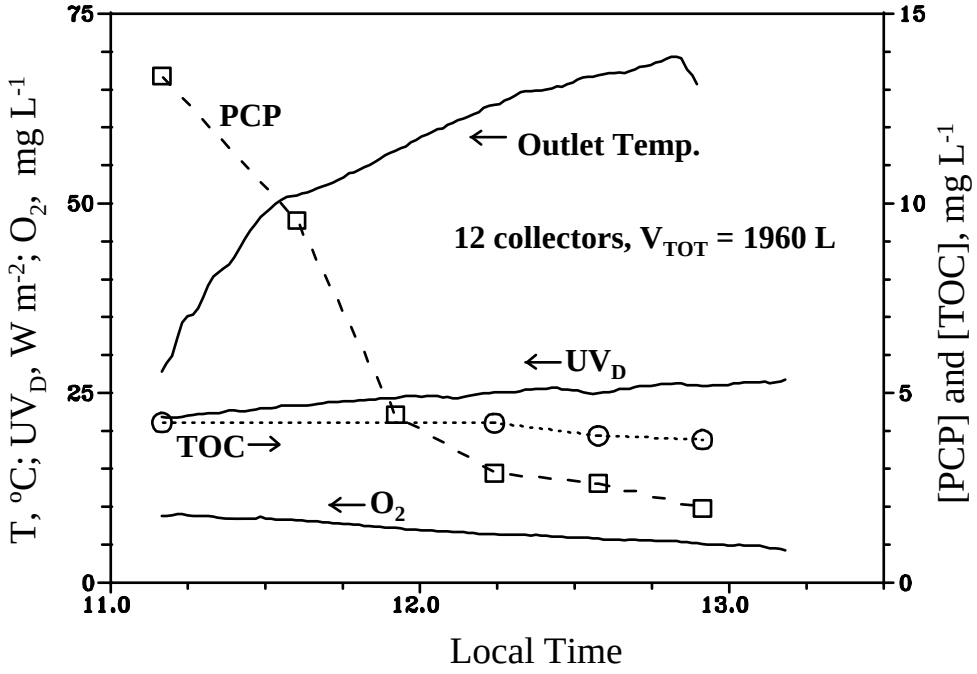

Figure 6.3. *Influence of different parameters on the photolytic decomposition of PCP*.

Figure 6.3 shows: a) PCP decomposition during the test, b) no mineralization of PCP, c) a decrease in the concentration of dissolved oxygen along with an increase in water temperature, and d) the evolution of direct UV radiation (data from the direct UV radiometer described in section 3.6). The results shown in this figure permit the following considerations:

1) Pentachlorophenol can be decomposed by photolysis, originating other organic compounds, as TOC does not decrease during the test. This is confirmed by the results of *Wong and Crosby* [*1981*] with regard to the formation of many different substances (See Figure 6.1). This means that this effect is not varied by the use of concentrated solar radiation.
2) The increase in temperature produced when solar radiation is concentrated does not affect TOC decomposition. The intermediates generated during photolysis do not seem to be volatile under the experimental conditions. There are no organic losses until 70ºC, which is the maximum temperature attainable in the plant.
3) Incident radiation on parabolic-trough collectors during relatively short periods (in this case about two hours) is practically constant when there are no clouds. The closer to solar noon the experiments are performed, the longer these periods will be. This behaviour allows many calculations, for which noticeable decomposition is necessary under conditions of almost constant power.
4) The decrease in concentration of the dissolved oxygen cannot be attributed to its consumption in the generation of CO_2, but is rather due mainly to the effect of temperature

increase (the amount of dissolved oxygen decreases as temperature rises). However, it never disappears completely, as occurs when TiO_2 is present (photocatalysis) as will be shown below.

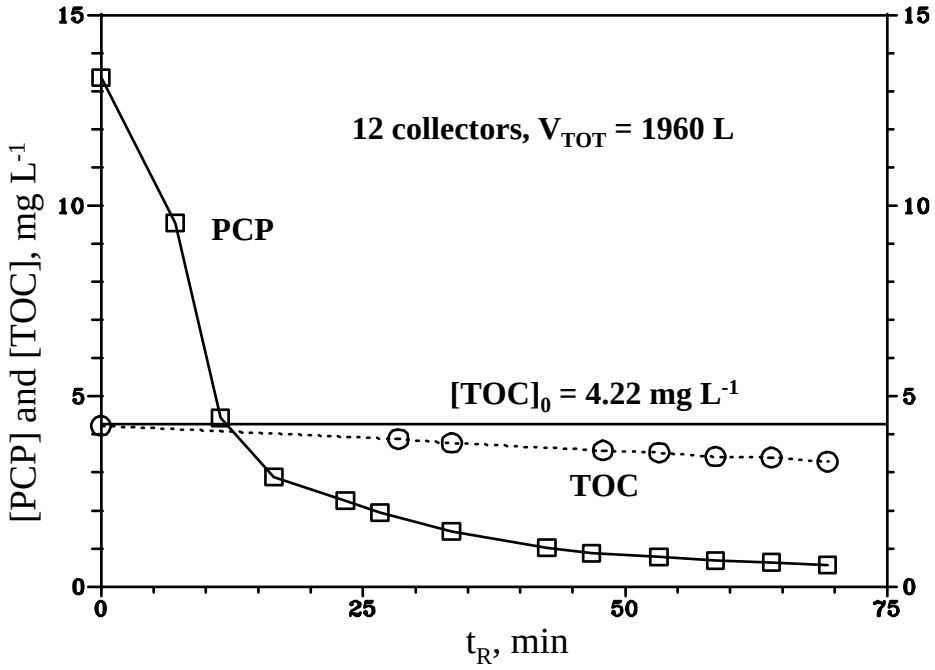

Figure 6.4. *PCP photolysis in the pilot plant, working in recirculation mode(see Figure 3.7.b) and using all the collectors.* $t_E \approx 4$ *hours.*

Figure 6.4 shows an experiment, in which $t_{1/2,PCP} \approx 10$ min, $r_{0,PCP} \approx 2.78$ μM min^{-1} and $r_{0,TOC} \approx 0.0136$ mg L^{-1} min^{-1}, long enough (total experimental time 4 hours) to produce a slight decrease in TOC. As observed in the HPLC chromatograms (Figure 6.5), PCP (largest peak on the left) nearly disappears completely (4.124 min peak, on the right). However, many new compounds appear in the chromatogram on the right (same figure) corresponding to the final TOC value. The discrepancy in retention time (2.86 and 4.13 min) between the two PCP peaks is due to little differences in pH in the HPLC mobile phase.

It must be pointed out that this experiment was carried out at $pH_0 \approx 7$ at which the reaction rate is higher than in acid medium, ($pH_0 = 7$, $t_{1/2} = 10$ min; $pH_0 = 4$, $t_{1/2} = 24$ min), although the difference is not as accentuated as that found by *Wong and Crosby* [*1981*] ($pH_0 = 7.3$, $t_{1/2}$=3.5 h; $pH_0 = 3.3$, $t_{1/2} = 100$ h) or by *Barbeni et al.* [*1985*] (See table 6.1). There is no difference if organic carbon decomposition ($r_{0,TOC}$), which is approximately the same in both cases, is observed (see table 3). Table 6.3 summarises all the results obtained in the PSA pilot plant (with 12 modules) during PCP degradation tests without catalyst

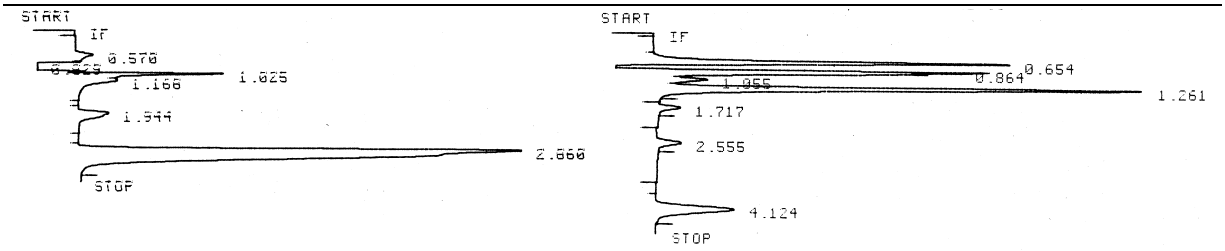

Figure 6.5. *HPLC chromatograms at 220 nm corresponding to the initial sample (left) and final sample (right) of the Figure 6.4 experiment.*

EXP. No.	C_0 (μM)	pH_0	$t_{1/2}$ (min)	r_0 (μM min^{-1})	$r_{0,TOC}$ (mg L^{-1} min^{-1})	UV_D/UV_G (1) (W m^{-2})	$\Phi_{E,0}$ (2) (%)
1	52.6	7	10	2.78	0.014	23.1/30.8	0.210
2	43.2	4	24	0.89		26.0/30.7	0.050
3	29.3	4	-	0.15	-	-/29.4 (3)	0.052
4	5.6	4	14	0.19	- (4)	24.0/31.5	0.014
5	33.8	7	-	0.0	0.0	0/0 (5)	-
6	30.7	4	-	0.0	0.0	0/0 (6)	-

(1) Average radiation during the test. (2) Obtained from equation 4.30. (3) Experiment carried out with the modules in horizontal position (without solar concentration) (4) In these cases (-), it is impossible to calculate the parameters because of the low degradation obtained. (5) and (6) Experiments carried out in the dark to check for PCP loss due to adsorption in the reactor walls (HDPE).

Table 6.3

Experiment 1 corresponds to Figure 6.4. The rest were performed using the same procedure and with an experimental time long enough to obtain representative results ($t_{E,No.2}$ = 4.5 h; $t_{E,No.3}$ = 6 h; $t_{E,No.4}$ = 2 h; $t_{E,No.4\ and\ 5}$ = 10 h). The results obtained in experiments 2 and 3, where the initial quantum yield estimated ($\Phi_{E,0}$) is practically the same, even though performed under very different conditions of illumination (with and without concentrating solar radiation), must be emphasised. This provides even greater support for the validity of the equations calculated in chapter 4.

This type of experiments have demonstrated that:

(i) The treatment is not feasible without a catalyst.
(ii) Increase in temperature in the reactor does not cause product loss.
(iii) There is no adsorption of PCP or its metabolites in the HDPE tubes of the pilot plant.

6.3 Photocatalytic destruction of PCP in the PSA pilot plant

After demonstrating that by solar radiation only it is impossible to mineralise pentachlorophenol at a reasonable rate, the first catalytic experiments were carried out. These were directed at proving that total mineralization is possible by solar photocatalysis. It will thus demonstrate that the mass balance adjusts to the stoichiometry proposed in Equation 3.16. In this phase of experimentation it was also attempted to optimize the injection of oxygen, which is necessary for the reaction to take place, in recirculation as well as in once-through tests. In addition to this, tests were carried out to prove whether PCP losses produced were by adsorption into the TiO_2, or by accumulation in certain zones of the reactor. Another aspect analyzed was the formation of PCP metabolites, in order to confirm whether the reaction mechanism takes place through similar steps as those described by other authors.

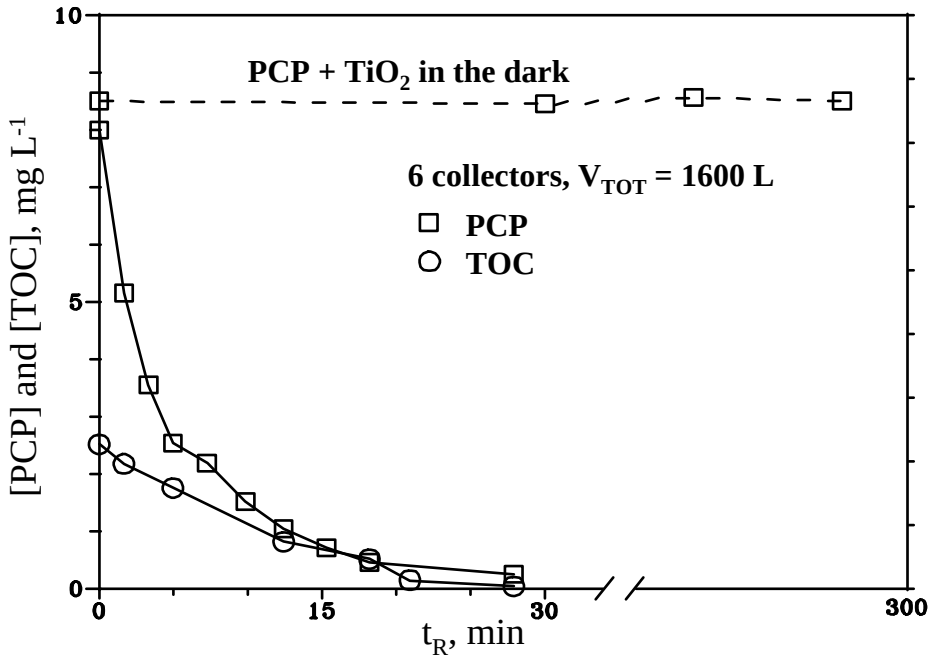

Figure 6.6. *PCP adsorption and photocatalytic degradation tests in the pilot plant, with 6 collectors and TiO_2 (100 mg L^{-1}). Recirculation 3000 L h^{-1}, $t_E \approx 3.0$ hours.*

At first, it was decided to use initial concentrations which were not very high (≤8 mg L^{-1} = 0.03 mM < = >2 mg L^{-1} TOC), in order to obtain total mineralization in a short time and, at the same time, ensure that the process and the plant are operated correctly. This concentration was also chosen so that the oxygen dissolved in the water would be sufficient (see Figure 6.3) to obtain all the initial TOC as CO_2.

The dashed line in Figure 6.6 indicates that: (i) appreciable PCP losses are not produced by adsorption on the catalyst, since the samples were filtered (see analytical method) before their injection in the chromatograph, (ii) there is no decomposition in the dark and (iii) in the reactor there are no "death zones", since the PCP added in the tanks originates the initial concentration desired and this is kept constant while there is no incident illumination. It was also confirmed that there was no sedimentation of the catalyst during the tests. A sample of specified volume was filtered and later the filter was weight in an analytical balance. In Figure 6.6, it is also demonstrated that the complete mineralization of initial TOC in a reasonable time by solar radiation and TiO_2 is possible.

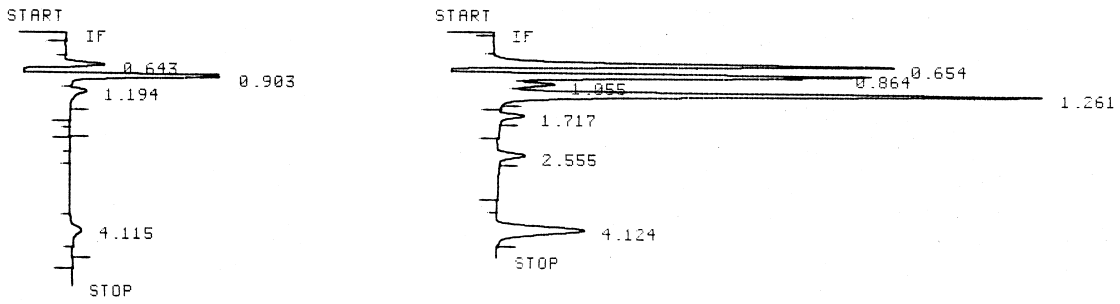

Figure 6.7. *Chromatograms (220 nm) corresponding to: (left) final sample of experiment shown in Figure 6.6 and (right) at the end of an experiment without TiO_2.*

6.3.1 Effect of oxygen concentration

After all the preliminary assays that demonstrated that the photocatalytic process is viable and that no phenomenon will obscure the results, an aspect related to the correct operation of the plant was analyzed. Continuation of all the testing as planned, under optimum conditions, depended on this factor: to keep a enough high concentration of dissolved oxygen (see Figure 6.3), throughout the reactor, in order to mineralize high amounts of PCP (1 mM of PCP requires 4.5 mM of O_2, see Eq. 3.16).

It seems that there is a consensus on the role of oxygen. It is necessary for complete mineralization and does not seem to be competitive with other reactives during the adsorption on TiO_2 [*Gerischer et al., 1992; Pelizzetti et al., 1990b; Turchi et al., 1989*], since the places where oxidation takes place are different from those of reduction (see Figure 1.1). According to *Pelizzetti et al.* [*1993d, 1995a*], the O_2 avoids the recombination of e^-/h^+ (Eq. 1.9) and, the photoactivated oxygen also reacts directly *[Minero et al., 1991a; Ollis, 1991b; Serpone, 1995a*]. *Serpone et al.* [*1995b*] have compared the effect of decomposing phenol in N_2O (able to capture e^-) and O_2 atmospheres, in such a way that no reaction is produced in the first.

Therefore, it seems clear that oxygen intervenes in more than just avoiding recombination of e^-/h^+ [*Lindsebigler et al., 1995*].

In any case, there are many examples in the bibliography that demonstrate that it is crucial. With PCP, *Puma et al [1993]* have demonstrated that in the absence of O_2, the decomposition rate is slower and TOC did not disappear. The same thing has been detected with 2,4-dichlorophenol [*Al-Ekabi et al., 1991*]; dichloroacetic acid [*Chemseddine et al., 1990*]; 4-chlorophenol [*Barbeni et al., 1984; Martin et al., 1995a; Mills et al., 1993a*]; and dodecylbencene sulphonate [*Hidaka et al., 1986*]. It is also known that its absence can provoke the formation of substances other than CO_2 (such as CH_4, C_2H_6 and H_2), as occurs in the degradation of propionic acid [*Bideau et al., 1992*].

Other authors have reflected that the concentration of oxygen also affects the reaction rate, which is faster when the partial pressure of oxygen (p_{O2}) in the atmosphere in contact with the water increases. *Okamoto et al.* [*1985a*] have determined this difference, for the decomposition of phenol, between p_{O2} =0.21 atm (air) and p_{O2} = 1 atm (pure oxygen) as 30%. *Mills et al*. [*1993a*] have detected that 4-chlorophenol decomposes 1.7 times faster when oxygen, instead of air, is bubbled inside the reactor. On the other hand, *Augugliaro et al.* [*1988*], have certified that the decomposition rate of phenol does not increase when p_{O2} has reached 0.5 atm and, the same occurs in the photodegradation of nitrophenols [*Augliaro et al., 1991*]. *Al-Ekabi et al.* [*1991*], have found no relation between [O_2] and 2,4-dichlorophenol decomposition rate. The latter author, who works with a tubular reactor illuminated by lamps and deposited TiO_2, has detected that, when the water is gas-saturated (whether by air or oxygen), the rate is much lower (50%) than if the gas is injected directly into the inlet, and this occurs throughout the reactor in the form of bubbles. It is assumed that there might be mass transfer problems since the catalyst is supported (see section 1.2.2). These problems are partly solved by the turbulence caused by the bubbles. The same behavior has been observed in other tubular-fix-catalyst reactors described in the literature [*Barni et al., 1995a; Bellobono et al., 1995; Matthews, 1987a, 1987c, 1992; Ollis et al., 1991a*], where the contaminant solution flow always affects the reaction rate (higher flow $\rightarrow$greater reaction rate). This is a clear symptom of the problems of mass transfer. In the case in hand, this problem does not arise since the catalyst is in suspension.

A dependence definitely could exist and is accepted as valid by many authors, between the photocatalytic reaction rate (r) and the concentration of oxygen (CO_2) in the water. This effect follows a L-H type relationship (see section 5.3):

$$r \propto \frac{K_{O_2} C_{O_2}}{1 + K_{O_2} C_{O_2}} \tag{6.2}$$

where K_{O2} is the oxygen adsorption constant on the catalyst. If this equation is combined with Eq. 5.2b:

$$r = k_r \frac{K_{O_2} C_{O_2}}{1 + K_{O_2} C_{O_2}} \frac{KC}{1 + KC} \tag{6.3}$$

*Augliaro et al., Okamoto et al. and Sczechowski (*taken from *Turchi et al.* [*1989*]) have calculated the value of K_{O2} making the above equation linear ($1/r_0 = a + [a/K_{O2}\, C_{O2}]$), where $a = (k_r K C_0)^{-1} + (k_r)^{-1}$. All of them obtain different results: K_{O2} = 11 atm^{-1}, 1.82 atm^{-1} and 110 atm^{-1} respectively, and only Sczechowski has worked with Degussa P-25 TiO_2. These results are logical since they used catalysts with different characteristics and the adsorption is different in each case. *Mills et al. [1993a*], however, calculate the value of the O_2 adsorption constant with Degussa P-25 too, and it also is different (4.4 atm^{-1}) from that calculated by Sczechowski. It is clear that the way in which oxygen affects the reaction rate is not only related to its adsorption in the catalyst. These constants are calculated assuming that r is directly proportional to the amount of oxygen adsorbed and the results that are obtained disagree. In any case, it seems that the difference between using air or pure oxygen is not drastic. In an industrial plant it will be purely a matter of economy of design.

In the once-through tests in the PSA pilot plant (See Figure 3.7a), the water, as it flows through the reactor, does not come into contact with the atmosphere at any time. When an important conversion has to be obtained, the residence time must be long (about 30 minutes). This means that the maximum flow rate must be about 500 L h^{-1} when working with six modules (see Eq. 3.4). For these situations, an oxygen injection system was installed at the reactor inlet and a sensor (O_2-selective electrode) at the outlet (See Figure 3.8). It had to be demonstrated that this system worked correctly.

In Figure 6.8 it is clear that when all the oxygen, that is contained in the feed tank water, has been consumed, photodecomposition of TOC comes to a halt. At the moment of injection of oxygen (done at the beginning of the reactor) reaches the end of the reactor, the photodecomposition continues. Therefore, in the once-through experiments at low flow rates, the injection of O_2 becomes necessary. At high flow rates, with six or less modules, with recirculation as well as in once-through, the addition of oxygen is not necessary since the residence time is short. The water recovers again the oxygen consumed when it reaches the tank (open to the atmosphere and stirred) [*Gerischer, 1995*].

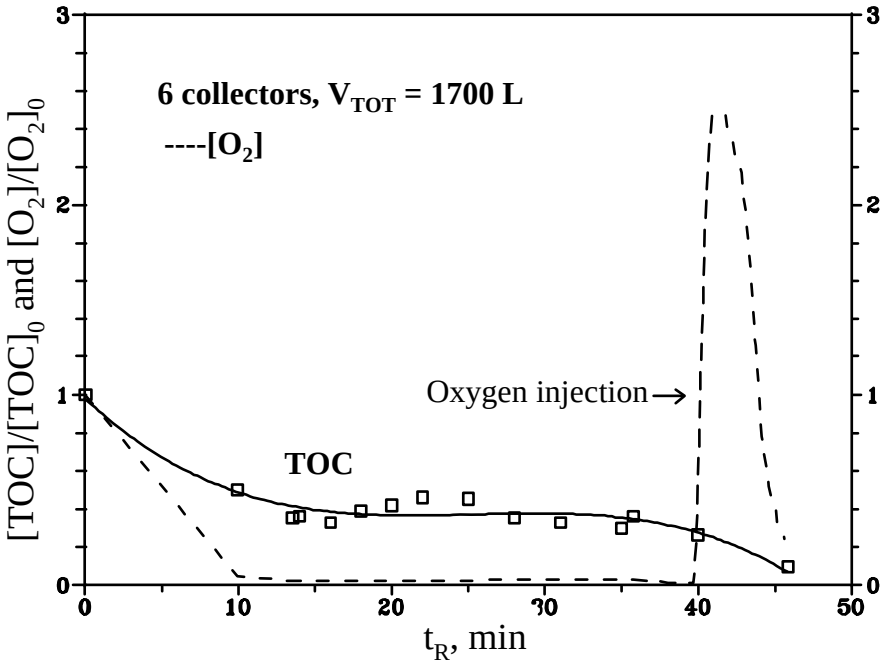

Figure 6.8. *Effect of the concentration of dissolved oxygen on PCP degradation. $[TOC]_0$ = 4 mg L^{-1}; $[O_2]_0$ = 8.5 mg L^{-1}; TiO_2 (100 mg L^{-1}). Flow rate = 500 L h^{-1}, $t_E \approx 3.5$ hours.*

It was not possible to carry out experiments varying p_{O2} (to find K_{O2}) as system conditions, not completely isolated from the atmosphere, did not allow it. Only experiments with and without oxygen injection were carried out, so that in the latter case, the oxygen concentration in the reactor tubes was high. In Figure 6.9 it may be observed how no difference was found between the two cases, since oxygen was not lacking at any time.

Some of the parameters, calculable from the experimental data, which give an idea of the PCP decomposition rate in each case are:

a) With injection: $E_{E,1/2}$ = 0.0059 Einstein L^{-1} and $r_{0,TOC}$ = 201 mg Einstein^{-1}

b) No injection: $E_{E,1/2}$ = 0.0063 Einstein L^{-1} and $r_{0,TOC}$ = 201 mg Einstein^{-1}

It is thus demonstrated that the in line injection of O_2 is not necessary if the time the water remains inside the reactor tubes, each time through, is low enough so that most of the oxygen is not consumed. When the water reaches the tank again it recovers the initial oxygen concentration. Therefore, although K_{O2} is unknown, it may be affirmed that, in this case $[K_{O2}C_{O2}/(1+K_{O2}C_{O2})] \approx$ constant.

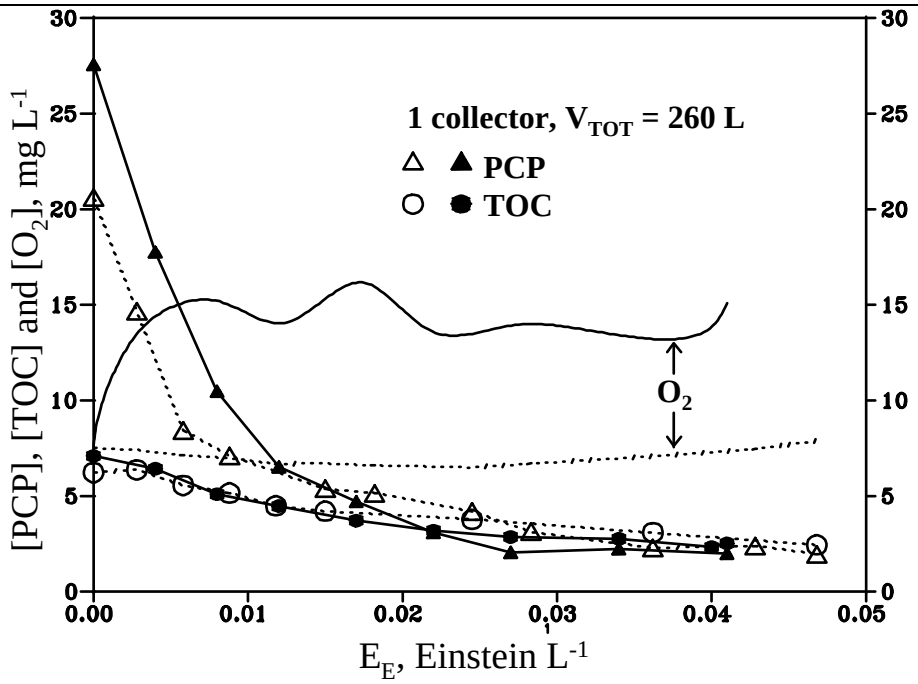

Figure 6.9. *Effect of the concentration of oxygen on PCP degradation. E_E is the accumulated energy. TiO_2 (200 mg L^{-1}); recirculation 3000 L/h; $t_E \approx 5$ hours. (a) Experiment with injection of oxygen (—), (b) no injection (---).*

6.3.2 Intermediate and final products of PCP photodecomposition

The effectiveness of degradation cannot be demonstrated only because all the initial PCP and TOC are decomposed. The stoichiometry proposed for the reaction (see Eq. 3.16) has to be demonstrated by a correct mass balance. Reactives and products might be lost in such a large reactor and this will originate not confident results.

The effectiveness is also confirmed by identifying some of the initial products of degradation. The evolution of three of them (see Figure 6.2), tetrachloride-1,4-benzoquinone (p-TCBQ), tetrachloride-1,2-benzoquinone (o-TCBQ) and tetrachlorohydroquinone (TCH), is shown in Figure 6.10a. All of them together do not make up 10% of the stoichiometric value at the beginning of the experiment, which is logical due to their high instability in water. Later, they disappear, which confirms that they are degraded and the process continues in a similar manner to that proposed by *Mills and Crosby* [*1983*] and *Mills and Hoffmann* [*1993*], until total mineralization.

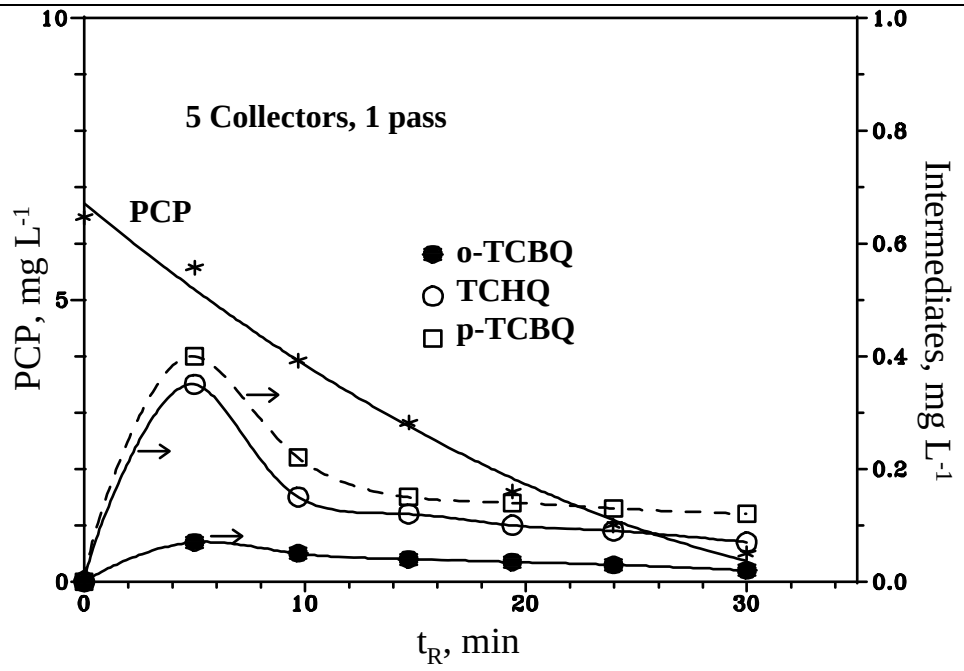

Figure 6.10a. *Evolution of three intermediate products during the degradation of PCP. TiO_2 (100 mg L^{-1}); once-through 500 L h^{-1}; $t_E \approx 1$ hour.*

Taking as a basis the indications of *Mills and Hoffmann* [*1993*] and *Minero et al.* [*1994*] for pentafluorophenol, and the intermediates of PCP decomposition detected in this study, (Figure 6.10a), a sequence may be proposed [*Minero et al., 1996a*] for the first steps of degradation (See Figure 6.10b). The beginning (oxidation, $k_{o,1}$ and $k_{o,2}$) is the addition of radicals $^{\bullet}$OH and loss of HCl, generating tetrachlorobenzoquinone, or o-TCBQ or p-TCBQ as also mentioned by Mills and Hoffmann. There are evidences of the formation of the adduct $^{\bullet}$OH/pentachlorophenolate [*Terzian et al., 1991*]. There is also a possible reduction ($k_{r,2}$), originating the radical tetrachlorophenoxile (R_2) which, through the later addition of $^{\bullet}$OH ($k_{o,3}$), produces tetrachlorohydroquinone (TCHQ). The halohydroquinones are common intermediates in the photocatalytic degradation of halogenated phenols. Therefore, chlorides ions may be formed either by oxidation following dechlorination or by photocatalytic hydrolysis (reductive dechlorination + oxidation). *Pichat et al.* [*1993a*] have proposed a similar mechanism for 2,4-dichlorophenol (intermediate of degradation of 2,4-dichlorophenoxiethanoic acid). Something very similar is proposed by *Minero et al.* [*1994*] for pentafluorophenol.

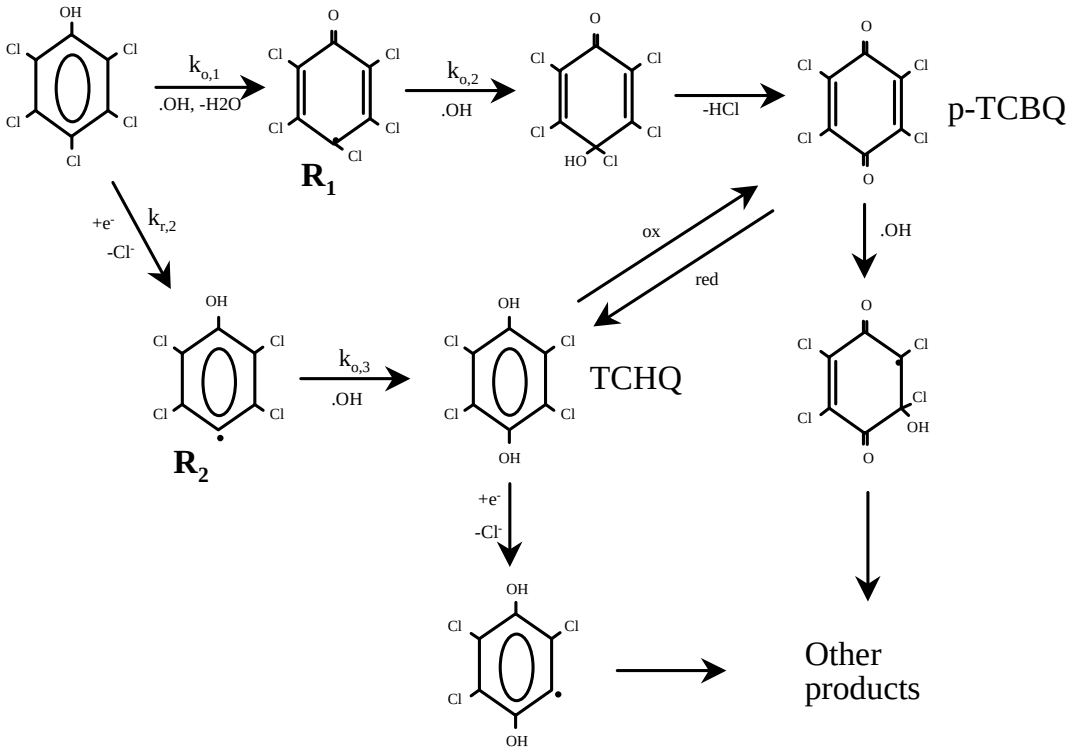

Figure 6.10b. *Proposed pathway for the first steps (formation of TCHQ and TCBQ) of PCP degradation, in the PSA pilot plant. Kinetic constants used in the text are also indicated. Different resonance forms of the intermediates are not shown.*

To validate the mass balance it must be confirmed that Cl^- and H^+ are also produced. In order to demonstrate that there are no product losses, the molar ratio must be $[Cl^-]_F = [H^+]_F = 5\ [PCP]_0$. This only occurs at the end of the experiment, when the TOC is almost 0. During the degradation, the formation of intermediates impedes this, since these intermediates contain differing amounts of chlorides. *Mills and Hoffmann* [*1993*] have detected, at the beginning of the reaction, production of only 2 Cl^- for each molecule of PCP degraded, which confirms even more strongly the mechanism proposed in Figure 6.10b. This relationship increases as the mineralization advances. The pH, likewise, does not reach the correct stoichiometric value until the end of decomposition of the TOC, since some of the intermediates generated have buffer characteristics.

In Figure 6.11 two complete PCP degradation tests are shown, at two different initial concentrations: ~0.1 mM and ~0.05 mM. In both cases the products obtained are practically the correct stoichiometric amounts. The slight difference may be attributed to the fact that all the TOC is not completely decomposed and to the analytical errors caused by comparing results obtained with four different analytical techniques (see section 3.8).

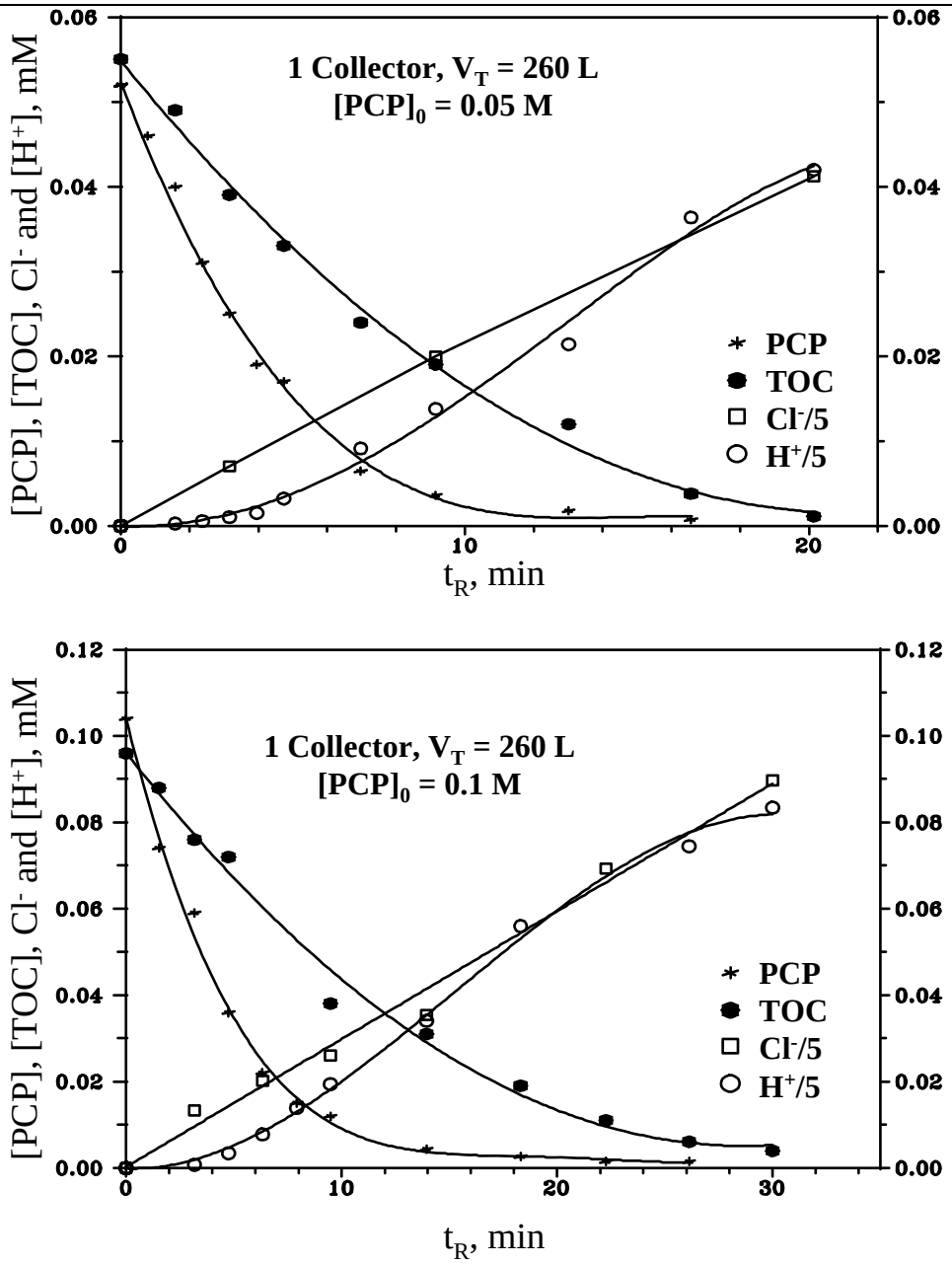

Figure 6.11. *Evolution of H^+ and Cl^- during PCP degradation. TiO_2 (200 mg L^{-1}); recirculation 4000 L h^{-1}; pH_0 ≈ 6.2. To demonstrate, more clearly, that reaction 3.16 is fulfilled, the concentration of TOC in mM is calculated considering 1 mMol TOC = 6 mMol of C = 72 mg and the concentration of H^+ and Cl^- is divided by 5 (1 mM PCP→5 mM HCl).*

In both experiments, the ratio between the chlorides produced/PCP decomposed changes: 1 (from initial C_0 to C ≈ 0.022 mM), 3 for concentrations between 0.022 mM and 0.01 mM and, from here on, continues increasing until the end. This again confirms that the first intermediates produced are tetrachlorides (like those that appear in Figure 6.10b) and also that dichloride compounds, similar to those in the mechanism proposed by *Mille and Crosby*

(Figure 6.1, compounds n°6 and 10), should be produced later. This effect is observed with all the PCP concentrations used (up to 200 mg L^{-1} < > 0.75 mM). This indicates that the mechanism of reaction must not vary when the initial PCP concentration is substantially increased, at least in the interval used in this work. H^+ formation is, at first, apparently slower than that of formation of Cl^-, due to the buffer characteristics of the PCP and the intermediates, as mentioned above.

6.3.3. Effect of initial pH

The pH value at which the surface of an oxide is uncharged is defined as the Zero Point Charge (pH_{zpc}), which for Degussa P-25 TiO_2 is 6.25 [*Kormann et al., 1991; Terzian et al., 1991*]. Above and below this value, the catalyst is negatively or positively charged according to:

$$-TiOH_2^+ \Leftrightarrow TiOH + H^+ \quad (6.4a)$$

$$-TiOH \Leftrightarrow -TiO^- + H^+ \quad (6.4b)$$

Kormann et al. [*1991*] have calculated these equilibrium constants, which are $pK_{TiOH,a}$ = 2.4 and $pK_{TiOH,b}$ = 8.0, and evaluate the abundance of all the species as a function of pH: -TiOH ≥ 80% when 3<pH<10; $-TiO^-$ ≥ 20% if pH>10; $-TiOH_2^+$ ≥ 20% when pH<3. Under these conditions, the photocatalytic degradation of the organic ionizing compounds is strongly affected by the pH of the solution [*Pelizzetti et al., 1990b, 1993d; Pichat et al., 1993b*]. Two extremes of this situation are: a) trichloroacetate, which at pH>6 does not degrade and the maximum degradation rate is obtained at pH≤1; b) Cl-ethylenammonium, which at pH<3 does not decompose and from pH>8 the photocatalytic reaction rate efficiency is maximum [*Kormann et al., 1991*]. The sodium dodecylbenzenesulfonate decomposes perfectly at neutral and basic pH but not at acid pH [*Hidaka et al., 1986*]. Numerous examples of similar effects appear in the literature, although not as extreme, for phenol and chlorophenols.

The effect of pH on the decomposition of phenol has been studied by *Abdullah et al.* [*1990*] and *Serpone et al.* [*1993a*]. The last mentioned authors have measured substrate decomposition (by HPLC) as well as the appearance of CO_2 and both parameters behaved in a similar manner (better at pH near 6.5). On the other hand, *Abdullah et al.* have determined that the maximum decomposition rate occurred at pH 3.5. The only important difference between the two experimental setups is that, in one case, the catalyst is in suspension and in the other is supported, but this should not modify the pH effect on the reaction rates. *Augugliaro et al.* [*1988*], however, found (also with TiO_2 in suspension) that at pH<3 the rate is very low, between that value and 12.5 it stays constant and then increases again from there on. *Kawaguchi* [*1984*] have proposed pH 3.5 as optimum. *Tseng et al.* [*1991*] have found the optimum zone to be between pH 5 and 9.

This lack of agreement in results is also found in results obtained with chlorophenols. With the three monochlorophenols, different results are obtained:

(i) For 2-chlorophenol the decomposition rate does not depend on pH_0 between pH 4 and 10 [*Tseng et al.; 1991*].

(ii) For 3-chlorophenol, the lowest rate is at pH<4 (minimum at pH 2.5), between 4 and 9 is constant and the highest rate is obtained at pH 12 [*D'Oliveira, 1990*].

(iii) For 4-chlorophenol the rate is similar between pH_0 4 and 8, with minimum at pH<3 [*Al-Sayyed et al., 1991; Matthews, 1986; Mills et al., 1993b*].

The decomposition rate of 2,4-dichlorophenol (pKa=7.85) is not affected when an important quantity of contaminant (20%) is adsorbed on the catalyst between pH 2 and 9 [*Serra et al., 1994*]. 2,4,6-trichlorophenol (pKa=6.0) at pH<6 is adsorbed on TiO_2 but is desorbed again, little by little, when the neutralization of the charges on the catalyst surface, in contact with water, proceeds. The reaction rate increases between pH 3.6 and 6.8 and from there on is constant [*Tanaka et al., 1994*].

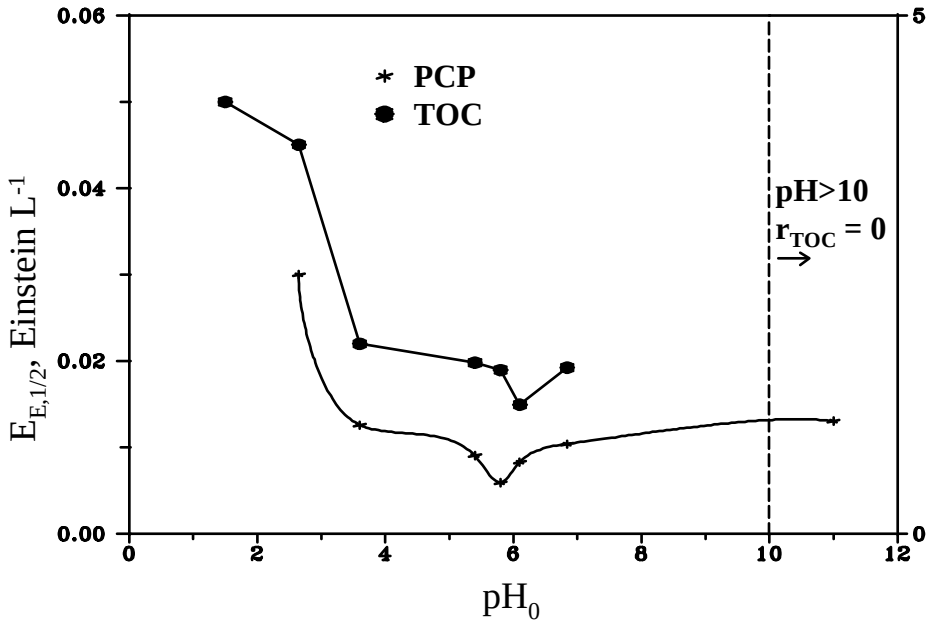

Figure 6.12. *Influence of initial pH in the photocatalytic destruction of PCP. TiO_2 (200 mg L^{-1}). $E_{E,1/2}$: moles of photons received to decrease C_0 one half (parameter calculated by Eq. 5.1 and equivalent to $t_{1/2}$).*

In many of these cases, a very important feature of photocatalysis is not taken into account when it is to be used for decontamination of water, and this is that during the reaction, a multitude of intermediate products are produced that may behave differently depending on the

pH of the solution. Therefore, to use only the rate of decomposition of the original substrate could yield an erroneous about the best initial pH for mineralization of the contaminant. In the case in hand, measurement of the TOC has mainly been used as the fundamental parameter for choosing the optimum pH.

As shown in Table 6.3, in the absence of TiO_2, the PCP decomposes faster if the initial pH of the solution is near 7. In the presence of the catalyst, this effect may vary and therefore tests were carried out at different pH_0. From the only preliminary information available, shown in Table 6.1, the initial decomposition rate of PCP appeared to be quite similar at pH 3 and 10.5. As may be observed in Figure 6.12, the optimum range of pH for mineralization is between 4 and 8. Therefore, all the experiments have been carried out in that range, but better between pH 6-8, which are the conditions in which PCP is found in the environment [*Crosby,1981*].

6.3.4 Conclusions

(I) The Pilot Plant designed and built at the Plataforma Solar de Almería is adequate to mineralize completely, in a reasonable length of time, large amounts of PCP through solar radiation and TIO_2.

(II) It must be assured that the water to be treated contains enough dissolved oxygen. In the case of the PSA pilot plant, this is attained because the system is open to the atmosphere.

(III) There are no reactive or product losses in the system except for those caused by the reaction itself. The analytical techniques selected allow the mass balance to be closed.

(IV) The mechanism is similar to that described in the literature for PCP (previously tested on a small scale with lamps), although in this case concentrated solar radiation and hundreds of liters of water are used. This allows much of the information already existing to be used and experiments do not have to be repeated.

(V) All the experiments designed to find out the influence of other parameters in the mineralization of PCP need to be carried out at pH ≈ 7.

6.4. Quantum Yield

6.4.1. Initial Considerations

In photochemistry, a concept called quantum yield is used to be able to evaluate the results obtained and to compare different experimental conditions. If equation 2.1 ($\Phi=\Delta n\ N_a^{-1}$) is recalled, the quantum yield of a photochemical reaction is defined with regard to the number of reacting molecules and the number of photons absorbed.

In this thesis, a heterogeneous system made up of a suspended solid (TiO_2), a gas (O_2) in bubbles and/or dissolved and an aqueous solution of a multitude of compounds (PCP, intermediates, H^+, Cl^-,...) was worked with. Finding out the amount of photons absorbed by the catalyst, from the behaviour of the radiation incident on a suspension such as this, is not the objective of this thesis. In order to calculate this, if so desired, one would have to: a) evaluate the absorption of a very complex reactive mixture, which, moreover, changes its composition throughout the reaction, b) from this basis, determine the photon flux that arrives at each particle of the catalyst to photoactivate it, and c) estimate the photons absorbed and dispersed. Furthermore, it seems that this is a feature which, for the moment is difficult to undertake [*Braun et al., 1993; Cabrera et al., 1996; Chamarro et al., 1990; Martin et al., 1993; Yue et al., 1994*], except under very special conditions [*Hacker et al., 1975; Valladares et al., 1993*].

It is necessary to remember that, in heterogeneous catalysis, it is usual to express the reaction rate as a function of the grams of catalyst. In photocatalysis, it should include the number of active centres, as well as the surface area of catalyst. But as a consequence of the above comments, the number of active centres is unknown and the surface of catalyst exposed to the light is undetermined [*Al-Ekabi et al., 1989*].

Because of this, a simplification has had to be employed. For calculation of N_a, only the radiation of a certain wavelength ($\lambda < 387$ nm) that is incident on the inside of the reactor is considered. The value obtained from this is called the estimated quantum yield: Φ_E. No distinction is made between the photons corresponding to each wavelength, assuming that all of them have the same effect on the surface of the catalyst. In all cases, this simplification is accepted as valid by a multitude of authors and widely used in the bibliography. [*Bideau et al., 1980; Bockelmann et al., 1992; D'Oliveira et al., 1990; Fox et al., 1994; Hilgendorf et al., 1992; Martin et al., 1995a; Matthews, 1988; Ollis et al., 1991a; Pruden et al., 1983a*]. The first step for the evaluation of the maximum quantum yield that can be obtained in the pilot plant consists of finding an optimum concentration of TiO_2 in the reactor. From here, in

so far as possible, the rest of the variables that could improve the conditions for PCP decomposition are studied.

6.4.2. Influence of TiO_2 concentration

There are a number of studies in the literature on the influence of catalyst concentration on process efficiency. The results are very different, but it may be deduced from all of them how radiation is incident on the reactor and the path length of it, inside the reactor, are fundamental in determining the optimum catalyst concentration:

- If the lamp is inside of the reactor and coaxial with it, [TiO_2] for r_{max} is very high (on the order of several grams per litre) [*Augliaro et al., 1988; Barni et al., 1995b*] if the path length is short (several mm). On the other hand, [TiO_2] for r_{max} is low (hundreds of mg per litre) if several centimetres are crossed [*Giménez et al., 1992a*; *Matthews, 1984, 1986a, 1986b, 1987b*].
- If the lamp is outside, but the path length is short (1-2 cm max.), r_{max} is obtained with 1-2 g L^{-1} of TiO_2 [*Ahmed et al., 1984; Al-Sayed et al., 1991; Ku et al., 1992; Minero et al., 1991a, 1993; Okamoto et al., 1985b; Pelizzetti et al., 1998; Serpone et al., 1993a; Tseng et al., 1991*].
- If the lamp is outside but the path length is several centimetres long, similar to what happens in a reactor illuminated by solar radiation, the appropriate catalyst concentration is several hundreds of milligrams per litre [*Augliaro et al., 1991; Cundall et al., 1978; Ollis, 1991b; Pacheco et al., 1990a; Turchi et al., 1994*].

From these extracts, only the reactors used by *Ahmed et al.* and *Pacheco et al*., correspond to reactors illuminated by solar UV, but the latter even uses one-axis parabolic trough collectors (See Fig. 2.4). This is the one that is most like the pilot plant conditions, since the photon source is from the outside (radiation from the parabolic trough) and the diameter of the reactor is 56 mm.

In all the cases described above, a "screening" effect is produced when the TiO_2 concentration is very high. The reaction rate diminishes due to the excessive opacity of the solution, which prevents the catalyst farthest in from being illuminated. The influence of this "screening" effect has also been demonstrated by *Magrini et al.* [*1994*]. Using two types of TiO_2 of different particle sizes (same surface area and at the same concentration), with the larger particles attaining the faster trichloroethylene degradation rate. The larger the size, the less the opacity of the suspension. According to *Ollis* [*1991b*], 1 g L^{-1} of catalyst reduces transmisivity to zero in a 1-cm-inner-diameter cylinder. Therefore, for a 56-mm tube, only an

outer strip is illuminated. When the radiation comes from a parabolic trough collector, something similar to what is shown in Figure 6.12 occurs.

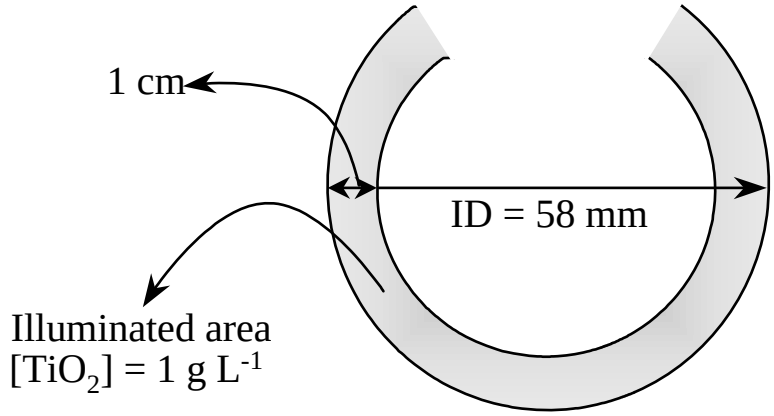

Figure 6.12. *Zone of pilot plant absorber tube where radiation penetrates, if the catalyst concentration is 1 g L^{-1}.*

This is only an approximation based on the results obtained by other authors: (i) *Ahmed et al.* [*1984*], for a tube (ID = 6 mm) directly illuminated by the sun (non-concentrated radiation), have obtained opacity with 3 g L^{-1}; (ii) *Pacheco et al.* [*1990b*], for a tube (ID = 38 mm) illuminated by two different parabolic trough collectors (concentrated radiation 20 and 50 times), the rate remains constant after 1 g L^{-1} in both.

In the PSA Pilot Plant, the situation is not very different from the above: ID = 58 mm and radiation concentrated 5-6 times. According to *Okamoto et al.* [*1985b*], the intensity of illumination affects the relationship between the reaction rate and the TiO_2 concentration. At higher intensity, the catalyst concentration can be higher. Furthermore, the dispersion and absorption of light causes photon density to diminish almost exponentially over the length of the optical path within a catalyst suspension [*Riegel et al., 1995*]. The number of photons incident on the absorber tube of the pilot plant, by unit of surface, is less than that incident on the parabolic trough collectors of *Pacheco et al.* [*1990a*] and, the diameter is also larger.

Because of all of the above, it is necessary to find out, experimentally, the optimum catalyst concentration for the plant studied. That is, the minimum concentration at which the maximum reaction rate is obtained. But it does not seem to be necessary to test concentrations over 1 g L^{-1}. To evaluate this optimum, it was elected to use, for greater security, different parameters calculable from the results of the experiments:

a) The estimated quantum yield (Φ_E) of the PCP and TOC initial decomposition rate.

b) The rate of Cl^- production, due to different ways in which reactants and products behave during photocatalysis.

c) The apparent constant k' (Eq. 5.4), since the initial PCP concentration used is not high (~ 0.1 mM) may be used and is a way to find out its behaviour until the end of the test.

d) $E_{E,1/2}$, which gives an idea of how long it takes for half of the initial product (PCP y COT) to disappear or for half of the stoichiometric chlorides to appear.

e) $E_{E,95\%}$ for TOC and Cl^-, which is the amount of photons that must be incident in one litre of reactor to decompose 95% of the TOC or obtain 95% of the chlorides foreseen.

To calculate k', E_E (Einstein L^{-1}) was used instead of t_R, for the reason explained in Section 5.2. For the same reason, $t_{1/2}$ was substituted for $E_{E,1/2}$. The catalyst concentration varied between 0 (photolysis) and 0.8 g L^{-1}, besides tests with no added catalyst, but with dirty tubes (as explained in Section 6.2). Since it is impossible to determine the amount of catalyst fixed on glass, these experiments were arbitrarily assigned $[TiO_2]$ = 5 mg L^{-1}.

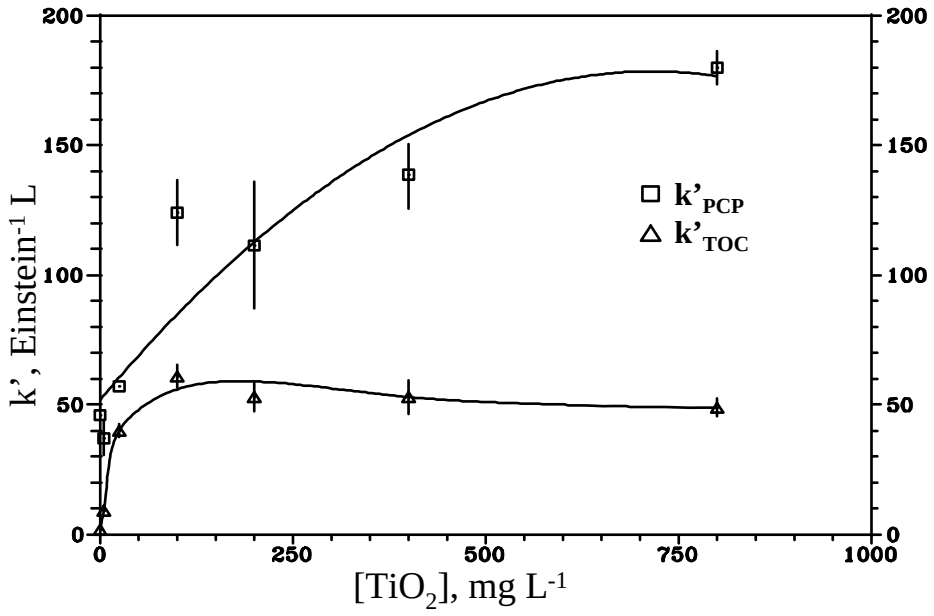

Figure 6.13. *Influence of catalysis concentration on the apparent rate constant ($ln(C_0/C) = k'E$). The continuous line is only intended to clarify the tendency of single values and the vertical lines show the idea of dispersion of the results, in repetitions of the same experiment. $C_{0,PCP}$ = 25 mg L^{-1} in all cases.*

In view of the results (as shown in Figure 6.13), PCP behaviour is not the same as that of TOC. This may be due to the influence of the intermediate products generated during the photocatalytic reaction. That is, the screening effect influences the decomposition of the original product in a different way than the other organic species present in the reaction. The

explanation for this could be the following:

a) The increase in [TiO_2] causes the PCP decomposition rate to increase because the generation of a larger amount of $^{\bullet}OH$, this effect being attenuated little by little by the screening. As seen in Figure 6.13, the increase in k'_{PCP} diminishes as the amount of catalyst increases, stabilising at a value of less than 0.8 g L^{-1}.

b) During PCP decomposition, photolytically degradable compounds must be generated. *Ollis* [*1984*, *1985*] notes that the oxidation of hydroquinones may be produced rather quickly without the presence of catalyst. The hydroquinones are intermediates of PCP degradation (See Figure 6.10b). Therefore, as the suspension becomes more opaque with the increase in TiO_2 concentration, the rate of hydroquinones decomposition decreases influencing the TOC rate.

This seems logical if the results obtained with other compounds in the same pilot plant are observed. *Curcó* [*1994*] and *Giménez et al.* [*1992b*, *1994*], for the reduction of Cr(VI) to Cr(III), found that when the TiO_2 concentration was increased, the reaction rate increased, even when more than 1 g L^{-1} was used, since in this process no intermediates of degradation are generated. Results analogous to those obtained with PCP, are produced when the TiO_2 concentration is varied during photodecomposition of formic acid and phenol [*Giménez et al.*, *1996a*], and with dichloroacetic acid [*Karpa*, *1995*]. In these cases, above 1 g L^{-1} of catalyst, the TOC decomposition rate stabilises. To confirm this, the rest of the system parameters must be used and see if they behave in a manner congruent with the above.

[TiO_2] (mg L^{-1})	**$\Phi_{E,0}$ (PCP) (%)[(1)]**	**$\Phi_{E,0}$ (COT)[(2)] (%º)**	**Φ_E (Cl^-)[(3)] (%)**	**$E_{E,95\%}$(COT) (Einstein L^{-1})**	**$E_{E,95\%}$(Cl^-) (Einstein L^{-1})**
0	0.21 ± 0.04	0.09 ± 0.01	-	-	-
5	0.22 ± 0.06	0.47 ± 0.08	0.26 ± 0.02	0.320 ± 0.014	0.178 ± 0.006
25	0.31 ± 0.02	1.00 ± 0.14	0.51 ± 0.04	0.090 ± 0.005	0.111 ± 0.007
100	0.46 ± 0.04	1.36 ± 0.02	0.68 ± 0.10	0.057 ± 0.004	0.090 ± 0.002
200	0.55 ± 0.07	1.83 ± 0.17	0.72 ± 0.11	0.044 ± 0.010	0.069 ± 0.018
400	0.82 ± 0.03	1.95 ± 0.13	0.80 ± 0.03	0.048 ± 0.002	0.066 ± 0.004
800	0.89 ± 0.19	1.85 ± 0.25	0.69 ± 0.02	0.046 ± 0.003	0.080 ± 0.002

(1) Estimated initial quantum yield; **(2)** Considering 1 mMol of TOC = 12 mg; **(3)** Correspond to complete degradation ([Cl] ≈ k E_E), 1 mMol of Cl^- = 35.5 mg.

Table 6.4

All the parameters given in Table 6.4 and Figure 6.14 indicate the same as in commented in Figure 6.13. That is, to mineralise PCP it is not necessary to use more than 200 mg L^{-1} of TiO_2. The rate of chloride formation (at the beginning of degradation, $E_{E,1/2,Cl}$, and when

degradation is complete, $E_{E,95\%}$ and Φ_E), as well as TOC decomposition (likewise, $\Phi_{E,0}$, $E_{E,1/2,COT}$ and $E_{E,95\%}$) are maximum around that concentration. The PCP does not behave in the same manner, but since the objective is complete mineralization, this amount of catalyst will be used from now on for all the following experiments.

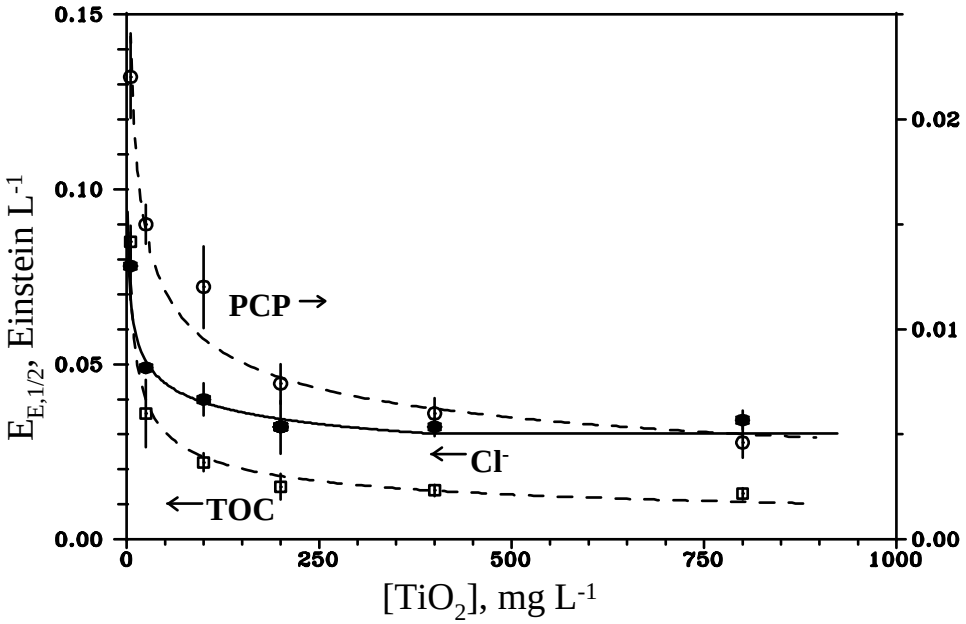

Figure 6.14. *Influence of catalyst concentration on $E_{E,1/2}$ (moles of photons necessary to reduce C_0 to half). The continuous lines are only intended to clarify the tendency of the values. $C_{0,PCP}$ = 25 mg L^{-1} in all cases.*

Another feature that it is of interest to know is the possibility of reusing the catalyst several times, since by this way its consumption would be considerably reduced.

In the literature, there are several examples with the same catalyst (P-25). For example, *Barbeni et al.* [*1987a*] do not find any decrease in degradation efficiency of 2,4,5-trichlorophenoxy acetic acid after using the same TiO_2 14 times. Likewise, *Al-Sayyed et al.* [*1991*] have reused it 10 times and the decomposition rate of 4-chlorophenol does not vary. *Mills et al.* [*1993b*] have arrived at the same conclusion also with 4-chlorophenol. *Hidaka et al.* [*1986*], with dodecylbenzene sulphonate, have used titanium dioxide P-25 up to four times without diminishing its efficiency. *Ahmed and Ollis* [*1984*] have obtained similar results with a different TiO_2 (Fischer, surface area 7 m^2 g^{-1}) in the mineralization of trichloroethylene. *Pacheco et al.* [*1990a*] also have reused the catalyst up to twelve times (in this case P-25 fixed on glass balls) with trichloroethylene with the same result.

In view of these results, something very similar must occur when PCP is mineralised. Table

6.5 shows the results of three repetitions of the same experiment reusing the catalyst and the water. That is, after reducing the PCP_0 to a certain value, more PCP is added and the experiment is repeated. More experiments were not considered necessary given the results of the authors mentioned above.

C_0 (mM)	$\Phi_{E,0}$ (COT) (%)	Φ_E (Cl^-) (%)	k'_{PCP} ($Einst^{-1}$ L)
0.090	0.75	0.64	45.8
0.102	0.83	0.84	40.1
0.095	0.97	0.77	52.0

Note: $[TiO_2] < 200$ mg L^{-1} was used, so any possible inhibition effect would be more accentuated.

Table 6.5

That catalyst is not deactivated after several uses. Logically, it will not do so during a single experiment either due to the possible effects of adsorption of reaction products or modification of the surface due to the effects of radiation, water or other factors that could diminish TiO_2 activity.

6.4.3. Application of the L-H model to PCP degradation in pilot plant

After knowing the initial optimum conditions of PCP degradation (pH and TiO_2 concentration), it is necessary to determine a useful model to predict the plant behaviour. This model must allow the calculation of the number of photons ($\lambda < 387$ nm) required for treating water contaminated with different amounts of PCP. From it, it can be approached the design of plants able to treat different flows. Nevertheless, the UV radiation data of the plants final location must be available.

Although different authors admit that the Langmuir-Hinshelwood (L-H) model is not an explanation of the mechanism of the photocatalytic process (as commented in paragraph 5.3), they agree on its usefulness. With it, the behaviour of the reaction rate versus the reactants concentration can be very often adjusted to a mathematical expression [*Doherty et al., 1995; Gerischer et al., 1993; Herrmann et al., 1983; Minero et al., 1991a, 1995; Okamoto et al, 1985a, 1985b; Serpone et al., 1993b; Turchi et al., 1990a*]. In fact, the utilisation of this model without any other consideration (applying directly Eq. 5.6 without the corresponding term of the intermediates adsorption) has been very usual in the case of chlorophenols [*Al-Ekabi et al., 1989; Al-Sayyed et al., 1991; Augliaro et al., 1988; D'Oliveira et al., 1990; Matthews, 1988; Serra et al., 1994*].

Due to this, a series of tests at different PCP initial concentration were performed to demonstrate if the experimental results could be adjusted with this model. Later, the details commented in section 5.3 will be discussed in depth for the case of PCP. The concentration interval was between 4 and 200 mg L^{-1}. The highest is very closed to the concentration detected in wood industries wastewater (see section 1.3). The lowest is the minimum possible to have enough experimental points with an acceptable analytical error (see section 3.8.1) and without complicating the analytical technique in excess.

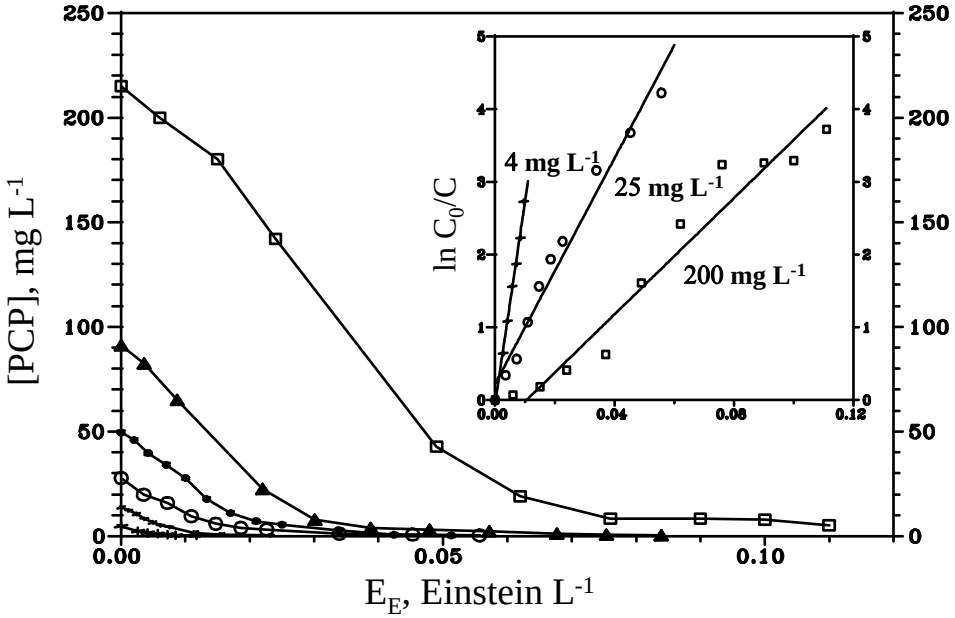

Figure 6.15. *PCP decomposition at different initial concentrations. TiO_2 = 200 mg L^{-1}. The adjustment of three of these experiments with $\ln(C_0/C) = k'E_E$ is shown in the inserted graphic. E_E is the accumulated energy.*

Figure 6.15 shows the results obtained in the commented concentration range. The adjustment of three of these experiments to a first order reaction is shown in the inserted graphic. As commented in section 5.3, this simplification is rather well but only when C_0 is small. This also occurs for the PCP in the PSA's pilot plant as the adjustment worsen when the initial concentration increases: $r^2_{C0=4}$ = 0.9942, $r^2_{C0=25}$ = 0.9799, $r^2_{C0=200}$ = 0.9450. Obviously, it is necessary to use a reliable model for a wide concentration interval.

The results shown in Figure 6.15 correspond to an example of each one of the experiments carried out but really they have been repeated at least once. From the slope of the line corresponding to the initial points, of each one of the experiments, the initial degradation rate has been calculated (see Figure 6.16), according to the procedure commented in section 5.3.

Figure 6.16 shows the calculated initial rate. It is observed that from de 0.2-0.4 mM (~ 50-100 mg L^{-1}) of PCP the initial rate is steady. At this concentration, catalyst saturation happens and the reaction rate becomes constant. Similar tests at higher catalyst concentration have not been done because solution opacity increases and no improvement in the mineralization will be obtained. (see Table 6.4).

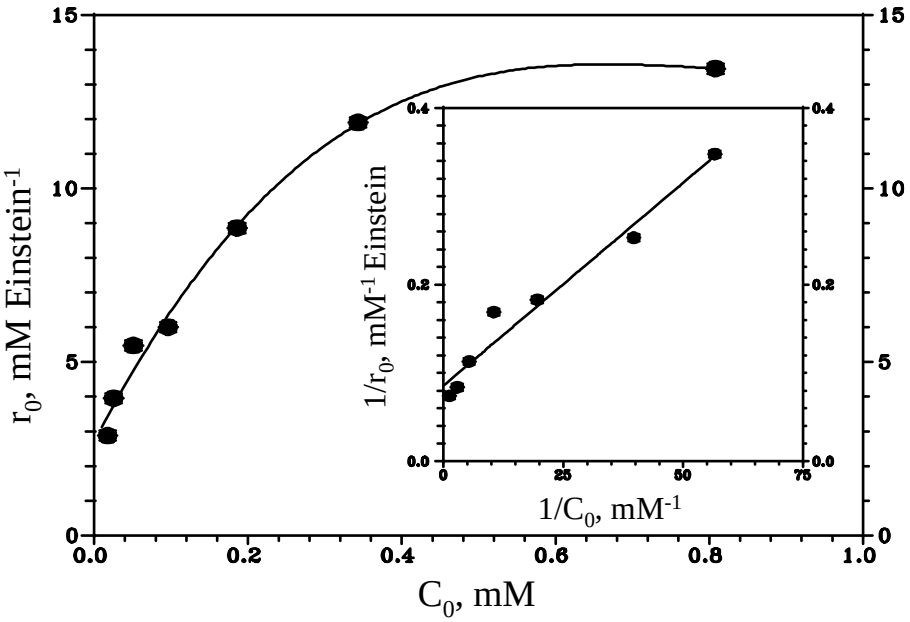

Figure 6.16. *Initial degradation rate as function of the PCP initial concentration. TiO_2 = 200 mg L^{-1}.Linealised Eq. 5.2 (L-H) are shown in the inserted graphic.*

From the graphic inserted in Figure 6.16, the constants can be calculated according to L-H model.

$$r_0 = \frac{k_r K C_0}{1 + K C_0} \rightarrow \frac{1}{r_0} = \frac{1}{k_r} + \frac{1}{k_r K}\frac{1}{C_0} \qquad (6.5)$$

$$k_r = 11.8 \text{ mMol Einstein}^{-1} = 0.0118 \text{ Mol Einstein}^{-1}$$
$$K = 18.3 \text{ mM}^{-1} = 1.83 \times 10^4 \text{ M}^{-1}$$

These constants can also be calculated from Eq. 5.5 (replacing $t_{1/2}$ by $E_{E,1/2}$), obtaining a very similar result (see Figure 6.17):

$$k_r = 13.6 \text{ mMol Einstein}^{-1} = 0.0136 \text{ Mol Einstein}^{-1}$$
$$K = 16.4 \text{ mM}^{-1} = 1.64 \times 10^4 \text{ M}^{-1}$$

The fittings are not perfect, as can be seen in Figures 6.16 and 6.17, but taking into account the experimental, and accumulative, errors the adjustment can be considered acceptable.

These errors are produced by the following experimental measurements: (i) flow rate, reactor volume and experimental time; (ii) analytical determinations; (iii) UV radiation and photon flux (iv) calculation of r_0 from.

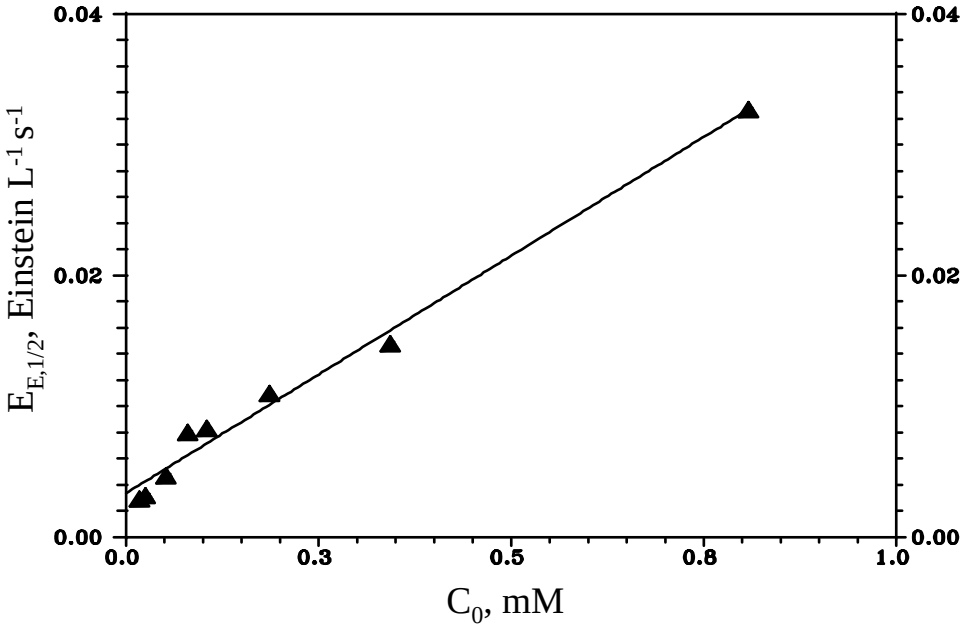

Figure 6.17. *$E_{E,1/2}$ (moles of photons to reduce C_0 one half) as function of the PCP initial concentration. TiO_2 = 200 mg L^{-1}.*

L-H model indicates that k_r is the reaction rate on the catalyst surface. In the case of photocatalytic reactions, where k_r has been calculated using moles of incident photons, instead of time, this constant is the estimated quantum yield (Φ_E). For the PCP in the actual pilot plant Φ_E = 0.0127 (average of the two former values), this is, ~1.3%.

The obtained constants are very similar to those indicated in the bibliography applying L-H to similar compounds (k_r and K have not been formerly determined for PCP). *Matthews* [*1988*] have obtained the following values: k_r = 1.1 x 10^{-4} M min^{-1}, K = 2.3 x 10^3 M^{-1} (phenol); k_r = 1.4 x 10^{-4} M min^{-1}, K = 1.3 x 10^3 M^{-1} (2-chlorophenol); k_r = 7.9 x 10^{-5} M min^{-1}, K = 4.9 x 10^3 M^{-1} (4-chlorophenol). In his experimental device (electrical lamps) the radiation was constant (I^*_E = 8.14 x 10^{-3} Einstein L^{-1} min^{-1}). Therefore, Φ_E = 1.4%, 1.7% and 1.0% respectively. The results shown by *D'Oliveira*'s [*1990*] with 3-chlorophenol were very similar: Φ_E = 2.2% and K = 1.6 x 10^3 M^{-1}. Also with 4-chlorophenol, *Al-Sayyed et al.* [*1991*] have attained similar values: Φ_E = 0.9-1.3% and K = 1.7 x 10^4 M^{-1}. Usually, quantum yields around 1% are very recurrent in heterogeneous photocatalysis [*Legrini et al., 1993; Matthews, 1993*]. Other authors have not clarified the value of I^*_E and, therefore, the rates (k_r) are not comparable. In these cases, the adsorption constants are: K = 4.1 x 10^3 M^{-1} (phenol [*Augliaro et al., 1988*]);

K = 5.7 x 10^3 M^{-1} (phenol [*Barni et al., 1995b*]); K = 1.9 x 10^4 M^{-1} (4-chlorophenol [*Al-Ekabi et al., 1989*]); K = 3.2 x 10^3 M^{-1} (2,4-dichlorophenol [*Serra et al., 1994*]); K = 7±3 x 10^4 M^{-1} (2-fluorophenol [*Minero et al. [1991a*]).

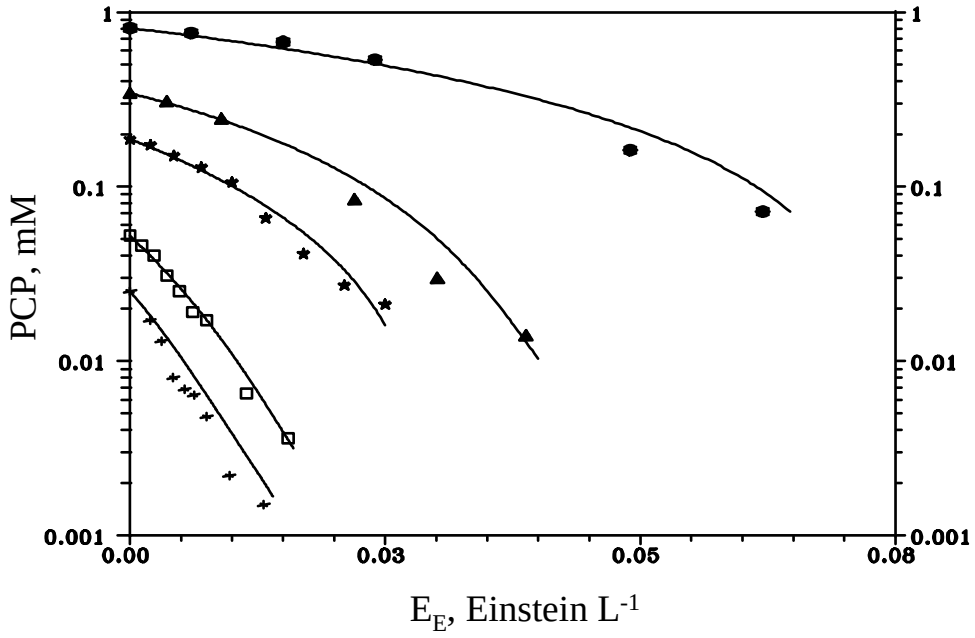

Figure 6.18. *Application of L-H to PCP degradation. The dots are experimental data. The lines are drawn with Eq. 6.5b.*

In agreement with the former, k_r and K obtained from Eqs. 6.5 and 5.5 fit acceptably the behaviour of PCP degradation in a wide range of concentrations. Figure 6.18 shows the performance of Eq. 5.3 using the calculated k_r and K. Eq. 5.3 with E_E instead of t becomes 6.5b:

$$\frac{\ln(C_0/C)}{k_r K} + \frac{(C_0 - C)}{k_r} = E_E \qquad (6.5b)$$

where E_E is accumulated energy, calculated from the illumination time and the photon flux density during the experiments, k_r = 12.7 mMol $Einstein^{-1}$ and K = 17.4 M^{-1}. Consequently, PCP photodegradation behaviour could be foreseen, with an acceptable reliability, knowing the UV radiation intensity and the initial concentration.

To confirm PCP adsorption constant (K), different experiments were carried out in the darkness with different PCP concentrations. No PCP loss has been detected (see Figure 6.6). Therefore, the adsorption has to be very low. A noticeable adsorption has to be detected when filtering the samples to be injected in the HPLC. The adsorbed PCP would have remained in the filter with the TiO_2. The experimental procedure was designed to obtain satisfactory results with low adsorption.

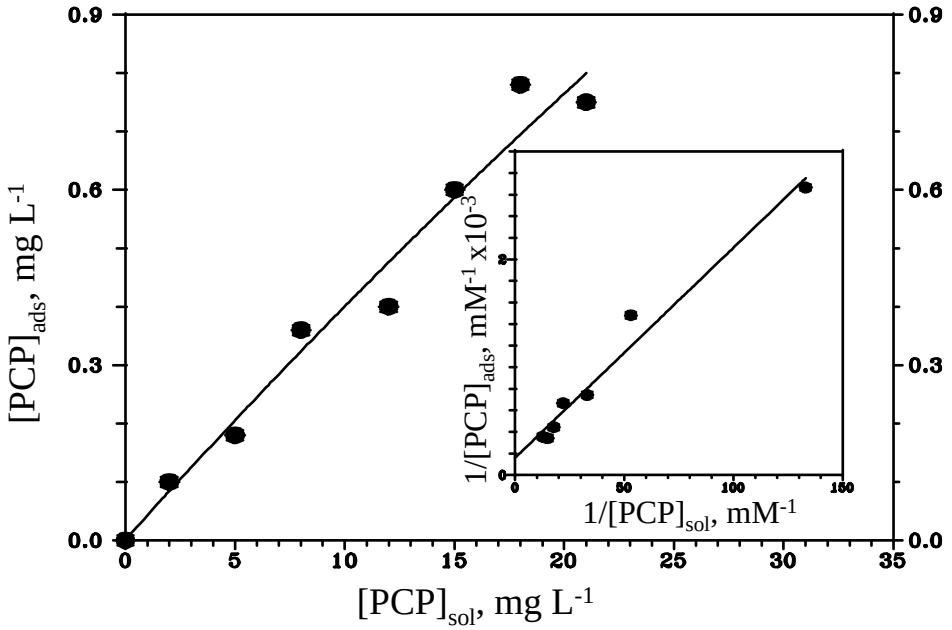

Figure 6.19. *PCP adsorption in the darkness on TiO_2 (200 mg/L). The adsorption isotherm (Eq. 6.6) is shown in the inset.*

The process [*Cunningham et al., 1990*] was the following: (i) weighting of an exact amount of PCP and adding to a 200 mg L^{-1} TiO_2 aqueous suspension of known volume, (ii) mixing during several hours, (iii) filtering (0.45 μm) and measuring by HPLC the PCP concentration in the filtered sample. The adsorption was very low: $[PCP]_{ads}/[PCP]_{sol} \approx 0.04$ (see Figure 6.19). This value is very similar to that found by *Al-Ekabi* [*1991*] for PCP, also in darkness. A large amount of TiO_2-PCP slurry was filtered for better appreciating the quantity of adsorbed PCP. The PCP retained in the filter was eluted with methanol later measured. Both measurements were in agreement.

According to L-H model, when the unique substance competing for the active centres is the solvent, PCP concentration on the catalyst surface is given by an adsorption isotherm:

$$[PCP]_{ads} = \frac{K\,[PCP]_{sol}\,N_C}{1 + K\,[PCP]_{sol}} \qquad (6.6)$$

where N_C is the number of active centres on the catalyst surface. The linearisation of this equation gives rise to the graphic inserted in Figure 6.19, being the intercept $1/N_C = 1.14 \times 10^5$ M^{-1} and the slope $1/(KN_C) = 17.7$. Therefore, $K = 6.4 \times 10^3$ M^{-1}, differs to the formerly obtained. This is, the adsorption constant, calculated with the L-H model, is not only related to the adsorption on the surface, further processes must be involved.

Al-Sayyed et al. [*1991*] have found something similar with 4-chlorophenol and *Cunningham et al.* [*1990, 1991*], with bencyl alcohol, salicylic acid, 4-aminobenzoic acid and 3-chloro-4-hydroxibenzoic acid. They have obtained very different values of K by both procedures. In these articles, it is proposed that it has been related with photoadsorption effects or with other reactions occurring on the surface, as explained in paragraph 5.3 (Eq. 5.8 and next.). *Davis et al.* [*1993*] have become to similar conclusions using a model proposed by them. The rigorous treatment of the kinetics give rises to L-H type equations, even if these are supported on photochemical and radical recombination processes and not on adsorption ones. The following kinetic model is based on the proposed by *Minero* [*1995*], but applied to the particular case of PCP.

6.4.4. Proposed kinetic model

The first steps of the process are, going back to the comments in Chapter 1:

$$h\nu + TiO_2 \xrightarrow{k_f} e^- + h^+ \tag{6.7a}$$

$$e^- + h^+ \xrightarrow{k_R} energy \tag{6.7b}$$

k_f involves the photon absorption rate, e^-/h^+ separation rate and electron migration rate to the catalyst surface. k_R is the electron/ hole recombination rate.

$$e^- + O_2 \xrightarrow{k_{r,1}} O_2^{\bullet -} \tag{6.8}$$

Reaction 6.8 avoids recombination. Also, the generated e^-/h^+ pairs can produce reactions 6.9a, 6.9b and 6.9c.

$$\begin{aligned} h^+ + H_2O &\xrightarrow{k_h} {}^{\bullet}OH + H^+ \quad \text{(a)} \\ h^+ \ (or\ {}^{\bullet}OH) + PCP_{ads} &\xrightarrow{k_{o,1}} R_1 \quad \text{(b)} \\ e^- + PCP_{ads} &\xrightarrow{k_{r,2}} R_2 + Cl^- \quad \text{(c)} \end{aligned} \tag{6.9}$$

where R_1 and R_2 are the intermediate compounds of the proposed degradation pathway (see Figure 6.10b). These reactions and the rests, in which radicals R_1 and R_2 are implied, lead to the following kinetic equations, representatives of the first photodegradation steps:

$$\frac{d[e]}{dt} = k_f I - k_R[e][h] - k_{r,1}[e][O_2] - k_{r,2}[e][PCP]_{ads} \tag{6.10a}$$

$$\frac{d[h]}{dt} = k_f I - k_R[e][h] - k_{o,1}[h][PCP]_{ads} - k_{o,2}[h][R_1] - k_{o,3}[h][R_2] \tag{6.10b}$$

$$\frac{d[R_1]}{dt} = k_{o,1}[h][PCP]_{ads} - k_{o,2}[h][R_1] \tag{6.10c}$$

$$\frac{d[R_2]}{dt} = k_{r,2}[e][PCP]_{ads} - k_{o,3}[h][R_2] \tag{6.10d}$$

This system can be elucidated, analytically, if the illumination is considered constant (at steady state, d[e]/dt = d[h]/dt = d[R_1]/dt = d[R_2]/dt = 0). It has been also supposed, to simplify the calculation, that the recombination rate (k_R[e][h]) is insignificant versus $k_{r,1}$[e][O_2]. The opposite hypothesis implies that [h] = 0, and the degradation would be null [*Minero, 1995*]. The resolution of the system for the PCP degradation rate (Eq. 6.11) is given by Eq. 6.12:

$$-\frac{d[PCP]_{ads}}{dt} = k_{o,1}[h][PCP]_{ads} + k_{r,2}[e][PCP]_{ads} \tag{6.11}$$

$$-\frac{d[PCP]_{ads}}{dt} = \frac{(k_{o,1}k_f^2 I^2[PCP]_{ads}) - (k_{o,1}k_{r,2}k_{r,1}[O_2][PCP]_{ads}^2) - (k_{o,1}k_{r,2}^2[PCP]_{ads}^3)}{(k_R k_{r,1}[O_2]) + (k_R k_{r,2}[PCP]_{ads}) + (2k_f I k_{o,1}[PCP]_{ads})} + \\ + \frac{(k_{r,1}[O_2]k_{r,2}[PCP]_{ads}) + k_{r,2}^2[PCP]_{ads}^2}{k_f I} \tag{6.12}$$

Eq. 6.12 is very complicated and, obviously, it is not useful for engineering design. Anyway it shows, qualitatively, that the reaction rate only depends (when I and [O_2] are constant) on the PCP concentration (concordant with the L-H model). In the present pilot plant, the concentration of oxygen in water is considered constant (the tank is open to the air). The radiation, using Eq. 5.1 as base for the reaction rate calculation, could be considered as a constant.

Hoffmann et al. [*1995*] have proposed approximated rates for reactions 6.7, 6.8 y 6.9. The generation of the e^-/h^+ pair is produced in femtoseconds (10^{-15} s), the recombination in nanoseconds (10 to 100 x 10^{-9} s), the scavenging of the e^- by the O_2 or the PCP in milliseconds (10^{-3} s) and the PCP oxidation in nanoseconds (100 x 10^{-9} s). Therefore, if k_f = k_R x10^8 = $k_{r,1}$ x10^{12} = $k_{r,2}$ x10^{12} = $k_{o,1}$ x10^8 are used in Eq. 6.12, the degradation rate, calculated for different and increasing PCP concentrations, changes in the same way that the experimental results shown in Figure 6.16. Consequently Eq. 6.12, which has been analytically deduced from the kinetic equations of the first steps of the photodegradation reactions (Eqs. 6.10 and 6.11), can behave like the L-H model.

If for the resolution of Eq. 6.11 only reactions 6.7, 6.8 and 6.9b are used (with the same considerations formerly assumed), then a simpler version of the system 6.10 is obtained and, in the same way, a equation similar to 6.12 but simpler (Eq. 6.15).

$$\frac{d[e]}{dt} = k_f I - k_{r,1}[e][O_2] \tag{6.13a}$$

$$\frac{d[h]}{dt} = k_f I - k_R[e][h] - k_{o,1}[h][PCP]_{ads} \tag{6.13b}$$

$$-\frac{d[PCP]_{ads}}{dt} = k_{o,1}[h][PCP]_{ads}$$
$$-\frac{d[PCP]_{ads}}{dt} = \frac{k_{o,1}k_f Ik_{r,1}[O_2][PCP]_{ads}}{k_f k_R I + (k_{o,1}k_{r,1}[O_2][PCP]_{ads})} \quad (6.14)$$

As ($[PCP]_{ads}/[PCP]_{sol}$) = 0.04, then $[PCP]_{sol} \approx [PCP]_0$ and the ratio between $[PCP]_{ads}$ and $[PCP]_0$ is given by Eq. 6.6. From this, Eq. 6.14 is transformed into Eq. 6.15:

$$-\frac{d[PCP]_0}{dt} = \frac{k_{o,1}k_f k_{r,1}[O_2]IKN_C[PCP]_0}{k_f k_R I(1+K[PCP]_0) + k_{o,1}k_{r,1}[O_2]KN_C[PCP]_0} \quad (6.15)$$

Grouping the constants (including $[O_2]$), this equation has the same structure than the L-H model:

$$-\frac{d[PCP]_0}{dt} = \frac{\alpha_1 I[TiO_2][PCP]_0}{\alpha_2 I + (\alpha_3 I + \alpha_4[TiO_2])[PCP]_0} \quad (6.16)$$

where $[TiO_2]$ has replaced N_C, because the catalyst and the experimental device have been always the same (N_C is function of the catalyst type and the reactor illumination method).

Equation 6.16, more exhaustive than Eq. 5.10, fits the experimental results obtained and can be linearised if I and $[TiO_2]$ are constant. During the calculation of k_r and K (Eq. 6.5) both conditions have occurred:

$$-\frac{1}{r_0} = \frac{\alpha_3}{\alpha_1[TiO_2]} + \left(\frac{\alpha_2}{\alpha_1 + [TiO_2]} + \frac{\alpha_4}{\alpha_1 I}\right)\frac{1}{[PCP]_0} \quad (6.17)$$

It is necessary to remind that, if E_E is used instead of t_R (Eq. 5.1), I could be considered constant. So, the intercept ($\alpha_3/\alpha_1[TiO_2]$) is equivalent to $1/k_r$ and the slope analogue to $1/k_rK$.

From Eq. 6.16, it is possible to deduce an overall one (Eq. 6.18). This equation is reminiscent of a Langmuirian rate equation but it has been obtained by an analytical treatment of the reaction mechanism. For this reason, as commented at the beginning of paragraph 6.4.3, the direct use of Eqs. 5.2 or 5.6 gives rise to satisfactory results in most cases. Clearly, although the analytical expression obtained for the rate of photooxidation may be analogous to the L-H relationship, nothing can be concluded about the operational mechanism in these photocatalytic experiments. Nevertheless, Eq. 6.18 is useful for plant design because it allows predicting how the behaviour of the most important variables (I, [PCP] and $[TiO_2]$) will affect the degradation rate.

$$r = \frac{\beta_1 X}{\beta_2 + \beta_3 X} \quad (6.18)$$

In this equation, when X is low, then $r \approx (b_1/b_2)\,X$ and the reaction rate follows a simple linear kinetics. When X is very high, then $r \approx (b_1/b_3)$ and the rate are constant. X could be: (i) $[PCP]_0$ and if $[TiO_2]$ and I are kept constant, then Eq. 6.18 fits the results shown in Fig. 6.16;

(ii) [TiO_2] and, by an analogous deduction, Eq. 6.18 fits with Fig. 6.13; (iii) I and results very similar to those shown in Fig. 2.5 would be obtained, as it will be commented later. Further details concerning this last question appear later in the corresponding section of this document devoted to the influence of the radiation intensity on the degradation rate.

6.4.5. Application of the proposed kinetic model to the Total Organic Carbon

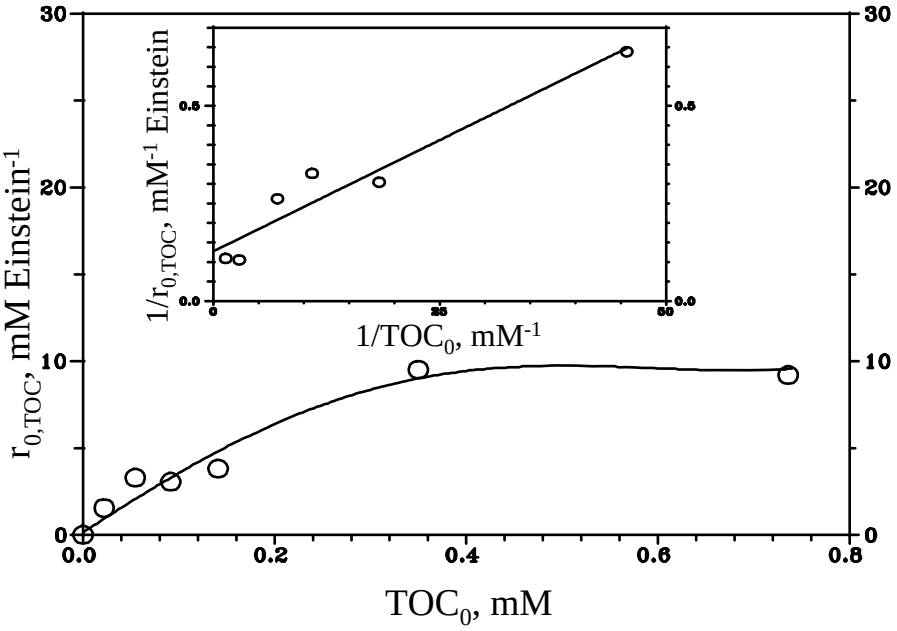

Figure 6.20. *Dependence of TOC degradation rate on TOC initial concentration. r_0 has been calculated using E_E. TiO_2 = 200 mg/L. The inset shows the fitting of these results with the inversion of Eq. 6.19.*

Equation 6.18 can also be used to predict the behaviour of the TOC degradation. For this purpose, it has been assumed that the last steps of the TOC degradation (from the ring breakage to the total mineralization) are a lot faster than the initial steps (generation of PCP equimolar intermediates, Fig. 6.10b). The opposite would mean that the TOC remains constant during most part of the decomposition, and this does not happen (see Figure 6.11). TOC decreases short after the beginning of PCP degradation. In this way, to calculate the TOC molar concentration, it has been considered that 1 Mol TOC = 72 g, this means, 6 atoms of carbon per mol of degraded total organic carbon. With these considerations, the rate of TOC disappearance is given by Eq. 6.19 (analogous to Eq. 6.18). Figure 20 shows experimental results and their successful fitting with the inversion of Eq. 6.19.

$$r_{0,TOC} = \frac{\beta_1 [TOC]_0}{\beta_2 + \beta_3 [TOC]_0} \qquad (6.19)$$

The inversion of Eq. 6.19 permits the calculation of the constants (β_i) from the intercept and

the slope of the fit line:

$$\frac{1}{r_{0,TOC}} = \frac{\beta_3}{\beta_1} + \frac{\beta_2}{\beta_1}\frac{1}{[TOC]_0}$$
$$\frac{\beta_3}{\beta_1} = 0.127 \text{ Einstein mMol}^{-1}; \quad \frac{\beta_2}{\beta_1} = 0.0114 \text{ Einstein L}^{-1} \tag{6.20a}$$

Using these values, experimental results and the corresponding fit lines are shown in Figure 6.21. The experimental results agree reasonably with the proposed model and the calculated constants. This equation will allow predicting the TOC degradation as function of the initial TOC and the available radiation. And the reverse, the number of photons required to reach a determined demineralisation level. Eq. 6.20b is analogue to 6.5b but replacing k_r^{-1} by β_3/β_1 and $(k_r K)^{-1}$ by β_2/β_1.

$$\frac{1}{\beta_1}\left\{\beta_2 \ln\left(\frac{[TOC]_0}{[TOC]}\right) + \beta_3\left([TOC]_0 - [TOC]\right)\right\} = E_E \tag{6.20b}$$

Remembering the similarities between Eqs. 6.20 and Eqs. 6.5, it is possible to relate the calculated constants with the TOC surface rate and TOC adsorption constant (considering these constants involve PCP and all its equimolar intermediates:

$$\beta_3/\beta_1 = 1/k_{r,TOC} \rightarrow k_{r,TOC} = 7.86 \text{ mMol Einstein}^{-1} = 0.00786 \text{ Mol Einstein}^{-1}$$
$$\beta_2/\beta_1 = 1/k_{r,TOC}K_{TOC} \rightarrow K_{TOC} = 11.1 \text{ mM}^{-1}$$

To obtain a correct comparison between these results and those obtained by other authors, who have applied the L-H model directly (k_r is constant of the surface reaction rate), it is necessary to use the produced CO_2 reaction rate. With this porpoise, it has been considered that 1 mol of TOC contains 6 atoms of carbon. As 6 molecules of CO_2 are produced from the TOC corresponding to one PCP molecule, the estimated quantum yield of CO_2 production is $\Phi_{E,CO2} = 0.00786$, this is ~0.8%. These values are of the same order to those obtained with similar compounds, by a direct application of the L-H model: 2-chlorophenol = 0.017, 4-chlorophenol = 0.0097, chlorobenzene = 0.007, phenol = 0.013 [*Matthews, 1988*].

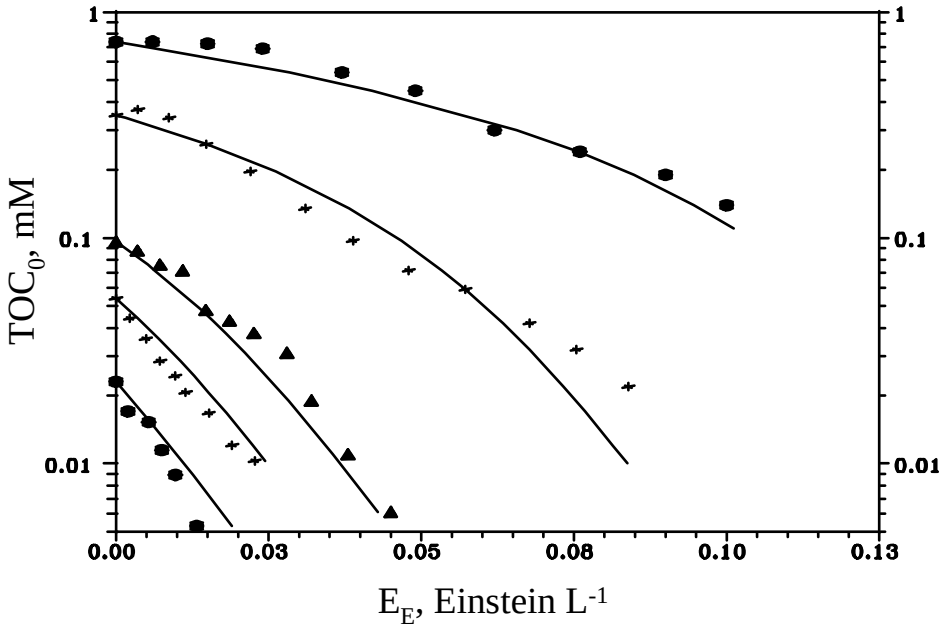

Figure 6.21. *Application of the proposed kinetic model to TOC mineralization. The dots are experimental data. The lines are drawn with Eq. 6.20b.*

Maximum efficiency is shown in Figure 6.20. This one is defined as the maximum degradation rate obtained when increasing the PCP initial concentration. For the production of 1 molecule of CO_2 is 6 x $r_{0,TOC,MAX} \approx 60$ mMol Einstein^{-1} (6%). The oxidation of one molecule of PCP needs, at least, 18 oxidative steps (PCP + $18h^+ \rightarrow 6CO_2$). Therefore, when the PCP concentration is high, the photonic efficiency of the whole system reaches 18% (6% x $18h^+/6CO_2$). This value is very similar to the formic acid quantum yield described in the literature (14-20% [*Sczechowski et al.,1993*]), which produces one molecule of CO_2 per each molecule of acid disappeared.

The obtained maximum quantum yield, calculated from $r_{0,TOC,MAX}$, has not been very high (~1%).In the bibliography there are only a few references where this parameter has been calculated: phenol 1% [*Terzian et al., 1990*], 4-chlorophenol 0.36% [*Linsebigler et al., 1995*] and 1.1% [*Mills et al., 1993b*], 2,4-dichlorophenol 0.4% [*Serra et al., 1994*], 2-etoxyethanol 1.2% [*Brezová et al., 1991*], atrazine 0.063% [*Minero et al., 1996b*], fenitrothion 0.07% [*Kerzhentsev et al., 1996*]. Usually, the mineralization quantum yield of this type of substances is always rather low. It is necessary to increase the quantum yield to avoid very large solar detoxification plants. In the following sections this aspect will be treated in depth.

6.4.6 Conclusions

(I) The optimum TiO_2 concentration in the PSA pilot plant is around 200 mg L^{-1}. Reutilization of the catalyst is possible.

(II) The direct application of the Langmuir-Hinshelwood model has produced an empirical

equation, which fits accordingly the PCP degradation experimental data. This equation is useful in a wide range of initial concentrations. This model is necessary for engineering plant design. Experimentation at pilot plant level is essential to obtain these equations.

(III) The kinetic parameters obtained with L-H application do not have the mechanistic meaning proposed by this model. The experimental data are correctly adjusted by an empirical equation, $r = \beta_1 X (\beta_2 + \beta_3 X)^{-1}$, which constants ($\beta_1$, β_2 and β_3) are very useful for the design. The value of these constants will be different when X is $[TiO_2]$ or I, instead of C_0.

(IV) Eq. 6.18 can also be applied to the total mineralization of PCP (final objective of the process). The following expression will allow the design of a plant to mineralize a determined quantity of PCP. Being $\beta_3/\beta_1 = 0.127$ Einstein $mMol^{-1}$ and $\beta_2/\beta_1 = 0.0114$ Einstein L^{-1}, it is possible to know E_E.

$$\frac{1}{\beta_1}\left\{\beta_2 \ln\left(\frac{[TOC]_0}{[TOC]}\right) + \beta_3\left([TOC]_0 - [TOC]\right)\right\} = E_E \qquad (6.21)$$

From this, it is possible to know the required solar collector area as function of: a) PCP concentration and quantity of water to be treated and, b) UV radiation data at the plant location.

6.5. Influence of the intensity of illumination on quantum yield

The photocatalytic reaction rate in heterogeneous phase depends, among other factors, on the intensity of the illumination. As mentioned in Section 2.2 (see Figure 2.5) there is a transition from a linear relationship ($r = k\ I$) to $r = k'\ I^{0.5}$. To evaluate the performance of a pilot plant, it is very important to find out whether the reaction rate behaves one way or another. If it increases by the square root of the intensity of illumination, Eq. 6.21 cannot be used directly, since incident radiation is not as well used at high intensities.

6.5.1. Bibliographic background

There are lots of articles on this aspect of photocatalysis, where the authors provide information concerning the level of light intensity where the change of order is produced. In some the value of illumination is provided in W_{UV} m^{-2}, in others as Einstein L^{-1} s^{-1} and in others in Einstein m^{-2} s^{-1}, depending on how this parameter was measured (radiometric or actinometric methods, see chapter 4). This causes some problems when attempting to compare results, since the relationship between W_{UV} and Einstein s^{-1} depends on the spectrum of the radiation source. But almost all those that mention W_{UV}, fortunately, use experimental equipment that provide radiation similar to solar (when not actually solar radiation) and

therefore, for the purposes of comparison, the standard: 22 W_{UV} m^{-2} = 6 x 10^{-5} Einstein m^{-2} s^{-1} [*ASTM, 1987a*] will be used. The relationship between volume and surface is more difficult to evaluate, since it depends on the configuration of the reactor, but it is possible to carry out the comparison with the pilot plant under study since it was calculated both ways (see Eqs. 4.15, 4.16, 4.20 and 4.21). In Table 6.6 the limits proposed by different authors, where the reaction rate is directly proportional to the intensity of illumination, are summarised.

Compound tested	**r = k I Limit**	**Bibliographic reference**
4-chlorophenol	I≤ 100 W_{UV} m^{-2}	*Al-Sayyed et al., 1991*
Chloroform	NO*****	*Bahnemann et al., 1991a*
Dichloroacetic acid	I<6 x 10^{-5} Eins L^{-1} s^{-1}	*Bahnemann et al., 1993a*
Acetic acid	I≤ 2 x 10^{-6} Eins L^{-1} s^{-1}	*Bideau et al., 1990*
Formic acid	I≤ 2 x 10^{-5} Eins L^{-1} s^{-1}	*Bideau et al., 1991*
Trichloroethylen	I≤ 2.3 x 10^{-4} Eins m^{-2} s^{-1}	*Blake et al., 1991*
Dichloroacetic acid	I≤ 10^{-4} Eins m^{-2} s^{-1}	*Bockelmann et al., 1992*
3-chlorophenol	I≤ 2.6 x 10^{-4} Eins m^{-2} s^{-1}	*D'Oliveira et al., 1990*
Chloroform	I≤ 5 x 10^{-7} Eins L^{-1} s^{-1}	*Kormann et al., 1991*
Trichloroethylen	I≤ 660 W_{UV} m^{-2}	*Magrini et al., 1990*
4-chlorophenol	I≤ 6 x 10^{-4} Eins L^{-1} s^{-1}	*Martin et al., 1995a*
Pentachlorophenol	I≤ 3.2 x 10^{-6} Eins L^{-1} s^{-1}	*Mills G. et al., 1993*
Phenol	I≤ 10^{-5} Eins m^{-2} s^{-1}	*Okamoto et al., 1985b*
Formiate	I≤ 7 x 10^{-5} Eins m^{-2} s^{-1}	*Sczechowski, 1993*
Phenol	I≤ 1.5 x 10^{-5} Eins L^{-1} s^{-1}	*Trillas et al., 1994*

*** Not linear at any interval**

Table 6.6

In other cases, this limit is not clear. *Al-Sayyed et al.* [*1991*] have found that the rate is proportional to $I^{0.5}$ for I>22 W m^{-2}, although up to I≤100 W m^{-2} the data also fit to r = k I. *Barni et al.* [*1995a*] have obtained similar results, for the degradation of phenol with lamps and fixed TiO_2, since r = k I and r = k' $I^{0.5}$ for the entire interval of intensities used (unspecified). *Ollis* [*1991b*] has commented, for the case of a parabolic trough collector illuminated by solar radiation, that the two situations cannot be distinguished. On the other hand, *Mills et al.* [*1993b*] have found that for illumination intensities between 8 x 10^{-6} and 10^{-4} Einstein m^{-2} s^{-1}, the reaction rate is related with I by r = k $I^{0.75}$. That is, there is a transition zone between r = k I and r = k' $I^{0.5}$.

The values found are very unlike. It may only be intuited that the intensity at levels of several suns (1 sun_{UV} = 22 W_{UV} m^{-2}), the quantum yield diminishes. *Ollis* [*1991b*] and *Herrmann* [*1995*] have proposed this limit as correct, although some authors indicate that even this would be produced at less than one sun. The pilot plant under study is made up of parabolic trough collectors which concentrate the solar radiation ten times, but, since the efficiency is approximately 60%, the final concentration is about six times. Considering maximum solar radiation of about 35 W_{UV} m^{-2} (direct) and 45 W_{UV} m^{-2} (global), and using equations 4.15c, 4.16c (both with R = 70%), 4.20c and 4.21c the following results are obtained:

$$I_{E(300\text{-}387)} = I_{D,E(300\text{-}387)} + I_{G;E(300\text{-}387)} = 6.0 \times 10^{-4} \text{ Einstein } m^{-2} s^{-1}$$

$$I^{*}_{E(300\text{-}387)} = I^{*}_{D,E(300\text{-}387)} + I^{*}_{G;E(300\text{-}387)} = 4.1 \times 10^{-5} \text{ Einstein } L^{-1} s^{-1}$$

The above data correspond to the maximums attainable in the pilot plant. As observed when compared to those in Table 6.6, the maximum intensities are on the same order as those proposed in some cases and higher in others. Due to this uncertainty, it becomes necessary to carry out a series of experiments to find out the behaviour of the pilot plant studied. But before entering into detail on the results obtained, it is advisable to explain the reason for this change of order.

The first authors who give an explanation for this effect were *Egerton and King* [*1979*]. Their reasoning is very simple, but nonetheless valid. In fact it is mentioned as correct in articles published a short time ago [*Serra, et al., 1994; Martin et al., 1995a*]. This reasoning is based on the first stages of the process. Recalling equation 6.13b, but applied to any reactant R:

$$\frac{d[h]}{dt} = k_f I - k_R [e] [h] - k_o [h] R \qquad (6.22)$$

If it is considered that [e] ≈ [h] (simplification considered as valid by other authors [*Turchi et al., 1990a; Gerischer, 1993; Martin et al., 1995a*]), then in stationary state:

$$\frac{d[h]}{dt} = 0 \rightarrow k_f I = k_R [h]^2 + k_o [h] R \qquad (6.23)$$

When I is very high, a large number of holes and electrons are generated (Eq. 6.7) and therefore $k_R[h]^2 \gg k_o[h]R$:

$$k_f I \approx k_R [h]^2 \rightarrow [h] \approx K I^{0.5} \qquad (6.24)$$

As the reaction rate depends on the amount of hydroxyl radicals present, and these are generated in the holes (see Eq. 1.1 to 1.9), then $r \propto I^{0.5}$ when I is high. Under these conditions, the quantum yield diminishes because of the high rate of recombination of e^-/h^+ pairs formed (k_R is the constant of the recombination reaction, Eq. 6.7). In the same manner, when I is small, the inverse is true, $k_R[h]^2 \ll k_o[h]R$:

$$k_f I \approx k_o [h] R \rightarrow [h] \approx K' I \qquad (6.25)$$

Several years later, *Turchi* and *Ollis* [*1990a*], in a very complete study on the mechanisms in which hydroxyl radicals are involved and used as a reference by many authors, went a little

further into this reasoning. Based on the principle that the reaction takes place between an adsorbed reactant (R_{ads}) and an $^{\bullet}OH$ radical in solution (situation ii of those commented in Section 5.3), the reaction rate is:

$$r \approx k_1 \left[{}^{\bullet}OH \right] \left[R_{1,ads} \right] \tag{6.26}$$

The reactions in which hydroxyl radicals are involved are:

$$Ti\text{-}OH^- + h^+ \underset{k_{2-}}{\overset{k_{2+}}{\leftrightarrow}} Ti\text{-}OH^{\bullet}; or\ Ti\text{-}H_2O + h^+ \underset{k_{2-}}{\overset{k_{2+}}{\leftrightarrow}} Ti\text{-}OH^{\bullet} + H^+ \tag{6.27}$$

$$Ti\text{-}OH^- \underset{k_{3-}}{\overset{k_{3+}}{\leftrightarrow}} Ti\text{-}OH^{\bullet} \tag{6.28}$$

$$^{\bullet}OH + R_{1,ads} \xrightarrow{k_1} R_{2,ads} \tag{6.29}$$

As the reactions in 6.27 depend on the pH of the solution (as commented in Section 6.3.3), no distinction is made between their constants, since in any case one or the other will be the case. In stationary state, the variation in the concentration of the hydroxyl radicals will be null:

$$\frac{d\left[{}^{\bullet}OH \right]}{dt} = k_{2+} \left[h \right] \left[Ti(OH) \right] - k_{2-} \left[TiOH^{\bullet} \right] - k_1 \left[OH^{\bullet} \right] \left[R_{1,ads} \right] = 0 \tag{6.30}$$

where (OH) may be OH^- or H_2O. As the Ti(OH) concentration is practically constant, $k_{2+}[Ti(OH)] \approx k'_{2+}$. Furthermore, $[TiOH^{\bullet}] = K_3 [OH^{\bullet}][Ti]$, where $K_3 = k_{3+}/k_{3-}$. Thus the concentration of hydroxyl radicals is:

$$\left[{}^{\bullet}OH \right] = \frac{k'_{2+} \left[h \right]}{k_{2-} K_2 \left[Ti \right] + k_1 \left[R_{1,ads} \right]} \tag{6.31}$$

Therefore, the concentration of hydroxyl radicals is directly proportional to that of holes. In order to find out [h] the procedure is similar:

$$\frac{d\left[h \right]}{dt} = k_f I - k'_{2+} \left[h \right] + k_{2-} \left[TiOH^{\bullet} \right] - k_R \left[e \right] \left[h \right] = 0 \tag{6.32a}$$

where k_f and k_R correspond to reaction 6.7.

Likewise *Egerton and King* [*1979*], Turchi and Ollis have assumed that [h] ≈ [e] and therefore $[h][e] \approx [h]^2$. Since recombination is faster than capture of holes by the surface of the catalyst (Eq. 6.27), as k_{2+} and k_{2-} are of the same order (later confirmed by *Hoffmann et al.* [*1995*]) and since if I is high [h] is also, then $k_R[h]^2 \gg (k'_{2+}[h] - k_{2-}[TiOH^-])$ is possible. This allows simplification of equation 6.32a and yields 6.33:

$$\frac{d\left[h \right]}{dt} = k_f I - k_R \left[h \right]^2 = 0 \tag{6.32b}$$

$$[h]_{high} = \left(\frac{k_f I}{k_R} \right)^{1/2} \tag{6.33}$$

If I is low, $k_R[h]^2$ « $(k'_{2+}[h] - k_{2-}[TiOH^{\cdot}])$:

$$[h]_{low} = \frac{k_f I + k_{2-}[TiOH^{\bullet}]}{k'_{2+}} \tag{6.34}$$

If equations 6.33 or 6.34 are substituted in 6.31 $[OH^{\cdot}] = f(I)^{0.5}$ or $[OH^{\cdot}] = f(I)$ is obtained. And in the expression for reaction rate (Eq. 6.26) the same is true. It may be observed that the treatment of the kinetics is more complex than that used by Egerton and King, but the result is the same. The change of order is due to the recombination of the pairs generated.

Also the same year, *Kormann et al.* [*1991*] have proposed a different theory based on the radiation absorbed by the catalyst (I_a). In this case, the hydroxyl radicals generated can be consumed by reaction 6.9b or by:

$$2^{\bullet}OH \xrightarrow[k_{H2O2}]{} H_2O_2 \tag{6.35}$$

and the equation for the speed of hydroxyl radical would be:

$$\frac{d[^{\bullet}OH]}{dt} = I_a \Phi_{\bullet OH} - k_o[^{\bullet}OH][S] - k_{H2O2}[^{\bullet}OH]^2 \tag{6.36}$$

where $\Phi_{\bullet OH}$ is the quantum yield of hydroxyl formation. Considering $\Phi_{\bullet OH} \approx 1$ and in stationary state:

$$I_a = k_o[^{\bullet}OH][S] - k_{H2O2}[^{\bullet}OH]^2 \tag{6.37}$$

The quantum yield of oxidation of the substrate S is:

$$\Phi_S = \frac{k_o[^{\bullet}OH][S]}{I_a} = \frac{k_o[^{\bullet}OH][S]}{(k_o[^{\bullet}OH][S]) + (k_{H2O2}[^{\bullet}OH]^2)}; \begin{cases} A = k_o[^{\bullet}OH][S] \\ B = k_{H2O2}[^{\bullet}OH]^2 \end{cases} \tag{6.38}$$

If the intensity of illumination is low, then the radiation absorbed is also and $[^{\bullet}OH]$. Under these conditions A » B and $\Phi_S \approx 1$. If I_a is high, B » A ($I_a \approx B$) and Eq. 6.38 can be simplified obtaining:

$$\Phi_S = \frac{k_o[S]}{(k_{H2O2} I_a)^{1/2}} \tag{6.39}$$

Therefore, the increase in intensity of illumination has a limit after which the reaction rate does not increase appreciably. Recombination of electron/hole pairs, as well the formation of H_2O_2 by combination of hydroxyl radicals, are both reactions competitive with substrate degradation. This effect may be appreciably attenuated if some product that reduces the importance of the two inhibiting reactions mentioned is added.

Pacheco et al. [*1990b*] and *Tyner et al.* [*1990*] are able to maintain a linear relationship between the degradation rate of salicylic acid and the intensity of illumination up to 450 W_{UV}

L^{-1} (~1.2 x 10^{-3} Einstein L^{-1} s^{-1}) by adding hydrogen peroxide. They use different reactors, but in the one on which the most radiation is incident, 1 L is equivalent to 0.35 m^2 of reactor. Similar results are obtained by *Halmann et al.* [*1992*] with tetrachloroethylene. In presence of H_2O_2 the reaction is linear up to 100 suns. The explanation for this may be based on the following reaction:

$$H_2O_2 + e^- \rightarrow {}^{\bullet}OH + OH^- \tag{6.40}$$

Thus, when the electrons are trapped, recombination of e^-/h^+ is impeded, although the importance of reaction 6.35 may also be reduced, or both at the same time. Either way, addition of oxidants can improve the efficiency of the process at high illumination intensities. Moreover, this type of compounds can increase the quantum yield even at low irradiation levels due to their strong oxidising character, as demonstrated later in section 6.6.

6.5.2. Pilot Plant Results

To accomplish experiments for finding out where in the pilot plant the relationship between intensity of illumination and reaction rate is, the value of I has had to be varied appreciably. For this it has been necessary to modify the usual solar collector conditions. The highest points of intensity in Figure 6.22 correspond to the normal situation (see Figures 4.8 and Eq. 4.29). The intermediate points correspond to tests performed with half of the parabolic trough collector mirrors covered (see Figure 4.9, Eq. 4.16f and Eq. 4.21c), in order to vary the concentration factor of the module. The lowest points of intensity were obtained by carrying out the experiments with the module completely horizontal and without solar tracking. Under these conditions no light is concentrated and the solar radiation only reaches the reaction through the glass tube (see Eq. 4.21c), without involvement of the mirrors. This procedure had already been followed previously by *Mehos et al.* [*1992b*], with 1-axis-tracking parabolic-trough collectors for the same purpose. At the same time, experiments were carried out at different hours of the day so that the intensity of solar radiation would vary.

The initial concentration of PCP was 25 mg L^{-1} and the rate shown the following figures corresponds to the initial reaction rata. This way the results correspond to the linear zone of degradation (see Figure 5.2). Likewise, the experiments were short. Therefore, the solar illumination did not vary appreciably during each test. In order to calculate I*, the average of UV_D y UV_G given by the radiometers, during the same interval for which the reaction rate (r) was calculated, was used.

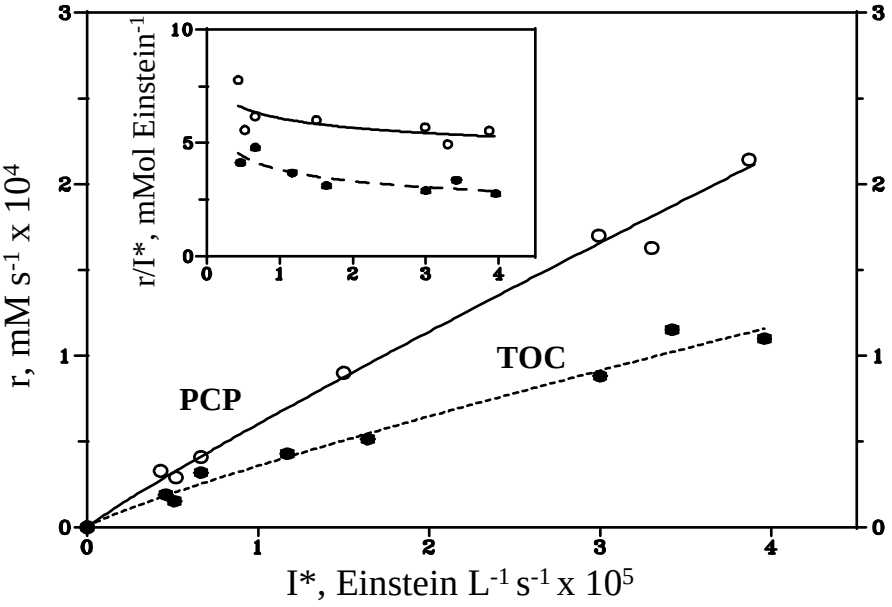

Figure 6.22. *Effect of the intensity of illumination per unit of reactor volume (I*<387 nm) on degradation rate. TiO_2 = 200 mg/L. In the graphic insert, the ratio between the reaction rate and I* as function of I* is shown.*

As shown in Figure 6.22, the effect of intensity of illumination on degradation of PCP and TOC (1 mMol = 72 mg) is similar. Practically linear dependence is observed in both cases. The graphic insert in Figure 6.22 shows that process efficiency diminishes slightly when I^* is increased. This indicates that the maximum zones of irradiation are in the transition between $r = k\ I$ and $r = k'\ I^{0.5}$. In Figure 6.22b this is confirmed even more. The reaction rate in the zone of highest irradiance seems to be proportional to the square root of intensity. However, for the parabolic trough collectors used for this work, it is reasonable to consider the rate directly proportional to the intensity of illumination throughout all the range of intensities. The use of a solar concentration similar to that of the pilot plant collectors would not diminish process efficiency.

In the graphic insert in Figure 6.22b and Figure 6.23, I was used (Eqs. 4.15 and 4.20) instead of I*. This was done in case some factor was masked by the use of reactor volume instead of reactor surface exposed to solar radiation. It should be remembered that $I_{D,E,1/2}$ is not half of $I_{D,E}$ (see Eq. 4.15), although $I^*_{D,E,1/2}$ is in fact half of $I^*_{D,E}$ (see Eq. 4.16). The results are similar when the illuminated reactor area is used instead of volume.

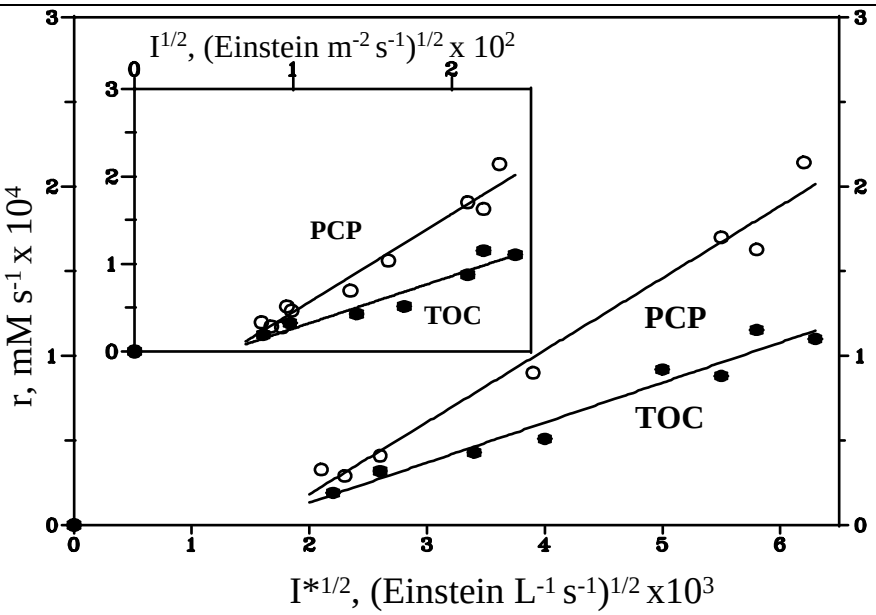

Figure 6.22b. *Ratio between the square root of intensity of illumination by unit of reactor volume (I*<387 nm) and degradation rate. TiO_2 = 200 mg/L. In the graphic insert, the ratio is the same, but by unit of reactor surface.*

Since only the first part, $r \approx (\beta_1/\beta_2)X$, of the model proposed (Eq. 6.18, X=I), is fulfilled, the graphic insert in Figure 6.23 allows acceptable fulfilment of the model to be confirmed. At the levels of illumination intensity attainable in the pilot plant, $r \approx \beta_1/\beta_3$ has never been reached.

6.5.3 Conclusions

(I) The reaction rate is directly proportional to the intensity of illumination in the pilot plant studied. Therefore, Eq. 6.21 may be used directly for the design.

(II) Since the maximum intensity obtained with the parabolic trough collectors is about 10 suns, these results are valid for collectors of lower or equal concentration factors. The diameter of the absorber tube must be very similar to extrapolate these results to other solar collectors (see Figure 6.12).

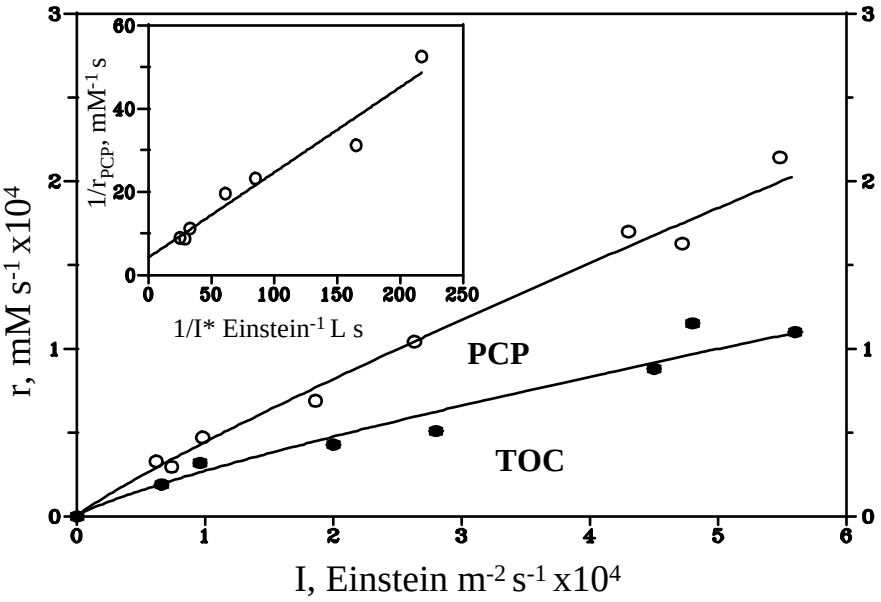

Figure 6.23. *Effect of the intensity of illumination by unit of reactor surface (I <387 nm) on degradation rate. TiO_2 = 200 mg/L. In the graphic insert linearization of Eq. 6.18 appears for X = I*.*

6.6 Quantum yield improvements by additional oxidants

As it has been commented before, oxygen is crucial for the photomineralization. The oxygen scavenges e^- avoiding e^-/h^+ recombination and it is also necessary for CO_2 production. The adding of other oxidising species must be considered, as different effects could be gain: (i) increasing the number of trapped e^- of the e^-/h^+ pairs and, consequently, avoid recombination; (ii) generating more quantity of $^\bullet OH$ as well as other oxidising species; (iii) increasing the oxidation rate of intermediate compounds; (iv) avoiding problems caused by a low $[O_2]$. The oxidising substance should not generate any toxic by-product. Hydrogen peroxide is the obvious candidate [*Bahnemann et al., 1994b*], proposed as intermediate in the photocatalytic process [*Pelizzetti et al., 1991a*]. H_2O_2 could increase the efficiency of the process at high irradiance level (see paragraph 6.5.2) and it has been tested with a large number of compounds, as explained bellow. Also, it is a very commonly and cheap chemical.

6.6.1 Hydrogen peroxide effect

H_2O_2 can generate $^\bullet OH$ by reaction 6.40, which also helps to avoid the recombination of e^-/h^+ pairs. The following reactions can also produce $^\bullet OH$ (reaction 6.42 does not take place with solar radiation, it needs λ < 300 nm [*Ollis et al., 1991a*]):

$$H_2O_2 + O_2^{\bullet -} \rightarrow {}^\bullet OH + OH^- + O_2 \qquad (6.41)$$

$$H_2O_2 + h\upsilon \rightarrow 2\,{}^\bullet OH \qquad (6.42)$$

Although, "a priori", the addition of this oxidant to the photochemical reaction should increase the reaction rate, it is not always so. *Brown et al*. [*1984*] have demonstrated that when using H_2O_2 the degradation rate of methyl orange decreases. The concentration used is very low (4.5 and 12 x 10^{-5} M, between 2 and 6 times higher than the dye). Years later, *Pichat et al.* [*1995a*] have shown a similar effect during the photodegradation of 1,2-dimetoxibencene (C_0 = 0.145 mM). When the molar ratio is <10, degradation rate decreases. However, when it is higher (molar ratio 30-100) the efficiency increases, decreasing again when the molar ratio is >100. *Brown et al.* have attributed this effect to the holes scavenging by hydrogen peroxide. Consequently, hydroxyl radicals formation is reduced:

$$H_2O_2 + 2h^+ \rightarrow O_2 + 2H^+ \qquad (6.43)$$

Pichat et al. [1995a] agree with this inference, but they propose that reaction 6.44 could also give rise, which decreases the amount of available hydroxyl radicals. The generated radical ($HO_2^{\bullet}$) is less reactive than $^{\bullet}OH$ [*Wolfrum et al., 1994*]:

$$H_2O_2 + {}^{\bullet}OH \rightarrow H_2O + HO_2^{\bullet} \qquad (6.44)$$

Besides this type of reactions, hydrogen peroxide can also influence the catalyst. *Boonstra et al.* [*1975*] have described that H_2O_2 is able to be adsorbed on TiO_2. *Klissurski et al.* [*1990*] have commented that, not only hydrogen peroxide is adsorbed, also hydroperoxide groups formed from H_2O_2. This effect produces competition between these species and the substrate by the catalyst active centres. The competition will depend upon the type of compound to be degraded.

Different authors have confirmed the situation described by Pichat. They demonstrate that the utilisation of hydrogen peroxide in excess can be negative for the process efficiency. *Tanaka et al.* [*1989a*] have found the optimum between 4 and 12 mM of H_2O_2 for 0.35 mM of tricloroethylene (molar ratio between 10 and 30, the rate is increased ~800%), decreasing clearly the rate for [H_2O_2] > 50 mM. These authors [*Tanaka et al., 1989b*], with chloral hydrate ($CCl_3CH(OH)_2$) 0.1 mM, obtained similar results: optimum between 0.34 and 7 mM of H_2O_2 (rate increases up to 2.5 times). Efficiency decreases clearly over 20 mM. *Hisanaga et al.* [*1990*] have shown very similar results with 12 chlorinated solvents (Cl_xC and Cl_xC_2). The optimum is $H_2O_2$10 mM with solvent 0.05 mM.

Treatment with $TiO_2/H_2O_2/UV_{solar}$ combination is also very effective for a large number of compounds: aromatics, halogenated aromatics, triacines, acetamides, halogenated hydroxybenzenenitrils, etc. All of them summarised in a very interesting work by *Muszkat et al.* [*1992*]. *Akmehmet et al.* [*1996*] have proposed an optimum (5-10 mM) for the decomposition of 17 compounds, among which several phenols and chlorophenols are included, at 0.1 mM. This agrees with other authors conclusions (molar ratio between 50 and

100 times). In these conditions decomposition rate (measured as produced CO_2) increases about 300%. A clear example of the requirement to optimise the use of hydrogen peroxide can be found in a work by *Enzweilwer et al.* [*1994*] about benzene degradation. When peroxide 0.02 M is added at the beginning of the process, the decomposition rate is 10 times slower than the same quantity added in 5 steps.

Some authors have described behaviours of the H_2O_2 which do not correspond exactly to the former comments. *Augliaro et al.* [*1990*], with phenol 1 mM, have obtained a rate increase from 0 to 6 mM of peroxide and, from then up to 20 mM (maximum tested concentration), the rate remains constant. These authors have explained such an effect (no inhibition at low H_2O_2 concentration) proposing that phenol and peroxide are adsorbed in different sites of the catalyst. This reasoning is based in H_2O_2 degradation rate. It is the same in presence and absence of phenol. The second part of the H_2O_2 effect (inhibition due to high oxidant concentration), it is not demonstrated nor rejected by the authors. They have not used a molar ratio enough high. In this year, *Chemseddine et al.* [*1990*] have tested the effect of H_2O_2 0.2 M during the photodegration of chloroacetic acid 0.2 mM. They have attained lower rate than with TiO_2 alone. They have justified it only from the effect of competitive adsorption. However, without testing other molar ratios (they have used a ratio of 1000), it can not be concluded that this inhibition effect should occur at lower ratio, too. *Pelizzetti et al.* [*1991a*] also have obtained inhibition with H_2O_2 10-100 mM and atrazine 0.12 mM, perhaps because they have used a very high peroxide concentration. *Hofstadler et al.* [*1994*], with 4-chlorophenol and a molar ratio of 50, have achieved an increase in the degradation rate. However, the TOC rate is not affected. In the previously commented article (*Akmehmet et al.*), the 4-chlorophenol mineralization rate is increased with a very similar H_2O_2/4-chlorophenol molar ratio. The explanation to this effect should be related with the illumination of the photoreactor (UV lamps with emission shorter than 300 nm). The TOC degradation rate increased in presence of peroxide because the radiation source emitted at wavelength shorter than 300 nm. In this case reaction 6.42 becomes important.

In a very exhaustive work, which includes calculations performed from L-H model and published by *Bellobono et al.* [*1994*], an intend to explain experimentally all the above mentioned is developed. With TiO_2 supported on a membrane and with different quantities of H_2O_2 and trichloroethylene the following results were obtained: (i) the adsorption constant of TCE decreases substantially when increasing [H_2O_2]; (ii) at a fixed molar ratio (30 = H_2O_2/TCE), degradation rate is lower when peroxide is present and TCE concentration is less than 0.25 mM; (iii) at higher concentration, H_2O_2 increases the efficiency when TCE concentration increases; (iv) up TCE 5 mM the rate is constant. This implies that the adsorption effect of H_2O_2 is very important.

Retrieving the L-H model, $r = k_r KC/(1+KC)$, when C is low ($r \approx k_r KC$) and, at the same time, H_2O_2 is added. Under these circumstances the substrate adsorption is reduced by the presence of H_2O_2 and therefore the rate could be lower with peroxide than without. Also, the additional $^{\bullet}OH$, generated by reaction 6.40 and 6.41, can not be efficiently used due to the low concentration of substrate. When C is higher, the rate also increases (see Eq. 6.26) and the additional hydroxyl radicals can be more efficient. When C is very high ($1+KC \approx KC$ and $r \approx k_r$), and the molar ratio H_2O_2/TCE is constant, the rate is invariable. At this time, the rate does not depend on adsorption and k_r only depends on [$^{\bullet}OH$]. The amount of available hydroxyl radicals is related with the reactions that produce them and those which consume them. Reactions 6.43 y 6.44 become important at high H_2O_2 concentration [*Peterson et al., 1991*] and the beneficial effect of reactions 6.40 and 6.41 lessen. At high molar ratios it is expected an inhibition effect because reactions 6.43 and 6.44 become more and more important.

Due to the disparity of the results shown in the bibliography about H_2O_2 effect, it is necessary to test it with PCP, from which, on the other hand there is no antecedent. The effect of hydrogen peroxide concentration on the photocatalytic rate depends on the treated compound and the experimental conditions [*Bahnemann et al. 1994b*]. H_2O_2 concentration has been selected in accordance with the results obtained by other authors and the restrictions imposed by the reactor. Before going ahead the photocatalytic experiments, tests were carried out in the darkness to determine the capacity of hydrogen peroxide to decompose PCP without radiation. Results are shown in table 6.7. Only a slight effect is produced on the PCP (none on the TOC) at very high concentration (120 mM). This concentration has not been used in the pilot plant.

$[H_2O_2]$, mM	**$[PCP]_0$, mg L^{-1}**	**$[COT]_0$, mg L^{-1}**	**$[PCP]^*_F$**	**$[COT]^*_F$**
120	27.1	9.3	22.0	9.6
60	26.6	9.6	24.9	9.5
12	26.3	8.0	25.2	8.0

*** After 24 h in the darkness**

Table 6.7

Figure 6.24 shows the first experiment carried out to adjust the optimum conditions. The initial PCP concentration used in all cases was ~0.1mM. Hydrogen peroxide (concentrated solution 12.3 M) is added directly to the tank E (see Figure 3.7.b). The mixture is recirculated at high flow rate (4000 L h^{-1}), with only one module, to reduce as much as possible the volume of the system. This procedure intends to minimise the reactants cost and to obtain a perfect mixture almost instantly. The former is very important because oxidant must be added

along the experiment. In this type of experiment a slight decomposition is produced prior to the experiment start (see 3rd point of paragraph 3.4.2). This decomposition (marked with 1 in figure 6.24) is originated by the interval existing between the peroxide addition and the first sample, done several minutes after to ensure a good mixture.

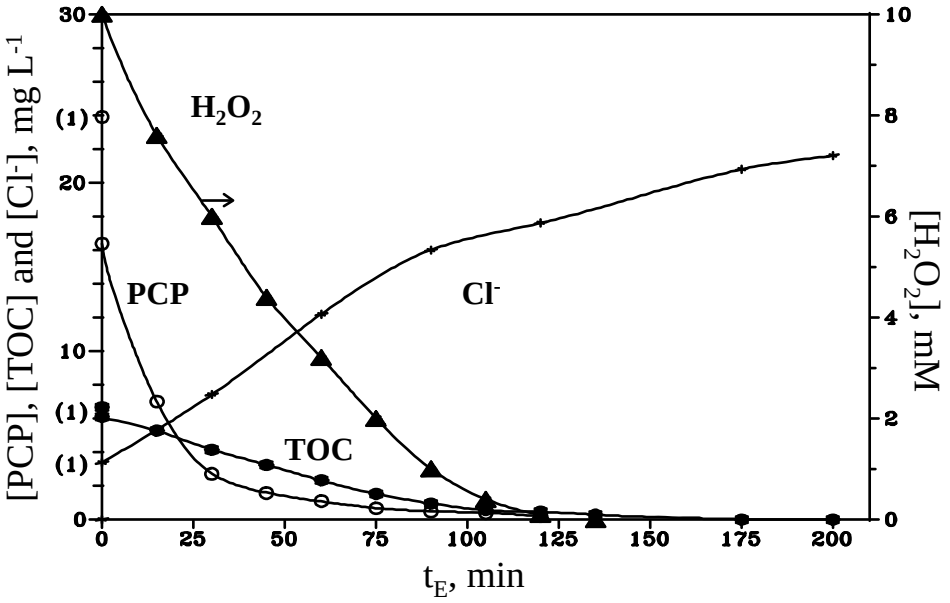

Figure 6.24. *PCP degradation with H_2O_2. 1 Module, TiO_2 200 mg L^{-1}.*

Taking into account the obtained results and being t_E (15 min) the sampling interval (see Eq. 3.5), the addition of peroxide along the experiment was necessary to keep a steady concentration. This concentration was 10±2.5 mM, because PCP or TOC decomposition rate does not change between this interval. As the pilot plant was not designed to inject in continuous, it had to be added by hand in the tank. The decomposition rate of H_2O_2 was approximately 7 mM h^{-1}, therefore 2.5 mM were added every 15 minutes (a little quantity in excess). To guarantee that H_2O_2 concentration was correct, this parameter was analysed in all the samples. The minimum initial concentration used was ~5mM. At smaller concentration it would be impossible to keep it stable. Figure 6.25 shows an experiment performed at H_2O_2 10 mM (constant). There was also a small decomposition during homogenisation in the reactor. The rest of conditions are similar to those in Figure 6.24.

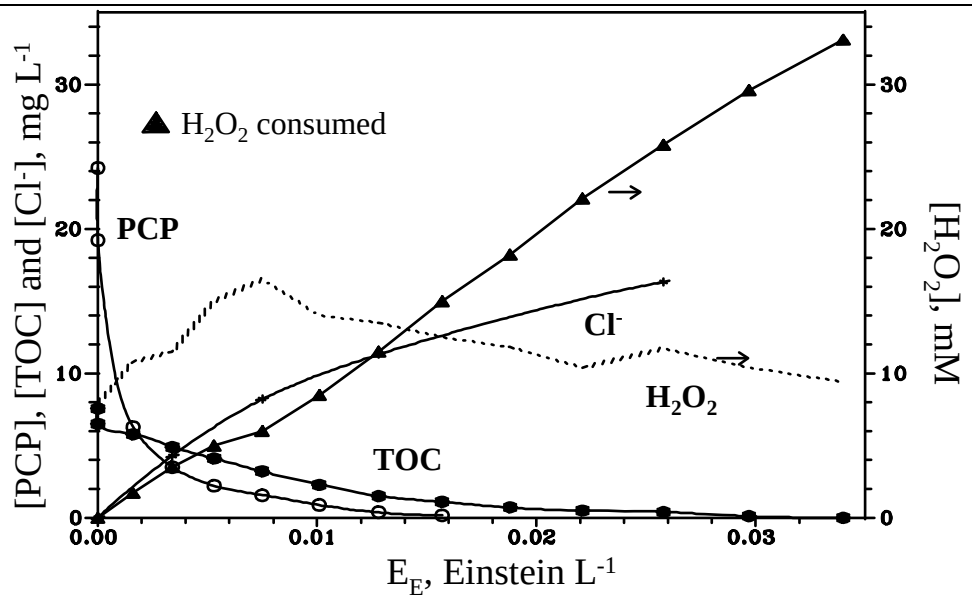

Figure 6.25. *PCP degradation with H_2O_2.10 mM. The doted line shows [H_2O_2] along the experiment.*

It has been possible to keep H_2O_2 concentration around 10 mM. The consumption of peroxide is constant during PCP mineralisation, indicating that there is no competition by the active sites of the catalyst between both species. Similar results have been obtained by *Augliaro et al.* [*1990*]. They gave determined that H_2O_2 decomposition rate is constant between 2 and 6 mM. *Jenny et al.* [*1991*] have obtained the same between 10 y 100 mM. Experiments like the former are very useful to know the influence of peroxide concentration on PCP decomposition rate in the pilot plant. A summary of them is shown in Table 6.8. The most suitable concentration of H_2O_2 in the PSA pilot plant is about 10 mM. In these conditions the mineralization rate increases twice and 23mM of peroxide are consumed to mineralise 95% of the initial TOC (~0.1 mM PCP). For higher concentrations, the efficiency of the process decreases.

[H_2O_2] mM	**Φ_E (H_2O_2) (%)**	**$\Phi_{E,0}$(PCP) (%)[(1)]**	**$\Phi_{E,0}$ (COT)[(2)] (%)**	**Φ_E (Cl^-)[(3)] (%)**	**$E_{E,95\%}$(COT) (Einstein L^{-1})**
0	-	0.55	1.83	0.72	0.044
6	64.0	-	3.03	2.65	-
10	99.8	2.98	3.29	2.46	0.026
50	90.0	0.91	1.78	1.00	0.051

(1), (2) y (3) have the same meaning than in Table 6.4.

Table 6.8

The H_2O_2 estimated quantum yield (Φ_E) when the concentration is higher than 10 mM is near 100%, even when the mineralisation rate have decreased. These results coincide with

Peterson et al. [*1991*] in the sense that, when H_2O_2 concentration is high, peroxide is consumed essentially by reactions 6.43 and 6.44. If 6.40 or 6.41 were important, inhibition of PCP decomposition should not be produced. Also, the decomposition rate of peroxide is constant although increasing considerably its concentration. It is confirmed that there is no competition with PCP by catalyst active sites.

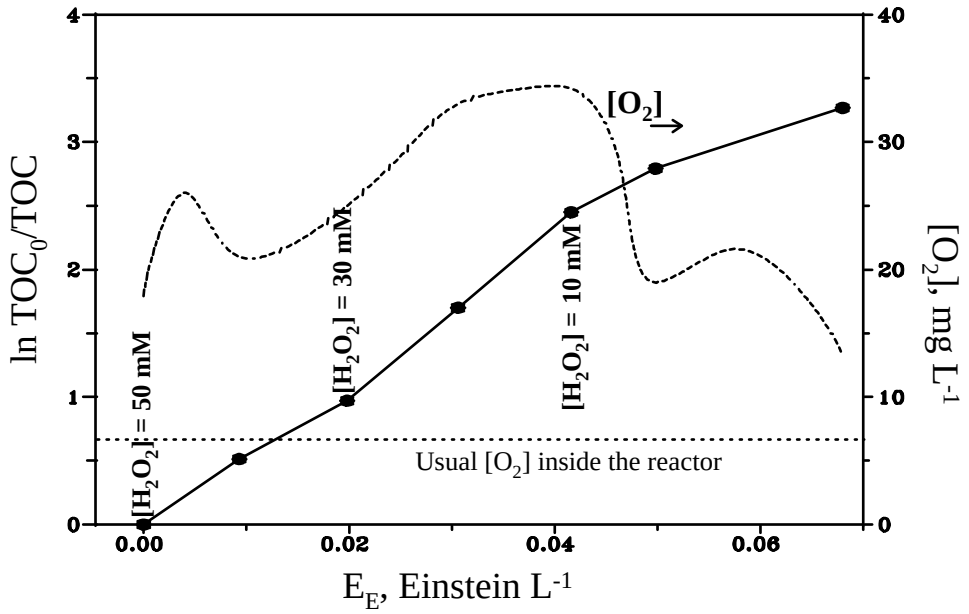

Figure 6.26. *PCP degradation with $[H_2O_2]_0$ = 50 mM (no addition along the experiment). The doted line shows $[O_2]$ along the experiment.*

Figure 6.26 illustrates an experiment with high concentration of peroxide at the beginning, without adding anything during the experiment. It can be seen how the degradation rate varies as function of the amount of H_2O_2 in each time. The maximum mineralization rate is attained between 10 and 30 mM, coinciding with the tests carried out at fixed peroxide concentration. The evolution of diluted oxygen is also shown. Oxygen has not been injected during the experiment (see Figure 6.9). This demonstrates that the application of hydrogen peroxide could be very useful when it is not possible to obtain an adequate concentration of oxygen in the reactor.

6.6.2 Persulphate effect

The use of hydrogen peroxide can double PCP mineralization rate and increase the treatment capacity of the plant. When the amount of wastewater to treat is invariable, the size of the plant could be reduced. However, there are different compounds candidates to be able of increasing reaction rate because they are also electrons scavengers. Among them, the most

utilised so far in heterogeneous photocatalysis have been:

$$\begin{aligned} IO_4^- + 8e^- &\xrightarrow{8H^+} 4H_2O + I^- \quad \text{(a)} \\ ClO_3^- + 6e^- &\xrightarrow{6H^+} 3H_2O + Cl^- \quad \text{(b)} \\ BrO_3^- + 6e^- &\xrightarrow{6H^+} 3H_2O + Br^- \quad \text{(c)} \\ S_2O_8^{2-} + e^- &\longrightarrow SO_4^{2-} + SO_4^{\bullet -} \quad \text{(d)} \end{aligned} \tag{6.45}$$

Chlorate has been proven inefficient to improve the effectiveness. Decomposition rate of 4-chlorofenol decreases in presence of $NaClO_3$ 0.1 M [*Martin et al., 1995a*]. The has been demonstrated with atrazine and 2,7-dichlorodibenzodioxine [*Pelizzetti et al., 1991a*]. However, both IO_4^- and bromate increase the mineralization rate in all the cases tested. *Grätzel et al.* [*1990*] have tried them with organophosphorous pesticides, being peryodate the most effective. *Martin et al.* [*1995a*] have obtained very similar reaction rates with both and 4-chlorophenol. *Pelizzetti et al.* [*1991a, 1993a*] have improved considerably the decomposition rate of atrazine, 2,7-dichlorodibenzodioxine and 2-chlorophenol in presence of IO_4^- 0.1 M. *Al-Ekabi et al.* [*1993*] have demonstrated that bromate increases the efficiency of 2,4-dichloroophenol, 1,1,2-trichloroetane, chlorobenzene y trichloroethylene decomposition rate. The inconvenient of both products is the cost. Their use in large quantities could increase considerable the plant operation costs.

The effect of persulphate on many organic compounds is known since long time ago. At high temperature (90-130 ºC) is capable to oxidise them completely in a few minutes [*Goulden et al., 1978*], if the concentration is high enough ($[S_2O_8^{-2}] \approx 200$ mM). A similar effect is obtained when electrons are generated in aqueous solution, which produce sulphate radicals (ec. 6.45d) from persulphate [*Neta et al., 1977*]. In fact, several TOC analysis methods based on these principles have been standardised years ago (EPA method 415.1).

Persulphate combined with TiO_2 has not been very usual, although it has been tested successfully and the cost (as sodium persulphate) is not high (about 100 ptas per mole). *Grätzel et al.* [*1990*] have increased up 5 times the decomposition rate of several organophosphorous, adding $S_2O_8^{2-}$ 0.2 M. *Pelizzetti et al.* [*1991a*] have improved considerably the decomposition rate of atrazine (5 times), 2,7-dichlorodibenzodioxine (3 times) and 2-chlorophenol (10 times) with persulphate 0.1 M. *Al-Ekabi et al.* [*1993*] have obtained similar results with 2,4-dichlorophenol. Sulphate, generated when persulphate is reduced, does not reduce the efficiency of the process, besides having been described inhibiting effects when sulphate ($[SO_4^{-2}]$>0.01M) is added to a photocatalytic reaction with TiO_2 [*Abdullah et al., 1990*].

The first experiments with PCP and persulphate were performed at the facilities of the

University of Torino (using lamps simulating solar radiation) and the results were promising [*Minero et al., 1993*]. The decomposition rate of 10 mg L^{-1} of PCP, in presence of persulphate 20 mM (4.8 g L^{-1} as $Na_2S_2O_8$) and 100 mg L^{-1} of TiO_2, was increased in more than one order of magnitude. This concentration of persulphate was very high to be used in the pilot plant, because it would mean the addition of a large amount of oxidant, due to the size of the reactor. The minimum volume (V_{TOT} = 260 L, Eq. 3.2) required to operate the pilot plat is obtained with one module and tank E. In this situation the plant has to be operated in recirculation mode (Eq. 3.5), as it was commented with hydrogen peroxide experiments. The preliminary tests were carried out at low concentration of sodium persulphate, to determine if there was possible to obtain considerable effects in the PCP mineralization with the addition of small amount of reactant.

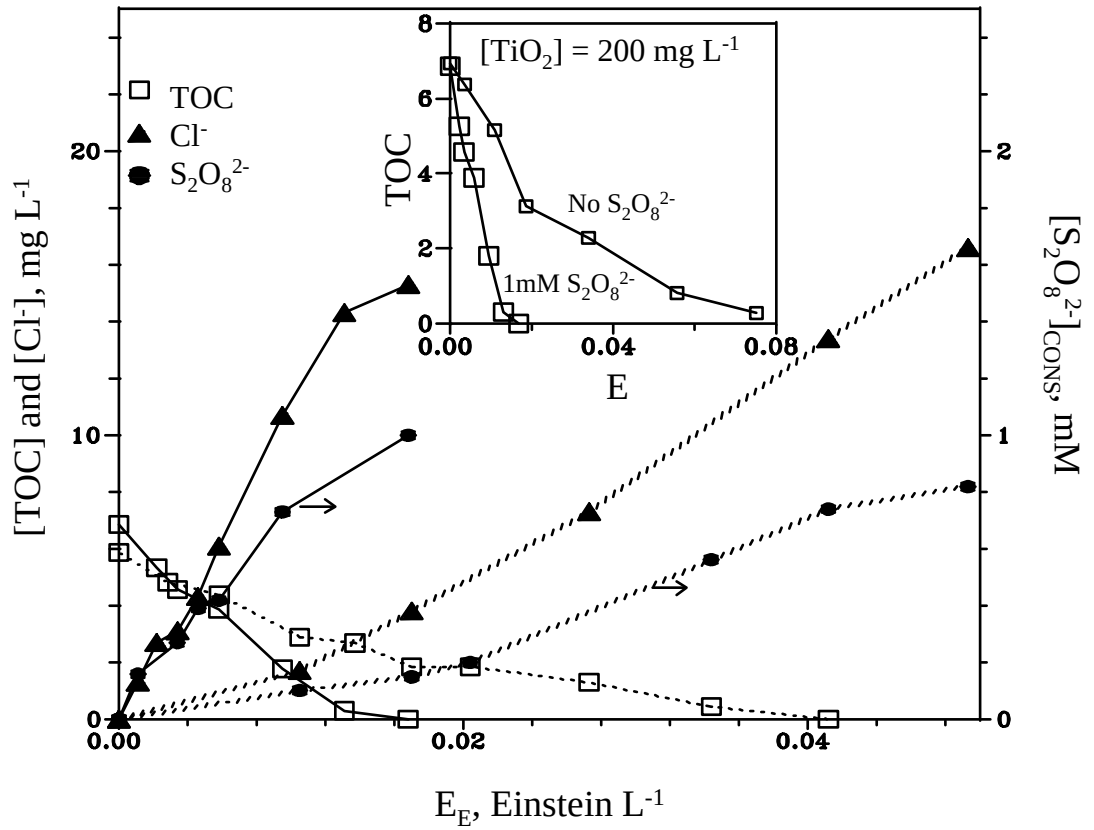

Figure 6.27. *PCP degradation with 1mM $S_2O_8^{2-}$. Right axis: consumed persulphate. Doted lines: no catalyst added. Solid lines: 200 mg L^{-1} TiO_2. In the inset a comparison with no persulphate experiment is shown.*

Figure 6.27, shows the results obtained during two experiments with persulphate 1mM, without any addition during the test. In one of them titanium dioxide is not added to the reactor. Nevertheless, a small amount is always present because a thin film of catalyst remains on the reactor glass tubes, as commented in paragraph 6.4, and it is not feasible to clean it. The graphic inserted in Figure 6.27 shows the results obtained with $S_2O_8^{2-}$ 1mM and

a typical experiment (PCP 25 mg L^{-1} and 200 mg L^{-1} of TiO_2) previously carried out in the pilot plant. Figure 6.27 demonstrates that persulphate could be very beneficial to increase the process efficiency. The effect is more noticeable in the last part of the reaction. The presence of persulphate seems to affect essentially the mineralization of the degradation intermediates. Something very similar has happened when using persulphate with atrazine, in this pilot plant [*Minero et al., 1996b*], and in previous studies [*Pelizzetti et al., 1991a*].

The initial persulphate concentration is low (1 mM), and although the complete amount is practically consumed, the mineralization rate is improved considerably. In these conditions, the last part of the degradation takes place at extremely low oxidant concentration. During the following experiments little amounts of persulphate were added, trying to keep a steady concentration equal to the initial one. For that purpose, samples were analysed (with the method described in paragraph 3.8.3) as they were taken from the pilot plant and the required amount of $S_2O_8Na_2$ was added to tank E, to retrieve the initial concentration. $Na_2S_2O_8$ has been selected because its low cost (~0.7 EURO/mol) and high water solubility (556 g L^{-1}, 20^oC). By this procedure, the amount of oxidant present in the dissolution has remained nearly unaltered.

In these preliminary experiments, the mineralization rate was low because the catalyst concentration was very low (TiO_2 adhered on the reactor glass), besides the persulphate presence. This one is also consumed very slowly. If reactions 6.45d and 6.46 were irrelevant, this means, if persulphate accelerates PCP oxidation directly (promoted by radiation or high temperature in the reactor), there would not be any difference in the persulphate consumption, when using higher or lower amount of catalyst. Also, the presence of both ($S_2O_8^{2-}$+200 mg L^{-1} of TiO_2) gives rise to the highest mineralization rate (see graphic inserted in Fig. 6.28). So, reaction rate increases because the recombination of e^-/h^+ (Eq. 6.7) decreases considerably and consequently reactions 6.9a, 6.9b and 6.9c are promoted. Other reactions that may occur due to the presence of persulphate and could also be beneficial are:

$$SO_4^{\bullet -} + e^- \rightarrow SO_4^{2-} \quad (6.46)$$

$$SO_4^{\bullet -} + H_2O \rightarrow SO_4^{2-} + OH^{\bullet} + H^+ \quad (6.47)$$

$$SO_4^{\bullet -} + PCP \rightarrow SO_4^{2-} + I_i \quad (6.48)$$

$$SO_4^{\bullet -} + I_i \rightarrow .... \rightarrow SO_4^{2-} + CO_2 \quad (6.49)$$

The importance of these reactions is demonstrated in Figures 6.28 and 6.29. Without persulphate (Figure 6.28), PCP decomposition nearly stops when the concentration is low (~ 2 mg L^{-1}), because the TiO_2 present is only that one remaining on the reactor tubes. In these conditions, the mass transfer becomes the limiting step and the reaction rate decreases considerably. The effect is the same that that one observed with fixed catalyst photocatalytic

reactors (see paragraph 1.2.2). When persulphate is added, the reaction occurs without problems right till the end, even a bit faster than with TiO_2 alone (2a and 1b from the graphic inserted in Figure 6.28).

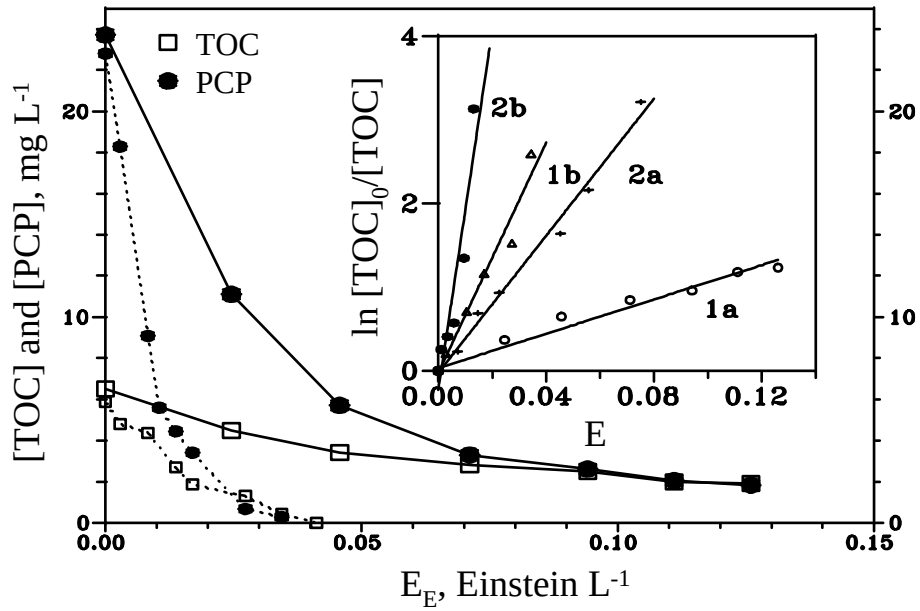

Figure 6.28. *PCP degradation (25 mg L^{-1}) without catalyst. With $S_2O_8^{2-}$ 1 mM (doted lines). Inset: (1) Without TiO_2 (a) without $S_2O_8^{2-}$ and (b) with $S_2O_8^{2-}$ 1 mM; (2) With TiO_2 200 mg L^{-1}, (a) without $S_2O_8^{2-}$ and (b) with $S_2O_8^{2-}$ 1 mM.*

If reactions 6.47, 6.48 and 6.49 were not kinetically important, the effect of persulphate would be noticeable only when the catalyst concentration is high (Figure 6.29). So, persulphate does not work just as an electron acceptor, because the mass transfer would be critical always at low TiO_2 concentration. This does not happen when persulphate is present. One fact, which demonstrates moreover the importance of the radical sulphate during the oxidation, is that the persulphate required, to mineralised a determined amount of PCP, does not depend on the oxidant concentration. It depends exclusively on the amount of PCP and catalyst (see Table 6.9, persulphate consumption). Figure 6.29 shows how the higher the initial persulphate concentration is, the higher persulphate decomposition rate is, but at the end, the consumption (2.8 mM) is always the same to mineralize initial TOC. According to this, the sulphate radical (E^o = 2.6 V) is able to oxidise PCP and its intermediates directly or by $^{\bullet}OH$ generation. In Figure 6.29 are also included the results obtained with 100 mg L^{-1} of PCP and persulphate 10 mM in the dark. The maximum temperature attained in the pilot plant during the experiments with persulphate has been 65^{o}C. The degradation was important (~50% TOC decomposition in 24 h), but irrelevant if it is compared with photocatalysis in presence of $Na_2S_2O_8$ 10 mM (~50% TOC decomposition in 10 minutes of illumination in the reactor).

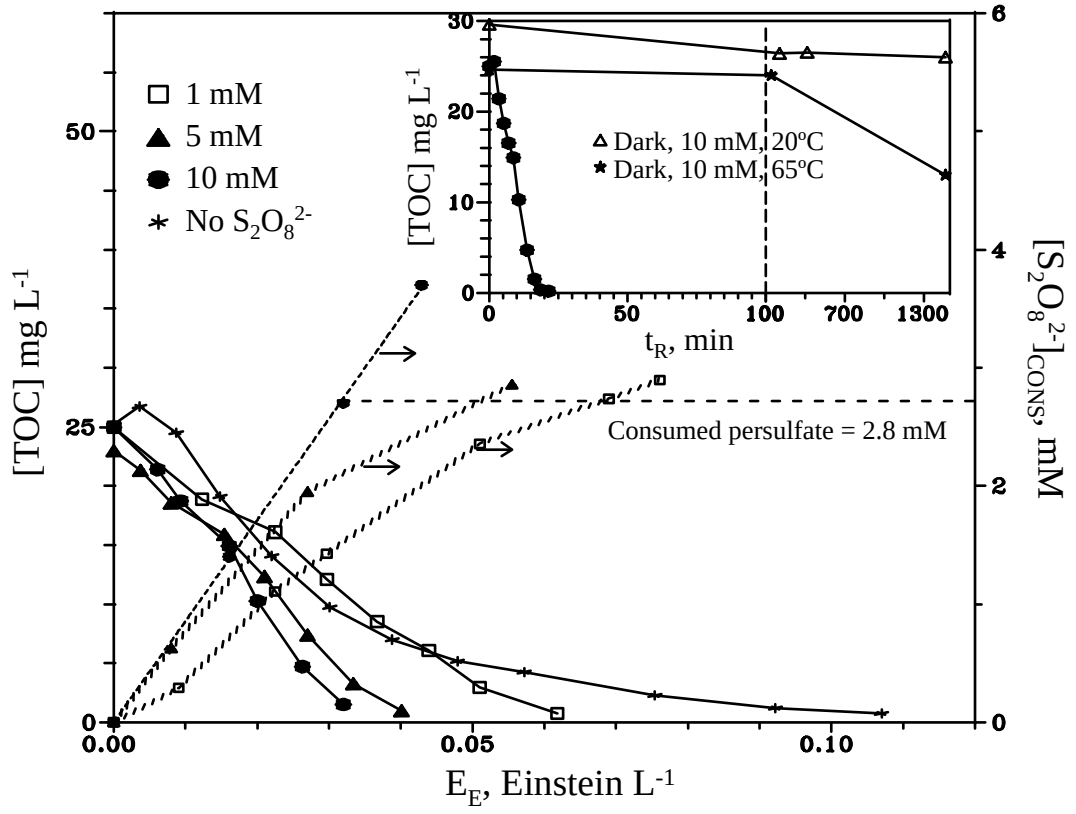

Figure 6.29. *Effect of persulphate concentration on PCP (100 mg L^{-1}) degradation with TiO_2 200 mg L^{-1}. Doted lines: persulphate consumption. Inset graphic: photocatalytic effect compared with persulphate effect at ambient temperature and 65 ºC.*

Persulphate produces higher effect during the last part of the degradation, therefore, the model described in paragraphs 6.4.4 and 6.4.5 is not valid any more. However, the equation to adjust the experimental data is a lot simpler in this case:

$$TOC_0 - TOC_i = k_{S_2O_8^{2-}} E_E ; k_{S_2O_8^{2-}} = \Phi_{E,COT} \frac{1}{100} \qquad (6.50)$$

where $k_{S_2O_8^{2-}}$ (Mol Einstein^{-1}) depends on the amount of persulphate used and on the catalyst concentration.

This equation is similar to 6.21 and can also be used for the plant design when persulphate is used to improve the degradation. Table 6.9 shows different values for the estimated quantum yield from which $k_{S_2O_8^{2-}}$ can be calculated.

$[TiO_2]$ mg L^{-1}	$[PCP]_0$ mg L^{-1}	$[Na_2S_2O_8]$ MM	$\Phi_{E,PCP}$ (%)[1]	$E_{E,95\%(COT)}$ Einst. L^{-1}	$\Phi_{E,COT}$ (%)[2]	Φ_{E,Cl^-} (%)[3]	$[Na_2S_2O_8]_{CONS}$ mM
[4]-	25	0	0.2	>0.130	0.6	0.3	--
-	25	1	0.9	0.035	3.5	1.0	0.6
-	25	5	1.1	0.026	5.4	2.8	0.8
-	25	10	2.4	0.015	7.3	3.0	0.7
-	100	10	1.9	0.061	6.2	2.8	2
200	25	0	0.6	0.044	1.8	0.7	--
200	25	1	>5	0.013	4.4	2.9	1.0
200	25	10	>5	0.008	-[5]	-[5]	1.0
200	100	0	1.2	0.091	3.7	1.5	-
200	100	1	7.4	0.051	3.8	1.9	2.9
200	100	5	>10	0.045	5.1	4.0	2.8
200	100	10	>10	0.033	6.6	5.2	3.0

(1), (2), (3) see table 6.4; (4) without catalyst; (5) degradation very fast, it is impossible to determine these values.

Table 6.9

6.6.3 Conclusions

(I) The use of oxidants (electron scavengers) can be very useful to improve the efficiency of PCP photocatalytic destruction.

(II) Hydrogen peroxide can double the reaction rate, but the addition has to be controlled and without exceeding $[H_2O_2]$ 30 mM. From that efficiency decreases.

(III) When it is difficult to keep an adequate concentration of dissolved oxygen, in the photocatalytic reactor, the use of H_2O_2 can be very advisable. Installation, operation and maintenance costs of an O_2 injection system must be compared with the application of this additive. It will be necessary to know in advance the effect of this peroxide on the compound to be treated.

(IV) Sodium persulphate, at not very high concentration (~5-10 mM), is able to increase the mineralization rate about 5 times. 25 mg L^{-1} of PCP need about 1 mM of $Na_2S_2O_8$ to be completely destroyed.

(V) In this case persulphate has been proven very efficient with supported catalyst. The

problem is that the reactor used has not been designed for this purpose and it is not possible to use it in these conditions. It is impossible to ensure that the amount of TiO_2 remaining in the tubes, due to the continuous circulation of suspensions, will keep stable and not be dragged little by little with the usage. If the reactor design solves this question, the efficiency can increase considerably. Problems caused by mass transfer, when catalyst suspensions are not used, could be diminished if persulphate were used.

(VI) Equation 6.50 is useful for reactors design. In the same way that 6.21, the required collector surface could be known as function of: a) flow rate and PCP concentration in the water to be treated and b) UV radiation data at the plant emplacement

7. CONCLUSIONS

(I) The first European plant for photocatalytic applications, based in the utilisation of solar energy, has been set up and operated.

(II) The optical efficiency of the collectors used is about 60%. Although they have not been specifically designed for photochemical applications the modifications, carried out on them, have not reduced drastically their efficiency. When the semiconductor is TiO_2, the material used, to manufacture the reflecting surface and the absorber tube, must be enough efficient to reflect and transmit radiation which wavelength is higher than 310-320 nm.

(III) On-line radiation measurement is essential to evaluate results in any photochemical reactor illuminated with solar radiation. Comparison with other results, obtained in different illumination conditions, is not possible if the spectral radiation distribution is not known. Working with solar UV radiation, it is not strictly necessary to know that distribution in real time.

(IV) All the experiences carried out in a pilot plant of large dimensions, where substance loses may occur, must be certified by appropriate analytical techniques. These techniques must be able to close the mass balance of reactants and products. Measurement of TOC by EPA 415.1 method (wet mode, without filtering the sample) has been extraordinarily useful. Analysis of TOC after filtering the sample, to remove TiO_2 and other solids in suspension, produces errors. Part of the sample components could be adsorbed on the solids and could remain in the filter.

(V) Chemical actinometers are adequate to evaluate the incident photonic flux in a photochemical reactor of large size, when it is not possible to know it directly by sensors located inside the reactor. They can also be used to check the output of electronic sensors.

(VI) Using the Sun as photon source produces additional uncertainties when treating the experimental kinetic data. It does not provide a constant flux of energy. To obtain an equation, relating experimental time and photonic flux (I), allows the evaluation of the kinetic data by the same procedures employed with a constant illuminating source.

(VII) Quantum yield, in heterogeneous photocatalysis, must be based only on the flux of energy capable to promote the formation of e^-/h^+ pairs in the catalyst (in this case

TiO_2, 3.2 eV). When it is not possible to calculate exactly the quantity of energy absorbed by the catalyst, the use of an estimated quantum yield is justified. The utilisation of energy fluxes corresponding to wavelength intervals out of catalyst band-gap gives rise to errors. So, it is essential to know the spectral radiation distribution inside the reactor.

(VIII) It is not possible to mineralise PCP in the pilot plant without using catalyst and without enough diluted oxygen (about 4-8 mg L^{-1}). The simpler way to introduce oxygen in the water is by stirring in the feeding tank, which it is in contact with the atmosphere. The oxygen could be replaced by other electron captor (hydrogen peroxide, sodium persulphate, etc.).

(IX) The best way to operate a solar photocatalytic plant is in batch mode. This is justified by the following:

(i) To avoid the water disposal before being completely treated. The use of an unstable source of energy (the Sun) originates unpredictability. It is impossible to foresee the residence time required achieving the outlet requirements. Analytical quality control must always be done, which it is not usually quick, before disposal.

(ii) Recirculation, using a stirred tank in contact with the atmosphere, can be the cheapest way to keep the right level of oxygen in the water.

(X) The optimum concentration of catalyst in the reactor is about 200 mg L^{-1}. This quantity depends on reactor diameter, light intensity and the way the reactor is illuminated. For other parabolic collectors, with a concentration ratio and an absorber tube diameter similar to those used in this thesis, the optimum will not change considerably. However, if the reactor configuration is different, it will be necessary to perform tests to determine the best catalyst concentration.

(XI) Useful design equations could be obtained by the application of a Langmuir-Hinshelwood (L-H) type model, even if it does not fit with the heterogeneous photocatalytic reaction mechanism. By now, these equations must be obtained in pilot plant level. They will be useful for large plants if the same type of collector is used at pilot and at industrial scale.

(XII) In the pilot plant used in this work, the reaction rate is proportional to the radiation intensity. The maximum tested intensity has been around 10 suns ($\sim 6 \times 10^{-4}$ Einstein m^{-2} s^{-1}). This does not agree with some publications, where it is commented that the

reaction rate increases with the square root of the intensity when it is higher than 1 sun. This point gives rise to uncertainties, because it seams that the experimental device also affects this question.

(XIII) The utilisation of electrons scavengers (oxidisers) can be very beneficial, although not all of them are valid. Hydrogen peroxide gives problems, if its concentration is not optimised, because it could constrain the process. Little quantities of sodium persulphate are very efficient. This oxidant could be very extremely effective when supported catalyst is used.

8. ECONOMIC ASSESSMENT

8.1 Introduction

This chapter attempts to compare the advantages, disadvantages and costs of PCP photocatalytic treatment, versus other more conventional technologies such as active carbon adsorption and air stripping. At the moment, the PCP in wastewater limit is 1 mg L^{-1}, so all calculations were made to achieve 0.1 mg L^{-1} so as not to exceed that value.

Air stripping involves the transfer of volatile organic compounds from a liquid (in this case water) to air. This is achieved by considerably increasing the contact area between the two phases. Packet or tray columns in which water usually flows downward and air flows upward are used for this purpose [*Weber et al., 1986*]. This treatment does not destroy the contaminant, but only transfers it into the air. The contaminant is removed from the air stream by adsorption or incineration before it is released into the atmosphere. In any case, PCP would not seem to be adequate for this procedure due to its low volatility (Henry's law constant = 0.16 atm/molar fraction).

Adsorption in active carbon consists of retaining the contaminants in a very porous carbon bed (500-1400 m^2/g). Organic compounds bond to the solid surface and when all the active centres of the adsorber have been saturated, it must be replaced. The saturated product must be stored or regenerated in a high-temperature furnace. A typical regeneration installation consists of a furnace where the carbon is heated up and the compounds retained are vaporised and later incinerated. PCP is efficiently retained in active carbon (between 100 and 600 mg of PCP can be adsorbed in 1 g of carbon). However, when the concentration in water is more than 10 mg L^{-1}, the active carbon treatment is expensive because the beds must be changed very often [*Solarchem, 1994*]. Furthermore, legislation with regard to the disposal of waste active carbon is becoming stricter while its regeneration is also expensive and, very often, environmentally unsafe.

For the treatment of water highly contaminated with PCP, a combination of photocatalysis and active carbon might be adequate (see Figure 8.1). PCP content can be reduced photocatalytically. Then the effluent from the photocatalytic process can be filtered through active carbon before disposal. As during the oxidation process many intermediate compounds may be produced from PCP, TOC is used as a fundamental parameter [*Serpone, 1994a*].

Below 10 mg L^{-1}, treatment by active carbon is always more advisable since the compounds to be removed are easily adsorbed [*Solarchem, 1994*]. Consequently, photocatalytic treatment

must be designed to reduce TOC to 2.7 mg L^{-1}. When the TOC is lower than this value, the concentration in water of PCP and its intermediates is always ≤ 10 mg L^{-1}, because the PCP molecule is 27% organic carbon. The carbon content of any intermediate of the reaction is always more than 27% TOC (see Figure 6.1. and 6.10b). It must also be assumed that intermediates will be efficiently retained in active carbon.

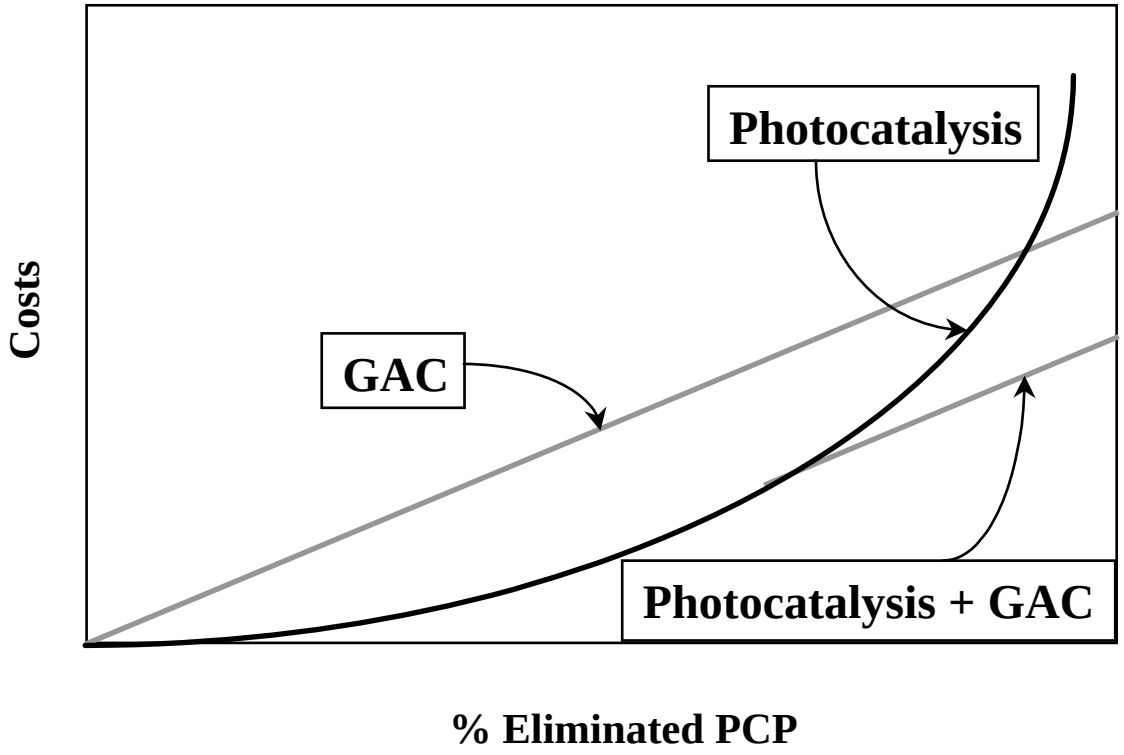

Figure 8.1. *Advantage derived from the combination of photocatalysis and active carbon.*

Due to the kinetics of the photocatalytic reaction, the rate decreases considerably when PCP concentration is low (See Figure 6.15). When active carbon is used as last step of the treatment, 0.1 mg L^{-1} before disposal, costs can be reduced considerably. This effect is not as noticeable when using peroxydisulphate (see Figure 6.29). The reaction follows zero order kinetics in the presence of this oxidant (see Eq. 6.50) and, so, when the concentration is low, the rate does not decrease very much. According to these possibilities, the treatment costs can be broached from different points of view, depending on plant design:

Case A. Photocatalytic treatment down to 0.1 mg L^{-1} of TOC.

Case B. Photocatalytic treatment with peroxydisulphate 10 mM down to 0.1 mg L^{-1} of TOC

Case C. Photocatalytic treatment with peroxydisulphate 10 mM down to 2.7 mg L^{-1} of TOC + active carbon

Case D. Photocatalytic treatment down to 2.7 mg L^{-1} of TOC + active carbon

Case E. Treatment with active carbon alone down to 0.1 mg L^{-1} TOC

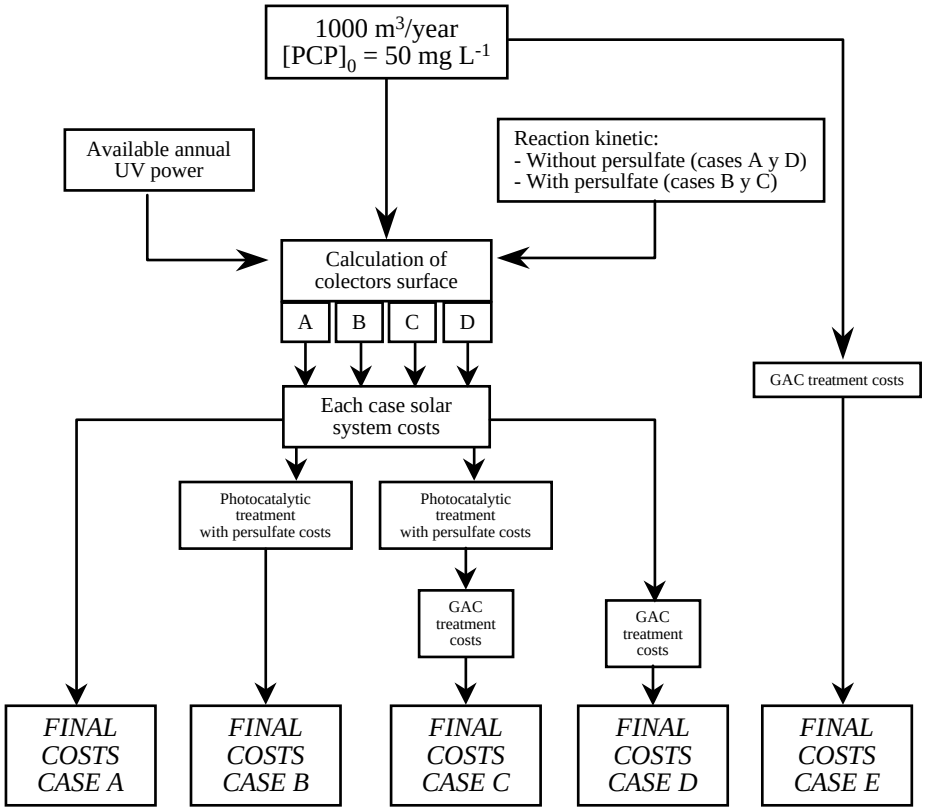

Figure 8.2. *Calculation of treatment costs for 1000 m^3 of PCP-contaminated water in the case of the five different options examined.*

8.2 Annual available ultraviolet radiation

For the calculation of the annual average of ultraviolet radiation, it is necessary to find out the so-called “cloud factor”. This factor is intended to be a measurement of atmospheric transparency and is affected by all the atmospheric components, which can absorb or scatter solar radiation (Eq. 4.3). In this way, the amount of energy that reaches the earth’s surface can be predicted for a given place at any time of the year.

As the photocatalytic reactor of the pilot plant is able to use direct radiation as well as global (Eq. 4.29), the “cloud factor” is calculated for both cases. It should be noted that the “cloud factor” for global radiation is always lower than the direct, as the diffuse component of solar radiation is maximum when direct radiation is absent (global = direct + diffuse). This is more noticeable in the case of UV, because the clouds do not absorb radiation in this range of the

solar spectrum, but only disperse it. The diffuse component of global solar UV radiation in the presence of clouds is very high compared to the rest of the spectrum.

This factor was calculated from the ratio between average radiation (affected by all atmospheric phenomena) and the highest attainable radiation at all times of the year. This is usually calculated for each month separately. To find out the highest radiation available each month, the best day of each month has been selected (completely clear sky during all the hours of sunlight) from among all the days considered for the calculation of the average radiation. The "cloud factor" was calculated from the data collected at the PSA meteorological station with radiometers which are not UV-specific, but sensitive to the whole spectrum. This was done because the UV-specific radiometers (see chapter 3.6) used in this thesis were only recently installed and the UV-radiation data base is thus not large enough to be considered statistically correct. In any case, the results obtained will be more conservative, because the total radiation is more affected by the atmospheric changes than UV radiation. The "cloud factor" will be greater, or at least the same as that obtained if the calculations were performed from data collected with specific UV solar sensors.

MONTH	**Sun h.(1) per day**	**No. filtered days**	**First day**	**Last day**	**$Rad_{dir,1}$(2) W m^{-2}**	**$Rad_{dir,2}$(2) W m^{-2}**	**$Rad_{glo,1}$(2) W m^{-2}**	**$Rad_{glo,2}$(2) W m^{-2}**
JANUARY	9.8	150	2-1-88	31-1-93	372	402	260	256
FEBRUARY	10.7	132	1-2-88	28-2-93	401	442	331	326
MARCH	11.8	155	1-3-88	31-3-93	375	402	383	383
APRIL	13.0	154	1-4-88	29-4-93	404	404	457	456
MAY	14.0	138	1-5-88	31-5-93	423	366	466	476
JUNE	14.5	151	3-6-87	27-6-93	456	409	480	435
JULY	14.2	165	1-7-87	31-7-93	450	482	508	461
AUGUST	13.3	182	1-8-87	31-8-93	411	453	476	481
SEPTEMBER	12.2	160	1-9-87	5-9-93	357	434	416	425
OCTOBER	11.0	156	1-10-87	31-10-92	384	430	347	349
NOVEMBER	10.0	146	3-11-87	30-11-92	424	394	281	279
DECEMBER.	9.5	142	1-12-87	30-12-92	329	414	227	222
ANNUAL	**12.0**	**1831**	**3-6-87**	**5-9-93**	**399**	**419**	**386**	**379**

(1) Monthly average. (2) There are two radiometers for direct and two for global.

Table 8.1

Of the period of 2286 days, or more than six years (1987-1993), selected for calculation of the averages, only 1831 days were used. The rest were unreliable, either because values were

excessively high or low, illogical for the time of the year or day, or due to uncongruencies among the different types of radiometers (direct-global-diffuse). This filtering (cancellation of erroneous data) was done by software specifically designed for PSA meteo station data [*Cáceres et al., 1992*]. The results obtained are shown in Table 8.1.

These radiometers are located in the meteorological station of the PSA (standardised by the Meteorological National Institute of Spain, No. 321-0). There are two units for direct and two for global, installed one by the other, to contrast the measurements. These sensors are calibrated periodically in the Actinometric Applications Unit of the Meteorological National Institute of Spain. The data are collected and stored in continuous in a data base managed by a computer. The most relevant characteristics of each radiometer are:

- Direct Radiation (2 units): Direct solar radiation sensor (EPPLEY. Model NIP), sensibility 8 μ Volts per W m^{-2}, measurement error $\pm$0.5%. It is mounted on a solar tracking system (EPPLEY. Model ST-1).

- Global Radiation (2 units): Global solar radiation sensors (EPPLEY Model PSP), sensitivity 9 μ Volts per W m^{-2}, measurement error $\pm$0.5%. It is mounted in a fixed horizontal position.

From the data shown in Table 8.1, it is possible to calculate the "cloud factor" in each case, using the average value of each pair of radiometers and the best day of each month, for which the following equation has been used:

$$f_{N,i,m} = 1 - \frac{\overline{D}_{i,m}}{D_{i,m,\max}}$$

$$\overline{D}_{i,m} = (\overline{Rad_{i,1} \text{ and } Rad_{i,2}})_m \times (\text{sun h. per day})_m \times 3.6 \qquad (8.1)$$

where $f_{N,i,m}$ is the monthly "cloud factor", $Rad_{i,1}$ and $Rad_{i,2}$ are the monthly averages obtained with the two direct and the two global radiometers, $\overline{D}_{i,m}$ (kJ m^{-2}) is the average monthly global or direct irradiance, $(\text{sun h. per day})_m$ are the monthly average hours of sunlight and $D_{i,m,max}$ is the irradiance of the best day in each month, also global or direct. Table 8.2 shows the "cloud factor" for both cases.

MONTH	$\overline{D}_{dir,m}$ KJ m^{-2}	$D_{dir,m,max}$ KJ m^{-2}	$f_{N,dir,m}$	$\overline{D}_{glo,m}$ KJ m^{-2}	$D_{glo,m,max}$ KJ m^{-2}	$f_{N,glo,m}$
JANUARY	13653	26813	0.49	9102	11443	.20
FEBRUARY	16247	31616	0.49	12697	16806	0.24
MARCH	16496	33660	0.51	16284	20992	0.22
APRIL	18846	35332	0.47	21324	25968	0.18
MAY	19807	38558	0.49	23688	29500	0.20
JUNE	22566	35474	0.36	23872	30276	0.21
JULY	23787	31762	0.25	24759	29704	0.17
AUGUST	20684	29085	0.29	22889	26164	0.12
SEPTEMBER	17277	30186	0.43	18371	24003	0.23
OCTOBER	16117	29840	0.46	13781	16312	0.16
NOVEMBER	14665	27776	0.47	10004	2220	0.18
DECEMBER	12675	26163	0.52	7653	10337	0.26
ANNUAL	**-**	**-**	**0.44**	**-**	**-**	**0.20**

Table 8.2

As explained above, the monthly "cloud factor" is calculated using the data collected by non-specific UV radiometers. Using this "cloud factor" and the data collected by the specific UV radiometers (see paragraph 3.6), it is possible to find out the average UV irradiance at the PSA. For this purpose, the best UV-radiation day of each month will be used. The result will be the monthly average UV with the exception, already commented on, that the result will be conservative. This value will be lower or similar to that obtained if the "cloud factor" were calculated directly with UV data. Therefore, the collector surface calculated in this way (see Figure 8.2) will be, at least, similar to that required to achieved the plant design settings. The plant will be, in the worse case, a little bit oversized. Table 8.3 shows the monthly UV average, global and direct, calculated by this procedure ($\overline{UV}_{D,m}$, $\overline{UV}_{G,m}$). Equation 8.2 has been used to calculate the monthly UV average

$$\overline{UV}_{i,m} = UV_{i,m,\max}\,(1 - f_{N,i,m})\,\frac{1}{3.6(sun\,hours)_m} \qquad (8.2)$$

where $UV_{i,m,max}$ is the UV irradiance of the best day of each month.

The annual UV available, as obtained from the monthly data, will be used as the basis of calculation to find out the total collector surface required for the photocatalytic treatment of 1000 m^3 of water per year (see Figure 8.2). Since Eq. 4.29 is a combination of Eq. 4.16c and

Eq. 4.21c, and UV_D and UV_G are annual averages, it is possible to find out the amount of UV energy available per year. Although the usual collector reflectivity used in this thesis is 60%, this is because they are old oil-heating solar collectors modified for use in photochemistry. In Eq. 4.16c, the reflectivity used for the parabolic mirrors is 80%, since in a plant specially designed for this application, the reflectivity of the Al-mirrors will be higher, in the range of 80-90%. The factor η_C (0.91, related to module construction) used in Eq. 4.11 will also be higher (0.95 will be assumed) for the same reason.

MONTH	**$UV_{D,m,max}$ KJ m^{-2}**	**$f_{N,dir,m}$**	**$\overline{UV}_{D,m}$ W m^{-2}**	**$UV_{G,m,max}$ KJ m^{-2}**	**$f_{N,dir,m}$**	**$\overline{UV}_{G,m}$ W m^{-2}**
JANUARY	511	0.49	7.4	503	0.21	11.3
FEBRUARY	796	0.49	10.5	823	0.24	16.2
MARCH	1096	1.51	12.6	972	0.22	17.8
APRIL	1223	0.47	13.9	1241	0.18	21.8
MAY	1270	0.49	12.8	1439	0.20	22.8
JUNE	1381	0.36	16.9	1472	0.21	22.3
JULY	1213	0.25	17.8	1423	0.17	23.1
AUGUST	1056	0.29	15.7	1265	0.13	23.0
SEPTEMBER	906	0.43	11.8	1023	0.23	18.0
OCTOBER	649	0.46	8.8	782	0.16	16.6
NOVEMBER	555	0.47	8.2	554	0.18	12.7
DECEMBER	555	0.52		461	0.26	10.0
ANNUAL		**0.43**	**12.5(1)**		**0.20**	**18.6(1)**

(1) Weighted average, considering the number of sunlight hours of each month and the number of days per month, taking into account that the year has 365 days and 4380 sun hours.

Table 8.3

With these considerations in mind, and using data from Table 8.3, Eqs. 4.16c, 4.21c and 4.29 give the following results:

$I^*_{D,E(300-387)} = 1.44 \times 10^{-5}$ Einstein L^{-1} s^{-1}

$I^*_{G,E(300-387)} = 3.00 \times 10^{-6}$ Einstein L^{-1} s^{-1}

$I^*_{E(300-387)} = 1.74 \times 10^{-5}$ Einstein L^{-1} s^{-1}

For 4380 sun hours per year, the total available energy per litre of reactor is **274 Einstein L^{-1} $year^{-1}$.**

8.3 Calculation of costs

8.3.1. Required collector surface in the cases studied

Using the available energy per litre of reactor, and Eqs. 6.21 and 6.50 (for 10 mM of $S_2O_8^{2-}$), the surface required to treat 1000 m^3 per year of water contaminated by PCP (50 mg L^{-1} = 0.19 mM) can be calculated for all the circumstances commented in Figure 8.2. 1mMol of TOC = 72 mg. was used in the calculations.

Case A

TOC_0 = 0.19 mM; TOC_F = 0.0014 mM; (Eq. 6.21) → $\mathbf{E_{E,A} = 0.080\ Einstein\ L^{-1}}$

Case B

TOC_0 = 0.19 mM; TOC_F = 0.0014 mM; (Eq. 6.50) → $\mathbf{E_{E,B} = 0.017\ Einstein\ L^{-1}}$

Case C

TOC_0 = 0.19 mM; TOC_F = 0.038 mM; (Eq. 6.50) → $\mathbf{E_{E,C} = 0.014\ Einstein\ L^{-1}}$

Case D

TOC_0 = 0.19 mM; TOC_F = 0.038 mM; (Eq. 6.21) → $\mathbf{E_{E,D} = 0.037\ Einstein\ L^{-1}}$

where $E_{E,I}$ is the energy per litre required to reduce the TOC to the desired level in each case. In 1000 m^3 of water to be treated per year:

$$\mathbf{E_{E,A,ANNUAL} = 80000\ Einstein\ year^{-1}}$$

$$\mathbf{E_{E,B,ANNUAL} = 17000\ Einstein\ year^{-1}}$$

$$\mathbf{E_{E,C,ANNUAL} = 14000\ Einstein\ year^{-1}}$$

$$\mathbf{E_{E,D,ANNUAL} = 37000\ Einstein\ year^{-1}}$$

Therefore, the required collector surface (A_{TOT}), including 20% overdimension is:

$$A_{TOT,i} = E_{E,i,ANNAL} \text{ x } (274\ \text{Einstein}\ L^{-1}\ year^{-1}) \text{ x } (0.77\ m^2\ L^{-1}) \text{ x } 1.2 \qquad (8.3)$$

$$\mathbf{A_{TOT,A} \approx 270\ m^2}$$

$$\mathbf{A_{TOT,B} \approx 57\ m^2}$$

$$\mathbf{A_{TOT,C} \approx 47\ m^2}$$

$$\mathbf{A_{TOT,D} \approx 125\ m^2}$$

The cost per square meter of an Al-collector has been estimated as 25.000 pts ($200, [*Parent et al., 1996*]). So, the differences in the four cases are not irrelevant.

8.3.2. Influence of insolation conditions and initial PCP concentration on calculation of the collector surface

When the atmospheric conditions are different from those at the Plataforma Solar de Almería, the calculation is similar, but from UV radiation data corresponding to the selected location. Figure 8.3 shows the results obtained applying Eq. 8.3 in each case. The available energy, per

litre of reactor and per year, has been calculated from Eq. 4.29. For this purpose, it has been assumed that the global UV is directly proportional to direct UV and the ratio between them is the same as at the PSA.

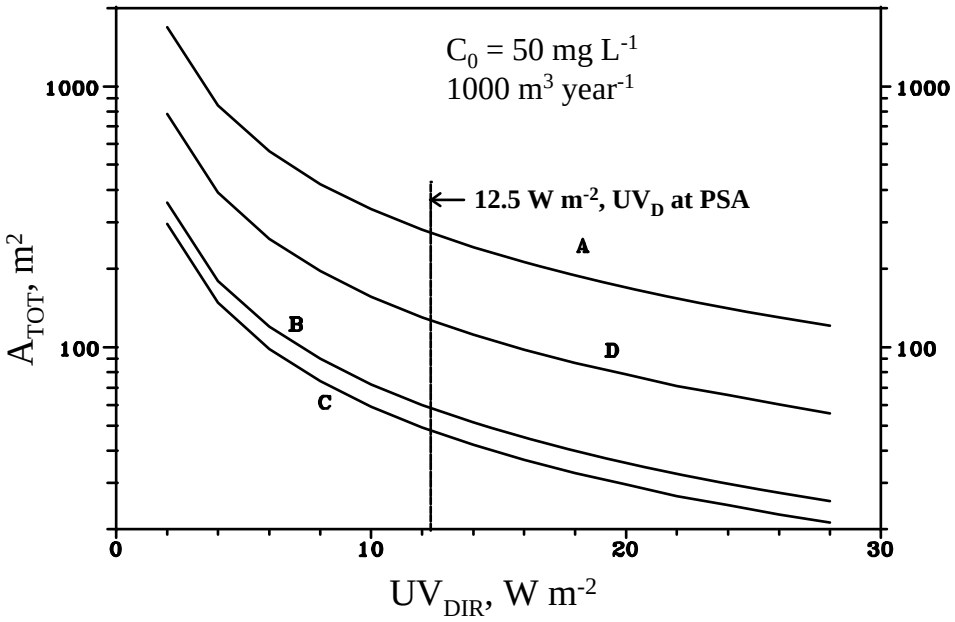

Figure 8.3 *Required collector surface, as a function of the average available UV for the four cases in Figure 8.2*

Likewise, when the initial PCP concentration is not 50 mg L^{-1}, the solar collector area required to reach the final concentration is different in each case (See Figure 8.4). In cases A and D, the A_{TOT}/PCP_0 ratio is not directly proportional. The lower the concentration per milligram of PCP mineralised, the larger the collector area required. However, in cases B and C, the relation is constant. In the graphic inserted in Fig. 8.4, it can be seen how the ratio between the collectors surface and the amount of contaminant mineralised shoots up when the initial PCP concentration is very low. This means that treatment is not feasible without peroxydisulphate for very large amounts of water, even though PCP content is low. Therefore, more collector surface is necessary to treat 1 gram of PCP diluted in 10 m^3 than in 1 m^3. In the range of concentration tested (up to 200 mg L^{-1}), it is cheaper to treat small volumes with high concentrations. This is not the case when peroxydisulphate is used as an additional oxidant.

8.3.3. Overall costs

Assuming that the costs of equipment and auxiliary installations (land, buildings, pumps, pipes, tanks, control systems, etc.), energy (pumping through the collectors or carbon beds,

etc.) and man power (operation and maintenance), are very similar in all the cases, included case E [*Klausner et al., 1992*], only those costs substantially affecting the differences between them are considered.

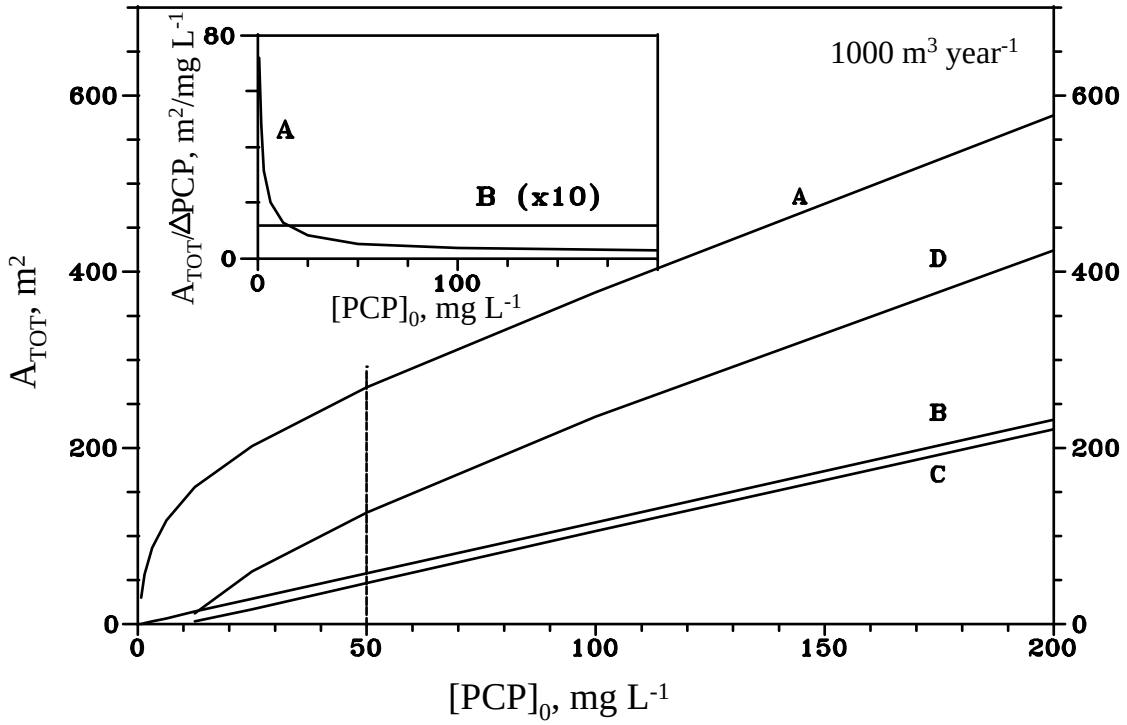

Figure 8.4. *Required collector surface as a function of initial PCP concentration. Graphic insert: Relation between collector surface and mineralised PCP (difference between C_0 and C_F) for cases A and B.*

In case A, the main cost is the solar collectors. 360 m^2 are required at a yearly cost of: (270 m^2) (25000 pts m^{-2}) (0.13) = **0.88 x 10^6 pts/year**. 13% is used as the yearly investment as recommended by the EPA (United States Environmental Protection Agency) for wastewater treatment plants [*Turchi et al., 1990b; Link et al., 1991*].

In case B, the cost corresponding to treatment with sodium peroxydisulphate must be included. According to the results obtained in experiments with peroxydisulphate (see Table 6.9), the consumption of peroxydisulphate (for TOC_F = 0.0014 mM) is ≈ 1.5 mMol per litre of contaminated water. This means a yearly consumption of 1500 moles of $Na_2S_2O_8$. The price of this reactant is ≈100 pts/mol. So, the yearly cost using peroxydisulphate is: [(57 m^2) (25000 pts m^2) (0.13)] + 150000 pts = **0.33 x 10^6 pts/year**.

Case C corresponds to treatment by peroxydisulphate and active carbon. The peroxydisulphate required to reduce TOC to 0.038 mM is a little bit less than in case B (1.2 mMol per litre of contaminated water), because the photocatalytic reaction stops a bit earlier. The cost of peroxydisulphate consumed is 120000 pts/year. The PCP remaining after the photocatalytic treatment is around 10 mg L^{-1}. Assuming medium quality active carbon (adsorption capacity = 300 mg of PCP per gram of carbon), 33 kg of carbon per year would be necessary. Active carbon is about 700 pts/kg, without including regeneration [*Information supplied by Aguas de Levante S.A., Barcelona 1996*], which is not going to be considered because regulations for active carbon regeneration after wastewater treatment are very strict. It would be extremely difficult to correctly regenerate PCP-saturated active carbon. Incineration at 1200ºC is very expensive, could generate dioxines [*Crosby, 1981*] and, at the same time, is rejected by many social sectors. So disposal of used active carbon residues should be managed only by an authorised company and the cost is about 350 pts/kg [*Information supplied by GEMASUR S.L. residue authorised manager AN-0002, Córdoba 1996.*]. Therefore, the cost of peroxydisulphate with active carbon is: [(47 m^2) (25000 pts m^2) (0.13)] + 120000 pts + 35000 pts = **0.31×10^6 pts/year**.

Case D is a combination of photocatalysis and active carbon without peroxydisulphate. Active carbon is employed in the last step (from 0.038 mM TOC to 0.0014) and the overall cost is: [(125 m^2) (25000 pts m^2) (0.13)] + 35000 pts = **0.44×10^6 pts/year**.

The last case (case E) is complete removal of 50 mg L^{-1} of PCP with active carbon. Although this not an environmentally "correct" solution because it would generate a dangerous toxic residue (PCP-saturated active carbon), it is legal and, very often, economically feasible. The final residue would be left in a controlled deposit. The yearly consumption of active carbon is 165 kg, which, with a 20% over dimension, is 200 kg/year. According to data supplied by *Aguas de Levante S.A.*, the cost of a container for approximately this amount of active carbon costs 100000 pts. The yearly cost for case E is therefore: [(100000 pts) (0.13)] + 210000 pts = **0.23×10^6 pts/year**.

8.3.4. Conclusions

(I) The active carbon treatment is a bit cheaper than the best (cases B or C) photocatalytic options. However, although this technology is very new, the costs are not far from others with many decades of development. On the other hand, the use of active carbon adsorption is feasible in this case only as long as current legislation allows this type of residue storage. In the European Union, regulations with regard to the generation of wastes which must be stored are stricter and stricter.

(II) These costs have been evaluated for the environmental conditions at the Plataforma Solar de Almería. The collector area required is directly proportional to the solar radiation available there. At another location with better insolation the collectors would cost less.

(III) PCP degradation, which is the objective of this thesis, does not have the fastest photocatalytic mineralization rate. At the same time, this compound is efficiently adsorbed on active carbon. Many compounds can be treated by photodegradation with TiO_2 that show low adsorption on active carbon and would therefore need more carbon than that calculated for PCP.

(IV) It is important to remark that this technology is in an experimental phase and many of its features could be improved, such as:

- More efficient collectors to improve the collection of diffuse UV radiation.
- Absorber tubes with completely solar UV-transparent materials.
- More efficient catalysts, to better and more cheaply utilise the solar spectrum.
- Optimisation of the use of additional oxidants

9. RECOMMENDATIONS FOR FURTHER RESEARCH ON THIS TOPIC

(I) The solar collectors used in this work are excellent to evaluate the photon flux inside the reactor. This has allowed the use of previous published work. This is very important when working with a large reactor, where any test means a considerable outlay of time and expense. So the more information available "a priori", the fewer experiments are necessary and the faster useful conclusions may be arrived at. Nevertheless, they are very expensive. It will be necessary the developing of new prototypes designed specifically for Solar Photocatalysis. It is very important to emphasise the importance of the reflecting surface. The reflectivity of an aluminised plastic is not enough. An aluminium surface will be the better solution.

(II) It is completely crucial the knowledge of the Solar Spectrum for calculation of quantum yields. Without this information is not possible the extrapolation of the results to different environmental conditions. Because of it, to design a photocatalytic plant it is necessary the measurement of Solar UV along several years. The "clouds factor" should be determined with these data.

(III) It is highly recommended the realisation of a Solar UV Map of the Mediterranean Region. This is one of the most industrialised areas all over the world and it is highly irradiated. This zone is very promising to install Solar Photocatalytic Detoxification plants.

(IV) The development of a model to predict the optimum concentration of catalyst as function of the type of solar collector is highly recommended This model is necessary for engineering plant design. If not, experimentation at pilot plant level is essential to obtain these equations.

(V) More efforts should be done to deposit efficiently the catalyst on an inert support. In this case persulphate has been proven very efficient with supported catalyst. The problem is that the reactor used has not been designed for this purpose. It is impossible to ensure that the amount of TiO_2 remaining on the tubes, due to the continuous circulation of suspensions, will keep stable and not be dragged little by little with the usage. If the reactor design solves this question, the efficiency can increase considerably. Problems caused by mass transfer, when catalyst suspensions are not used, could be diminished if additional oxidants were used.

(VI) The results presented in this work have clearly demonstrated that one attractive way to markedly enhance the photocatalytic degradation of PCP in water streams is to add an

efficient electron acceptor to the system. This reduction would also reduce the solar collector surface. It necessary more research to evaluate the best oxidant concentration and its relationship with the catalyst concentration.

(VII) It is necessary to develop a procedure to obtain a model similar to Eq. 6.21 with a minimum number of experiments.

(VIII) A combination between photocatalysis and more conventional wastewater treatment methods should be investigated. Toxicity measurements of photocatalysis intermediates will be very helpful to couple this technique with biological treatment systems. Photocatalysis produce, from the original substrate, more oxidised compounds. Biological reactors operate better as more oxidised products are treated.

10. NOMENCLATURE

a: Semi-aperture of the parabolic collector.

A_{TiO2}: Surface area of the catalyst ($m^2\ g^{-1}$).

A_{TOT}: Parabolic collector area.

b: Radio of the absorber tube

c: Light speed (2.99×10^{17} nm s^{-1}).

C: Response curve, normalised, at the reactor outlet.

C_0: Initial reactant concentration.

C_F: Final reactant concentration.

C_{O2}: Oxygen concentration in water (mg L^{-1}).

C_S: Solvent concentration in the L-H model (M).

D_i: Irradiance, corresponding to the total solar spectrum on the PSA (kJ m^{-2}).

E: Age distribution at the reactor outlet.

E_E: Accumulated energy, in the reactor, per unit of volume (Einstein L^{-1}).

$E_{E,1/2}$: Accumulated energy, in the photocatalytic reactor, per unit of volume and necessary to reduce one half the initial reactant concentration (Einstein L^{-1}).

$E_{E,95\%}$: Accumulated energy, in the photocatalytic reactor, per unit of volume and necessary to reduce the 95% of the initial reactant concentration (Einstein L^{-1}).

E_G: Catalyst band gap (3.2 eV for TiO_2 anatase).

f: Focal distance of the parabolic collectors.

f_{CR}: Correcting factor of the reflectivity measurements (1.22).

$f_{i\lambda}$: Power fraction of a polychromatic source associated to each wavelength

f_n: Clouds factor (%)

h: Plank constant (6.63×10^{-34} J s).

hυ: Abbreviation to symbolise the light participation in a chemical reaction

I: Photonic flux density (Einstein $m^{-2}\ s^{-1}$).

I_D: Photonic flux density corresponding to direct radiation (Einstein $m^{-2}\ s^{-1}$).

$I_{D,E}$: Photonic flux density corresponding to direct radiation in the pilot plant reactor (Einstein $m^{-2}\ s^{-1}$).

$I^*_{D,E}$: Photonic flux density, per unit of volume, corresponding to direct radiation inside the absorber of the pilot plant (Einstein $L^{-1}\ s^{-1}$).

$I_{E:}$ Photonic flux density in the pilot plant reactor (Einstein $m^{-2}\ s^{-1}$).

I^*_E: Photonic flux density, per unit of volume, inside the absorber of the pilot plant (Einstein $L^{-1}\ s^{-1}$).

I_G: Photonic flux density global radiation (Einstein $m^{-2}\ s^{-1}$).

$I_{G,E}$: Photonic flux density corresponding to global radiation in the pilot plant reactor (Einstein $m^{-2}\ s^{-1}$).

$I^*_{G,E}$: Photonic flux density, per unit of volume, corresponding to global radiation inside the absorber of the pilot plant (Einstein $L^{-1}\ s^{-1}$).

k': Apparent rate constant (s^{-1}). In this thesis, when using Eq. 5.1, the units are L Einstein^{-1}.

k_f: Reaction constant of the e^-/h^+ pairs formation.

k_h: Reaction constant of hydroxyl radicals formation from H_2O and h^+ (Eq. 6.8).

k_{OH}: Sum of the reaction constants of $^\bullet OH$ radicals formation.

$k_{o,i}$: Constant of the oxidation reactions involved in the PCP decomposition

k_r: Constant of the surface reaction rate in the L-H model (Ms^{-1}). In this thesis, when using Eq. 5.1, the units are Mol Einstein^{-1}.

$k_{r,2}$: Constant of tetrachlorophenoxyl radical formation reaction rate (R_2, figure 6.10b).

k_R: Constant of the electrons and holes recombination reaction rate.

K: Adsorption constant of the reactants in the L-H model (M^{-1}).

K_{O2}: Adsorption constant of the oxygen in the L-H model (M^{-1}).

K_s: Adsorption constant of the solvent in L-H model (M^{-1}).

M: Air mass (sunlight pathlength).

N: Number of photons emitted by a polychromatic light source.

N_a: Number of absorbed photons.

N_c: Number of active sites on the catalyst surface.

N_D: Number of photons corresponding to direct radiation.

$N_{D,E}$: Number of photons corresponding to direct radiation, inside the absorber of the pilot plant.

N_G: Number of photons corresponding to global radiation.

$N_{G,E}$: Number of photons corresponding to global radiation, inside the absorber of the pilot plant.

N_0: Avogadro's number (6.023×10^{23}).

N_λ: Number of photons emitted by a monochromatic light source.

P_a: Number of photons absorbed per unit of time.

PH_{zpc}: pH value at which the surface of an oxide does not content electric charge.

PKa: -log (acid ionisation constant)

$PK_{TiOH,i}$: -log (TiOH dissociation constant)

Po_2: Oxygen partial pressure (atm)

Q: Volumetric flow.

Q_λ: Number of photons emitted by a monochromatic light source.

r: Reaction rate.

r_{CALC}: Oxalic acid decomposition rate, obtained from radiometric data and the characteristics of the solar collectors

$r_{D,OXAL}$: Oxalic acid decomposition rate, obtained from the direct incident radiation and the characteristics of the solar collectors

$r_{G,OXAL}$: Oxalic acid decomposition rate, obtained from the global incident radiation and the characteristics of the solar collectors

r_0: Initial reaction rate. In the photocatalytic reactions studied in this thesis, it is considered initial rate that one calculated during the first steps of the reaction, when the rate is directly proportional (zero order) to the energy received.

$RADi_{,\lambda}$: Radiation flux measured by an spectroradiometer ($W\ m^{-2}$).

R: Reflectivity of the aluminised surface of the collectors, measured periodically by a portable reflectometer.

$R_{C,g}$: Concentration ratio calculated from the collectors geometry.

$R_{C,op}$: Concentration ratio calculated from the collectors optic characteristics.

s_T: Area of the cylindrical surface of the absorber tube (m^2).

S_p: Area of the collecting surface of each collector (m^2).

t_{exp}: Time in which the water circulates through all the reactor at determined flow.

$t_{E,i}$: Time from the beginning of the experiment until sample "i" is taken.

$t_{R,i}$: Residence time inside the reactor, or illumination time, of each sample

$t_{1/2}$: Half life time, this means, from the beginning of the reaction until the initial concentration is reduced one half.

$T_{a,\lambda}$: Transmittance to solar light of the atmosphere, resulting from the dispersion produced by aerosols (solid or liquid particles which are suspended in the air).

$T_{g,\lambda}$: Transmittance to solar light of the atmosphere, resulting from the absorption provoked by atmospheric gases.

$T_{o,\lambda}$: Transmittance to solar light of the atmosphere, resulting from the absorption of ozone.

$T_{v,\lambda}$: Transmittance to solar light of the atmosphere, resulting from the absorption of water vapour.

$T_{R,\lambda}$: Transmittance to solar light of the atmosphere, resulting from the dispersion produced by air molecules.

$T\lambda$: Transmittance to solar light of the atmosphere.

UV_D: Radiation flux measured by the sensor of direct UV (W m^2).

$UV^*_{D,\lambda}$: Direct radiation flux of a determined wavelength calculated from $f_{D,\lambda}$ and UV_D (W m^2).

UV_G: Radiation flux measured by the sensor of global UV (W m^2).

$UV^*_{G,\lambda}$: Global radiation flux of a determined wavelength calculated from $f_{G,\lambda}$ and UV_G (W m^2).

$UV_{I,\lambda}$: Ultraviolet radiation flux, corresponding to each wavelength, measured by the spectroradiometer (W m^{-2} nm^{-1}).

$UV_{\Sigma,i}$: Ultraviolet radiation flux measured by the spectroradiometer (W m^{-2}).

V_A: Volume of the feeding tank.

V_{HDPE}: Volume of the polyethylene pipes of the pilot plant.

V_M: Volume inside each collector (helioman).

V_{TOT}: Total volume of the system.

V_R: Volume of the absorber tubes used in each experiment.

W_λ: Energy content of one photon.

X: Reactants conversion.

β: Fraction of catalyst illuminated particles.

η_C: Loss factor due to the construction characteristics of the solar collectors (0.91).

$\eta_{R,0}$: Loss factor due to the reflectivity of the aluminised surface immediately after being installed on the collectors (0.85).

$\eta_{R,i}$: Loss factor due to the reflectivity of the aluminised surface, which varies with environmental conditions, calculated from the measurements of R.

$\eta_{R,\lambda}$: Loss factor due to the reflectivity of the aluminised surface (average value = 0.872) before being installed on the collectors.

$\eta_{T,\lambda}$: Loss factor due to the transmisivity of the absorber glass.

η_S: Loss factor due to errors of the collectors sun tracking system (0.92).

θ: Aperture angle of the parabolic trough collectors.

θ_m: Acceptance semi-angle of the parabolic trough collectors.

θ_x: Fraction of surface of catalyst covered by the compound to be degraded (in this case PCP).

λ: Wavelength (nm).

μ_λ: Absorption coefficient (cm^{-1}).

τ: Average lifetime of the radicals $^\bullet$OH.

Φ: Quantum yield (%).

Φ_E: Quantum yield estimated from I^*_E, photonic flux per unit of volume, (%).

Φ_{OH}: Quantum yield of the $^\bullet$OH radicals formation.

$\Phi_{E,D}$: Quantum yield estimated from the direct radiation (%).

$\Phi_{E,0}$: Quantum yield estimated from the initial reaction rate (%).

Φ_λ: Quantum yield at fixed wavelength (%).

ε_λ: Extinction coefficient or molar absorption (M^{-1} cm^{-1}).

11. REFERENCES

Abdullah, M.; et al.; "Effects of Common Inorganic Anions on Rates of Photocatalytic Oxidation of Organic Carbon over Illuminated Titanium Dioxide". *J. Phys. Chem., 94, pp. 6820-6825 (1990).*

Acher, A.; Saltzman, S.; "Photochemical Inactivation of Organic Pollutants from Water". *Ecological Studies, Vol. 73 (Toxic Organic Chemicals in Porous Media), pp. 302-319. Springer-Verlag Ed. (1989).*

Ahmed, S.; Ollis, D.F.; "Solar Photoassisted Catalytic Decomposition of the Chlorinated Hydrocarbons Trichloroethylene and Trichloromethane". *Solar Energy, Vol. 32, No. 5, pp. 597-601 (1984).*

Akmehmet, I.; "Accelerated Photocatalytic Mineralization of Organic Pollutants Suspension of TiO_2". *Int. Conf. on Oxid. Tech. for Water and Waste Water Treatment. Goslar, Germany. May (1996).*

Al-Ekabi, H.; Serpone, N.; "Kinetic Studies in Heterogeneus Photocatalysis. Photocatalytic Degradation of Chlorinated Phenols in Aerated Aqueous Solutions over TiO_2 Suported on a Glass Matrix". *J. Phys. Chem., Vol. 92, pp. 5726-5731. (1988).*

Al-Ekabi, H.; Serpone, N.; Pelizzetti, E.; Minero, C.; Fox, M.A.; Barton, R.; "Kinetics Studies in Heterogeneous Photocatalysis. TiO_2-Mediated Degradation of 4-Chlorophenol alone and in Three-Component Mixture of 4-Chlorophenol, 2,4-Dichlorophenol and 2,4,5-Trichlorophenol in Air-Equilibrated Aqueous Media". *Langmuir, 5, pp. 250-255. (1989).*

Al-Ekabi, H.; et al.; "Advanced Technology for Water Purification by Heterogeneous Photocatalysis". *Int. J. of Environ. and Pollution, Vol. 1, 1/2, pp. 125-136. (1991).*

Al-Ekabi, H.; et al.; "TiO_2 Advanced Photo-Oxidation Technology: Effect of Electron Acepptors". *Photocatalytic Purification and Treatment of Water and Air, Ollis, D.F. and Al-Ekabi, H. (eds.). Elsevier Sci. Publish. B.V., pp. 321-335. (1993).*

Al-Ekabi, H.; "Advanced Oxidation Technologies for Water and Air Remediation". *1st Intern. Conf. on AOTs, London, Ontario, Canada. June 1994.*

Al-Sayyed, G.; et al.; "Semiconductor-sensitized Photodegradation of 4-Chlorophenol in Water". *J. Photochem. Photobiol., 58, pag. 99-114. (1991).*

Alpert, D.J.; Sprung, J.L., et al. "Sandia National Laboratories'Work in Solar Detoxification of Hazardous Wastes". *Solar En. Mat., 24, pp. 594-607. (1991).*

Amalric, L.; et al. "The Photodegradation of 2,3-benzofuran and its Intermediates, 2-Coumaranone and Salicylaldehyde in TiO_2 Aqueous Suspensions". *J. Photochem. Photobiol. A: Chem., 85, pp 257-262. (1995).*

American Society for Testing and Materials (ASTM); "Standard Tables for Terrestial Direct Normal Solar Spectral Irradiance for Air Mass 1.5". *Designation: E891-87. (1987a).*

American Society for Testing and Materials (ASTM); "Standard Tables for Terrestial Solar Spectral Irradiance at Air Mass 1.5 for a 37º Tilted Surface". *Designation: E892-87. (1987b).*

Anderson, J.V.; Link, H.; Bohn, M.; Gupta, B.; "Development of U.S. Solar Detoxification Technology: An Introduction". *Solar En. Mat., 24, pp. 538-549. (1991).*

Augugliaro, V.; Pelizzetti, E.; Minero, C.; et al.; "Photocatalytic Degradation of Phenol in Aqueous Titanium Dioxide Dispersions". *Toxicol. and Environ. Chem., Vol. 16, pp. 89-109. (1988).*

Augugliaro, V.; Davì, E., et al.; "Influence of Hydrogen Peroxide on the Kinetics of Phenol Photodegradation in Aqueous Titanium Dioxide Dispersion". *App. Catalysis, Vol. 65, pp. 101-116. (1990).*

Augugliaro, V.; et al.; "Photocatalytic Degradation of Nitrophenols in Aqueous Titanium Dioxide Dispersion". *App. Catalysis, 69, pp. 323-340. (1991).*

Bahnemann, D.W.; et al.; "Mechanism Studies of Water Detoxification in Illuminated TiO_2 Suspensions". *Solar En. Mat., 24, pp. 564-583. (1991a).*

Bahnemann, D.W.; et al.; "Mechanism of Organic Transformations on Semiconductor Particles". *Photochemical Conversion and Storage of Solar Energy, in E. Pelizzetti and M. Schiavello (eds.), pp. 251-276, Kluwer Academic Publish. (1991b).*

Bahnemann, D.W.; et al.; "Photocatalytic Detoxification: Novel Catalyst, Mechanism and Solar Applications". *Photocatalytic Purification and Treatment of Water and Air, D. Ollis and H. Al-Ekabi (eds.), Elsevier Science Publishers, pp. 301-319. Amsterdam. (1993a).*

Bahnemann, D.W.; et al.; "Photocatalytic Detoxification of Polluted Aquifers: Novel Catalyst and Solar Applicationas". *Aquatic and Surface Photochemistry. G.R. Helz, R.G. Zepp and D.G. Crosby (eds.). Lewis Publishers. pp.349-368. (1994a).*

Bahnemann, D.W.; et al.; "Photocatalytic Treatment of Water". *Aquatic and Surface Photochemistry. G.R. Helz, R.G. Zepp and D.G. Crosby (eds.). Lewis Publishers. pp.261-316. (1994b).*

Barbeni, M.; et al.; "Photodegradation of 4-Chlorophenol Catalyzed by Titanium Dioxide Particles". *Nouveau J. de Chim., Vol. 8, pp. 547-550. (1984).*

Barbeni,M.; et al.; "Photodegradation of Pentachlorophenol Catalyzed by Semiconductor Particles". *Chemosph., Vol. 14, 2, pp. 195-208. (1985).*

Barbeni, M.; Pramauro, E.; Pelizzetti, E.; "Photochemical Degradation of Chlorinated Dioxins, Biphenyls Phenols and Benzene on Semiconductor Dispersions". *Chemosphere, Vol. 15, No. 9, pp. 1913-1916. (1986).*

Barbeni, M.; et al.; "Sunlight Photodegradation of 2,4,5-Trichlorophenoxy-Acetic Acid and 2,4,5-Trichlorophenol on TiO_2. Identification of Degradation Pathway". *Chemosphere, Vol. 16, 6, pp. 1165-1179. (1987a).*

Barni, B; et al.; "Pilot-Plant-Scale Photodegradation of Phenol in Aqueous Solution by Photocatalytic Membranes Inmobilizing Titanium Dioxide". *Chemosphere, Vol- 30, nº 10, pp. 1861-1874. (1995a).*

Barni, B; et al.; "Laboratory-Scale Photodegradation of Phenol in Aqueous Solution by Photocatalytic Membranes Inmobilizing Titanium Dioxide". *Chemosphere, Vol. 30, nº 10, pp. 1847-1870. (1995b).*

Bellobono, I.R.; et al.; "Laboratory - and Pilot-Plant-Scale Photodegradation of Chloroaliphatics in Aqueous Solution by Photocatalytic Membranes Inmovilizing Titanium Dioxide". *J. Photochem. Photobiol. A: Chem., 84, pp.83-90. (1994).*

Bellobono, I.R.; et al.; "Pre-Industrial Experience in Advanced Oxidation and Integral Photodegradation of Organics in Potable Waters and Waste Waters by PHOTOPERM^{TM} Membranes Inmovilizing TiO_2 and Promoting Photocatalysis". *J. Membrane Sci., 102, pp. 139-147 (1995).*

Bideau, M.; Claudel, Otterbein, M.; "Photocatalysis of Formic Acid Oxidation by Oxygen in an Aqueous Medium". *J. of Photochem., Vol. 14, pp. 291-302. (1980).*

Bideau, M.; Claudel, B; Faure, L.; Rachimoellah, M.; "Homogeneous and Heterogeneous Photoreactions of Decomposition and Oxidation of Carboxylic Acids". *J. of Photochem., Vol. 39, pp. 107-128. (1987).*

Bideau, M.; Claudel, B; Faure, L.; Rachimoellah, M.; "Photo-Oxidation of Formic Acid by Oxygen in the presence of Titanium Dioxide and Dissolved Copper Ions: Oxygen Transfer and Reaction Kinetics". *Chem. Eng. Comm., Vol. 93, pp. 167-179. (1990).*

Bideau, M.; et al.; "The Photo-Oxidation of Acetic Acid by Oxygen in the Presence of Titanium Dioxide and Dissolved Copper Ions". *J. Photochem. Photobiol. A: Chem., 61, pp. 269-280. (1991).*

Bideau, M.; et al.; "The Photo-Oxidation of Propionic Acid by Oxygen in the Presence of TiO_2 and Dissolved Copper Ions". *J. Photochem. Photobiol. A: Chem., 67, pp. 337-348. (1992).*

Blake, D.; Webb, J.; Turchi, C.; Magrini, K.; "Kinetic an Mechanistic Overview of TiO_2 Photocatalyzed Oxidation Reactions in Aqueous Solution". *Solar En. Mat., 24, pp. 584-593. (1991).*

Blake, D.M.; "Bibliography of Work on the Photocatalytic Removal of Hazardous Compounds from Water and Air". *National Technical Information Service, U.S. Depart. of Commerce, Springfield, VA22161, USA. May 1994.*

Blake, D.M.; "Bibliography of Work on the Photocatalytic Removal of Hazardous Compounds from Water and Air. Update Number 1". *Nat. Tech. Inform. Serv., U.S. Dept. of Commerce, Sprinfield, VA22161, USA. June 1995.*

Blanco, J. and Malato, S.; "Final Configuration of the PSA Solar Detoxification Loop". *Plataforma Solar de Almeria. IER-CIEMAT. Report 6/91. (1991a).*

Bockelmann, D.; et al.; "Preparation and Characterization of Novel Mixed Titanium/Iron Oxide Photocatalyst for the Detoxification of Polluted Aquifers". *Private Communication, ISFH. Hannover (1991).*

Bockelmann, D.; et al.; "Solar Detoxification of Polluted Water: Comparing the Efficiencies of a Parabollic Trough Reactor and a Novel Thin-Film-Fixed-Bed Reactor". *Proceedings of 1st. Intern. Conf. on TiO_2 Photocatalytic Purification and Treatment of Water and Air. London (Ontario), Canada. Nov. (1992).*

Bockelmann, D.; et al.; "Concentrating versus non-Concentrating Reactors for Solar Water Detoxification". *Sol. En. Mat. and Sol. Cells, 38, pp. 441-451. (1995).*

Boonstra, A.H.; et al.; "Adsorption of Hydrogen Peroxide on the Surface of Titanium Dioxide". *J. Phys. Chem., 79, pp. 1940-1943. (1975).*

Borello, R.; et al.; "Photocatalytic Degradation of DDT Mediated in Aqueous Semiconductor Slurries by Simulated Sunlight". *Env. Tox. and Chem., Vol. 4, pp. 997-1002. (1989).*

Borthen, J.; Leviten, D.; "Making Solar Detoxification of Contaminated Groundwater a Reality". *Solar Eng., Vol. 1, pp. 57-63. ASME (1992).*

Braun, A. M.; et al.; "Up-Scaling Photochemical Reactions". *Adv. in Photochem, 18, pp. 235-313. (1993).*

Brezová, V.; et. al.; "Photocatalytic Oxidation of 2-etoxy ethanol in a Water Suspension of Titanium Dioxide". *J. Photochem. Photobiol. A: Chem., 56, pp. 125-134. (1991).*

Brown, G.T.; et al.; "Methyl Orange as a Probe for Photooxidation Reactions of Colloidal TiO_2". *J. Phys. Chem., 88, pp. 4955-4959 (1984).*

Cabrera, M.I.; et al.; "Parameteres for Photocatalytic Reactor Design. Absorption and scatering Coefficients of Titanium Dioxide Suspension". *Int. Conf. on Oxid. Technologies for Water and Wastewater Treatm., Goslar, Germany. May (1996).*

Cáceres, J.; García, G.; Pérez, M.; "Filtrado de la Base de Datos de la Estación Meteorológica". *Plataforma Solar de Almería, R-25. (1992).*

Carey, J.H.; Lawrence, J.; Tosine, H.M.; "Photodechlorination of PCBS in the Presence of TiO_2 in Aqueous Suspensions". *Bull. of Environ. Contamination & Toxicol., Vol. 16, 6, pp. 697-701. (1976).*

Cassano, A.E.; "Uso de Actinómetros en Reactores Tubulares Contínuos". *Revista de la Facultad de Ing. Química, Santa Fe (Argentina), 37, pp. 469-501. (1968).*

Chamarro, E.; Esplugas, S.; "Efecto de la dispersión de la Luz sobre el Campo de Radiación de un Fotorreactor Plano". *Anales de Química, Vol. 86, pp. 439-442. (1990).*

Chang, W. et al.; "Bactericidal Activity of TiO_2 Photocatalyst in Aqueous Media: Toward a Solar-Assisted Water Desinfection System". *Environ. Sci. Technol, 28, pp. 934-938 (1994).*

ChemService; "Pesticides and Metabolites". *Chem. Service Inc. (1992).*

Chemseddine, A. and Boehm, H.P. "A Study of the Primary Step in the Photochemical Degradation of Acetic Acid and Chloroacetic Acids on a TiO_2 Photocatalyst". *J. Mol. Catal., 60, pp. 295-311. (1990).*

Chen-Yung Hsiao; Chung-Li Lee; Ollis, D.F.; "Heterogeneous Photocatalysis: Degradation of Diluted Solutions of Dichloromethane (CH_2Cl_2), Chloroform ($CHCl_3$), and Carbon Tetrachloride (CCl_4) with Illuminated TiO_2 Photocatalyst". *J. Catal., 82, pp. 418-423. (1983).*

Crosby, D.G.; "Environmental Chemistry of Pentachlorophenol". *Pure Appl. Chem., 53, pp. 1051-1080 (1981).*

Cundall, R.B.; et al.; "The Photocatalytic Oxidation of Liquid Phase Propan-2-ol by Pure Rutile and Titanium Dioxide Pigments". *J. Oil Col. Chem. Assoc., 61, pp. 351-355. (1978).*

Cunningham, J.; et al.; "Factors Influencing Efficiencies of TiO_2-Sensitized Photodegradation. Part 1., Substitued Benzoic Acids: Discrepancies with Dark-adsorption Parameters". *J. Chem. Soc. Faraday, Trans., 86(23), pp. 3835-3941. (1990).*

Cunningham, J.; et al.; "Sensitized Photo-oxidations of Dissolved Alcohols in Homogeneous and Heterogeneous Systems Part 2. TiO_2-Sensitized Photodehydrogenations of Benzyl Alcohol". *J. Photochem. Photobiol. A: Chem., 58, pp. 361-371. (1991).*

Curcó, D.; "Modelos Cinéticos y de Radiación en Procesos Fotocataliticos". *Tésis Doctoral, Universidad de Barcelona. (1994).*

Curcó, D.; et al.; "Photocatalytic Degradation of Phenol: Comparison between Pilot-Plant Scale and Laboratory Results". *Sol. En., Vol. 56, 5, pp. 387-400. (1996a).*

Curcó, D. et al.; "Photocatalysis and radiation absorption in a solar plant". *Sol. En. Materials and Sol. Cells, 44, pp. 199-217. (1996b).*

Davis, A.P.; et al.; "A Kinetic Model Describing Photocatalytic oxidation using Illuminated Semiconductors". *Chemosphere, Vol. 56, 6, pp. 1119-1135. (1993).*

Degussa Corporation; "Technical Bulletin Pigments". *Nº 56, 60, 64, 72. Germany.*

Doherty, S.; et al.; "Kinetics and Products of the Photocatalytic Degradation of Morpholine in TiO_2 Aqueous Suspensions". *J. Chem. Soc. Faraday Trans., 91(12), pp. 1853-1859. (1995).*

D'Oliveira, J.C.; et al.; "Photodegradation of 2- and 3-Chlorophenol in TiO_2 Aqueous Suspensions". *Environ. Sci. Technol., 24, pp. 990-996. (1990).*

Egerton, T.A.; King, C.J.; "The Influence of Light Intensity on Photoactivity in TiO_2 Pigmented Systems". *J. Oil Chem. Assoc., 62, pp. 386-391. (1979).*

Enzweilwer, R.J.; et al.; "A Pilot Scale Investigation of Photocatalytic Detoxification of BETX Water". *ASME Inter. Solar En. Conf. San Francisco, USA. March (1994).*

Environmental Protection Agency; "Notice of the Second Prioritary List of Hazardous Substances Commonly Found at Superfund Sites". *Environ. Reporter, pp. 1255-1260. (1988).*

Fabero, F.; Chenlo, F.; "Análisis de la Distribución Espectral de la Irradiancia Solar en Madrid". *V Congreso Ibérico de E. Renovables. ISES. Madrid. Octubre (1990).*

Feister, V.; et al.; "Instruments for Broad-Band UV radiation Measurements". *Sol. En., Vol. 49, 6, pp. 535-540. (1992).*

Fernandez, A.; et al.; "Preparation and Characterizacion of TiO_2 Photocatalysts Supported on Various Rigid Supports (Glass, Quartz and Stainless Steel). Comparative Studies of Photocatalytic Activity in Water Purification". *App. Catalysis B: Environ., 7, pp. 49-63. (1995).*

Fox, M.A.; "Organic Heterogeneus Photocatalysis: Chemical Conversions Sensitized by Irradiated Semiconductors". *Acc. Chem. Res., 16, pp. 314-321. (1983).*

Fox, M.A.; et al.; "The Effect of the "Inert" Support on Relative Photocatalytic Activity in the Oxidative Decomposition of Alcohols on Irradiated Titanium Dioxide Composites". *Res. Chem. Interm., Vol. 20,7, pp. 711-722. (1994a).*

Froilán, J.; "Pentachlorophenol Degradation by Flavobacterium sp. and its Application to Soil Decontamination". *Tesis Doctoral, Universidad de Minnesota, USA. (1990).*

Gao, Y-M; et al.; "Preparation and Photocatalytic Properties of Titanium (IV) Oxide Films". *Mat. Res. Bull., Vol. 27, pp. 1023-1030. (1992).*

Gerischer, H.; et al.; "Photocatalytic Oxidation of Organic Molecules at Ti*O_2 Particles by Sunlight in Aerated Water". J. Electrochem. Soc., Vol. 139, 1, pp. 113-118. (1992).*

Gerischer, H.; "Conditions for an Efficient Photocatalytic Activity of TiO_2 Particles". *Photocatalytic Purification and Treatment of Water and Air, Ollis, D.F. and Al-Ekabi, H. (eds.). Elsevier Sci. Publish. B.V., pp. 1-17. (1993).*

Gerischer, H.; "Photocatalysis in Aqueous Solution with Small TiO_2 Particles and the Dependence of the Quantum Yield on Particle Size and Light Intensity". *Electrochim. Acta, Vol. 40, 10, pp. 1277-1281. (1995).*

Giménez, J.; Cervera S.; Aguado M.; Borrell L.; "Aprovechamiento Fotocatalítico de la Energía Solar en el Tratamiento de la Contaminación y Producción de Combustibles". *Era Solar 50, pp. 6-12. (1992a).*

Giménez, J.; et al.; "The Photocatalytical Use of Solar Energy as an Alternative Way in the Pollution Treatment". *6th Intern. Symp. on Solar Thermal Concentrating Techn. Mojacar (Almería), Spain. Sept. (1992b).*

Giménez, J.; et al.; "Photoreactor Design for Photocatalytical Detoxification: Kinetic and Radiation Studies". *ASME Intern. Solar En. Conf. San Francisco, USA. March (1994).*

Giménez, J.; et al.; "Photocatalytic Oxidation of Organic Pollutants by Using Solar Energy". *Inter. Symposium on Environ. Appl. of Advan. Oxid. Tech. San Francisco USA. Febrero (1996a).*

Giménez, J.; et al.; "Reactor Modelling in the Photocatalytic Oxidation of Wastewater". *Int. Conf. on Oxid. Tech. for Water and Wastewater Treatm., Goslar, Germany. May (1996b).*

Giménez, J.; et al.; "Photocatalytic Treatment of Phenol in a Solar Plant". *Int. Symp. on Solar Thermal Concentrating Tech.; Colonia, Germany. October (1996c).*

Glatzmaier, G.C.; "Cost Comparison of Solar Detoxification with Conventional Alternatives for Destruction of Trichloroethylene". *Solar Eng., Vol. 1, pp. 43-49. ASME (1992).*

Goswami, D.Y.; " Engineering of solar Photocatalytic Detoxification and Disifection Processes". *Advances in Solar Energy. K.W. Böer (ed.) Am. Solar En. Soc. pp. 165-209. (1995).*

Goulden, P.D.; et al.; "Kinetics of Uncatalyzed Peroxydisulphate Oxidation of Organic Material in Fresh Water". *Anal. Chem., Vol. 50, nº 7, pp. 953-958. (1978).*

Grätzel, C.K.; Jirousek, M.; Grätzel, M.; "Decomposition of Organophosphorous Compounds on Photoactivated TiO_2 Surfaces". *J. Mol. Cat., 60, pp. 375-387.(1990).*

Guillard, Ch.; et al.; "The GC-MS Analysis of Organic Intermediates from the TiO_2 Photocatalytic Treatment of Water Contaminated by Lindane". *J. Adv. Oxid. Technol., Vol. 1,1, pp. 53-60. (1996).*

Haag, W.R.; et al.; "Rate Constant for Reaction of Hydroxyl Radicals with Several Drinking Water Contaminants". *Environ. Sci. Technol., 26, pp. 1005-1013. (1992).*

Hacker, D.S.; "Photocatalysis in a Slurry Reactor". *Chem. Eng. Sc., Vol. 30, pp. 1149-1158. (1975).*

Halmann, M.; et al.; "Photodegradation of Dichloromethane, Tetrachloroethylene and 1,2-dibromo-3-chloropropane in Aqueous Suspensions of TiO_2 with Natural, Concentrated and Simulated Sunlight". *Solar En. Mat. and Solar Cells, 26, pp. 1-16. (1992).*

Hass, R.; "Applied Optics and Optical engineering", *Vol. VIII. pp. 309-330. Academic Ress, Inc., New York. (1965).*

Herrmann, J.M.; Pichat, P.; "Heterogeneous Photocatalysis Oxidation of Halide Ions by Oxygen in Ultraviolet Irradiated Aqueous Suspensions of Titanium Dioxide". *J. C. S. Faraday I, 76, pp. 1138-1146. (1980).*

Herrmann, J.M.; Mozzanega, M.N.; Pichat, P.; "Oxidation of Oxalic Acid in Aqueous Suspensions of Semiconductors Illuminated with UV or Visible Light". *J. Photochem., 22, pp. 333-343. (1983).*

Herrmann, J.M.; et al.; "Photocatalytic Oxidation at Romm Temperature in Various Media". *New developments in Selective Oxidations, G. Centi and F. Trifiro (eds.), pp. 675-682. Elsevier Sci. Pub. (1990a).*

Herrmann, J.M.; "Heterogeneous Photocatalysis: an Emerging Discipling Involving Multiphase System". *Catal. Today, 24. pp. 157-164. (1995).*

Hidaka, H.; et al.; "Photodegradation of Surfactants II: Degradation of Sodium Dodecylbenzene Sulphonate Catalysed by Titanium Dioxide Particles". *J. Photochem., 35. pp. 219-230. (1986).*

Hilgendorff, M.; et al.; "Photocatalytic Decomp. of Aliphatic Halogenated Hydroc. in Water: Lab. Studies and Solar Applications". *6th Intern. Symp. on Solar Thermal Conc. Techn. Mojacar (Almería), Spain. Sept (1992).*

Hisanaga, T.; et al.; "Photocatalytic Degradation of Organochlorine Compounds in Suspended TiO_2". *J. Photchem. Photobiol., A: Chem., 54, pp. 113-118. (1990).*

Hoffmann, M.R.; et al.; "Environmental Applications of Semiconductor Photocatalysis". *Chem. Rev., 95, pp. 69-96. (1995).*

Hofstadler, K.; et al.; "New Reactor Desing for Photocatalytic Wastewater Treatment with TiO_2 Inmovilized on Fussed Silica Glass Fibers: Photomineralization of 4-Chlorophenol". *Environ. Sci. Technol., Vol. 28, 4, pp. 670-674. (1994).*

Howe, R.F.; Grätzel, M.; "EPR Study of Hydrated Anatase under UV Irradiation". *J. Phys. Chem., 91, pp. 3906-3909. (1987).*

Hulstrom, R.; Bird, R.; Riordan, C.; "Spectral Solar Irradiance Data Sets for Selected Terrestial Conditions". *Solar Cells, 15, pp. 365-391. (1985).*

Iqbal, M.; "An Introduction to Solar Radiation". *Academic Press, Canada. (1983).*

Jacobsen, B.N.; et al.; "Microbial Degradation of Pentachlrophenol and Lindane in Laboratory-Scale Activated Sludge Reactor". *EEC Workshop, Organic Micropollutants in the Aquatic Environment. Helsinki, Finland. May (1989).*

Jenny, B.; Pichat, P.; "Determination of the Actual Photocatalytic Rate of H_2O_2 Decomposition over suspended TiO_2. Fitting to the Langmuir-Hinshelwood Form". *Langmuir, 7, pp. 947-954 (1991).*

Jorgensen, G.; Govindarajan, R.; "Ultraviolet Reflector Materials for Solar Detoxification of Hazardous Waste". *Report SERI/TP-257-4418. DE91 002196. Solar Energy Research Institute. July (1991).*

Kamat, P.V.; Dimitrijevic, N.; "Colloidal Semiconductors as Photocatalysts for Solar Energy Conversion". *Solar Energy, Vol. 44, 2, pp. 83-98. (1990).*

Karpa, L.; "Solar-photokatalytische Behandlung eines Industrieabwassers auf der Plataforma Solar de Almeria, Spanien". *Diplomarbeit, Tech. Univ. Clausthal. (1995).*

Kawaguchi, H.; "Photocatalytic Decomposition of Phenol in the Presence of Titanium Dioxide". *Env. Tech. Letters, Vol. 5, pp. 471-474. (1984).*

Kawaguchi, H.; "Dependence of Photocatalytic Reaction Rate on Photocatalyst Concentration in Aquous Suspensions". *Environ. Technol., Vol. 15, pp. 183-188. (1994).*

Kennes, Ch.; et al.; "Biodegradación de Compuestos Orgánicos Tóxicos". *Ing. Quim., 302, pp. 119-123. (1994).*

Kerzhentsev, M.; et al.; "Photocatalytic Pollutant removal in Water at Room Temperature: Case Study of the Total Degradation of the Insecticide Fenitrotion". *Catalysis Today, 27, pp. 215-220. (1996).*

Klausner, J.F.; Goswami, D.Y.; Wyness, P.R.; "Energy Consumption of Wastewater Treatment Technologies". *Solar Eng., Vol. 1, pp. 29-36. ASME (1992).*

Klissurski, D.; et al.; "Study of Peroxide-Modified Titanium Dioxide (Anatase)". *J. Chem. Soc. Faraday Trans., 86, pp. 385-388. (1990).*

Kormann, C; et al.; "Photolysis of Chloroform and other Organic Molecules in Aqueous TiO_2 Suspensions". *Environ. Sci. Technol., 25, pp. 494-500. (1991).*

Kratz, W.; Gruttke, H.; "Pentachlorophenol. A Wood Preservative. Its Distribution in an Invertebrade Food Chain". *EEC Workshop, Organic Micropollutants in the Aquatic Environment. Helsinki, Finland. May (1989).*

Ku, Y. and Hsieh, Ch. B.; "Photocatalytic Decomposition of 2,4-dichlorophenol in Aqueous TiO_2 Suspensions". *Wat. Res., Vol. 26, 11, pp. 1451-1456. (1992).*

Kuehl, D.W.; Dougherty, R.C.; "Pentachlorophenol in the Environment. Evidence for its Origin from Commercial Pentachlorophenol by Negative Chemical Ionization Mass Spectrometry". *Environ. Sci. Technol., Vol. 14, 4, pp. 447-449. (1980).*

Kuhn, H.I.; et al.; "Chemical Actinometry". *Pure and Appl. Chem., Vol. 61, 2, pp. 187-210. (1989).*

Legrini, O.; et al.; "Photochemical Processes for Water Treatment". *Chem. Rev., 93, pp. 671-698. (1993).*

Leighton, W.G. and Forbes, G.S.; "Precision Actinometry with Uranyl Oxalate". *J. Am. Soc., 52, pp. 3139-3152. (1930).*

Lensch, G.; et al.; "FH-PTL WEDEL Reflectometer Type 02-1 No. 3". *Final Report and Report on the Test Program, No. 2/83, SSPS, Plataforma Solar de Almería. (1983).*

Levenspiel, O.; "Ingeniería de la Reacción Química". *Ed. Reverté, Barcelona. (1975).*

Li, X.; et al.; "Sensitized Photodegradation of Chlorophenols in a Continuous Flow Reactor System". *Wat. Sci. Tech., Vol. 26, 1-2, pp. 367-376. (1992).*

Lindner, M.; et al.; "Photocatalytic Degradation of Organic Compounds: Accelerating the Process Efficiency". *Int. Conf. on Oxid. Techn. for Water and Wastew. Treatment, Goslar, Germany, May. (1996).*

Lindsebigler, A.L.; et al; "Photocatalysis on TiO_2 Surfaces: Principles, Mechanisms and Selected Results". *Chem. Rev., 95, pp. 735-758. (1995).*

Link, H.; Turchi, C.S.; "Cost and Performance Projections for Solar Water Detoxification Systems". *Proceedings for ASME International Solar Energy Meeting. Reno, Nevada. March (1991).*

Magrini, K.A.; Webb, J.D.; "Photocatalytic decomposition of aqueous organic compounds as a function of solar irradiation intensity". *ASME Inter. Solar En. Conf. Miami (Florida), USA. April (1990).*

Magrini, K.A.; et al.; "Improving Catalyst Performance for Solar-based Photocatalytic Oxidation of Organics". *ASME Inter. Solar En. Conf. San Francisco, USA. March (1994).*

Mäkinen, P.M.; et al.; "Chlorophenol Toxicity Removal and Monitoring in Aerobic Treatment: Recovery from Process Upsets". *Environ. Sci. Technol., 27, pp. 1434-1439 (1993).*

Malato, S.; Blanco, J.; "Photocatalytic Decomposition of Pentachlorophenol by Solar UV Light and TiO_2 Powder". *Proceedings of 6th Intern. Symp. on Solar Thermal Concentrating Technologies. Mojacar (Almería), Spain. September (1992).*

Malato, S.; et al.; "Photocatalytic Degradation of Industrial Residual Waters". *Sol. En., Vol., 56, 5, pp. 401-410. (1996a).*

Malato, S.; et al.; "Low-Concentrating CPC Collectors for Photocatalytic Water Detoxification. Comparison with a Medium Concentrating Solar Collector". *Int Conf. on Oxidation Tech. for Water and Wastewater Treatment. Goslar, Germany. (1996b).*

Manilal, V.B. et al.; "Photocatalytic Treatment of Toxic Organics in Wastewater: Toxicity of Photodegradation Products". *Wat. Res. Vol.26, 8, pp. 1035-1038. (1992).*

Martin, C.A.; et al.; "Photocatalytic Reactors I. Optical Behaviour of Titanium Oxide Particulate Suspensions". *J. Photochem. Photobiol. A: Chem., 76, pp. 199-208. (1993).*

Martin, S.T.; et al.; "Chemical Mechanism of Inorganic Oxidants in the TiO_2/UV Process: Increased Rastes of Degradation of Chlorinated Hydrocarbons". *Environ. Sci. Technol., 29, pp. 2567-2573. (1995a).*

Martin, S.T.; et al.; "Photochemical Destruction of Chemical Contaminants on Quantum Sized Semiconductor Particles". *Solar Engineering, Vol 1, ASME 1995, pp. 409-413 (1995b).*

Matthews, R.; "Hydroxylation Reactions Induced by Near-Ultraviolet Photolysis of Aqueous Titanium Dioxide Suspensions". *J. Chem. Soc., Faraday Trans., I, 80, pp. 457-471. (1984).*

Matthews, R.W.; "Photo-oxidation of Organic Material in Aqueous Suspensions of Titanium Dioxide". *Wat. Res., Vol. 20, 5, pp. 569-578. (1986a).*

Matthews, R.W.; "Photocatalytic Oxidation of Chlorobenzene in Aqueous Suspensions of Titanium Dioxide". *J. Catalysis, 97, pp. 565-568. (1986b).*

Matthews, R.W.; "Photo-oxidation of Organic Impurities in Water Using Thin Films of Titanium Dioxide". *J. Phys. Chem., 91, pp. 3328-3333. (1987a).*

Matthews, R.W.; "Carbon Dioxide Formation from Organic Solutes in Aqueous Suspensions of Ultraviolet Irradiated TiO_2; Effect of Solute Concentration". *Aust. J. Chem., 40, pp. 667-75. (1987b).*

Matthews, R.W.; "Solar-Electric Water Purification using Photocatalytic Oxidation with TiO_2 as a Stationary Phase". *Sol. En., Vol. 38, 8, pp. 405-413. (1987c).*

Matthews, R.W.; "Kinetics of Phtocatalytic Oxidation of Organic Solutes over Titanium Dioxide". *J. Catalysis, 111, pp. 264-272. (1988).*

Matthews, R.W.; et al.; "Photocatalytic Oxidation for Total Organic Analysis". *Anal. Chym. Acta, 233, pp. 171-179. (1990).*

Matthews, R.W.; McEvoy, S.R.; "Photocatalytic Degradation of Phenol in the Presence of Near-UV Illuminated Titanium Dioxide". *J. Photochem. Photobiol. A: Chem., 64, pp. 231-246. (1992).*

Matthews, R.W.; "Photocatalysis in Water Purification: Possibilities, Problems and Prospects". *Photocatalytic Purification and Treatment of Water and Air, Ollis, D.F. and Al-Ekabi, H. (eds.). Elsevier Sci. Publish. B.V. pp. 121-138. (1993).*

Mehos, M.S.; et al.; "Measurement and Analysis of Near Ultraviolet Solar Radiation". *Solar Eng., Vol. 1, pp. 51-55. ASME (1992a).*

Mehos, M.; Turchi, C.; "The Solar Detox. Field Exp.: A Pilot-Scale Invest. of the Solar Detox. Techn.". *6th Intern. Symp. on Solar Thermal Concentrating Techn. Mojacar (Almería), Spain.(1992b).*

Mille, M.J.; Crosby, D.G.; "Pentachlorophenol and 3,4-Dichloroaniline as Model for Photochemical Reactions in Seawater". *Marine Chem., 14, pp. 111-120. (1983).*

Miller, R.M.; et al.; "Sequential Degradation of Chlorophenols by Photolytic and Microbial Treatment". *Envirn. Sci. Technol., 22, pp. 1215-1219. (1988).*

Millipore Corporation; "A10 Total Organic Carbon Monitor". *(1995).*

Mills, A.; et al.; "Water Purification by Semiconductor Photocatalysis". *Chem,. Soc. Rev., pp. 417-425. (1993a).*

Mills, A.; et al.; "Photo mineralization of 4-Chlorophenol Sensitized by Titanium Dioxide: a Study of the Initial Kinetics of Carbon Dioxide Photogeneration". *J. Photochem. Photobiol. A: Chem., 71, pp. 75-83 (1993b).*

Mills, G.; et al.; "Photocatalytic Degradation of Pentachlorophenol on TiO_2 Particles: Identification of Intermediates and Mechanism of Reaction". *Environ. Sci. Technol., 27, pp. 1681-89. (1993a).*

Minero, E.; et al.; "Kinetic Studies in the Heterogeneous Photocatalysis 6. AM1 Simulated Sunlight Photodegradation over Titania in Aqueous media: A First Case of Fluorinated Aromatics and Identification of Intermediates". *Langmuir, pp. 928-936 (1991a).*

Minero, C.; Pelizzetti, E.; Malato, S.; Blanco, J.; "Large Solar Plant Photocatalytic Water Decontamination: Degradation of Pentachlorophenol". *Chemosphere, Vol. 26, 12, pp. 2103-2119. (1993).*

Minero, C.; et al.; "Reactions of Hexafluorobencene and Pentafluorophenol Catalyzed by Irradiated TiO_2 in Aqueous Suspensions". *Langmuir, Vol. 10, pp. 692-698. (1994).*

Minero, C.; "A Rigurous kinetic Approach to Model Primary Oxidative Steps of Photocatalytic Degradations". *Sol. En. Mat. Sol. Cells., 38, pp. 421-430. (1995).*

Minero, C., et al.; "Large Solar Plant Photocatalytic Water Decontamination: Effect of Operational Parameters". *Sol. En., Vol. 56, 5, pp. 411-420. (1996a).*

Minero, C.; Pelizzetti, E.; Malato, S.; Blanco, J.; "Large Solar Plant Photocatalytic Water Decontamination: Degradation of Atrazine". *Sol. En., Vol. 56, 5, pp. 421-428. (1996b).*

Muradov, N.Z.; "Solar Detoxification of Nitroglycerine Contaminated Water Using Inmovilized Titania". *Sol. En., Vol. 52, 3, pp. 283-288 (1994).*

Muszkat, L.; et al.; "Solar Photodegradation of Xenobiotic Contaminants in Polluted Well Water". *J. Photochem. Photobiol. A. Chem., 65, pp. 409-417 (1992).*

Muszkat, L.; et al.; "Solar Photocatalytic Mineralization of Pesticides in Polluted Waters". *J. Photochem. Photobiol. A: Chemistry, 87, pp. 85-88. (1995).*

Nargiello, M.; et al.; "Physical-Chemical Characteristics of P-25 Making it Extremely Suited as the Catalyst In Photodegradation of Organic Compounds". *Photocatalytic Purification and Treatment of Water and Air. Ollis, D.F. and Al-Ekabi, H. (eds.). Elsevier Sci. Publish.B.V.pp. 801-805 (1993).*

Neta, P.; et al.; "Rate Constant and Mechanism of Reaction of SO_4^{o-} with Aromatic Compounds". *J. Am. Chem. Soc., 99, 1, pp. 163-164. (1977).*

Nguyen, T. et al.; "Complete Heterogenously Photocatalyzed Transformation of 1,1- and 1,2- Dicromoethane to CO_2 and HBr". *J. Phys. Chem., 88, pp. 3386-3388 (1984).*

Oberg, V.; et al.; "On Photocatalytic Detoxification of Water Containing VOC's". *ASME Intern. solar En. Conf. San Francisco, USA. March (1994).*

Okamoto, K. et al.; "Heterogeneus Photocatalytic Decomposition of Phenol over TiO_2 Powder". *Bull. Chem. Soc. Jpn., 58, pp. 2015-2022. (1985a).*

Okamoto, K. et al.; "Kinetics of Heterogeneus Photocatalytic Decomposition of Phenol over Anatase TiO_2 Powder". *Bull. Chem. Soc. Jpn., 58, pp. 2023-2028. (1985b).*

Ollis, D.F.; "Heterogeneous Photoassisted Catalysis: Conversions of Perchloroethylene, Dichloroethane, Chloroacetics Acids, and Chlorobenzenes". *J. Catalysis, 88, pp. 89-96. (1984).*

Ollis, D.F.; "Contaminant Degradation in Water. Heterogeneus Photocatalysis Degrades Halogenated Hydrocarbon Contaminants". *Environ. Sci. Technol., Vol. 19, 6, pp. 480-484. (1985).*

Ollis, D.F.; et al.; "Destruction of Water Contaminants". *Environ. Sci. Technol., Vol. 25, 9, pp. 1523-1528. (1991a).*

Ollis, D.F.; "Solar-Assisted Photocatalysis for Water Purification: Issues, Data, Questions". *Photochemical Conversion and Storage of Solar Energy, pp. 593-622. Kluwer Academic Publishers. (1991b*).

Ollis, D.F.; "Photocatalytic Purification and Treatment of Water and Air". *Elsevier Sciencie Publishers B.V. Nehterlands. (1993).*

Pacheco, J.E.; Carwile, C.; "Developments in Solar Photocatalysis for Destruction of Organics in Water". *Waste Management 90. Proc. Interna. Tucson (Arizona), February (1990a).*

Pacheco, J.E.; Tyner C.E.; "Enhancement of Processes for Solar Photocatalytic Detoxification of Water". *1990 ASME Solar Energy Division. International Solar Energy Conference. Maimi, Florida, April (1990b).*

Pacheco, J.; Prairie, M.; Evans, L.; Yellowhorse, L.; "Engineering-Scale Experiments of Solar Photocatalytic Oxidation of Trichloroethylene". *25th Intern. Society Energy Conversion Engineering Conference. Reno, Nevada. August (1990c).*

Pacheco, J.E.; Prairie, M.; Yellowhorse, L.; "Photocatalytic Destruction of Chlorinated Solvents with Solar Energy". *Proceedings 1991 ASME-JSME-JSES International Solar Energy Conference. Reno, Nevada. March (1991).*

Pacheco, K.; Watt, A.S.; Turchi, C.S.; "Solar Detoxification of Water: Outdoor Testing of Phototype Photorreactors". *Joint Solar Eng. Conf., ASME. pp. 43-49. (1993).*

Parent, Y.; et al.; "Solar Photocatalytic Process for the Purification of Water: State of Development and Barrires to Commercialization". *Sol. En., Vol. 56, 5, pp. 429-438. (1996).*

Pelizzetti, E.; "Homogeneus and Heterogeneus Photocatalysis". *La Chimica e L'Industria, Vol. 68, 10, pp. 51-52. (1986a).*

Pelizzetti, E.; et al.; "Photocatalytic Degradation of Polychlorinated Dioxins and Polychlorinated Byphenyls in Aquous Suspensions of Semiconductors Irradiated with Simulated Solar Light". *Chemosphere, Vol. 17, 3, pp. 499-510. (1988).*

Pelizzetti, E.; et al.; "The Role of Colloidal Particles in the Photodegradation of Organic Compounds of Environmental Concern in Aquatic Systems". *Adv. Colloid Interf. Sci., 32, pp. 271-316. (1990).*

Pelizzetti, E.; et al.; "Enhancement of the Rate of Photocatalytic Degradation on TiO_2 of 2-Chlorophenol, 2,7-Dichlorodibenzodioxin and Atrazine by Inorganic Oxidizing Species". *New J. Chem., Vol. 15, 5, pp. 351-359. (1991a).*

Pelizzetti, E.; et al.; "Photocatalytic Process for Surfactant Degradation". *Photocatalytic Purification and Treatment of Water and Air, Ollis, D.F. and Al-Ekabi, H. (eds.). Elsevier Sci. Publish. B.V. (1993a).*

Pelizzetti, E.; et al.; "Formation and Disappearance of Biphenyl Derivates in the Photocatalytic Transformation of 1,2,4-Trichlorobenzene of Titanium Dioxide". *Photocatalytic Purification and Treatment of Water and Air, Ollis, D.F. and Al-Ekabi H. (eds.). Elsevier Sci. Publish. B.V. pp. 291-300. (1993b).*

Pelizzetti, E.; et al.; "Photocatalytic Process for Destruction of Organic Water Contaminants". *Chem. Reactor Techn. for Environ. Safe Reactors and Products, pp. 577-608. Kluwer Ac. Publ., Netherlands. (1993c).*

Pelizzetti, E.; Minero, C.; "Mechanism of the Photo-Oxidative Degradation of Organic Pollutants over TiO_2 Particles". *Electrochimica Acta, Vol. 38, 1, pp. 47-55. (1993d).*

Pelizzetti, E.; et al.; "Metal Oxides as Photocatalyst for Environmental Detoxification". *Comments Inorg. Chem., Vol. 15, 5, pp. 297-337. (1994a).*

Pelizzetti, E.; "Concluding Remarks on Heterogeneous Solar Photocatalysis". *Sol. En. Mat. and Sol. Cells, 38, pp. 453-457. (1995).*

Peterson, M.W.; Turner, J.A.; Nozik, A.J.; "Mechanistic Studies of the Photocatalytic Behavior of TiO_2 Particles in a Photoelectrochemical Slurry Cell and the Relevance to Photodetoxification Reactions". *J. of Phys. Chem., 95, pp. 221-25. (1991).*

Pichat, P.; et al.; "Destruction of 2.4-dichlorophenoxyethanoic Acid(2,4-D) in Water by TiO_2-UV, H_2O_2-UV or Direct Photolysis". *Photocatalytic Purification and Treatment of Water and Air, Ollis, D.F. and Al-Ekabi, H. (eds.). Elsevier Sci. Publish. B.V. pp. 683-688. (1993a).*

Pichat, P.; et al.; "TiO_2 Photocatalytic Destruction of Water Aromatic Pollutants: Intermediates; Properties-Degradability Correlation; Effects of Inorganic Ions and TiO_2 Surface Area; Comparison with H_2O_2 Processes". *Photocatalytic Purification and Treatment of Water and Air, Ollis, D.F. and Al-Ekabi, H. (eds.). Elsevier Sci. Publish. B.V. pp. 207-223. (1993b).*

Pichat, P.; et al.; "Assessment of the Importance of the Role of H_2O_2 and $O_2^{\cdot-}$ in the Photocatalytic Degradation of 1,2-Dimethoxybenzene". *Solar Energy Mat. and Sol. Cells, 38, pp. 391-399. (1995a).*

Pruden, A.L.; Ollis, D.F.; "Photoassisted Heterogeneous Catalysis: the Degradation of Trichlroethylene in Water". *J. Cat., 82, pp. 404-417. (1983a).*

Puma, G.L.; et al.; "Photodegradation of Pentachlorophenol". *Photocatalytic Purification and Treatment of Water and Air, Ollis, D.F. and Al-Ekabi, H. (eds.). Elsevier Sci. Publish. B.V. pp. 689-694. (1993).*

Rabek, J.F.; "Experimental Methods in Photochemistry and Photophysics". *Chap. 27.2, John Wiley and Sons, New York (1982).*

Riegel, G.; and Bolton, J.R.; "Photocatalytic Efficiency Variability in TiO_2 Particles". *J. Phys. Chem.; 99, pp. 4215-4224. (1995).*

Riordan, C.J.; Hulstrom, R.L.; Myers, D.R.; "Influences of Atmosferic Conditions and Air Mass on the Ratio of Ultraviolet to Total Solar Radiation". *Solar Energy Research Institute (SERI)/TP-215-3895. August (1990).*

Rupert, G.; et al.; "Possibilities of Wastewater Treatment with Light Assistance". *ISES Solar World Cong. Budapest, Hungary. (1993a).*

Rupert, G.; et al.; "UV-0_3, UV-H_2O_2, UV-TiO_2 and the Photo-Fenton Reaction. Comparison of Advanced Oxidation Processes for Waste Water Treatment". *Chemosphere, Vol. 28, 8, pp. 1447-1454. (1994).*

Sabin, F.; et al.; "Photo-oxidation of Organic Compounds in the Presence of Titanium Dioxide: Determination of the Efficiency". *J. Photochem. Photobiol. A: Chem., 63, pp. 99-106. (1992).*

Saltiel, C.; et al.; "Performance Analysis of Solar Water Detoxification System by Detailed Simulation". *Solar Eng. Vol. 1, pp. 21-28. ASME (1992).*

Sánchez, M.; "Fabricación y Caracterización Optica de Polímeros Reflectantes con Alta Reflectancia en el UV". *IER-CIEMAT. Proy. M8H01. Informes de Progreso. (1991 y 1992).*

Sclafani, A.; et al.; "Photocatalytic Degradation of Phenol in Aqueous Polycrystalline TiO_2 Dispersions: the Influence of Fe^{+3}, Fe^{+2} and Ag^{+} on the Reaction Rate". *J. Photochem. Photobiol. A: Chem., 56, pp. 113-123. (1991).*

Sczechowski, J.G.; et al.; "Evidence of Critical Illumination and Dark Recovery Times for Increasing the Photoefficiency of Aqueous Heterogeneous Photocatalysis". *J. Photochem. Photobiol. A: Chem.; 74, pp. 273-278. (1993).*

Serpone, N.; Pelizzetti, E.; "Photocatalysis: Fundamentals and Applications". *Wiley-Interscience. John Wiley & Sons. (1989).*

Serpone, N. et al.; "Heterogeneous Photocatalyzed Oxidation of Phenol, Cresols, and Fluorphenols in TiO_2 Aqueous Suspension". *Adv. Chem. Ser., 238, pp. 281-314 (1993a).*

Serpone, N.; et al.; "Identifying Primary Events and the Nature of Intermediates formed during the Photocatalyzed Oxidation of Organics mediated by Irradiated Semiconductor". *Photocatalytic Purification and Treatment of Water and Air, Ollis, D.F. and Al-Ekabi, H. (eds.). Elsevier Sci. Publish. B.V. pp. 225-250. (1993b).*

Serpone N.; "A Decade of Heterogeneous Photocatalysis in our Laboratory: Pure and Applied Studies in Energy Production and Environmental Detoxification". *Res. Chem. Interm., Vol. 20, 9, pp. 953-992. (1994a).*

Serpone, N.; "Brief Introductory Remarks on Heterogeneous Photocatalysis". *Solar Energy Mat. and S. Cells, 98, pp. 369-379 (1995a).*

Serpone, N.; et al.; "Exploiting the Interparticle Electron Transfer Process in the Photocatalyzed Oxidation of Phenol, 2-Chlorophenol and Pentachlorophenol: Chemical Evidence for Electron and Hole Transfer between Coupled Semi conductor". *J. Photochem. Photobiol. A: Chem. 88, pp. 247-255. (1995b).*

Serra, F.; et al.; "Titanium Dioxide-Photocatalized Oxidation of 2,4-Dichlorophenol". *J. Environ. Sci. Health, A29(7), pp. 1409-1421. (1994).*

SGE Scientific Pty. Ltd., "ANATOC, Total Organic Carbon Analyzer". *Melbourne, Australia. (1993).*

SERI (Solar Energy Research Institute); "Shedding a New Light on Hazardous Waste". *SERI/TP-220-3771. February (1991).*

Solarchem Environmental Systems; "The UV/Oxidation Handbook". *1994.*

Spacek, W.; et al.; "Heterogeneous and Homogeneous Wastewater Treatment Comparison between Photodegradation with TiO_2 and the Photo-Fenton Reaction". *Chemosphere, Vol. 30, 3, pp. 477-484. (1995).*

Sullivan, J.M.; et al.; "TiO_2 Catalyzed Photo Oxidation of Atrazine in Dilute Aqueous Solutions Under Solar Irradiation: Process Development". *ASME Intern. Solar En. Conf. San Francisco, USA. March (1994).*

Suzuki, T.; "Metabolism of Pentachlorophenol by Soil Microbore". *J. Environ. Sci. Health, B12(2), pp. 113-127. (1977).*

Tanaka, K.; et al.; " Photocatalytic Degradation of Organohalide Compounds in Semiconductor Suspension with added Hydrogen Peroxide". *New J. Chem., 13, pp.5-7. (1989a).*

Tanaka, K.; et al.; "Efficient Photocatalytic Degradation of Chloral Hydrate in Aqueous Semiconductor Suspension". *J. Photochem. Photobiol., A: Chem., 48, pp. 155-159. (1989b).*

Tanaka, S.; et al.; "Effects of pH on Photocatalysis of 2,4,6-Trichlorophenol in Aqueous TiO_2 Suspensions". *Wat. Sci. Tech., Vol. 30, 9, pp. 47-57. (1994).*

Terzian, R.; Serpone, N.; et al.; "Kinetic Studies in Heterogeneous Photocatalysis 4. The Photomineralization of a Hydroquinone and Cathecol". *J. Photochem. Photobiol. A: Chem., 55, pp. 243-249. (1990).*

Terzian, R.; et al.; "Pulse Radiolytic Studies of the Reaction of Pentahalophenols with OH Radicals: Formation of Pentahalophenoxyl, Dihydroxypentahalocyclohexadienyl and Semiquinone Radicals". *Langmuir, 7, pp. 3081-3089. (1991a).*

Terzian, R.; et al.; "Photocatalyzed Mineralization of Cresols in Aqueous Nedia with Irradiated Titania". J. Catal., 128, pp.352-365. (1991b). *J. Catal., 128, pp.352-365. (1991b).*

Tinuzzi, L.; et al.; "Treatment of Industrial Wastewaters by Photocatalytic Oxidation on TiO_2". *Photocatalytic Purification and Treatment of Water and Air, Ollis, D.F. and Al-Ekabi, H. (eds.). Elsevier Sci. Publish. B.V. pp. 585-594. (1993).*

Trillas, M.; et al.; "Photocatalytic Oxidation of Phenol and 2,4-dichlorophenol over TiO_2". *ASME Intern. Solar En. Conf. San Francisco, USA. March (1994).*

Tseng, J.M.; et al.; "Removal of Chlorophenols from Water by Photocatalytic Oxidation". *Wat. Sci. Tech. Vol. 23, pp. 377-387 (1991).*

Turchi, C.S.; Ollis, D.F.; "Mixed Reactant Photocatalysis: intermediates and Mutual Rate Inhibition". *J. Cat., 119, pp. 487-496. (1989).*

Turchi, C.S.; Ollis, D.F.; "Photocatalytic Degradation of Organic Water Contaminants: Mechanisms Involving Hydroxyl Radical Attack". *J. Cat., 122, pp. 178-192.(1990a).*

Turchi, C.S.; Link, H.F.; "Relative Cost of Photons from Solar or Electric Sources for Photocatalytic Water Detoxification". *Proceedings of International Solar Energy Society 1991 Solar World Congress, Denver, Colorado. August (1990b).*

Turchi, C.S.; Mehos, M.S.; "Solar Photocatalytic Detoxification of Groundwater: Developments of Reactor Design". *Chem. Oxid., 2, pp. 301-314. (1994).*

Tyner, C.E.; "Application of Solar Thermal Technology to the Destruction of Hazardous Wastes". *Solar Energy Materials, 21, pp. 113-129. Elsevier Science Publishers, (1990).*

Valo, R.; et al.; "Bioremedation of Chlorophenol Contaminated Ground Water". *EEC Workshop, Organic Micropollutants in tha Aquatic Environment. Helsinki, Finland. May (1989).*

Valladares, J.E.; et al.; "A Method for the Determination of Quamtum Yields in Heterogeneous Systems: the TiO_2 Photocatalyzed Bleaching of Methylene Blue". *Photocatalytic Purification and Treatment of Water and Air, Ollis, D.F. and Al-Ekabi, H. (eds.). Elsevier Sci. Publish. B.V. pp. 111-120. (1993).*

Vidal, A; "Degradación Fotocatalítica de Contaminantes en Agua: Ensayos de Validación con Acido Salicílico". *IER-CIEMAT Proy. M8H01. Diciembre (1991a).*

Vidal, A; "Degradación Fotocatalítica de Lindano en Agua con Radiación Solar". *3º Congreso Intern. de Química de la ANQUE. Tenerife, Diciembre 1994.*

Vogelpohl, A.; "Oxidation Technologies for Water and Wastewater Treatment". *Papierflieget Verlag, Clausthal-Zellerfeld, Germany. (1996).*

Watts, R.J. et al.; "Sedimentation and Reuse of Titanium Dioxide: application to Suspended Photocatalyst Reactors". *J. Environ. Engin., Vol. 121, 10, pp. 730-735. (1995).*

Weber, K.; Ernst, W.; "Levels and Pattern of Chlorophenols in Water of the Weser Estuary and the German Bight ". *Chemosph., 11, pp. 873-879. (1978).*

Weber, W.J.; et al.; "Removing Dissolved Organic Contaminants from Water". *Environ. Sci. Technol., Vol. 20, 10, pp. 970-979. (1986).*

Wilkins, F.W.; et al.; "Use Solar Energy to Drive Chemical Process". *Chem. Eng. Progress, pp. 41-49. June (1994).*

Wolfrum, E.J.; et al.; "Hydrogen Peroxide in Heterogeneous Photocatalysis". *Aquatic and Surface Photochemistry, Helz, G.R. and Crosby, D.G. (eds.). Lewis Publisher. pp. 451-465. (1994).*

Wong, A.S.; Crosby, D.G.; "Photodecomposition of Pentachlorophenol in Water". *.J. Agric. Food Chem., 29, pp. 125- 130. (1981).*

Yue, P.L.; " Modelling Scale-up and Design of Multiphasic Photoreactors". *Photocatalytic Purification and Treatment of Water and Air, Ollis, D.F. and Al-Ekabi, H. (eds.). Elsevier Sci. Publish. B.V. pp. 495-510. (1994).*

Zarza Moya, E.; "Typical Direct Solar Radiation and Ambient Temperature Data". *Internal Report Nº R.18/89 E.Z., Plataforma Solar de Almería. September, (1989).*